AD-A172 880 PARAMETRIC INVESTIGATION OF FACTORS INFLUENCING THE MECHANICAL BEHAVIOR O..(U) MASSACHUSETTS UNIV AMHERST DEPT OF CIVIL ENGINEERING W A NASH ET AL. 30 MAY 86 1/5

UNCLASSIFIED AFOSR-TR-86-0858 AFOSR-83-0025 F/G 22/2 NL

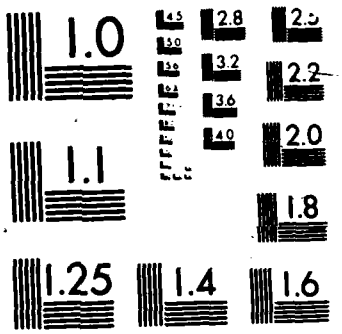
1.0
2.8
3.2
3.6
4.0
2.2
2.0
1.1
1.8
1.25
1.4
1.6

UNCLASSIFIED

SECURITY CLASSIFICATION OF THIS PAGE (When Data Entered)

(2)

AD-A172 880

REPORT DOCUMENTATION PAGE

AFOSR-TR- 86-0858

READ INSTRUCTIONS BEFORE COMPLETING FORM

1. REPORT NUMBER

2. GOVT ACCESSION NO.

3. RECIPIENT'S CATALOG NUMBER

4. TITLE (and Subtitle)

Parametric Investigation of Factors Influencing the Mechanical Behavior of Large Space Structures

5. TYPE OF REPORT & PERIOD COVERED

FINAL TECHNICAL
1 Nov 82-30 June 85

6. PERFORMING ORG. REPORT NUMBER

7. AUTHOR(s)

William A. Nash
Thomas J. Lardner

8. CONTRACT OR GRANT NUMBER(s)

AFOSR-83-0025

9. PERFORMING ORGANIZATION NAME AND ADDRESS

University of Massachusetts
Amherst, MA 01003

10. PROGRAM ELEMENT, PROJECT, TASK AREA & WORK UNIT NUMBERS

61102F
2302/B1

11. CONTROLLING OFFICE NAME AND ADDRESS

AFOSR/NA
Building 410
Bolling AFB, D.C. 20332-6448

12. REPORT DATE

30 May 1986

13. NUMBER OF PAGES

7+299+138

14. MONITORING AGENCY NAME & ADDRESS (if different from Controlling Office)

AFOSR/NA
Building 410
Bolling AFB, D.C. 20332-6448

15. SECURITY CLASS. (of this report)

Unclassified

15a. DECLASSIFICATION/DOWNGRADING SCHEDULE

Not applicable

16. DISTRIBUTION STATEMENT (of this Report)

Approved for public release,
distribution unlimited

DTIC
ELECTE
OCT 0 8 1986
S D
D

17. DISTRIBUTION STATEMENT (of the abstract entered in Block 20, if different from Report)

18. SUPPLEMENTARY NOTES

19. KEY WORDS (Continue on reverse side if necessary and identify by block number)

Space structures
Very large structures
Flexible structures
Truss-like structures
Structural vibrations
Thermal effects in structures

20. ABSTRACT (Continue on reverse side if necessary and identify by block number)

The investigation has two objectives: (I) To investigate the relative importance of factors such as thermal gradients, differential gravitational effects, solar radiation pressure, albedo effects, and spatial pressure gradients on structural behavior of large space structures; and (II) To investigate structural behavior of a very thin membrane subject to combined internal pressure as well as mechanical and thermal loadings. It was

DTIC FILE COPY

DD FORM 1 JAN 73 1473

UNCLASSIFIED

SECURITY CLASSIFICATION OF THIS PAGE When Data Entered

TABLE OF CONTENTS

Introduction 1

Objectives of Research Program 2

Summary of Results 2

Publications 5

Personnel Involved in the Research 6

Advanced Degrees Awarded 6

Papers Presented 6

Advisory Functions 7

Patents 7

Appendix I I-1

Appendix II II-1

PARAMETRIC INVESTIGATION OF FACTORS INFLUENCING THE MECHANICAL BEHAVIOR OF LARGE SPACE STRUCTURES

William A. Nash
Thomas J. Lardner

INTRODUCTION

The problem of investigating extremely large deformations of very flexible large space structures began to assume importance more than two decades ago with launching of the ECHO I satellite into orbit. This system was fabricated from 0.001 cm (0.0005 inch) thick Mylar coated with a vacuum deposited molecular film of aluminum to provide reflectivity to radio frequency transmissions. The final design of the vehicle indicated that its rigidity was sufficient to retain its shape during earth orbit at 1600 km (1000 miles) altitude, but that buckling might occur at somewhat lower altitudes. In ECHO II a two-layer aluminum foil with an inner layer of Mylar was utilized to overcome this buckling problem. During development of the ECHO vehicles, consideration was given to design of expandable structures for space application in the form of reflectors, solar collector, solar sails, scientific equipment packages, and re-entry bodies. Factors examined included design against the hazards of meteoroid particles, high energy radiation, thermal effects, and other environmental factors.

More recently, in 1981, serious attention has been given to development of design criteria for a very large reflector antenna in orbit. One of the more promising preliminary designs of this 800 meter (2600 feet) diameter system involves a truss supporting a parabolic reflector with the outer edge of the reflector being stiffened with a tension truss.

An extremely interesting conceptual design was that of SOLAR SAIL, carried out at the Jet Propulsion Laboratory. This involved a vehicle in the form of a square sail of area 64,000 m^2 fabricated from very thin Mylar. Solar radiation pressures were found to be of extreme importance in the projected flights of this system.

Availability Codes
Dist | Avail and/or Special
A-1

These investigations, together with others, have emphasized the need for a better understanding of the relative importance of a number of environmental parameters involved in the design of any large space structure. These parameters include (a) effect of thermal gradients on the structure -- such influences may cause thermal buckling, thermally induced vibrations, thermal stresses, etc.; (b) differential gravitational forces acting between remote points of a large space structure having a characteristic dimension of several kilometers (one to two miles) in length; (c) pressure gradients along the length of the structure; (d) solar radiation pressure effects; (e) albedo effects; and others.

OBJECTIVES OF RESEARCH PROGRAM

The present research has two objectives:

(Task I) To investigate the relative importance of factors (a) through (e) on design of large space structures operating over a range of altitudes from 200 km (120 miles) to 32,000 km (20,000 miles) above the earth.

(Task II) To investigate structural behavior of an extremely lightweight film-like structure stabilized by internal gas pressure. Such a system could possibly be employed as an instrument carrier, or alternately as an appendage to a somewhat more rigid large space structure, perhaps of a truss-like configuration.

SUMMARY OF RESULTS

Task 1

For the range of altitudes of interest in this investigation and mentioned earlier, and for large space structures having a characteristic

length of several kilometers (one to two miles) the following results were found:

1. Differential gravitational forces do not have any significant effect on the length or attitude of the structure. Nor can such forces alter the orbit appreciably.

2. Radiation heating is very significant in causing structural deformation and in producing libration in attitude motion. However, the effect on orbital parameters due to radiation heating is negligible.

3. Radiation pressure has a negligible effect on changing the axial dimensions of the structure but it can disturb the attitude and orbital motion significantly. Of the three external disturbing sources, namely differential gravitational forces, radiation heating, and radiation pressure, the radiation pressure causes the largest perturbation in the orbital parameters of the system.

4. In low earth orbit, effects of the earth's albedo and its direct radiation should be included in analysis and design. At high altitude orbits, albedo and direct earth radiation effects may be neglected and only direct solar radiation need be considered.

5. A change in differential value of the end masses in the case of a very long dumbbell-like space structure causes a change in the differential gravitational force, but the effects due to this on the space structure are negligible.

6. A change in the length of a space structure does not produce any appreciable change in the effect of the differential gravitational force on the system. However, the dimensions of the large space structure are of great importance in the radiation thermal and pressure effect analyses since

increasing the characteristic length of the structure leads to an increase in surface area exposed to radiation.

7. Increasing the value of the initial attitude angle causes an increase in the libration of the large space structure about its center of mass. An initially imposed attitude misalignment does not, however, produce any noticeable change in length of the structure.

8. An initially induced axial deformation of a large space structure has a significant effect in changing the length and attitude of the structure, but has a negligible effect on perturbing the orbit parameters.

9. Any increase in initial angular velocity of a large space structure induces a greater eccentricity of the orbit and greatly disturbs the attitude motion. For highly eccentric orbits, the structure may tumble continuously. The orbit eccentricity, however, has an insignificant effect in producing structural deformations.

10. Differential gravitational effects vary only very slightly with altitude of the large space structure above the earth. However, radiation thermal and pressure effects vary with changes in lower altitudes. Both terrestrial radiation and direct solar radiation should be considered in design of structures to operate at lower altitudes of approximately 200 km (120 miles).

11. For the range of altitudes considered, for a long space structure in the form of a dumbbell, the attractive forces between the two end masses are negligible.

12. Radiation thermal and pressure effects are greatly enhanced by an increased area-to-mass ratio of the structure. This ratio is one of the most important parameters leading to an increase in thermal and radiation pressure effects on a large space structure.

13. A change of total mass of the large space structure produces only a very minor change in differential gravitational effects. However, the change of mass does produce a significant change in thermal and radiation pressure effects because such a change is often accompanied by an increase in the area-to-mass ratio of the system.

The entire analysis as well as detailed numerical results leading to these conclusions are presented in Appendix A of this report.

Task II

The mechanical behavior of an extremely thin, internally pressurized film-like membrane subject to combined mechanical and thermal loadings was investigated. The material was assumed to be of a Mooney-type and governing equations were derived using the constitutive relations of this material together with thermodynamic relations. The dependence of deformations and thermal stress resultants on internal pressure, axial force, and materials parameters has been determined and presented in parametric form. Regions of stable equilibrium as well as of wrinkling in the vicinity of constraining reinforcements have been determined. Some unexpected phenomena were discovered, such as development of a barrel-shaped contour of an originally cylindrical membrane due to loading with nearly constant axial forces.

The entire analysis as well as detailed results leading to these conclusions are presented in Appendix B of this report.

PUBLICATIONS

Two research papers have been prepared thus far, with several more to follow. The first two are:

"Finite Deformations and Thermal Stresses of Axisymmetric Membranes," B.Q. Yu, William A. Nash, and Thomas J. Lardner. Submitted to The International Journal of Solids and Structures.

"Inflation Instability of an Initially Cylindrical Membrane," B.Q. Yu, William A. Nash, and Thomas J. Lardner. Submitted to The Journal of Applied Mechanics, Transactions, ASME.

PERSONNEL INVOLVED IN THE RESEARCH

Prof. William A. Nash, Department of Civil Engineering, University of Massachusetts, Amherst, MA 01003.

Prof. Thomas J. Lardner, Department of Civil Engineering, University of Massachusetts, Amherst, MA 01003.

Mr. Ramesh B. Malla, Doctoral student in Civil Engineering, University of Massachusetts.

Mr. Bao-qing Yu, Doctoral student in Civil Engineering, University of Massachusetts.

ADVANCED DEGREES AWARDED

Mr. Ramesh B. Malla will receive the Ph.D. from the University of Massachusetts in August, 1986. He is currently employed on the faculty of the University of Connecticut, Storrs, Ct.

Mr. Bao-qing Yu will receive the Ph.D. from the University of Massachusetts in August, 1986.

PAPERS PRESENTED

At the Air Force Office of Scientific Research Second Forum on Large Space Structures held at Texas A & M University, July 1985, Prof. Nash

presented a paper "Finite Deformations and Thermal Stresses in Axisymmetric Membrane Structures."

Also, in January 1985 at Howard University, Washington, D.C., and in September 1985 at Clarkson University, Potsdam, NY, Prof. Nash presented seminars based upon the present AFOSR investigation.

Additional papers based upon Task I of this work are in preparation. They will essentially be condensations of Appendix A of the current report.

ADVISORY FUNCTIONS

Prof. Nash serves as a consultant to the Flight Dynamics Laboratory, Wright-Patterson AFB, Ohio.

PATENTS

No patents were developed during the course of this investigation.

APPENDIX I

Dynamic and Thermal Effects in Very Large Space Structures

CHAPTER I

INTRODUCTION

Introduction and Scope of the Problem

"....To Survive on Earth We Must Expand into Space," writes Ben Bova, editor of Omni magazine in his book, The High Road [1]. At the present time when the world is suffering from overwhelming population growth, drastic decrease in natural resources, and pitiful environmental conditions, the statement of Ben Bova seems to indicate the next resort for solving this global problem. In view of tremendous modern scientific achievements, the possibility of exploring the moon, nearby planets, and asteroids for minerals and other natural resources and transporting them, after processing in space, to the planet earth has become very near to reality. Since 1981, the success of space shuttle aircraft traveling back and forth between the earth and space may have solved the problem of transportation. The successful operation of the Manned Maneuvering Unit (MMU) during various missions of the space shuttle beginning in February 1983 has shown the world that the deployment, assembly, and repair of a structure in space is not an impossible job. Many advantages in both the civilian and

defense fields created by erecting a large orbiting structure in space have been recognized for almost two decades. The number of advantages from the deployment of a large space structure is constantly growing with new developments in space technology. Listed below are a few of them:

1. A large space structure can be used for solar power stations, large space mirrors, large antennas, space-based radar, and multipurpose large space platforms.
2. Deploying a permanent large station in low earth orbit (LEO) may facilitate industrial experiments in material processing, a research laboratory, a staging base for spacecraft refueling and maintenance, a medical laboratory, a dormitory for work crews, and a center for large-scale construction projects.
3. A large space structure can act as a towing vehicle which can carry pay loads from the low orbits attainable by the space shuttle aircraft to higher, more useful orbits.
4. One large manned space station built in geosynchronous earth orbit (GEO, the 24-hour "Clarke Orbit") could consolidate many smaller satellites and allow continuous maintenance of the sensors. Hence, it will be able to decrease the congestion created by placing many smaller satellites in space. The GEO is currently

the most preferred site for communication, navigation, and meteorological satellites.

5. Finally, the technology developed for the large space structures may gradually evolve and expand for use for the establishment of a space colony.

It is clear that there are many benefits that mankind can enjoy from the deployment of a very large structure in space. Although there has been a great deal of development in design and deployment concepts and technology needed for this regard, unfortunately, the core of the subject has still not been fully explored. The deployment of very large structures in space which have characteristic dimensions of several kilometers operating at altitudes ranging from 200 to 35900 km above the earth's surface gives rise to a number of new and significant problem areas that may not have been associated with smaller systems.

The objective of the present research is to investigate these probable problem areas for very large light weight orbiting systems. It is believed that these problems not only need to be thoroughly understood for the formulation of good design criteria for the successful and efficient functioning of the large orbiting systems, but that these problem areas may suggest additional uses for very large structures in space. The effects on very large space structures which are being investigated in this research include the following more significant areas:

(1) Differential gravitational force effects,

(2) Thermal effects, and

(3) Radiation pressure effects.

Both the radiation thermal and pressure effects include direct solar, direct earth, and earth's albedo radiation.

Since earlier investigations deal with relatively small size structures orbiting in space, almost all of them treat the orbital motion of the space structure unafffected by the attitude motion [30, 78]. However, this may not be true in the case of a very large space structure. In addition to taking this matter into consideration, the present work does not put any restriction on the shape of the orbit in which a space structure moves. Further, the structural behavior (deformation), at least in the longitudinal direction, of a space structure is investigated here.

The section below gives a brief historical review pertaining to the developement, design and deployment of space structures in general. In the chapters following this, the effects of the external disturbances are studied on an axially flexible dumbbell-shaped space structure in a general orbit. Chapter II presents the theoretical developments. In Chapter III the numerical method for solution of the equations of motion is discussed. In Chapter IV the results and discussion of the results from the numerical analysis are presented. Finally, in Chapter V

conclusions from the present study are drawn, and some recommendations for further work in related areas are presented.

Historical Review

The successful launch and deployment of the Echo I communication satellite on August 12, 1960 [2] represented the first introduction of a medium size, inflatable thin-walled structure into orbit. The satellite was placed near the 1668-kilometer circular orbit. It was a balloon-shaped satellite with a diameter 30.48 meters (100 feet) and was constructed from a 0.00127 cm (0.0005 inch) thick PolyEthylene Terephthalate (PET) plastic film with aluminum vapor deposited on the outside surface in order to provide reflectancy to radio frequency transmission and to protect the film from damaging ultraviolet radiation. Inside the balloon, sublimating powders were added so as to develop sufficient vapor pressure for inflation in the vacuum of space. The magnitude of equilibrium pressure developed inside the satellite was dependent on the magnitude of the membrane skin temperature. The variation of temperature around the orbit was from 132 °C to -107 °C or a change of 239 °C. The final design of Echo I indicated that its rigidity was sufficient to retain its shape in the orbit of a 1668 kilometer altitude, but it would require a slight

increase in rigidity to prevent buckling at lower orbit altitude. In Echo II, this rigidity was provided by two layers of very thin aluminum foil with an inner layer of Mylar. The Echo II vehicle was 41 meters in diameter.

The Echo missions were followed by the PAGEOS (Passive Geodetic Earth Orbiting Satellite) missions. PAGEOS I was identical to Echo I in shape, size, and basic principles of its function. It was also fabricated of 1.27×10^{-2} mm PET film coated on the outside surface with vapor deposited aluminum to make it highly reflective of sunlight. It was placed in a near polar and circular orbit of 4237 kilometers altitude on June 24, 1966 [3]. PAGEOS I was a technologically advanced version of Echo I. The objective of this mission was to provide a luminous target in near earth-space that fulfills the requirement for worldwide satellite triangulation. The temperature variation in this orbit was predicted to be from 119 °C to -130 °C. The predicted life of PAGEOS I was about 5 years while that of Echo I was considerably less. Another difference in Echo I and PAGEOS I was that PAGEOS I spent a large percentage of its orbital lifetime in the inner Van Allen belt - a region of high intensity, magnetically trapped, particulate radiation which extends from 2000 to 4800 km above the earth.

At about the time of development of the Echo and the PAGEOS vehicles, consideration was given to design of other

space structures for application in the form of reflectors, solar collectors, scientific equipment packages, and an orbiting astronomical observatory. These systems were of relatively smaller sizes orbiting in the range of altitudes 500 to 800 km. For this range of dimensions and altitudes, a number of investigations were carried out pertinent to design against the hazards of meteroid particles, high energy radiation, thermal effects, and environmental factors. Mention should be made of the Radio Astronomy Explorer (RAE) satellite which was launched by NASA at about this time (July 1968), but it was of relatively larger size. The main purpose of this satellite was to carry out some measurements in longwave radio signals from outer space [60]. The satellite had four, 750 feet STEM (Storable Tubular Extendible Member) type, Be-Cu antennas in the orbital plane.

During the last decade or so, there have been numerous studies involving large space structures. Various missions which require large lightweight structures, the major design requirement of such structures, and the prediction of their future have been summerized by Hedgepeth and Brodsky [4] and [5]. Although prioritized specific missions are not yet defined, several novel and innovative design concepts have been suggested for future applications [6-16]. Here, specific mention should be made of the Solar Sail concept, the idea of which was envisioned more than two decades ago

[17, 18] and was studied in detail and designed recently as a square kite-like spacecraft for practical use by the Jet Propulsion Laboratory [19, 20]. Each side of the square sail was 850 meters, and a rendezvouz with Halley's comet was considered as a first mission application. Unfortunately, this project remained incomplete due to monetary reasons. Heliogyro is another proposed solar space vehicle [60]. It consists of twelve 6 km twisted blades which rotate in a solar radiation field generating the required propulsive forces. The Tethered Orbiting Interferometer (TOI) is yet another proposed RAE satellite consisting of two end bodies joined by a flexible lightweight cable several kilometers (5 km) long [60]. The entire structure is gravity gradient stabilized with its long axis pointed towards the earth.

These conceptual ideas have provided valuable information regarding the future technology needed for developing and deploying structurally efficient, reliable, and relatively low-cost systems in space.

CHAPTER II

THEORETICAL DEVELOPMENT

Formulation of Problem

Background

The very large space structure upon which the effects of a differential gravitational force, radiation thermal and radiation pressure, including direct solar and the earth's albedo and its direct radiation are to be studied is shown in Figure 1. In general, the orbital motion of the center of mass of a space structure and the librational motion about its center of mass are mutually coupled. The extent of such coupling depends on the size and shape of the space structure. The larger the ratio (x/r_c), the larger is the influence of librations on the orbital motion where x and r_c are the length of the space structure and the distance of the structure from the center of the earth, respectively.

The coupling between the two motions was first studied by Lagrange while considering the librations of the moon. One of the first studies in satellite librations was carried out on a dumbbell-shaped satellite [45].

Subsequently, there have been numerous works on dumbbell-shaped satellites regarding attitude determination and coupled motion in circular and elliptical orbits [30, 46-55]. All of these investigations are confined to the rigid orbiting dumbbell and are under the sole influence of the earth's gravitational field.

As noted in the previous section, in recent years, there has been a tendency to focus the major research efforts towards very large and flexible space vehicles in response to various mission requirements. These flexible structures possess a potentially large source of elastic energy. Early work, accounting for the satellite extensibility, was carried out on the dumbbell-shaped satellite (for example, see [55, 56]). However, these works were confined to a circular orbit, only the gravitational force effect, and employed reduced (simplified) equations of motion. Later, greater generality was introduced in the derivation of the equations of motion and in the studies of stability, dynamics, and control of flexible space vehicles [31-33, 57-62]. These studies show that elastic deformation or flexibility of a space structure has certain effects on the stability, performance, and overall body orbital motion. In these works, actual analysis to obtain a solution is based on only the gravitational force effects and in some cases, gravitational force and solar radiation effects on

the orbital or attitude motion separately. More recently, algorithms which enable one to simulate numerically the large motions of unrestrained and restrained space structures have been developed [63, 64].

Fundamental Equations of Motion

The geometric configuration which is under consideration representing a very large space structure consists of two point masses, m_1 and m_2 connected by an axially flexible link structure which moves in a general non-circular orbit (Figures 1 and 2). The weight of the link structure can be considered to be negligible in comparison with the weight of the total system, and thus for a light weight system the mass of the linked structure may be taken to be lumped at the two ends. This dumbbell structure is assumed to move in the orbital plane (coplanar motion). It is also assumed that the orbit of the structure is defined by the motion of its center of mass C. There are two important reasons in chosing this dumbbell model to represent a space structure. First, the dumbbell configuration is employed to facilitate the study of differential gravitational force effects. Second, the link joining the two dumbbell masses can be considered to be a plate-like structure which, in turn, may well represent a very large truss-like structure. It has been currently

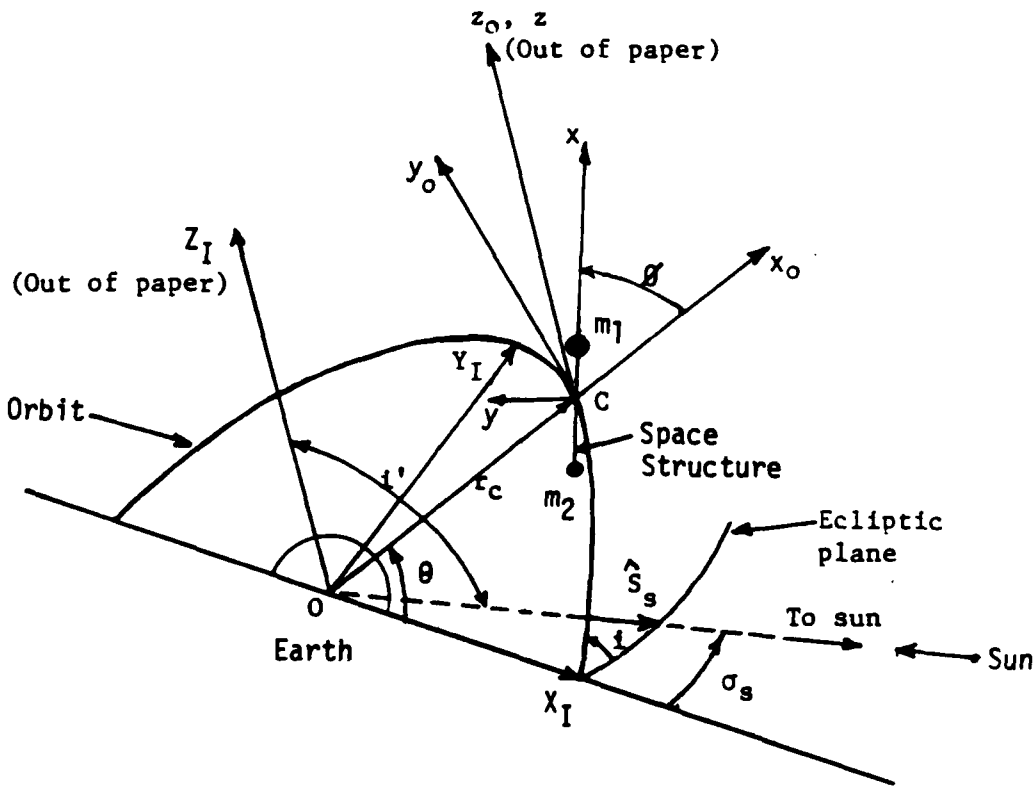

Figure 1. Space Structure in Orbit

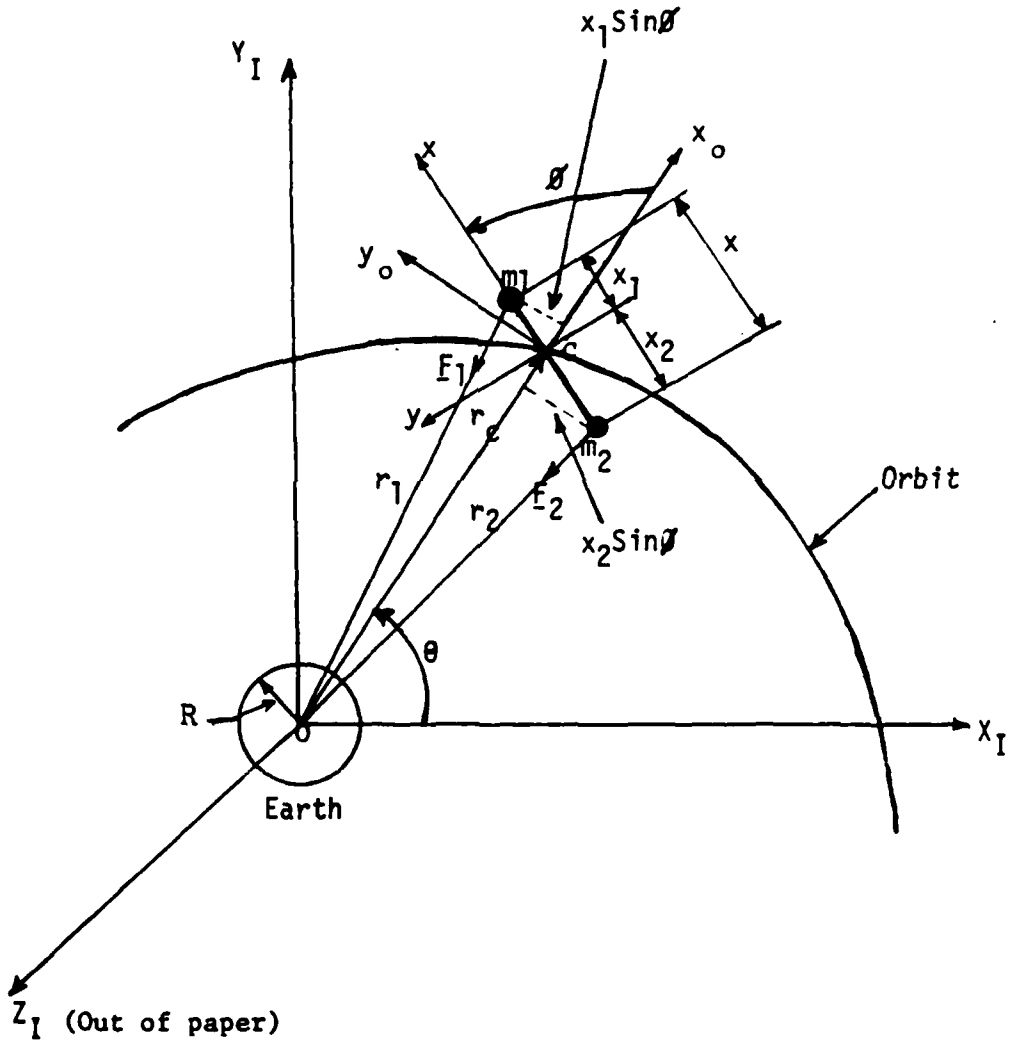

Figure 2: Space Structure Subjected to Earth's Gravitational Forces

envisioned that a strong candidate for a low-mass and high-stiffness structure is an open-truss configuration.

The equations of motion of such a structure moving in an orbit around the spherical earth of radius R_E whose center is at point O (Figure 2) will be derived using Lagrange's procedure. The generalized coordinates of the problem will be (1) the radial distance r_c between the center of the earth and the center of mass of the space structure, (2) the angle θ describing the sweep of the radial line r_c in the plane of motion, (3) the distance x between the two dumbbell masses m_1 and m_2, and (4) the angle ϕ between the local vertical line OC and the line joining the two masses.

<u>Kinetic energy</u>. The total kinetic energy of the system with respect to earth-fixed axes (X_I, Y_I, Z_I) (Figure 2) can be determined quite readily (see Appendix A) and is given by

$$K_E = \left(\frac{1}{2}\right)\{m[\dot{r}_c^2 + (r_c\dot{\theta})^2] + m_1[\dot{x}_1^2 + x_1^2(\dot{\theta} + \dot{\phi})^2] + m_2[\dot{x}_2^2 + x_2^2(\dot{\theta} + \dot{\phi})^2]\} \tag{2.1}$$

where

$$m = m_1 + m_2 \tag{2.2}$$

and

x_1 and x_2 are the distances of the masses, m_1 and m_2 from the C. M. of the space structure C , respectively and are given by

(a) $x_1 = (m_2/m)x$

(b) $x_2 = (m_1/m)x$

(c) $x = x_1 + x_2$

(2.3)

The first term in the right hand side of Equation (2.1) is the kinetic energy of the mass center of the system, and the second and third terms represent the kinetic energies of the masses m_1 and m_2, respectively. Noting the reduced mass

$$\bar{m} = (m_1 m_2)/m \tag{2.4}$$

the above equation (2.1)can be written as below

$$K_E = \left(\frac{1}{2}\right) \{m[\dot{r}_c^2 + (r_c\dot{\theta})^2] + \bar{m}[\dot{x}^2 + x^2(\dot{\theta} + \dot{\phi})^2] \tag{2.5}$$

<u>Potential energy</u>. Of all the external forces acting on the system, the forces given below are conservative in nature, and hence, can be derived from a potential function.

(a) The earth's gravitational force on the point masses can be derived from the well-known potential function (Ref. 67, pp 287; also see Appendix A)

$$V_g = -\mu\left(\frac{m_1}{r_1} + \frac{m_2}{r_2}\right) \tag{2.6}$$

where

$$\mu = gR^2 \tag{2.7}$$

is a constant quantity, g represents the acceleration due

to gravity at the earth's surface, and R is the radius of the spherical earth, r_1 and r_2 are distances of the mass centers of masses, m_1 and m_2 from the center of the earth (O), respectively. These are given by the following relations.

(a) $r_1 = [r_c^2 + x_1^2 + 2r_c x_1 \cos\emptyset]^{1/2}$

(b) $r_2 = [r_c^2 + x_2^2 - 2r_c x_2 \cos\emptyset]^{1/2}$

(2.8)

(b) The attractive force between the two masses m_1 and m_2 can be obtained from the potential function as given below

$$V_m = -(Gm_1m_2)/x \tag{2.9}$$

where G is the Universal Gravitational Constant.

(c) Lastly, the force produced due to the deformation of the structure can be derived from the strain energy U_e. Expressions for U_e will be derived in the sections below for various operational parameters of the space structure.

Thus, the total potential energy of the system under consideration is given by summing up V_g, V_m, and U_e

$$P_E = -\mu\left(\frac{m_1}{r_1} + \frac{m_2}{r_2}\right) - G\frac{m_1m_2}{x} + U_e \tag{2.10}$$

<u>Generalized forcing functions</u>. Besides the conservative external forces that are treated above, other external

forces which are nonconservative and which the system is subjected to, are thermal forces and radiation pressure forces. Within the framework of this study, these forces may arise from (a) direct solar radiation, (b) the earth's albedo and (c) its direct radiation. The mathematical expressions to represent these forces will be presented in the sections below. In general, these forces can be obtained by the method of virtual work. Let F_i be an external force, then the work dw_i done by the force in an infinitesimal virtual displacement or deformation $d\delta_i$, is

$$dw_i = F_i \, d\delta_i \tag{2.11}$$

The generalized force Q_i corresponding to the coordinate i is defined by

$$Q_i = dw_i / d\delta_i = F_i \tag{2.12}$$

At present, it will suffice to represent the generalized forces due to the above sources by Q_r, Q_θ, Q_α, and Q_ϕ corresponding to the generalized coordinates r_c, θ, α, and ϕ, respectively.

General equations of motions. For the generalized coordinates and forces described above, Lagrange's equations (Ref. 69, pp 273), are

$$\text{(a)}\quad \frac{\partial}{\partial t}\left(\frac{\partial K_E}{\partial \dot{r}_c}\right) - \frac{\partial K_E}{\partial r_c} + \frac{\partial P_E}{\partial r_c} = Q_r$$

$$\text{(b)}\quad \frac{\partial}{\partial t}\left(\frac{\partial K_E}{\partial \dot{\theta}}\right) - \frac{\partial K_E}{\partial \theta} + \frac{\partial P_E}{\partial \theta} = Q_\theta$$

$$\text{(c)}\quad \frac{\partial}{\partial t}\left(\frac{\partial K_E}{\partial \dot{x}}\right) - \frac{\partial K_E}{\partial x} + \frac{\partial P_E}{\partial x} = Q_x$$

$$\text{(d)}\quad \frac{\partial}{\partial t}\left(\frac{\partial K_E}{\partial \dot{\phi}}\right) - \frac{\partial K_E}{\partial \phi} + \frac{\partial P_E}{\partial \phi} = Q_\phi$$

(2.13)

where a dot indicates differentiation with respect to time, t. Upon substitution of K_E and P_E respectively from Equations (2.5) and (2.10) into Equations (2.13) and minor algebraic work (Appendix A), one gets

$$\text{(a)}\quad m\ddot{r}_c - mr_c\dot{\theta}^2 + \mu\left[\frac{m_1(r_c + x_1\cos\phi)}{r_1^3} + \frac{m_2(r_c - x_2\cos\phi)}{r_2^3}\right] = Q_r$$

$$\text{(b)}\quad mr_c(r_c\ddot{\theta} + 2\dot{\theta}\dot{r}_c) - \bar{m}\,\mu\left[\frac{(-1)}{r_1^3} + \frac{1}{r_2^3}\right]x r_c\sin\phi = (Q_\theta - Q_\phi)$$

$$\text{(c)}\quad \bar{m}\ddot{x} - \bar{m}x(\dot{\theta} + \dot{\phi})^2 + \bar{m}\,\mu\left[\frac{(x_1 + r_c\cos\phi)}{r_1^3} + \frac{(x_2 - r_c\cos\phi)}{r_2^3}\right] + \frac{Gm_1m_2}{x^2} + \frac{\partial U_e}{\partial x} = Q_x$$

$$(d)\ \bar{m}[x^2(\dot{\theta} + \dot{\phi}) + 2x\dot{x}(\dot{\theta} + \dot{\phi})] + \bar{m}\ \mu[\frac{(-1)}{r_1^3} + \frac{1}{r_2^3}]x r_c \sin\phi = Q_\phi \tag{2.14}$$

These differential equations of motion are coupled and non-linear. A study of the equations of motion reveals that the basic parameters r_c, θ, x, and ϕ are coupled to each other by themselves and by their first and second derivatives. Therefore, the natural period of the libration in ϕ and the natural period of oscillation in x are seen to depend on other variables.

Differential Gravitational Force Analysis

The effect of differential gravitational forces acting between remote points is negligible for a small system, but it is not so for a very large flexible structure, particularly in low earth orbit [29]. One of the first studies of this effect, besides the classical study of the oscillation of the moon, was on a dumbbell-shaped satellite [30, 45]. Because of the large distances between masses at the ends of the very large structure, gravitational effects cause secular motion of the masses. Hence, these effects give rise to anomalous overall structural motion (for example, see Refs. [29-33]).

For a situation where the dominant external force is due to earth's gravity alone, then

(a) $Q_r = 0$

(b) $Q_\theta = 0$

(c) $Q_x = 0$

(d) $Q_\phi = 0$

(2.15)

For an axially flexible structure, the strain energy corresponding to axial force is

$$dU_e/dx = K_a\ (x - x_s) \tag{2.16}$$

where K_a is the force required to stretch the structure by a unit distance and is given by

$$K_a = A_{cs}E/x_s \tag{2.17}$$

in which, A_{cs} is the area of the cross-section of the structure, and E is the modulus of elasticity of the material of the structure. Also x_s is the static stress free (reference) length of the dumbbell structure.

The equations of motions are now given by Equations (2.14) with the above values of Q_r, Q_θ, Q_x, Q_ϕ, and dU_e/dx. The equations thus obtained agree completely with equivalent equations derived by Hall and Smith [79] when $m_1 = m_2$ and with no damping.

In the equations of motion (2.14) the gravitational force terms are as below:
The earth's gravitational forces on mass m_1 and m_2 are, respectively

$$\text{(a)}\quad F_{g1} = \frac{\mu}{m}\left[\frac{m_1(r_c + x_1\cos\phi)}{r_1^3}\right]$$

$$\text{(b)}\quad F_{g2} = \frac{\mu}{m}\left[\frac{m_2(r_c - x_2\cos\phi)}{r_2^3}\right] \tag{2.18}$$

Total earth's gravitational force F_g on the system is given by adding Equations (2.18a) and (2.18b)

$$F_g = \frac{\mu}{m}\left[\frac{m_1(r_c + x_1\cos\phi)}{r_1^3} + \frac{m_2(r_c - x_2\cos\phi)}{r_2^3}\right] \quad (2.19)$$

At time t = 0, the initial total earth's gravitational force on the system can be written as

$$F_{g0} = \frac{\mu}{m}\left[\frac{m_1(r_0 + x_{10}\cos\phi)}{r_{10}^3} + \frac{m_2(r_0 - x_{20}\cos\phi)}{r_{20}^3}\right] \quad (2.20)$$

where the subscript "0" represent the corresponding quantities at t = 0.

The differential gravitational force ΔF_g on the structure can be obtained by subtracting Equation (2.18b) from Equation (2.18a)

$$\Delta F_g = \frac{\mu}{m}\left[\frac{m_1(r_c + x_1\cos\phi)}{r_1^3} - \frac{m_2(r_c - x_2\cos\phi)}{r_2^3}\right] \quad (2.21)$$

As we have seen in Appendix A, in the case where the space structure is subjected to gravitational force only, the second Lagrange's relation in Equations (2.13) yields an expression (Equation (A-26)) which can be put in self adjoint form as below

$$m\frac{d}{dt}(r_c^2\dot{\theta}) + m\frac{d}{dt}\{x^2(\dot{\theta} + \dot{\phi})^2\} = 0 \quad (2.22)$$

Integrating this relation with respect to time, we have

$$mr_c^2\dot{\theta} + \bar{m}(\dot{\theta} + \dot{\phi})^2x^2 = \text{constant} \quad (2.23)$$

This expression shows that the angular momentum ($r_c^2\dot{\theta}$) about the center of the earth is no longer a constant as it would be in the case for a single point mass in an unperturbed orbit. While the total angular momentum of the orbit must still remain constant, Equation (2.23) shows that for the structure this constant has two variable components: the angular momentum due to the orbital motion and the angular momentum due to the libratory motion. Hence, any change in the libratory component due to variation in x and ϕ must therefore be accompanied by a compensating change in the orbital component. Therefore, there exists an energy exchange between orbit and libration motion, and the orbit will be perturbed by variations in x and ϕ. It is interesting to note that Hall and Smith [79] reached the same conclusion while investigating the simplified (approximate) equations of motion.

Thermal Analysis

In one orbit the structure will be exposed to a wide range of temperature which can cause thermally induced vibrations (for example, see Refs. [21], [23], and [25]), thermal buckling, surface material degradation (for example, see [22]), thermally induced nutational body motion [24], and thermal stresses. Although for a structure having a length of a few kilometers the temperature may remain constant while it is completely in the sunlight portion or on the earth-shadow portion of an orbit, there may arise a differential temperature along the structure while it is entering the earth-shadow and exiting from it. This may give rise to thermally induced deformation, possible skin buckling, and overall distortion of the shape of the structure that may change the geometry sufficiently so as to alter the attitude and/or render the system incapable of carrying out its assigned mission. For example, this could happen if a large antenna distorts sufficiently so that it reflects the signal inaccurately [16].

It was observed that a thermal gradient gives rise to anomalous spacecraft body motion. Spacecraft booms exposed to solar radiation have been known to exhibit thermally induced oscillatory instabilities (thermal flutter) [26-28].

This effect may well arise in very large space structures, especially if they consist of structural components with thin open sections.

For any thermal analysis, an accurate determination of temparature variation around an orbit of a structure in space is most essential. This is done in the section below.

Temperature Variation

It can be deduced from the fundamental hypothesis of the mathematical theory of conduction of heat in solids [80] that, if there is no heat generated within, or radiated away, the differential equation that defines the heat flow in a one-dimensinal structure is

$$K_{th} V \frac{\partial^2 T(x,t)}{\partial x^2} - M c \frac{\partial T(x,t)}{\partial t} = 0 \qquad (2.24)$$

where

K_{th} = thermal conductivity

v = volume of the structure

M = mass of the structure effective to radiation

c = specific heat of material

x = longitudinal length measured from the center of mass of the structure

t = coordinate used to measure time

T = absolute temperature at the position x at time t

If it is assumed that the structure radiates heat $\dot{q}_{out}$ as a black body and that the heat input can be defined by the function $\dot{q}_{in}$, then the thermodynamic equation of heat conduction and radiation is given by

$$K_{th} V \frac{\partial^2 T(x,t)}{\partial x^2} - M\,c \frac{\partial T(x,t)}{\partial t} = \dot{q}_{out}(x,t) - \dot{q}_{in}(x,t) \qquad (2.25)$$

For a space structure of a few kilometers characteristic dimension, orbiting at altitudes of our contemporary concern, it can be assumed without significant loss in accuracy, that the temperature remains constant throughout the structure at a given time. For example, in geosynchronous orbit a one kilometer long structure travels fast enough to enter into or exit from the earth's shadow in about 0.3 seconds. In lower orbits the time is even shorter. Then, the above thermodynamic equation will reduce to

$$M\,c \frac{\partial T(t)}{\partial t} = \dot{q}_{in}(t) - \dot{q}_{out}(t) \qquad (2.26)$$

In general, the specific heat of a substance is dependent on pressure and temperature. However, theories show, and experiments verify, the fact that there is very little pressure dependence of the specific heat of solids until extremely high pressures are encountered which is unlikely

in the present problems. Even the temperature dependence is slight for moderate changes in temperature. For example, for aluminium at temperatures equal to 32°F, 572 °F, 1112 °F, and 1292 °F (i. e., 0 °C, 300 °C, 600 °C, and 700 °C, respectively) the values of specific heat are found to be equal to 0.2106, 0.2463, 0.2821, and 0.2590 Btu/lb_m-°F, respectively [87]. So, in the absence of any other information, the specific heat of the solid under the present circumstances is considered to be constant at a value of 0.21 Btu/lb_m-°F.

An accounting of energy to and from, or stored in, a space structure serves to determine the temperature of the structure. The following assumptions are made in determining the temperature variation in the structure: (1) The internal heat generated by power sources, net internal radiation absorbed, heating due to the impingement of micrometeorites, molecules, atoms, ions, or atomic nuclei, and aerodynamic heating although it may be significant up to 200 miles above the earth's surface, are ignored; (2) The material of the structure is homogeneous and isotropic i. e., thermal conductivity of the structure is constant; (3) The heat energy transferred is assumed to be only radiative; (4) The temperature remains constant throughout the structure at any specific instant, so the temperature is a function of time only; (5) The heat absorbed at a point on the sunlight side of the structure is proportional to the cosine of the angle

between the surface normal and the sun line; (6) The main structure connecting the two end masses is considered to be plate-like with mass (M); (7) The sun is a fixed source of collimated electromagnetic radiation; (8) The type of orbit (polar, equatorial, etc.) is assumed to produce only small changes in the structure. In actual practice the amount of radiation reflected and emitted from the earth might vary with the type of orbit; and (9) The earth and its atmosphere is represented by the earth alone.

Assuming the space structure is a black body, the radiative heat output is given by

$$\dot{q}_{out} = \epsilon_1 \sigma A_{sd1} T_1^4 + \epsilon_2 \sigma A_{sd2} T_2^4 \qquad (2.27)$$

where

ϵ = emissivity

σ = Stephan-Boltzmann constant

T = temperature of the structure as defined before

A_{sd} = total area of one side of the plate-like structure

Subscripts 1 and 2 refer to side 1 and side 2 of the structure. Assuming identical surface and geometric properties on both sides of the structure, the above equation reduces to

$$\dot{q}_{out} = \epsilon \sigma A_{sf} T^4 \qquad (2.28)$$

In which, total surface area $A_{sf} = 2A_{sd}$, and $T_1 = T_2 = T$.

The radiation effects received by a space structure are of mainly three types. These are the major sources which cause the change in temperature of the structure.

1. The most important heat source is direct solar radiation.
2. The second source of heat is solar radiation reflected from the earth and atmosphere.
3. The last heat source is the radiation emitted by the earth and atmosphere.

In brief,

$$\dot{q}_{in} = \underset{(\dot{q}_s)}{\text{Direct solar}} + \underset{(\dot{q}_r)}{\text{reflected from earth \& atmosphere}} + \underset{(\dot{q}_e)}{\text{emitted from earth \& atmosphere}} \qquad (2.29)$$

In this section, an expression to determine the heat energy from each source will be presented.

Let us define the celestial sphere (Figure 3(a)) as below: O is the center of the earth. The X_I Y_I - plane coincides with the orbit plane ($x_o y_o$ plane) of the space structure. C is the instantaneous position of the center of mass (C. M.) of the structure. The direction of the sun is S inclined by an angle $i' = ZS$ (see Figure 3a) from the

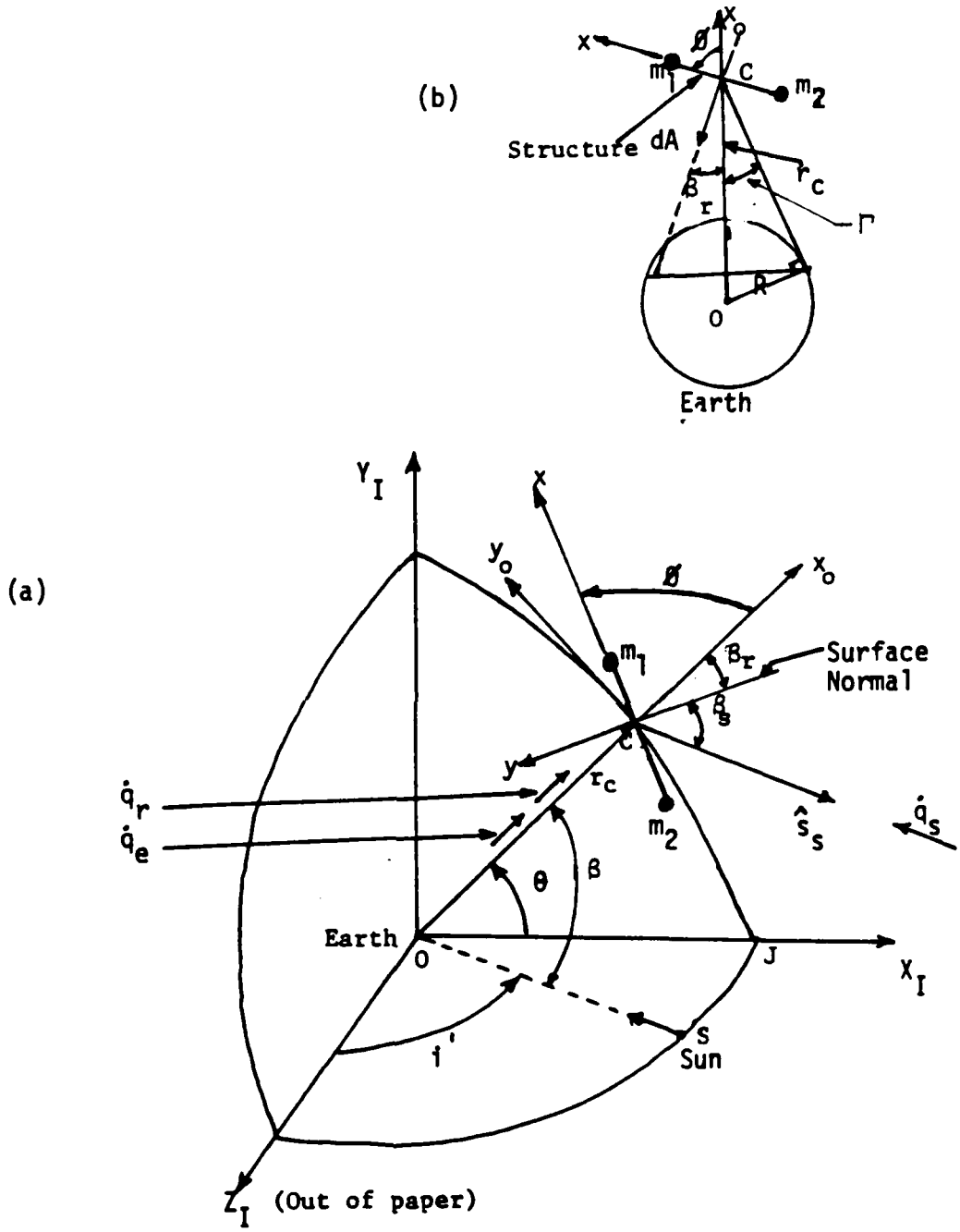

Figure 3. Space Structure Subjected to Heating from Various Radiation Sources

orbit normal (OZ). The J direction defines the direction of the X_I - axis and is the intersection of the orbit plane and a perpendicular plane which contains the sun. The instantaneous position of the space structure is defined by an angle θ measured from the X_I - axis.

The angle β is a measure of the orientation of the plane of the orbit with respect to the earth-sun line. $\beta = 0$ corresponds to the earth-sun line lying in the plane of orbit. As the space structure revolves about the earth, it passes from the earth's shadow into sunlight and back into shadow again. When the structure is on the sun side of the earth, the amount of incident solar and reflected radiation varies with time. But, when it is in the earth's shadow the incident radiation remains constant, because in such a case the only radiation the structure receives is direct earth radiation, which is constant at any altitude. Direct solar and earth reflected radiations are zero in the earth's shadow region.

<u>Direct solar radiation heating.</u> When the sun heats a structure in space directly, the amount of heat absorbed is a function of the surface absorptivity, a_s, and the projected surface area normal to the sun flux. Thus, the total solar heating is

$$\dot{q}_s = \delta \, a_s \, G_s \, A_{sd} \, |\cos\beta_s| \qquad (2.30)$$

where β_s is the angle between the surface normal and sun direction (Figure 3a). The quantity within | | indicates the absolute value for the corresponding term. It is assumed that the solar energy flux G_s is essentially independent of orbit altitude. This is the case in the present study also. A_{sd} is the total plan area of the structure and δ is a step function which is given by

$$\delta = 1 \text{ in the sunlight portion of the orbit}$$
$$= 0 \text{ in the earth's shadow portion of the orbit} \qquad (2.31)$$

In theory, it is possible that sunlight may be incident on both sides of the flat plate-like structure. In practice, it is very unlikely that a space structure will be operated so close to the sun or at such an angle from the perpendicular to the sun so that the backside will be irradiated. Therefore, direct solar radiation incident only on one side of the structure has been considered in the above expression.

<u>Earth's albedo radiation heating.</u> Albedo refers to the influence of light reflected from the earth to an object in the atmosphere. The earth acts as a reflector of solar radiation. The albedo factor A_r is a measure of the fraction of solar energy reflected. It has been shown by Modest [70] that although the reflected heat is a

complicated function of attitude (θ, ϕ), sun's position, and altitude of the space structure, good accuracy can be obtained by using Cunningham's view factor F_{e1} and F_{e2} [42] in the following equation

$$\dot{q}_r = \delta(a_{r1}F_{e1}A_{sd1} + a_{r2}F_{e2}A_{sd2})A_rG_s\cos\beta \quad \text{for } |\beta| \leq \pi/2$$
$$= 0 \quad \text{for } |\beta| > \pi/2 \tag{2.32}$$

where β is the angle between the earth-sun line and the earth-orbiting body line (Figure 3a), and a_r is surface absorptance to radiation reflected from the earth. Subscripts 1 and 2 refer to side 1 and side 2 of the plate-like structure. The view factors F_{e1} and F_{e2} as reported by Cunningham, are given below

(a) When $0 \leq |\beta_r| \leq (\pi/2 - \Gamma)$

$$F_{e1} = \sin^2\Gamma \cos\beta_r$$
$$F_{e2} = 0$$

(b) When $(\pi/2 - \Gamma) \leq \beta_r \leq (\pi/2 + \Gamma)$

$$F_{e1} = [\sin^2\Gamma \cos\beta_r \cos^{-1}(-\cot\Gamma \cot\beta_r) + \cos^{-1}(\cos\Gamma/\sin\beta_r) - \cos\Gamma \sqrt{(\sin^2\Gamma - \cos^2\beta_r)}]/\pi$$
$$F_{e2} = F_{e1} \quad \text{with } \beta_r = (\pi - \beta_r) \tag{2.33}$$

where Γ is the angle between the line OC and a tangent from C to the planet surface (Figure 3(b)). β_r is the angle between the line OC and the surface normal to the orbiting structure.

As is seen in the above relations, the view factor is a function of the altitude of the orbiting surface, the size of the sphere, attitude of the orbiting structure, and other basic geometric quantities. The sphere (radiation emitting body) is assumed to be gray and diffuse.

For a structure having the same surface and geometric characteristics on both sides, Equation (2.32) becomes

$$\dot{q}_r = \delta a_r A_r G_s (F_{e1} + F_{e2}) A_{sd} \cos\beta \qquad \text{for } |\beta| \leq \pi/2$$
$$= 0 \qquad \text{for } |\beta| \geq \pi/2 \qquad (2.34)$$

<u>Direct earth radiation heating.</u> The heat absorbed by a surface is a function of the surface absorptivity a_e and view factor F_e. The view factor between an orbiting flat plate and a sphere was developed by Cunningham [42]. The amount of heat absorbed by the surface from earth emission is given by

$$q_e = a_e E_e (F_{e1} + F_{e2}) A_{sd} \qquad (2.35)$$

where E_e is the earth emitted radiation intensity. It can

be expressed in the following manner

$$E_e = \epsilon_e \sigma T_e^4 \tag{2.36}$$

In which,

ϵ_e = emissivity of the earth.

T_e = temperature of the earth

σ = Stephan-Boltzmann constant

The view factors are again given by Equations (2.33). In deriving Equation (2.35), we have again assumed that the surface and geometric characteristics of both sides of the structure are identical.

Geometric consideration gives us the following relations (Figure 3a)

(a) $\beta_r = (\emptyset - \pi/2)$

(b) $\sin r = R/r_c$

(c) $\cos\beta = \sin i' \cos\theta$

(d) $\cos\beta_s = \sin i' \sin(\theta + \emptyset)$

(2.37)

The total heat energy input to the space structure now is given by substituting Equations (2.30), (2.34), and (2.35) into Equation (2.29).

$$q_{in} = \delta a_s G_s A_{sd} |\cos\beta_s| + (\delta a_r A_r G_s \cos\beta + a_e E_e)(F_{e1} + F_{e2}) A_{sd} \quad \text{for } |\beta| \leq \pi/2$$

$$= \delta a_s G_s A_{sd} |\cos\beta_s| + a_e E_e (F_{e1} + F_{e2}) A_{sd} \quad \text{for } |\beta| \geq \pi/2 \tag{2.38}$$

The recommended average value of the earth albedo is 0.30. The corresponding equivalent black body temperature of the earth is 254°K which leads to an average emitted radiation E_e at the earth's surface of 237 W/m^2 (0.34 cal cm^{-2} min^{-1}) [74, 75].

<u>Equilibrium Temperature.</u> The equilibrium temperature can be determined from Equation (2.26) by setting the left-hand side equal to zero

$$\text{i. e.,} \quad \dot{q}_{in} - \dot{q}_{out} = 0 \tag{2.39}$$

Substituting Equations (2.28) and (2.38) into Equation (2.39) and arranging terms, the following relation can be obtained

$$T_{eq} = \left[\frac{\delta a_s G_s A_{sd} \cos\beta_s + (\delta a_r A_r G_s \cos\beta + a_e E_e)(F_{e1} + F_{e2}) A_{sd}}{\epsilon \sigma A_{sf}}\right]^{1/4} \quad \text{when } |\beta| \leq \pi/2$$

$$= \left[\frac{\delta a_s G_s A_{sd} \cos\beta_s + a_e E_e (F_{e1} + F_{e2}) A_{sd}}{\epsilon \sigma A_{sf}}\right]^{1/4} \quad \text{when } |\beta| \geq \pi/2 \tag{2.40}$$

where T_{eq} is the equilibrium temperature.

Equations of Motion

Generalized Forcing Functions. Let Q_{th} be the external forcing function due to thermal effects on the structure. Then it can be written that

$$Q_x = Q_{th} \tag{2.41}$$

Since the force Q_{th} does no work when x is kept fixed and other variables, namely, r_c, θ, and ϕ are varied, it follows that the generalized forces Q_r, Q_θ, and Q_ϕ corresponding to coordinates r_c, θ, and ϕ, respectively , are equal to zero. That is,

$$\begin{aligned} &(a)\ Q_r = 0 \\ &(b)\ Q_\theta = 0 \\ &(c)\ Q_\phi = 0 \end{aligned} \tag{2.42}$$

If only the axial deformation is considered, the force in this direction due to temperature variation in the space

structure is given by Booley and Weiner [83] as:

$$Q_{th} = E[-\alpha_{th}(T - T_s) + \int_A \alpha_{th}(T - T_s)dA] \qquad (2.43)$$

Here, α_{th} is the coefficient of thermal expansion or contraction and T_s is the reference temperature (°K). Other notations are as defined earlier. In a case where the temperature is only a function of time, Equation (2.43) gives

$$Q_{th} \equiv 0 \qquad (2.44)$$

i. e., the axial normal stress due to temperature change is zero. But, there will be a thermally induced strain. Thus, the expression for strain energy will be different than that when the temperature effect is not considered.

<u>Strain energy.</u> The total strain energy, U_e is given by

$$U_e = (\text{Volume})(\text{Strain Energy Density}) \qquad (2.45)$$

Or, $$U_e = (A_{cs})\{(1/2)E\epsilon_x^2\} \qquad (2.46)$$

where, ϵ_x is the axial normal strain under the mechanical loading.

The structure can be considered to be subjected to

(first) only a thermal effect which causes the strain $\alpha_{th}(T - T_s)$, and (second) only a mechanical effect which causes the strain, ϵ_x. The total normal strain, ϵ_T is then given by

$$\epsilon_T = \alpha_{th}(T - T_s) + \epsilon_x \tag{2.47}$$

Therefore,

$$\epsilon_x = \epsilon_T - \alpha_{th}(T - T_s) \tag{2.48}$$

The total normal strain is also given by

$$\epsilon_T = (x - x_s)/x_s \tag{2.49}$$

Upon substitution of Equation (2.49) into Equation (2.48), we get,

$$\epsilon_x = \left(\frac{x - x_s}{x_s}\right) - \alpha_{th}(T - T_s) \tag{2.50}$$

Substituting for ϵ_x from the above equation into Equation (2.46), we obtain,

$$U_e = \frac{1}{2} A_{cs} x_s E \left[\left(\frac{x - x_s}{x_s}\right) - \alpha_{th}(T - T_s)\right]^2 \tag{2.51}$$

The quantity (dU_e/dx) is now

$$dU_e/dx = \frac{A_{cs}E}{x_s}(x - x_s) - A_{cs}E_\alpha(T - T_s) \qquad (2.52)$$

where, the thermoelastic property in the longitudinal direction is

$$E_\alpha = E\,\alpha_{th} \qquad (2.53)$$

The equations of motion of the space structure are now given by Equations (2.14) where the generalized forcing functions are given by Equations (2.41) and (2.44), and the quantity (dU_e/dx) is given by Equation (2.52). These equations contain the effects of gravitational and thermal forces.

Effect of the Earth's Shadow

To evaluate the effect of the earth's shadow, we must know the values of angles θ_i and θ_e at which the space structure enters and exits the earth's shadow, respectively (Figure 4b). Without appreciable error, it can be assumed that the shadow is a circular cylinder of radius R. The intersection of the orbit plane with this half-cylinder is a semi-ellipse as shown in Figures 4 (a and b). Its equation in the coordinate system described above is [71]

$$\frac{X_I^2}{a^2} + \frac{Y_I^2}{b^2} = 1 \qquad (X_I \leq 0) \qquad (2.54)$$

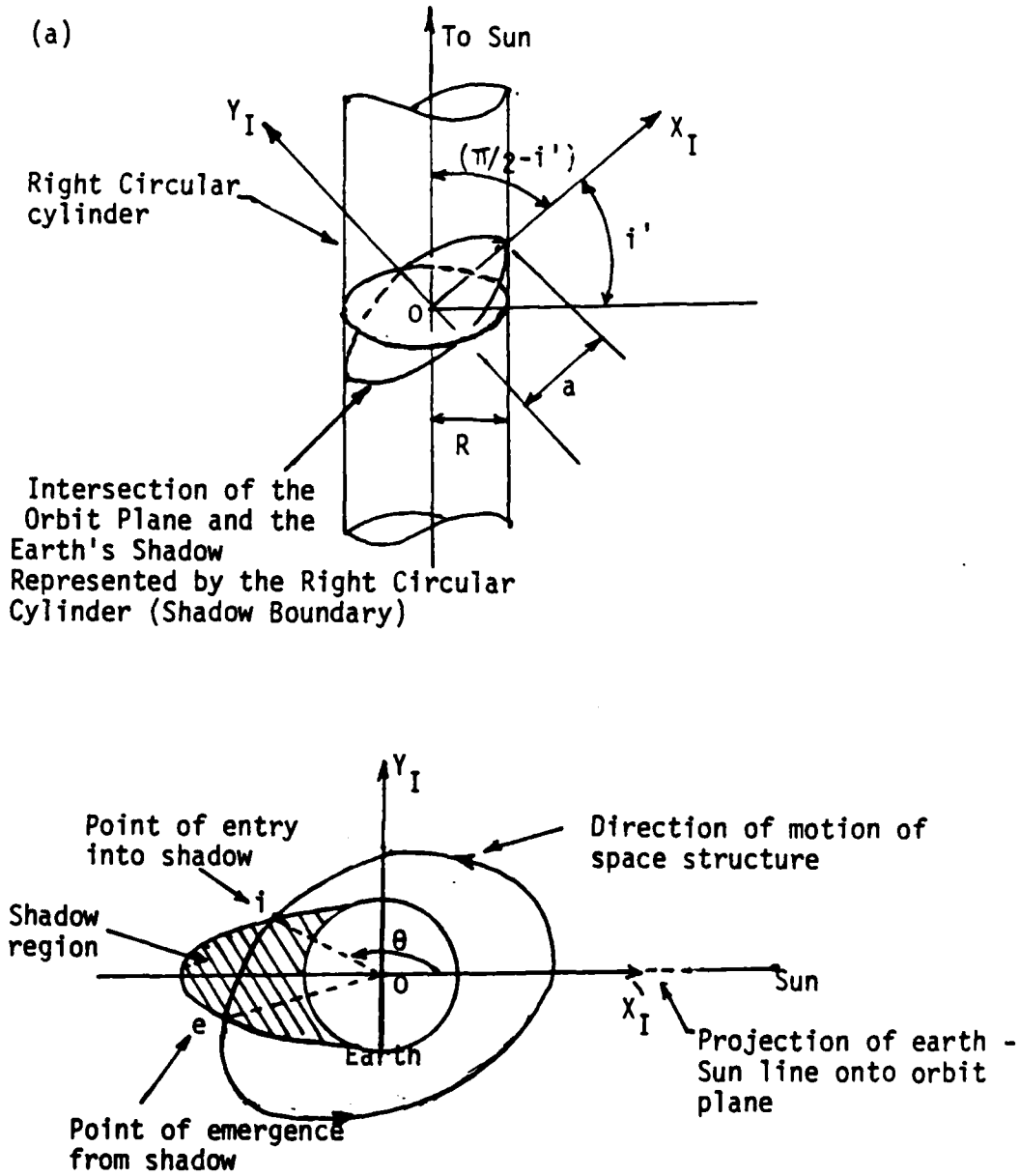

Figure 4. (a) Geometry of Shadow Boundary and (b) Passage of a Space Structure Through the Earth's Shadow

Since $a = R/\mathrm{Cos}\,i'$ (Figure 4b) (2.55)

we have,

$$X_I^2 \mathrm{Cos}^2 i' + Y_I^2 = R^2 \qquad (X_I \leq 0) \qquad (2.56)$$

In polar coordinates x_I and y_I can be represented as

$$\text{(a)} \quad X_I = r_{sb}\mathrm{Cos}\theta$$

$$\text{(b)} \quad Y_I = r_{sb}\mathrm{Sin}\theta \qquad (2.57)$$

Thus, the above Equation (2.56) can be written as

$$r^2_{sb} = \frac{R^2 E}{1 - \mathrm{Cos}^2\theta\ \mathrm{Sin}^2 i'} \qquad \left(\frac{\pi}{2} \leq \theta \leq \frac{3\pi}{2}\right) \qquad (2.58)$$

where r_{sb} is the radial line describing the shadow boundary.

To obtain an analytical solution of the equation except for a circular orbit is next to impossible. Therefore, this equation should be solved numerically in conjuction with the equations of motion (2.14) for every revolution. Hence, in general, to determine angles the θ_i and θ_e, the above equation for r_{sb} is equated with that for r_c of orbit of the structure. As the value for r_c at a certain time t is evaluated numerically, the above Equation (2.58) should also be evaluated with $r_c = r_{sb}$. If this equation is also satisfied, the corresponding value

of θ is θ_i or θ_e. The following conditions are of importance:

(a) If $r_c > r_{sb}$ for all time, then the space structure is in sunlight continuously.

(b) If $r_c = r_{sb}$ and $\pi/2 \leq \theta \leq 3\pi/2$ the structure crosses the shadow boundary.

(c) If $r_c < r_{sb}$ and $\pi/2 \leq \theta \leq 3\pi/2$ the structure lies within the earth's shadow.

(2.59)

The angle i' is required to be computed every few days. The angle i' in Equation (2.58) is found from the equation below [71].

$$\mathrm{Cos}i' = \mathrm{Cos}i_o\mathrm{Sin}\delta_o + \mathrm{Sin}i_o\mathrm{Cos}\delta_o\mathrm{Sin}(\alpha_N - \alpha_o) \qquad (2.60)$$

where i_o is the inclination of the orbit plane to the equator, and α_o and δ_o are the right ascension and declination of the sun respectively, and α_N is the right ascension of the ascending node.

Radiation Pressure Analysis

Ever since the first exhibition of solar radiation perturbation effects upon an earth satellite (the Vanguard I, launched on March 17, 1958), many aspects of solar radiation induced orbital perturbations have been studied [34-41]. In particular, the anomalous behavior of the Echo I balloon satellite received a great deal of attention [35]. Similarly, solar radiation pressure on PAGEOS was found to give rise to spin and precession torques [40] and affect the orbit of the satellite [41]. The effects of solar radiation pressure on a gravity gradient satellite [36] and the Communications Technology Satellite [38] were also investigated. The feasibility of utilizing solar radiation forces for controlled orbital transfer was assessed quite early in the space age. In 1958 Garwin [17] envisioned an exploration of the planetary system by means of large solar sails made of aluminized Mylar. The concept was further substantiated in subsequent studies [18-20, 39]. This effect depends almost exclusively on the distance from the sun. Thus it may be nearly constant within the altitudes of contemporary interest.

Besides direct solar radiation, terrestrial radiation is also important. The earth radiates energy over a wide range of wavelengths and particularly in the infrared and

optical regions of the spectrum. The infra red is largely a re-emission of radiation received from the sun at other wavelengths. This is henceforth referred to as direct radiation from the earth and its atmosphere. On the other hand, the radiation in the optical wavelengths is a reflection, both diffuse and specular, of the incident sunlight. The reflected radiation, measured as a fraction of the incident radiation, is called the albedo. The mechanical pressure exerted on an orbiting body by terrestrial radiations has been recognized long ago for near-earth satellites. The effects of terrestrial radiations exclusively depend on the distance of a space vehicle from the earth. The larger the distance, the lesser will be the effects. A study by Flanagan and Modi [77] revealed that below 6000 miles altitude, the earth-emitted and -reflected radiation pressure effects should be considered although these effects are smaller than that of direct solar radiation. Numerous studies have been done to determine the effects of the terrestrial radiations upon the orbit of a space vehicle [see for example ref. 84 through 88]. All of these studies showed that the terrestrial radiations affected the orbital elements of a satellte. More recently, Zerbini showed that the earth's albedo affected the orbit of PAGEOS I [41].

In addition to orbital perturbations, the radiation pressures can also affect the attitude motion and structural

deformation of a large flexible space structure. In the early nineteen seventies, Modi and Flanagan [89], studied the attitude dynamics of a gravity oriented satellite under the influence of direct solar, direct earth, and earth reflected (albedo) radiation pressures. Their study revealed a relatively small effect from the terrestrial radiations. This may be the reason that research on the attitude dynamics of a space structure has since then been centered around the effect due to direct solar radiation pressure only (for example, see ref. 91 through 95). As far as the effects of radiation pressures on the structural deformation is concered, very little has been understood to date. A study conducted by Krishna and Bainum [90] of uncontrolled and controlled dynamics of a thin flexible beam in orbit in the presence of direct solar radiation disturbances suggests that there can be deformations of space structure due to radiation pressures. For a very large space structure which will most probably have a large area-to-mass ratio, there is no doubt that the effects of radiation pressures are very significant.

Light Pressure

Before proceeding further, a brief account of the fundamentals behind the mechanical action of light exerted on reflecting and absorbing bodies called the "Pressure of Light" will be presented. Maxwell developed the

electromagnetic theory of light in 1872. An experimental verification that light waves exert a pressure was achieved by the Russian physicist P. W. Lebedev in 1899. Theoretically, the pressure of light can be interpreted on the basis of Maxwell's electromagnetic theory of light or from quantum theory. According to either theory, the pressure exerted on a surface by a plane electromagnetic wave which falls on a normally oriented reflecting surface is given by

$$p = S\ (1 + C_r)/v_l \text{ [force/length]} \tag{2.61}$$

where S is the power of the incident electromagnetic wave per unit surface (erg/cm^2-sec), and C_rS is the power of the corresponding reflected wave (erg/cm^2-sec). Here C_r denotes the reflection coefficient, and v_l is the speed of light. In the above expression, the energy consists of the energy of both incident and reflected waves (Figure 5).

In a general case, if a surface is oriented at an angle β_s with respect to the light ray, the radiation pressure is

$$p = [S(1+C_r)/v_l]\ \cos^2\beta_s \tag{2.62}$$

For a celestial body which is at a distance d_i from the

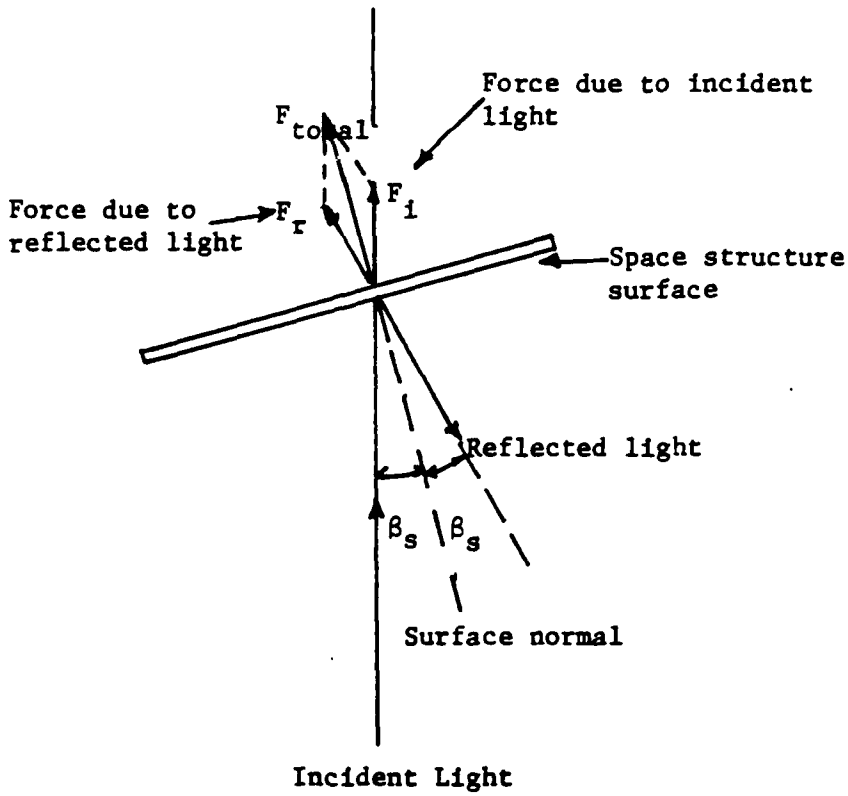

Figure 5. Solar Radiation Pressure on a Surface

sun, the solar constant S for this distance is determined by the formula

$$S = S_o \ (d_o/d_i)^2 \tag{2.63}$$

where d_o is the mean earth-sun distance, and S_o is the " Solar Constant" which is the power of solar radiation which falls on a unit area of earth surface per unit time and has the value

$$S_o = [2.0 + 0.04]\text{cal/cm}^2\text{-min} = 1.35 \times 10^6 \text{ erg/cm}^2\text{-sec}$$

This shows that the light pressure is very small even for such a powerful radiation source as the sun. Substituting Equation (2.63) into Equation (2.62), we finally obtain,

$$p = [S_o(1 + C_r)/v_l][d_o/d]^2 \cos^2\beta_s \tag{2.64}$$

For a space structure orbiting around the earth, $d_i = d_o$ for all practical cases. Therefore, Equation (2.64) reduces to

$$p = [S_o(1 + C_r)/v_l]\cos^2\beta_s \tag{2.65}$$

The acceleration experienced by a body of mass m and effective area A under the action of radiation pressure can be determined by the formula

$$a = p\ A/m \quad [\text{length/time}^2] \tag{2.66}$$

The quantity (A/m) is a parameter called the "area-to-mass" ratio. This quantity is generally constant for each body, and is of decisive importance in estimating the effect of radiation pressure on the motion of space structures.

The gravitational force of the sun and the force due to solar radiation pressure act in opposite directions. If a space structure (for example a gas-inflated balloon of the type "Echo 1") is of spherical shape, then the sun's gravitational force is proportional to the volume, i. e., to a^3, where a is the radius of the sphere, whereas the force due to radiation pressure is proportional to the effective area, i. e., to a^2. The ratio of these forces is proportional to 1/a. So, in the case of a light sphere of sufficiently small size, both forces can balance each other, or the radiation pressure force can exceed the gravitational force of the sun. If the latter case is true, the body will leave the solar system under the effect of radiation pressure. This is precisely the principle behind "Solar Sailing" - employing solar radiation pressure on a space ship to create a small, steady thrust for interplanetary voyage. Motion of this kind would take place along a spiral orbit and a change in the orientation of the sail with respect to the solar radiation from which it acquires its power would permit it move toward and away from the sun

[18].

Forces and Moments due to Radiation

The chief sources of radiation which cause forces and possibly torques on an orbiting space structure are:

1. direct solar radiation,
2. solar radiation reflected by the earth and its atmosphere,
3. direct radiation emitted from the earth and its atmosphere, and
4. radiation emitted by the space structure.

The analysis of the last source requires knowledge of the temperature in the structure, and, in general, it is a much smaller effect compared to the first three cases. However, there are special situations when this effect is also comparable to the other three. For example, the pressure experienced by emission from a "black " flat plate receiving solar radiation (and thus emitting the same amount of radiation) is equal to two-thirds of the pressure due to direct solar radiation [73]. The space structure, in general, does not act as a "black body", and, moreover, it emits radiation in all directions, thus tending to produce no resultant force. Hence, for these reasons, this effect will be neglected in the present analysis.

Radiation pressure on a surface is a function of its

absorptivity (C_a), reflectivity (C_r, specular and C_{rd}, diffuse), and transmissibility (C_t) as well as its position relative to the emitting body. Further, C_a, C_{rs}, C_{rd}, and C_t themselves vary with surface temperatures, the wave length of the incident radiation and the angle of incidence. It is also possible that the surface properties including C_a, C_{rs}, C_{rd}, and C_t of a particular space structure may change with time as a result of external factors. However, such variations are generally small and will be neglected. Some other small effects which will be ignored in this study are: (1) possible variations of the solar constant; (2) the small change in the solar distance; (3) the slight motion of the sun in right ascension and declination; and (4) the Poynting-Robertson effect, which is ascribed to the action of radiation pressure and is conditioned on the nonvanishing velocity of a space structure in a given reference frame and has relativistic background [85, 86].

Let us consider the general case as shown in Figure 6. The incoming radiation of intensity I (parallel to the unit vector $\underline{e}_1$) makes an angle β_i with the normal $\underline{n}$ to the surface element dA which has radiation properties C_a, C_{rs}, C_{rd}, and C_t (Coefficients of absorption, specular reflection, diffuse reflection, and transmission, respectively). The radiation, after striking the surface, is partly absorbed, partly reflected specularly, partly

reflected diffusely, and partly transmitted by the surface. The specularly reflected radiation (parallel to the unit vector $\underline{e}_2$) makes an angle β_r with the surface normal $\underline{n}$. The unit vector $\underline{e}_3$ perpendicular to $\underline{n}$ and coplanar with $\underline{n}$, $\underline{e}_1$, and $\underline{e}_2$ can be defined by the relation [73]

$$\underline{e}_3 = \underline{n} \times (\underline{e}_1 \times \underline{n}) / \mathrm{Sin}\beta_i \tag{2.67}$$

If the surface is assumed to be a specular reflector, geometric optics gives $\beta_i = \beta_r$. Continuity demands that, at the intercepting surface,

$$C_a + C_{rs} + C_{rd} + C_t = 1 \tag{2.68}$$

According to Einstein's electromagnetic mass-energy equivalence relationships, the incoming photons may be considered to have an equivalent mass

$$E_{Ph} = m_{ph} v_l^2 \tag{2.69}$$

where E_{Ph} and m_{ph} represent the energy and mass of radiant energy, and v_l, the speed of light. From this, the photon equivalent momentum $\underline{P}_{Ph}$ may be expressed as

$$\underline{P}_{Ph} = m_{ph} \underline{v}_l = E_{Ph} / \underline{v}_l \tag{2.70}$$

The force developed as a result of photon momentum transfer at a surface is entirely defined by the vector relationship

$$\underline{F} = d\underline{P}_{Ph}/dt \tag{2.71}$$

For an intercepting plate that is arbitrarily oriented, the incident energy is given by

$$E_i = I \cos\beta_i dA \tag{2.72}$$

The power density I is the energy per unit time through a unit area. Thus,

$$d\underline{F}_i = -(I/v_1)\cos\beta_i dA \ \underline{e}_1 \tag{2.73}$$

where $d\underline{F}_i$ is the force due to total incident radiation energy (see Figure 6).

Let us define a fundamental quantity,

$$p_f = I/v_1 \tag{2.74}$$

p_f is the radiation pressure (force per unit area) acting on a nonreflective surface normal to the incoming radiation. Now,

$$d\underline{F}_i = -p_f \cos\beta_i dA \ \underline{e}_1 \tag{2.75}$$

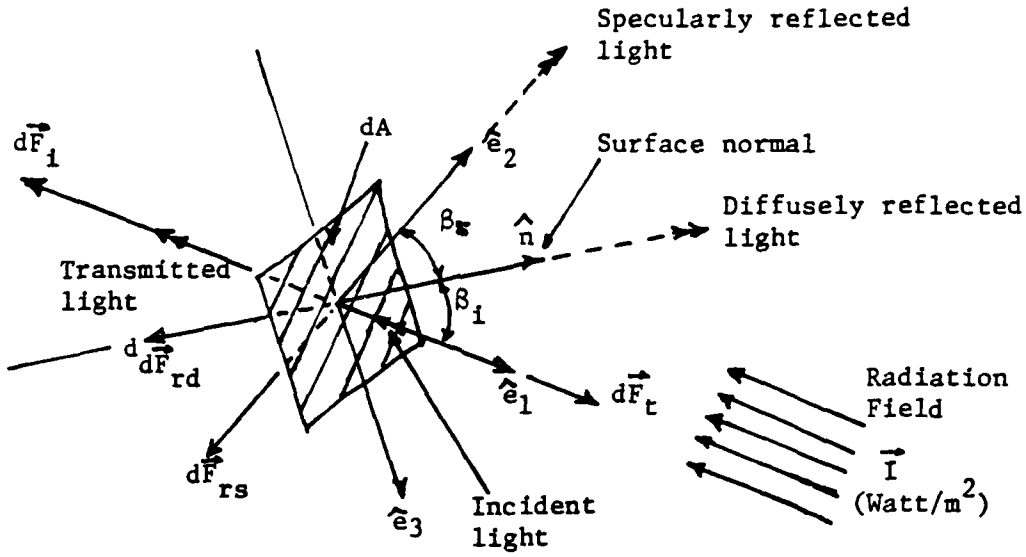

Figure 6. Surface Geometry for Incident, Reflected, and Transmitted Radiation

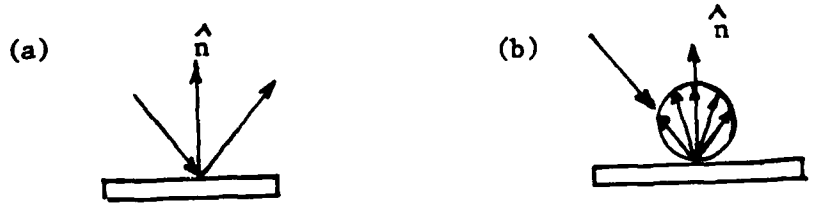

Figure 7. Reflection Geometry (a) Specular and (b) Diffuse

The specularly reflected light produces a force,

$$d\underline{F}_{rs} = -C_{rs}(p_f \mathrm{Cos}\beta_i)dA\ \underline{e}_2 \tag{2.76}$$

The outgoing momentum of diffusely reflected photons may be calculated by integrating over the hemisphere and making use of the symmetry about the normal to the surface. It is apparent that the tangential components of outgoing momentum will be cancelled due to symmetry leaving only the normal components to integrate over the hemisphere (Figure 7b). The result shows that the effective momentum transfer to the surface due to to outgoing diffusely reflected photons is just two-thirds what it would have been if the same number of photons were reflected along the normal [97, 98]. That is,

$$d\underline{F}_{rd} = -(2/3)C_{rd}p_f \mathrm{Cos}\beta_i dA\ \underline{n} \tag{2.77}$$

Lastly, the force produced by the transmitted photons is

$$d\underline{F}_t = C_t p_f \mathrm{Cos}\beta_i dA\ \underline{e}_1 \tag{2.78}$$

The total force on the element of area dA can be obtained by adding Equations (2.75) through (2.78), which is,

$$d\underline{F} = - p_f \mathrm{Cos}\beta_i dA \, [\underline{e}_1 + C_{rs}\underline{e}_2 + (2/3)C_{rd}\underline{n} - C_t\underline{e}_1] \qquad (2.79)$$

Resolving $\underline{e}_1$ and $\underline{e}_2$ in the $\underline{n}$ and $\underline{e}_3$ directions (normal and tangential components), we get

$$\underline{e}_1 = \mathrm{Cos}\beta_i \underline{n} + \mathrm{Sin}\beta_i \underline{e}_3 \qquad (2.80)$$

$$\underline{e}_2 = \mathrm{Cos}\beta_i \underline{n} - \mathrm{Sin}\beta_i \underline{e}_3 \qquad (2.81)$$

Making use of these relations in Equation (2.79)

$$d\underline{F} = -p_f \mathrm{Cos}\beta_i dA \, [\{(1 + C_{rs} - C_t)\mathrm{Cos}\beta_i + (2/3)C_{rd}\}\underline{n} + \{(1 - C_{rs} - C_t)\}\mathrm{Sin}\beta_i \underline{e}_3] \qquad (2.82)$$

Separating into normal and transverse components,

$$d\underline{F}_N = -p_f \mathrm{Cos}\beta_i dA \, [\{(1 + C_{rs} - C_t)\mathrm{Cos}\beta_i + (2/3)C_{rd}\}\underline{n} \qquad (2.83)$$

$$d\underline{F}_T = -p_f \mathrm{Cos}\beta_i dA \, [(1 - C_{rs} - C_t)\mathrm{Sin}\beta_i \underline{e}_3] \qquad (2.84)$$

The force $d\underline{F}_T$ parallel to the surface will act to translate the spacecraft (move sideways) but, in general, will not act to rotate the spacecraft [75]. However, it is not always safe to assume that the radiation force parallel to the spacecraft surfaces does not produce torque - both forces perpendicular to the surface (which often produce torque) and those parallel to the surfaces (which may also

produce torques) should be considered.

Let us now deduce the elemental radiation pressure force expressions for some special surfaces.

1. For a well-insulated surface at equilibrium,

$$C_t = 0 \text{ and } C_a + C_{rs} + C_{rd} = 1 \tag{2.85}$$

Equation (2.82) becomes

$$d\underline{F}_I = -p_f \cos\beta_i dA \, [\{(1 + C_{rs})\cos\beta_i + (2/3)C_{rd}\}\underline{n} + \{(1 - C_{rs})\}\sin\beta_i \underline{e}_3] \tag{2.86}$$

2. For a completely absorbing surface

$$C_a = 1 \text{ and } C_{rs} = C_{rd} = C_t = 0 \tag{2.87}$$

The governing force Equation (2.82) becomes

$$d\underline{F}_A = -p_f \cos\beta_i dA \, [\cos\beta_i \underline{n} + \sin\beta_i \underline{e}_3] \tag{2.88}$$

3. For a perfect mirror (i. e., a completely specular reflecting surface)

$$C_{rs} = 1 \text{ and } C_a = C_{rd} = C_t = 0 \tag{2.89}$$

The radiation force Equation (2.82) reduces to

$$d\underline{F}_{rs} = -p_f \cos^2\beta_i dA \, \underline{n} \tag{2.90}$$

4. For a completely diffuse surface

$$C_{rd} = 1 \text{ and } C_a = C_{rs} = C_t = 0 \tag{2.91}$$

The force on the area dA is given by (Equation (2.82))

$$d\underline{F}_{rd} = -(2/3)p_f \cos\beta_i dA \, \underline{n} \tag{2.92}$$

Metals tend to have $C_{rs} > C_{rd}$ while paints, black as well as white, usually have $C_{rd} > C_{rs}$. In the absence of specific information it has been customary to assume $C_{rs} = 0$ for paints and $C_{rd} = 0$ for metals. The effects of such assumptions upon the torques are not large (typically $\leq$ 20 percent) [75].

The equations of motion of the space structure under the influence of the earth's gravitational force and the forces due to radiation pressure are again given by Equation (2.14). In this case, Q_r, Q_θ, Q_x, and Q_ϕ are forces and moments due to the radiation effects. Q_r is the force along the r_c vector; Q_θ is the moment about the center of the earth (O) axis; Q_x is the force along the length of the structure; and Q_ϕ is the moment about the structure's center of mass (C). These external forces and moments are complicated functions of many parameters pertaining to the sun, earth, and the structure. Clancy and Mitchell [73] derived integral relations to express some of these forces and torques acting on an arbitrarily shaped satellite under the influence of the three sources of radiation mentioned above. On the other hand, Flanagan and Modi [77] derived closed form relations for some of these forces and torques acting on a flat plate shaped space vehicles under the influences of the above radiation pressure disturbances.

However, these expressions for radiation forces and torques are too complicated and also incomplete for the

present analysis. Therefore, a simpler, practically feasible, and complete set of relations to express all the radiation forces and torques required in the present context will be developed below. For this purpose, it will be assumed that the sun lies in the orbit plane, and the earth-sun line is coincident with the X_I axis. Of course, this will give the most severe solar radiation pressure effects. The space structure surface will be considered to be completetly absorbing. Also, as in a thermal effect analysis, the space structure will be considered as a flat rectangular plate and has both dynamic and geometric symmetry.

<u>The direct solar radiation pressure.</u> Consider a space structure represented by a flat plate undergoing a planar librational motion (Figure 8). At present, the sun is in an arbitrary position inclined at an angle i' from the normal to the orbit plane. P is the center of radiation pressure at the structure. The distance from C (c.m. of the structure) to P is l_p. Here l_p is positive along the positive x-axis and r_p is the distance of the center of pressure P from the center of the earth O. r_p is given as below

$$r_p = [r_c^2 + l_p^2 + 2r_c l_p \cos\emptyset]^{1/2} \qquad (2.93)$$

where l_p is given by

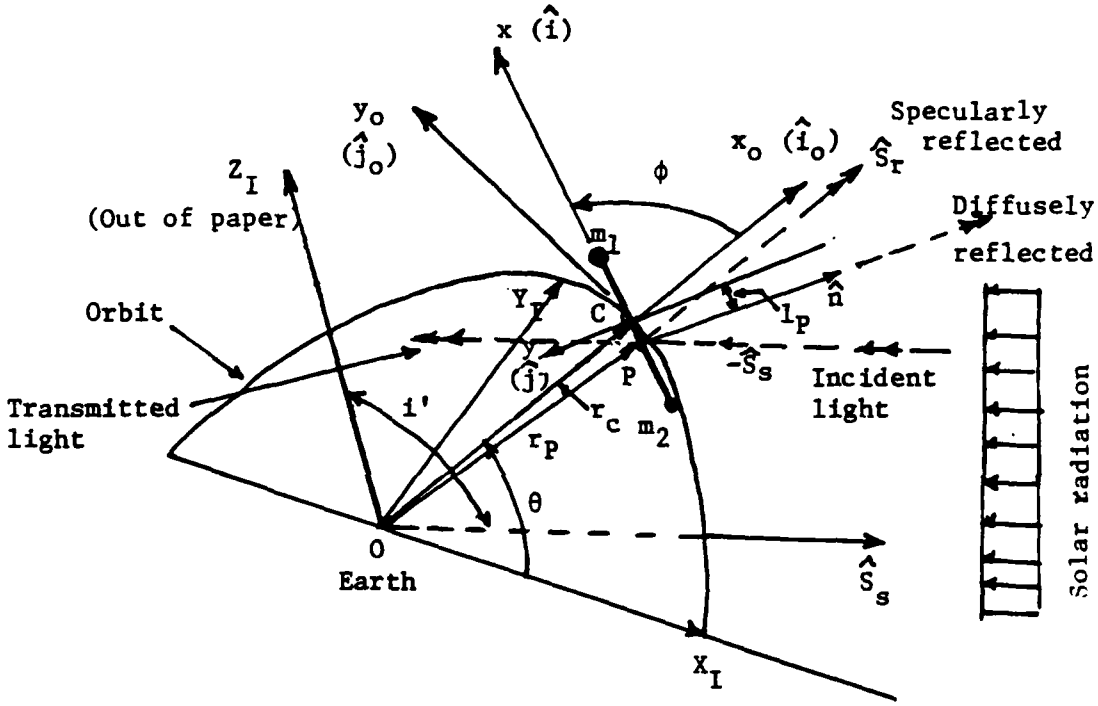

Figure 8. Direct Solar Radiation and Orbital Geometry

$$l_p = x_1 - (x/2) \text{ for } m_1 \geq m_2$$
$$= (x/2) - x_2 \text{ for } m_1 \leq m_2 \tag{2.94}$$

in which, x_1 and x_2 and x are given by Equations (2.3). For a plate structure with uniform rectangular cross section l_p is positive when $m_1 < m_2$, negative when $m_1 > m_2$, and zero when $m_1 = m_2$. Hence,

(a) For $m_1 \geq m_2$

the maximum value of $r_p = r_c - l_p$ at $\emptyset = \pi$; and

the minimum value of $r_p = r_c + l_p$ at $\emptyset = 0$

(b) For $m_1 \leq m_2$

the maximum value of $r_p = r_c + l_p$ at $\emptyset = 0$; and

the minimum value of $r_p = r_c - l_p$ at $\emptyset = \pi$

(2.95)

The force on an element of area dA of the structure due to direct solar radiation, which is taken parallel to the earth-sun line amd constant over the spacecraft's orbit, can be written as (refer to Equation (2.79))

$$d\underline{F}_{ds} = -\delta\, p_{ds} |\cos\beta_s|\, [(1 - C_t)\underline{S}_s + C_{rs}\underline{S}_r + (2/3)C_{rd}\underline{n}]dA \tag{2.96}$$

where δ is 1 in the sunlight side of an orbit and is 0 in the earth's shadow side of an orbit, β_s is the angle of

incidence of the direct solar radiation flux on the plate, and $\underline{S}_s$, $\underline{S}_r$, and $\underline{n}$ are unit vectors along the incident light, reflected light, and surface normal respectively. The positive sign conventions for these unit vectors are as shown in Figure 8. The quantity within | | indicates the absolute value for the corresponding term. p_{ds} is the direct solar radiation pressure (force per unit area) acting on a surface normal to the incoming solar radiation and is given by

$$p_{ds} = S_o/v_1 \tag{2.97}$$

in which S_o is the solar constant. Equation (2.96) agrees with the equivalent equation derived by Wertz [96] when $C_t = 0$, and with the corresponding equation derived by Flanagen and Modi [77] for $C_{rd} = 0$.

Let us now express the direct solar radiation pressure force in body coordinates (x, y, z) and orbital coordinates (x_o, y_o, z_o).

1. In body coordinates, we may write

   (a) $\underline{S}_s = S_1\underline{i} + S_2\underline{j} + S_3\underline{k}$

   (b) $\underline{S}_r = S_{r1}\underline{i} + S_{r2}\underline{j} + S_{r3}\underline{k}$

(2.98)

where,

$\underline{i}$, $\underline{j}$, $\underline{k}$ = unit vectors along x, y, z axes, respectively

S_1, S_2, S_3 = components of $\underline{S}_s$ along x, y, z, axes, respectively

S_{r1}, S_{r2}, S_{r3} = components of $\underline{S}_r$ along x, y, z axes, respectively

Substituting for S_s and S_r from Equation (2.98) into Equation (2.96) and noting that $\underline{n} = -\underline{i}$, the total direct solar radiation pressure force on the flat plate can be written as:

$$\underline{F}_{ds} = -\delta\, p_{ds} |\cos\beta_s| A_{sd} [\{(1 - C_t)S_1 + C_{rs}S_{r1}\}\underline{i} + \{(1 - C_t)S_2 + C_{rs}S_{r2} - (2/3)C_{rd}\}\underline{j} + \{(1 - C_t)S_3 + C_{rs}S_{r3}\}\underline{k}] \tag{2.99}$$

where A_{sd} is the area of the plate effective for solar radiation (here, one side of the plate).

2. Similarly, in orbital coordinates, we can write

(a) $\underline{S}_s = S_{o1}\underline{i}_o + S_{o2}\underline{j}_o + S_{o3}\underline{k}_o$

(b) $\underline{S}_r = S_{ro1}\underline{i}_o + S_{ro2}\underline{j}_o + S_{ro3}\underline{k}_o$

(2.100)

where,

$\underline{i}_o$, $\underline{j}_o$, $\underline{k}_o$ = unit vectors along x_o, y_o, z_o, respectively

S_{o1}, S_{o2}, S_{o3} = components of $\underline{S}_s$ along x_o, y_o, z_o axes, respectively

S_{ro1}, S_{ro2}, S_{ro3} = components of $\underline{S}_r$ along x_o, y_o, z_o axes, respectively

The total direct solar radiation pressure force on the space structure in orbital coordinates can now be obtained by substituting Equations (2.100) into Equation (2.96), which is given below:

$$\underline{F}_{ds} = -\delta\, p_{ds} |\cos\beta_s| A_{sd} [\{(1 - C_t)S_{o1} + C_{rs}S_{ro1}\}\underline{i}o + \{(1 - C_t)S_{o2} + C_{rs}S_{ro2}\}\underline{j}o + \{(1 - C_t)S_{o3} + C_{rs}S_{ro3}\}\underline{k}o + (2/3)C_{rd}\underline{n}] \qquad (2.101)$$

Geometric considerations give (Appendix B)

(a) $S_1 = \cos(\theta + \emptyset)\sin i'$

(b) $S_2 = -\sin i' \sin(\theta + \emptyset)$

(c) $S_3 = -\cos i'$

(2.102)

(a) $S_{r1} = -S_1$

(b) $S_{r2} = S_2$

(c) $S_{r3} = -S_3$

(2.103)

(a) $S_{o1} = \cos\theta \sin i'$

(b) $S_{o2} = -\sin\theta \sin i'$

(c) $S_{o3} = -\mathrm{Cos}i'$

(2.104)

(a) $S_{ro1} = -(S_1\mathrm{Cos}\emptyset + S_2\mathrm{Sin}\emptyset)$

(b) $S_{ro2} = -S_1\mathrm{Sin}\emptyset + S_2\mathrm{Cos}\emptyset$

(c) $S_{ro3} = -S_3$

(2.105)

Also, it can be easily seen that

$$\mathrm{Cos}\beta_s = \mathrm{Sin}i'\mathrm{Sin}(\theta + \emptyset) \qquad (2.106)$$

Now, let us impose the assumptions that the sun lies along the X_I axis and that the surface is completely absorbing which requires that the resultant force be along the direction of the earth-sun (or structure-sun) line. With these assumptions, we can write

(a) $i' = \pi/2$

(b) $C_a = 1$

(c) $C_{rs} = C_{rd} = C_t = 0$

(2.107)

and then,

$$\mathrm{Cos}\beta_s = \mathrm{Sin}(\theta + \emptyset) \qquad (2.108)$$

In such case, the total forces on the space structure due to

direct solar radiation can be directly obtained from Equations (2.99) in the body coordinates and from (2.101) in the orbital coordinates as below:

$$\underline{F}_{ds} = -\delta\ p_{ds}|\mathrm{Cos}\beta_s|A_{sd}(S_1\underline{i} + S_2\underline{j}) \tag{2.109}$$

in body coordinates and

$$\underline{F}_{ds} = -\delta\ p_{ds}|\mathrm{Cos}\beta_s|A_{sd}(S_{o1}\underline{i}o + S_{o2}\underline{j}o) \tag{2.110}$$

in orbital coordinates.

The direct solar radiation force along the r_c-vector can be obtained from Equation (2.110) as

$$(Q_r)_{ds} = -\delta\ p_{ds}|\mathrm{Cos}\beta_s|A_{sd}S_{o1} \tag{2.111}$$

where S_{o1} is given by Equation (104a) which is now

$$S_{o1} = \mathrm{Cos}\theta \tag{2.112}$$

Taking the anticlockwise moment to be positive, the moment about point O (center of the earth) is (see Figure 9)

$$(Q_\theta)_{ds} = l_{ds}F_{ds} \tag{2.113}$$

where

$$l_{ds} = r_c\mathrm{Sin}\theta + l_p\mathrm{Sin}\eta \tag{2.114}$$

$$\eta = \theta + \emptyset \tag{2.115}$$

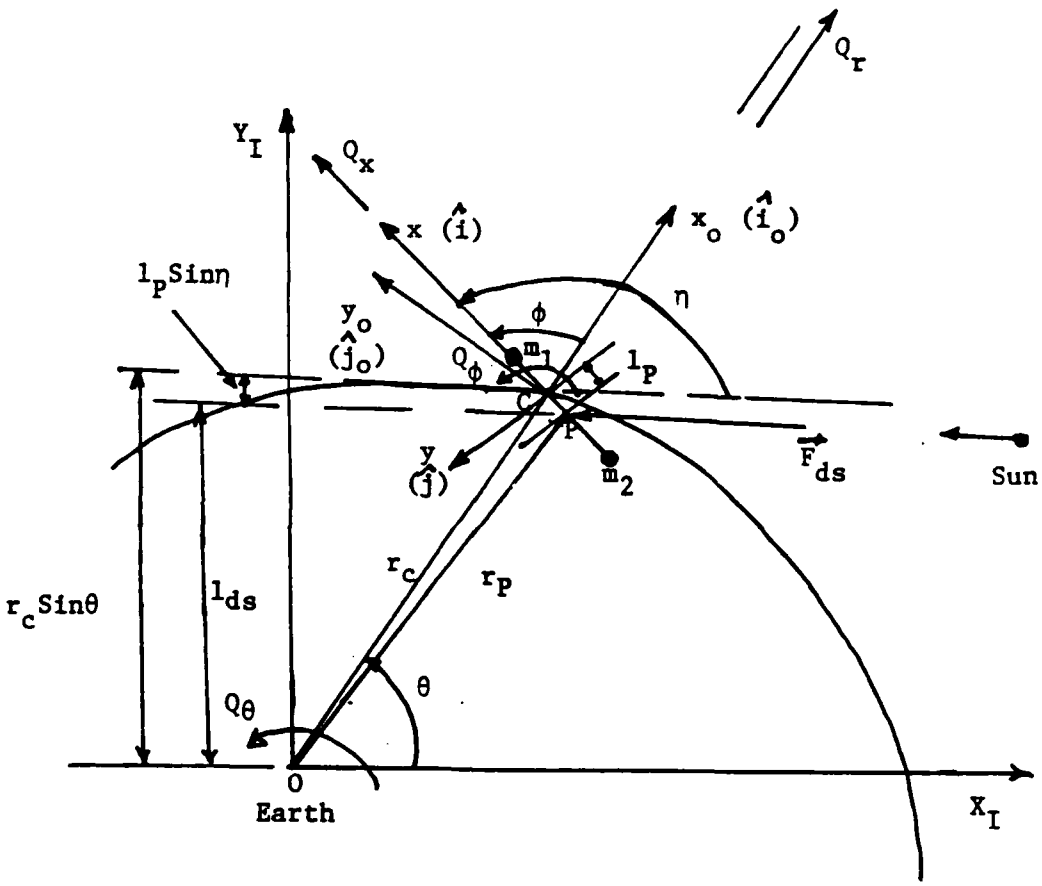

Figure 9. Direct Solar Radiation Forces and Moments

l_p can be positive or negative and is given by Equation (2.94). From Equation (2.109), magnitude of F_{ds} is:

$$F_{ds} = \delta\ p_{ds} |\cos\beta_s| A_{sd} (S_1^2 + S_2^2) \qquad (2.116)$$

in which, from Equations (2.102a and b)

$$\text{(a)}\ S_1 = \cos(\theta + \emptyset)$$
$$\text{(b)}\ S_2 = -\sin(\theta + \emptyset)$$
$$(2.117)$$

The direct solar radiation force along the length of the structure can be deduced from Equation (2.109)

$$(Q_x)_{ds} = -\delta\ p_{ds} |\cos\beta_s| A_{sd} S_1 \qquad (2.118)$$

Lastly, the moment due to the direct solar radiation pressure about the point C (c. m. of the structure) is given by (see Figure 9)

$$(Q_\emptyset)_{ds} = \delta\ p_{ds} |\cos\beta_s| A_{sd} S_2 l_p \qquad (2.119)$$

The numerical value of the direct radiation force intensity can be taken to be $p_{ds} = 4.66 \times 10^{-06}$ Newton/meter [75].

The terrestrial radiation pressure. As we have already mentioned, terrestrial radiations are of two kinds - one, radiation emitted directly from the earth and its atmosphere and two, solar radiation reflected from the earth and its atmosphere (albedo). The disturbing effects of direct solar radiation are well known and understood, but comparatively little attention has been given to the indirect effects of radiation re-emitted or reflected from the earth. This lack of attention is probably due, partly, to the fact that all estimates of the latter effects suggest that its magnitude is considerably smaller than that of direct solar radiation, and partly, due to the fact that the problem is much more difficult mathematically.

Earlier investigations by Wyatt [84], Shapiro [85], Sehnal [86], and Prior [88] give the maximum estimated perturbations of orbital motion due to the terrestrial (direct earth and its albedo) radiation as to be 25 percent of the direct solar radiation pressure. The effect from terrestrial radiation pressure on the attitude motion is reported by Modi and Flanagan [89] to be relatively small compared to the direct solar radiation pressure. In the present study, we intend to investigate the effects of radiation pressure on the axial deformation of the structure. Since the space structure is usually very light, flexible, and may have very large area to mass ratio, we have included the terrestrial radiation pressure

effects in our investigation.

Instead of going into unnecessary detail, we intend to investigate the terrestrial radiation pressure effects for a specific orientation of the space structure which will give us the maximum effects. Levin [76] examined the relative contribution of reflected radiation from the earth and received by a spherical satellite. He found that the principal component of the reflected radiation on a spherical satellite is in the radial direction and that this component diminishes to approximately 10 percent of the magnitude of the direct radiation at an altitude approximately equal to the earth's radius. Components other than in the radial direction generally may be neglected. Therefore, the configuration where the space structure remains perpendicular to the radial vector r_c, that is, $\emptyset = \pi/2$ (which gives the maximum radial component) has been selected for the analysis. In addition to the assumptions made before, it is assumed that the reflectivities of the structure's surface for solar radiation, both direct and reflected, and the earth's radiation are taken to be the same. In the real situation, there arises a difference in the values of the reflectivities because the earth radiates in a longer wavelength region than that of the sun. As in the thermal effect analysis, the solar radiation reflected by, and the radiation emitted directly from, the earth and its

atmosphere can be represented by reflection and emission from a sphere of radius R.

In such a situation, the terrestrial radiation pressure correspond to forces and moments on the space structure which can be expressed as below (Figure 10):

1. For earth's albedo radiation, we can write the following relations

   (a) The total radiation force, using the inverse square law is:

$$\underline{F}_{alb} = \delta\, p_{alb} (R/r_c)^2 A_{sd} \cos\beta\ \underline{i}_o$$

$$\text{with } \cos\beta = 0 \text{ if } \cos\beta < 0 \qquad (2.120)$$

   where β is the angle between the earth-sun line and the earth-orbiting body line line (Figure 3a), and p_{alb} is the magnitude of the earth's albedo radiation pressure at the surface of the earth with $\beta = 0$ and $\emptyset = \pi/2$. According to Flanagan and Modi [77], $p_{alb} = 1.20658 \times 10^{-06}$ N/m² and from Equation (2.37c) with $i' = \pi/2$,

$$\cos\beta = \cos\theta \qquad (2.121)$$

   (b) The force in the radial direction (normal) is the same as given by Equation (2.120):

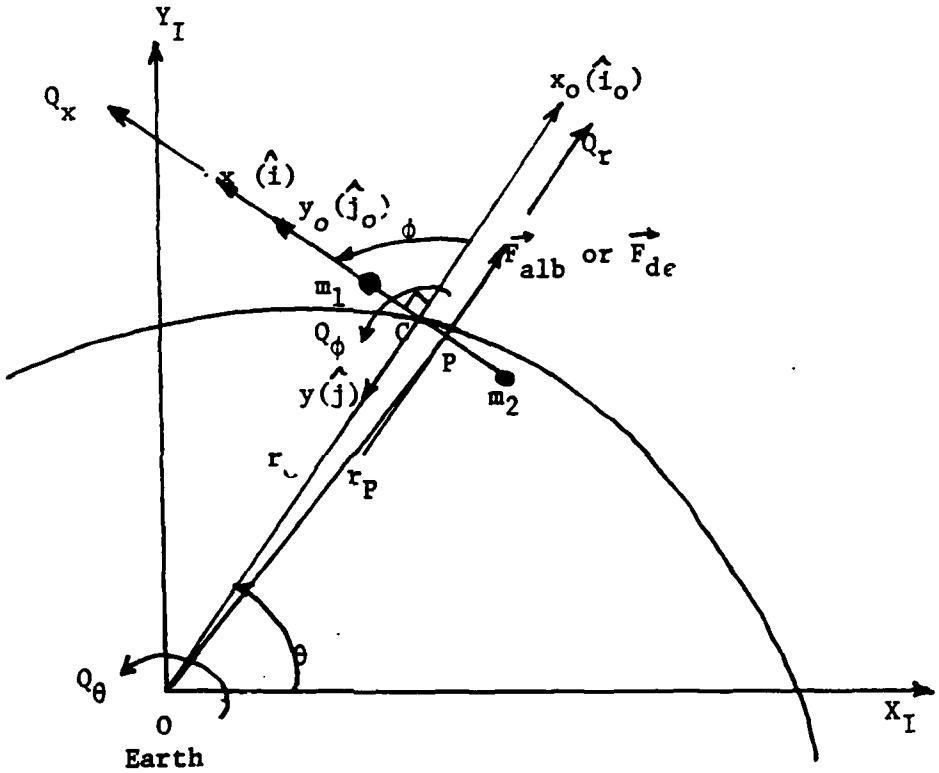

Figure 10. Terrestrial Radiation Forces and Moments

$$(Q_r)_{alb} = \delta\, p_{alb}(R/r_c)^2 A_{sd}\cos\beta$$

with $\cos\beta = 0$ when $\cos\beta < 0$ (2.122)

(c) The moment about point O is (see Figure 10):

$$(Q_\theta)_{alb} = -\delta l_p (Q_r)_{alb} \quad (2.123)$$

(d) The force along the structure is:

$$(Q_x)_{alb} = 0, \quad (2.124)$$

and

(e) The moment about point C (c. m. of the structure) is (Figure 10):

$$(Q_\phi)_{alb} = -l_p (Q_r)_{alb} \quad (2.125)$$

2. For direct earth radiation, we can write the following:

(a) The total force, using the inverse square law, is given by

$$\underline{F}_{de} = p_{de}(R/r_c)^2 A_{sd}\underline{i}_o \quad (2.126)$$

where p_{de} is the magnitude of the direct earth radiation pressure for the structure at the earth's surface when $\phi = \pi/2$. According to Flanagan and Modi [77], $P_{de} = 4.9795\times10^{-7}$ N/m^2

(b) The force in the radial direction is the same as given by Equation (2.126)

$$(Q_r)_{de} = p_{de}(R/r_c)^2 A_{sd} \quad (2.127)$$

(c) The moment about the point O (center of the earth) is:

$$(Q_\theta)_{de} = -l_p (Q_r)_{de} \quad (2.128)$$

(d) The transverse force is:

$$(Q_x)_{de} = 0, \tag{2.129}$$

and

(e) The moment due to the direct earth radiation pressure about the point C (c. m. of the structure) is (Figure 10):

$$(Q_\emptyset)_{de} = -l_p(Q_r)_{de} \tag{2.130}$$

In all the above expressions l_p is given by Equation (2.94).

<u>Total radiation pressure forces and moments.</u> Total forces and moments due to all three sources of radiation are now obtained by summing up the individual corresponding terms derived above. They are:

(a) The total radiation force in the radial direction:

$$Q_r = (Q_r)_{ds} + (Q_r)_{alb} + (Q_r)_{de} \tag{2.131}$$

$(Q_r)_{ds}$, $(Q_r)_{alb}$, and $(Q_r)_{de}$ are given by Equations (2.111), (2.122), and (2.127), respectively.

(b) The total moment due to the radiation pressure about the center of the earth (O):

$$Q_\theta = (Q_\theta)_{ds} + (Q_\theta)_{alb} + (Q_\theta)_{de} \tag{2.132}$$

$(Q_\theta)_{ds}$, $(Q_\theta)_{alb}$, and $(Q_\theta)_{de}$ are given by Equations (2.113), (2.123), and (2.128), respectively.

(c) The total r diation force along the longitudinal

direction of the structure:

$$Q_x = (Q_x)_{ds} + (Q_x)_{alb} + (Q_x)_{de} \tag{2.133}$$

$(Q_x)_{ds}$, $(Q_x)_{alb}$, and $(Q_x)_{de}$ are given by Equations (2.118), (2.124), and (2.129), respectively.

(d) The total moment due to the radiation pressure about the center of mass of the structure (C):

$$Q_\emptyset = (Q_\emptyset)_{ds} + (Q_\emptyset)_{alb} + (Q_\emptyset)_{de} \tag{2.134}$$

$(Q_\emptyset)_{ds}$, $(Q_\emptyset)_{alb}$, and $(Q_\emptyset)_{de}$ are given by Equations (2.119), (2.125), and (2.130), respectively.

The strain energy term (dU_e/dx) is as derived in the differential gravitational force effect analysis and is given by Equation (2.16). The equations of motion are now given by Equations (2.14) with the above expressions (Equations (2.131 through 2.134) for the radiation forces and moments to be used as forcing functions.

CHAPTER III

GENERAL APPROACH TO SOLUTION

The analyses reported here of the motion of a large axially flexible dumbbell-shaped space structure executing a planar motion in a general orbit under various external disturbances in space, including differential gravitational forces, radiation thermal and radiation pressure forces, has led the writer to the development of four non-linear, coupled, differential equations of motion and one equation which gives the temperature variation of the structure in an orbit as a function of time. An analytical solution of the equations is not possible. The equations therefore are solved by a numerical integration method. The purpose of this section is to indicate the selection of a physical model and essential system parameters and an outline of the numerical method to obtain a solution of the complete equations of motion.

System Parameters and Initial Conditions

Selection of Physical Model and System Parameters

One of the strong candidates for the preliminary

design and deployment of a space structure is an open truss-like configuration. We have therefore selected a tetrahedral truss configuration (Figure 11) for the numerical analysis. The space structure is a dumbbell-shaped system. The mass of the truss may be considered negligible compared to the total mass of the system in the case of a relatively massive system. Otherwise, the mass of the truss may be considered to be lumped at the two ends of the structure. Although for a refined design, thermal and dynamic analyses should be done for every member of the truss structure, here we intend to study only overall response of the structure. Therefore, the truss-like structure linking the two masses m_1 and m_2 is viewed as a continuous plate-like model. The equivalent dynamic mechanical and thermal properties of the truss system [65, 66] are determined in Appendix C and are tabulated in Table 1 along with other general parameters.

To have a better understanding of the impact of changing the values of the physical parameters on the structure, the analysis is done with different values of certain more relevant parameters such as mass and length. To give a more practical significance of the result which will be obtained from the present study, all the system parameters are selected within today's practical range.

The tetrahedral truss-like space structure is

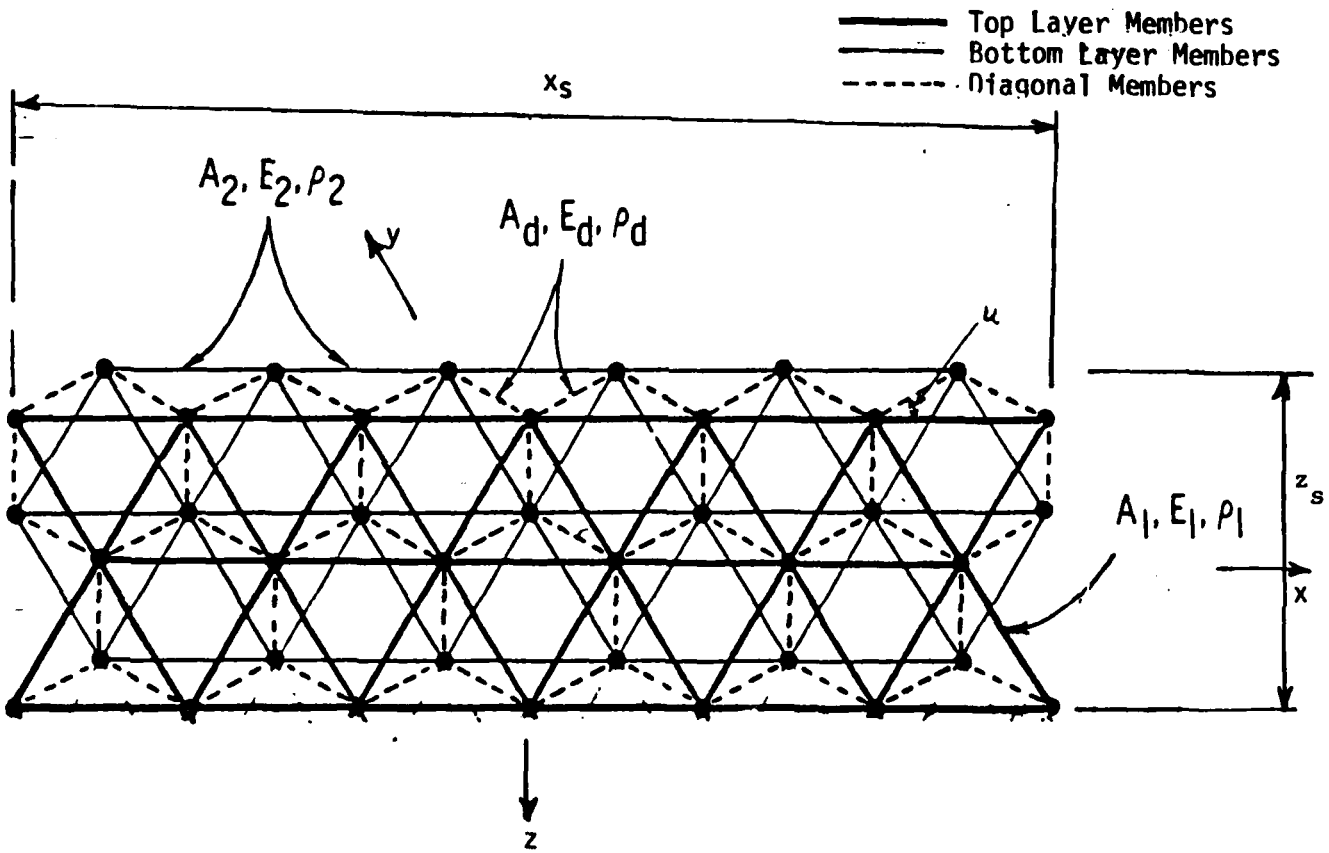

Figure 11. Tetrahedral Truss Configuration

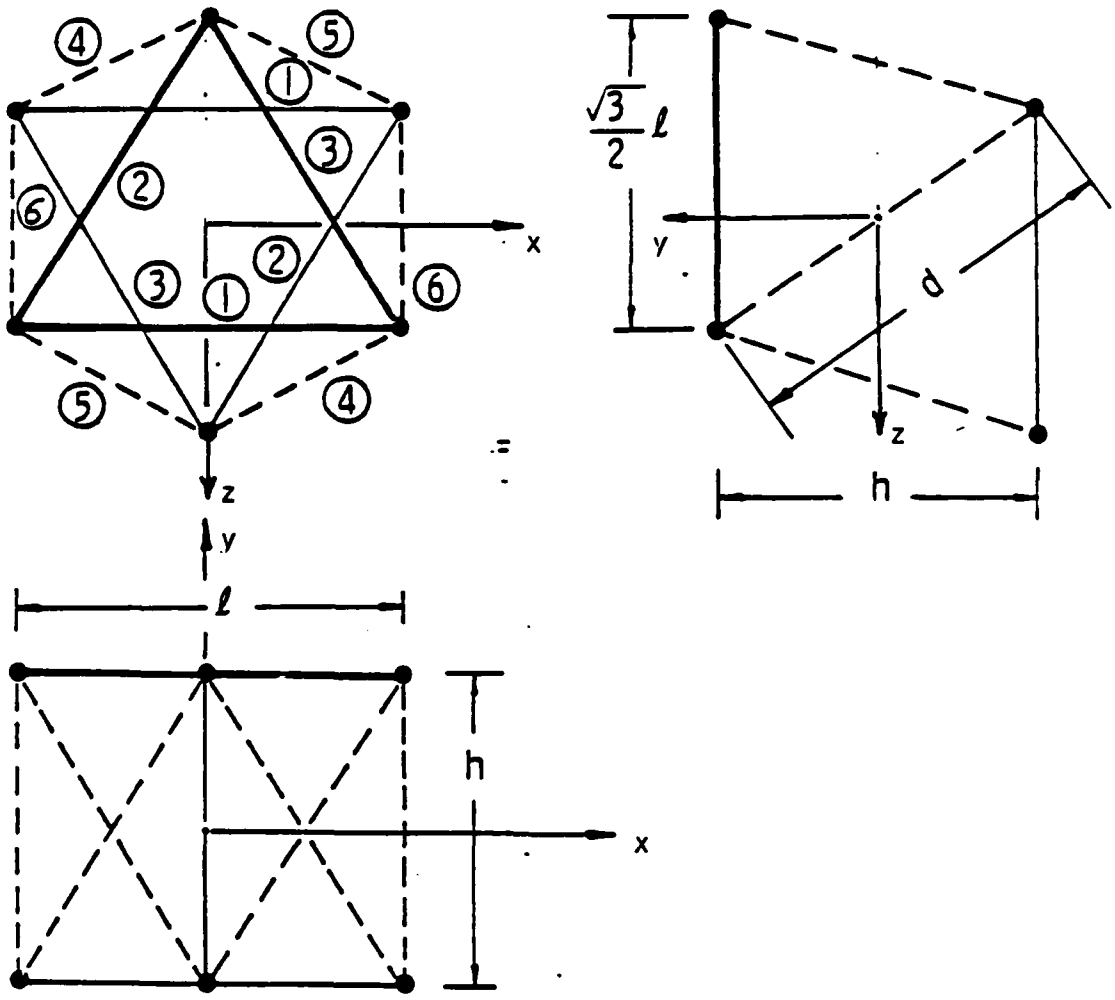

Figure 12. Repeating Element of Tetrahedral Truss

Table 1. Constant Parameter values Used in Numerical Examples

(Refer Appendix C for detail.)

Solar and Terrestrial Constants

$G = 8.64432 \times 10^{-16}$ km^4/N-min^4 (6.670×10^{-8} dyne cm^2/gm^2)
$g = 35.316$ km/min^2
$R = 6374.33$ km
$E_e = 237.0 \times 10^6$ watt/km^2
$A_r = 0.3$
$P_{de} = 0.49795$ N/km^2
$P_{alb} = 1.20658$ N/km^2
$G_s = 1.353 \times 10^9$ watt/km^2
$P_{ds} = 4.66$ N/km^2

Space Structure

Material : Aluminum
Geometric Configuration : Tetrahedral truss
Cross-section : rectangular
Member size : 1.13 cm diameter bars
$h = 4.899 \times 10^{-3}$ km
$z_s = 0.05\ x_s$ km
$A_{cs} = (2.4495 \times 10^{-4})\ x_s$ km^2
$E = 6.689496 \times 10^{10}$ N/km^2
$M = 6658.7678$ (N-min^2)/km (24 metric tons)
$A_{sd}/A_{sf} = 0.5$
$E_\alpha = 24.34976 \times 10^6$ N/km^2-°k
$a_s = 1.0$ $a_e = 1.0$ $a_r = 1.0$ $\epsilon = 1.0$
$\sigma = 5.67 \times 10^{-2}$ watt/km^2-°k^4
$c = 52.75368$ watt-km/N-min-°k (879.228 joule/kg °c)

Completely absorbing surface:
$C_a = 1$, $C_{rs} = C_{rd} = C_t = 0$

considered to be made of a number of identical aluminum bars of approximately 1.13cm diameter. In a particular layer, these bars are spaced 6m from each other. The height of the truss structure is determined to be 4.899m (Appendix C). The truss is assumed to be rectangular in cross-section. The width of the truss is 0.05 times the length of the structure. The total mass of the system is chosen to be 3600 metric tons at first and later 36 metric tons. The formal value of m is selected to satisfy the equilibrium state at t = 0 (Appendix D). This is a rather massive system. The later value of m is selected to be just 1.5 times that of the mass of the truss. The mass of the truss structure alone is about 24 metric tons. The static length of the structure selected varies from 0.5 km to 5 km. An outline is presented in Appendix C to determine the mass (M) and areas (A_{sd} and A_{sf}) of the truss effective in receiving radiation flux.

Selection of Initial Conditions

In order to solve the four second order differential equations of motion (2.14), we need to specify eight initial conditions: r_0, θ_0, x_0, ϕ_0, $\dot{r}_0$, $\dot{\theta}_0$, $\dot{x}_0$, and $\dot{\phi}_0$, where the subscript indicates the values of a variable at the beginning of the motion of the structure in an orbit at t = 0. In addition to these eight

initial conditions, we require one more initial condition, T_0 for thermal analysis in order to determine the temperature variation of the structure in an orbit. Table 2 gives the values for these initial conditions used in the analysis to investigate the effects on the space structure due to the differential gravitational forces, radiation heating, and radiation pressure forces. Together with the initial conditions, this table also lists the values used for various system parameters which appear in the equations; and some of which are changed occasionally to study their effects on the structure.

In general, any set of values may be assigned to the initial conditions. However, to be able to judge the validity of the results in practice and to draw a useful conclusion from the results, it is necessary to limit ourselves to certain more relevant sets of initial conditions. Selection of each initial value is noted below:

Selection of altitudes. Two values of r_0 are selected 6574.33 km (altitude of 200 km from the surface of the earth) and 42274.33 km (altitude of 35900 km). These altitudes represent low earth orbit (LEO) and Geosynchronous orbit (GEO), respectively. It is very desirable to investigate the effects of the external factors on the space structure at different altitudes. In particular, in studying radiation thermal and pressure effects, we should have a knowledge of the

relative magnitude of the effects due to direct solar, direct earth and earth's albedo on the space structure as a function of altitude. A space structure orbiting at a higher altitude spends more time inside the earth's shadow. Therefore, the effects of the earth's shadow can be critical at higher altitudes.

Selection of orbits. Two type of orbits, one circular and another elliptical, are selected for the analysis. The value of $\dot{\theta}_0$ determines the amount of ellipticity in the orbit. The greater the value of $\dot{\theta}_0$, the larger will be the ellipticity. In space, structures may be deployed mainly in circular or elliptical orbits depending on the functional requirements and purpose of the missions. In the present analysis, there are two good reasons for selecting an elliptical orbit. One, contributions of various sources can be compared at different altitudes in the same orbit. This eliminates the need of considering many circular orbits corresponding to different altitudes. Two, the amount of time a space structure spends in the earth's shadow is critical for radiation thermal and pressure analyses. In an elliptical orbit with its major axis along the earth-sun line, the structure spends more time in the earth's shadow than in the circular orbit at the same altitude.

Selection of initial length. In the first set of initial conditions, the value of the initial length x_0 and

AD-A172 880 PARAMETRIC INVESTIGATION OF FACTORS INFLUENCING THE MECHANICAL BEHAVIOR O..(U) MASSACHUSETTS UNIV AMHERST DEPT OF CIVIL ENGINEERING W A NASH ET AL. 30 MAY 86 2/3

UNCLASSIFIED AFOSR-TR-86-0858 AFOSR-83-0025 F/G 22/2 NL

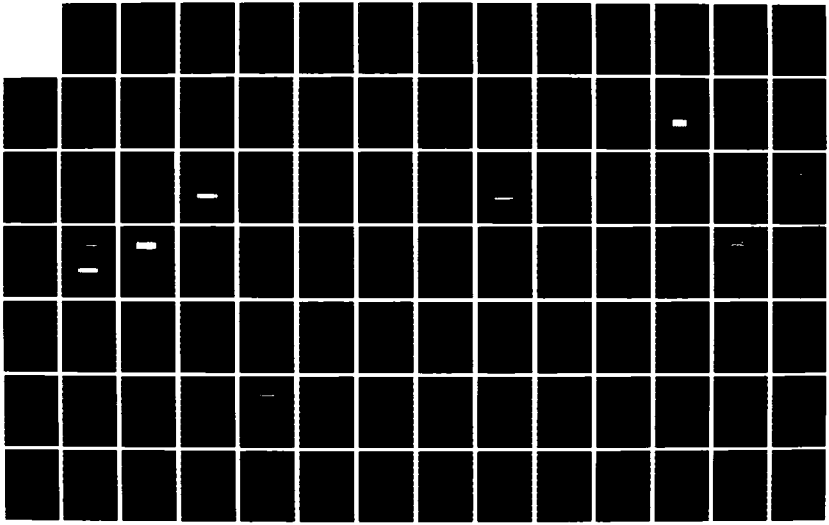

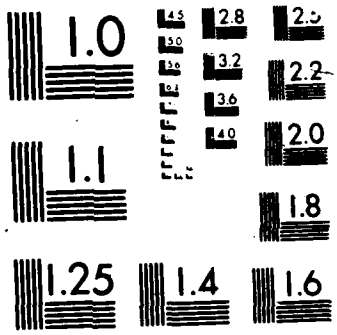
1.0
2.8
3.2
3.6
4.0
2.2
2.0
1.1
1.8
1.25
1.4
1.6

initial angular velocity $\dot{\theta}_0$ are determined from the equilibrium state of the space structure in a circular orbit (Appendix D) with r_0 = 6574.33 km, $\theta_0 = 0$, $\phi_0 = 0$, $\dot{r}_0 = \dot{x}_0 = \dot{\phi}_0 = 0$ and $x_s = 1$ km. In order to study the effects of the initial axial deformation on the response of the structure, other values of x_0 selected are $1.01x_s$, $1.05x_s$ and $0.95x_s$.

Selection of initial attitude angle. Three values of ϕ_0 are chosen - 0 radians, 0.1 radians (small initial misalignment), or $\pi/2$ radians (large initial misalignment) depending on the libration desired.

Initial conditions on rest of the orbital and body parameters. Since for all cases the structure is considered to begin its motion at perigee, the value of $\dot{r}_0$ is zero. The direction of perigee defines the x_I-axis, and θ is measured from this axis. Therefore , the value of θ_0 is also zero. Other initial conditions $\dot{x}_0$ and $\dot{\phi}_0$ are set equal to zero for all cases.

Selection of initial temperature. For thermal analysis, the reference temperature T_s of the space structure is taken to be room temperature (290°K). The structure is assumed to have this temperature when in the stress-free condition. Also, it is considered that the space structure begins travelling in an orbit with this temperature initially. Hence, we take a $T_0 = T_s = 290$ °K for all cases.

For radiation pressure effects, there is no need to consider additional initial conditions.

Special Cases (Orientations)

In a general case, the effects of various external factors can be seen in the space structure's orbit, attitude motion and structural deformation simultaneously. Besides the general case, it is of great importance to investigate the effects of the external space disturbances on the structure oriented in a specific direction. To facilitate the purpose of various mission requirements, the space vehicle may be operated in a particular orientation by means of control and guidance mechanisms. We study four different orientations which are considered to be most significant in the present context. These are given below:

Special Case 1 ($\theta + \phi = \pi/2$). The normal to the space structure is kept parallel to the earth-sun line for all values of time, i.e., the space structure is always at a right angle to the earth-sun vector (Figure 13(a)). In such case, the space structure experiences the greatest impact from direct solar radiation. From the functional point of view, such a mission may be desirable to obtain maximum solar power.

Special Case 2 ($\phi = \pi/2$). In this case, the normal to the space structure is kept parallel to the

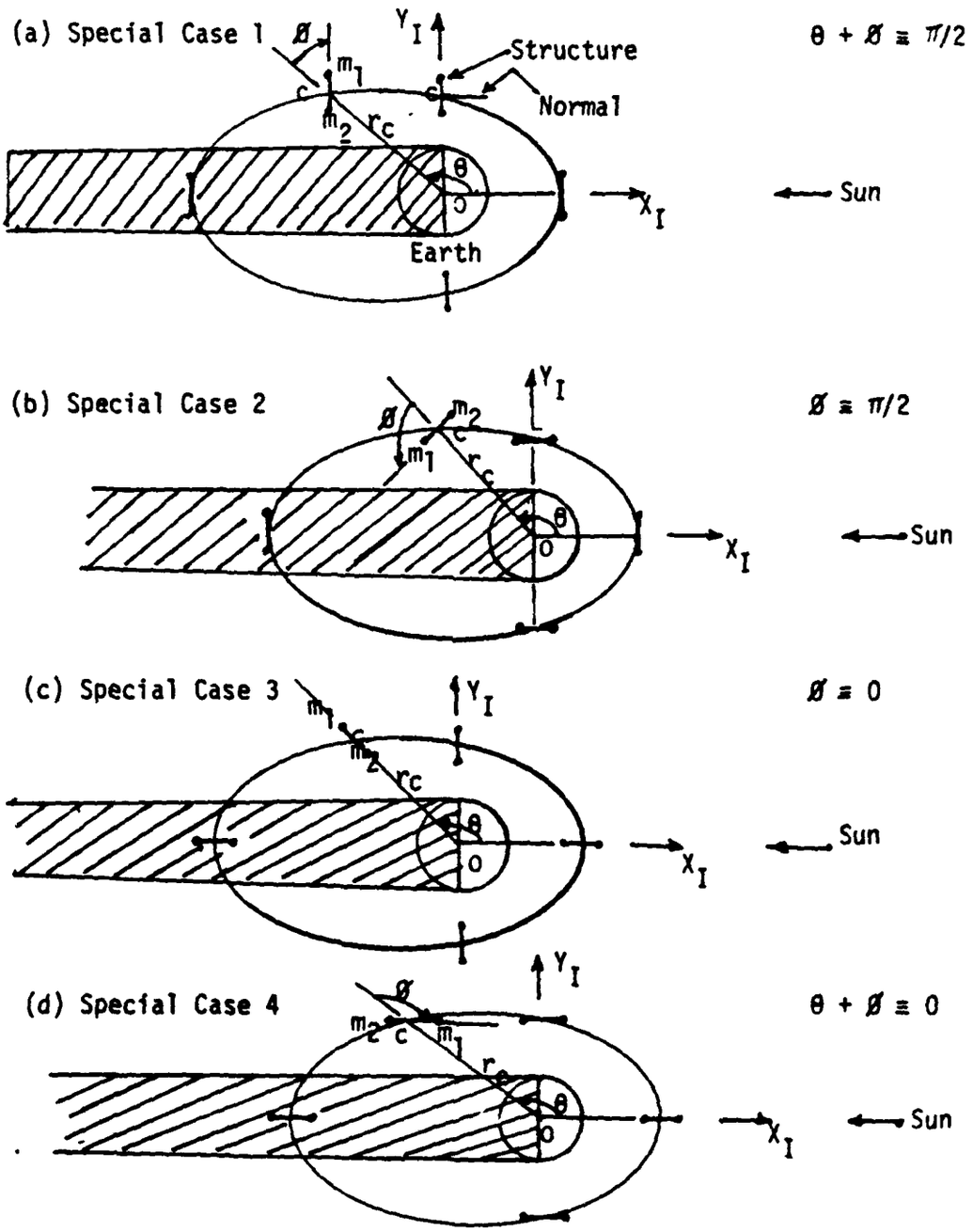

Figure 13. Some Controlled Orientations of a Space Structure

earth-structure line for all values of time, i.e., the space structure is at a right angle to the radial (r_c) vector (Figure 13(b)). In this orientation, the space structure experiences maximum effects due to direct earth emitted radiation and the earth's albedo. Such orientation of a space vehicle may be desirable to obtain the largest area of the structure exposed to the earth for various functional requirements.

Special Case 3 ($\phi = 0$). Here, the normal to the structure is at a right angle to the earth-structure line at any instance, i.e., the structure is aligned along the radial (r_c) vector for all values of time (Figure 13(c)). The space structure in an such orientation experiences the least effects from the direct earth and the earth's albedo radiation. Moreover, since the two point masses at the ends of the structure are farthest apart with respect to the earth, this orientation gives greatest response to the differential gravitational forces. The structure may be required to be in such an orientation for various purposes. For example, once a rigid space structure of dumbbell shape is so oriented in a circular orbit, it continues to remain in this position [45] eliminating the need for any additional control mechanism.

Special Case 4 ($\theta + \phi = 0$). In this case, the normal to the structure is perpendicular to the earth-sun line for all values of time, i.e., the structure is always

aligned with the direction of direct solar radiation (Figure 13(d)). This orientation experiences minimum solar radiation effects all along the orbit. Such an orientation must be attained for any space structure on which the radiation thermal and pressure effects have to be minimized.

Numerical Method

The equations of motion developed in chapter II are programmed using FORTRAN computer language for the Cyber 175 digital computer. The computer programs are written using an IMSL subroutine DVERK to solve the equations of motion. The method of integration used in the subroutine is fifth and sixth order Runge-Kutta-Verner method. Throughout the computer analysis the tolerance limit is maintained at 1.0×10^{-6}. The step size and the total duration of time chosen for the analysis vary depending on which kind of external disturbances are applied to the structure. All computations are done with single precision accuracy. A brief outline follows:

Differential Gravitational Forces

A computer program is written to solve the equations of motion (2.14) in conjunction with Equations (2.15) and

(2.16). A sample listing of the program (Computer Program I), sample input data, a sample run session and sample output data are shown in Appendix E. The step size for integration is 0.2 minutes. The total duration of time is 400 minutes at lower perigee altitude (200 km) and 1500 or 1700 minutes depending on whether the orbit is circular or elliptical at higher perigee altitude (35900 km). In order to study the effects of the differential gravitational forces on the space structure, the m_1/m_2 ratio is varied keeping the total mass m constant. Other parameters which are varied and whose effects are studied are total mass (m), lengh (x_s), orbit eccentricity (e), initial axial deformation ($x_0 - x_s$), and initial attitude misalignment ($\emptyset_0$). In addition to general orientation of the space structure, all four special orientations (cases) described in an earlier section are investigated. Table 2 (a) gives the summary of the values of these parameters and initial conditions selected for the computer investigations.

Differential Gravitational Force and Radiation Heating

In order to study the combined effects of the differential gravitational forces and radiation heat in the space structure, the equation of motion (2.14) in conjuction with Equations (2.42), (2.44), (2.52) and

Table 2: List of Computer Runs with Associated Initial Conditions and Other Parameter Values

$\theta_0 = 0 \quad \dot{r}_0 = 0 \quad \dot{x}_0 = 0 \quad \dot{\phi}_0 = 0$ (Note: These initial contitions are kept the same throughout the computer investigations.)

(a) Differential Gravitational Force Effects

Step size for the computations = 0.2 minutes

Example No.	Figure No.	r_0 (km)	$\dot{\theta}_0$ (rad/min)	ϕ_0 (rad)	x_0 (km)	x_a (km)	m_2 ($\frac{N\text{-}min^2}{km}$)	m_1/m_2	A_{ca} (km^2)	Orbit Type	Orientation of Structure	Comments
1	14(a),(b) 16(a),17(a) 18(a)	6574.11 (200 km from the surface of the earth)	.0710629041142	0.0	1.000023	1.0	5.0×10^5 (1800 t)	1.0	.00024495	Circular	General	Equilibrium state. Check for stability
2	15(a),16(a) 17(a)						4.0×10^5	1.5				Effects of m_1/m_2 Ratio (m=3600 t)
3							2.5×10^5	3.0				
4							7.5×10^5	1/3				
5	18(a),19(a) 20(a)				1.000069	3.0	5.0×10^5 (1800 t)	1.0	.00073485			Effects of Length
6					5.000115	5.0			.00122475			
7					0.5000115	0.5			.000122475			
8	21(a),22(a) 23(a),23(c)			0.1	1.000023	1.0			.00024495			Effects of Initial Libration
9				1.5707963								
10	24(a),25(a) 25(b),26(a) 27(a)			0.0	1.01							Effects of Initial Axial Deformation
11					1.05							
12					0.975							
13					1.000023							Neglecting Attraction between m_1 and m_2
14	28(a),28(b) 30(a),31(a) 32(a),33(a) 33(c)		.0738							Elliptical		Effects of Orbit e Small e (=0.0785)
15			.08883									Large e (=0.56)

Table 2: List of Computer Runs with Associated Initial Conditions and Other Parameter Values (Continued ...)

(a) Differential Gravitational Force Effects (Continued ...)

Step size for the computations = 0.2 minutes

Example No.	Figure No.	r_0 (km)	$\dot{\theta}_0$ (rad/min)	θ_0 (rad)	x_0 (km)	x_a (km)	m_2 ($\frac{N\text{-}min^2}{km}$)	m_1/m_2	A_{cs} (km^2)	Orbit Type	Orientation of Structure	Comments
16 17 18	15(b),16(b) 17(b)	42274.33 (35900 km from the surface of the earth)	.0043581803426	0.0	1.000023	1.0	5.0×10^5 2.5×10^5 7.5×10^5	1.0 3.0 1/3	.00024495	Circular	General	Effects of m_1/m_2 (m = 3600 t)
19	18(b),19(b) 20(b)				5.000115	5.0	5.0×10^5 (1800 t)	1.0	.00122475			Effects of Length
20 21	21(b),22(b) 23(b),23(d)			0.1 1.5707963	1.000023	1.0			.00024495			Effects of Initial Libration
22	24(b),26(b) 27(b)			0.0	1.05							Effects of Initial Axial Deformation
23					1.000023							Neglecting Attraction between m_1 and m_2
24	29(a),(b) 30(b),31(b) 32(b)		.004526							Elliptical		Effects of Orbit e Small e (=0.0785)
25	42(c),43(b)	6574.33	.08883	1.5707963						Elliptical (e=0.56)	Special Case 1	Effects of Special Orientations
26	44,45(b)										Special case 2	
27	31(a),32(a) 46(b)			0.0							Special Case 3	
28	47,48(b)										Special Case 4	
29 30	34,35(a), 35(b)						5.0×10^3 2.5×10^3	1.0 3.0			General	Effects of Total Mass m (m = 36 t)

Table 2: List of Computer Runs with Associated Initial Conditions and Other Parameter Values (Continued ...)

(b) Differential Gravitational Force and Radiation Thermal Effects

x_0 = 1.000023 km x_s = 1.0 km A_{cs} = 0.00024495 km^2 T_0 = 290°K Step size for the computations = $\begin{cases} 0.2 \text{ minutes for } |\theta| \leq \pi/2 \\ 0.1 \text{ minutes for } |\theta| \geq \pi/2 \end{cases}$

Example No.	Figure No.	r_0 (km)	$\dot{\theta}_0$ (rad/min)	θ_0 (rad)	A_{sd} (km^2)	m_2 ($\frac{N\text{-}min^2}{km}$)	m_1/m_2	A_{sf} (km^2)	Orbit Type	Orientation of Structure	Comments
31	37(a), 38(a) 39(a)	6574.33	.07106292041142	0.0	.000375188	5.0×10^5 (1800 t)	1.0	.00175038	Circular	General	All 3 sources of radiation heating are considered with equal importance. For each case, runs are made for following situations: 1. Gravity (G) + Direct Solar (D.S.) 2. G + D.S. + Albedo (ALB) 3. G + D.S. + ALB + Direct Earth (D.E.) For these cases, (A_{sf}/m) = .000486 m^2/kg
32	37(b), 38(b) 39(b)	42274.33	.0043581803426								
33	40,41(a) 41(b)	6574.33	0.08883						Elliptical (e = 0.56)		
34	42,43(a) 43(b)			1.5707963						Special Case 1	
35	44,45(a) 45(b)									Special Case 2	
36	46(a), 46(b)			0.0						Special Case 3	
37	47,48(a) 48(b)									Special Case 4	
38	49,50(a) 50(b)					5.0×10^3 (18 t)				General	Effects of A_{sf}/m on Total Thermal Response (A_{sf}/m) = .0486 m^2/kg (A_{sf}/m) = 2.778 m^2/kg
39					0.05			0.1			
40	51(a), 51(b)		.07106292041142	1.5707963					Circular	Special Case 2	For these runs, (A_{sf}/m) = 2.778 m^2/kg 1. G. + D.S. 2. G. + D.S. + ALB 3. G. + D.S. + ALB + D. E.

NOTE: G Gravitational forces D.S. Direct solar radiation ALB Albedo radiation D.E. Direct earth radiation

Table 2: List of Computer Runs with Associated Initial Conditions and Other Parameter Values (Completed)

(c) Differential Gravitational Force and Radiation Pressure Force Effects

x_0 = 1.000023 km x_s = 1.0km A_{cs} = 0.00024495 km^2 Completely absorbing structural surface

Step size for the computations = $\begin{cases} 0.2 \text{ minutes for } |\theta| \leq \pi/2 \\ 0.1 \text{ minutes for } |\theta| \geq \pi/2 \end{cases}$

Example No.	Figure No.	r_0 (km)	$\dot{\theta}_0$ (rad/min)	ϕ_0 (rad)	A_{sd} (km^2)	m_2 ($\frac{N\text{-}min^2}{km}$)	m_1/m_2	A_{sf} (km^2)	Orbit Type	Orientation of Structure	Comments
41 42 43	52 53(a),53(b) 54(a),54(b)	6574.33	0.08883	0.0	.000875188	5.0×10^5 2.5×10^5 7.5×10^5	1.0 3.0 1/3	.00175038	Elliptical	General	G + D.S. Effects (A_{sf}/m) = .000486m^2/kg l_p = 0.0 km l_p = $-0.25x_s$ km l_p = $+0.25x_s$ km
44 45						5.0×10^3 2.5×10^3	1.0 3.0				G + D.S. Effects (A_{sf}/m) = .0486m^2/kg l_p = 0.0 km l_p = $-0.25x_s$ km
46 47 48	55,56(a) 56(b),57(a) 58(b)				0.05	5.0×10^3 2.5×10^3 7.5×10^3	1.0 3.0 1/3	0.1			G + D.S. Effects (A_{sf}/m) = 2.778 m^2/kg l_p = 0.0 km l_p = $-0.25x_s$ km l_p = $+0.25\ x_s$ km
49	42,58(a) 58(b),59(a) 59(b)			1.5707963		5.0×10^3	1.0			Special Case 1	G + D.S. Effects (A_{sf}/m) = 2.778m^2/kg l_p = 0.0 km
50	60(a),60(b) 61(a),61(b)									Special Case 2	1. G + D.S. 2. G + D.S. + ALB 3. G.+ D.S. + ALB + D.E. For these runs, $(A_{sf}/m$ = 2.778m^2/kg l_p = 0.0 km

NOTE: G Gravitational forces D.S. Direct solar radiation ALB Albedo radiation D.E. Direct earth radiation

(2.26) are solved numerically. A listing of a sample computer program (Computer Program II) written for this purpose is given in Appendix E together with the listing of sample input data, a sample run session and sample output data. The step interval for all numerical integration is taken to be 0.2 minutes for $|\theta| \leq \pi/2$ whereas it is 0.1 minutes for $|\theta| \geq \pi/2$. The latter interval includes the earth's shadow region. The step size is decreased from 0.2 minutes to 0.1 minutes to determine the earth's shadow entry and exit locations more accurately. The total duration of time considered is more than enough for at least one orbit. For the circular orbit at altitude 200 km, this is 400 minutes (more than 4 orbit periods). For the elliptical orbit, the duration is 437.2 minutes, and for circular orbit at 35900 km altitude it is taken to be 1500 minutes.

To obtain the most severe thermal effects, the sun direction is taken to be coincident with the x_I-axis, and the surface of the structure is taken as an ideal "black body" for radiation heat. All the three major sources of radiation heat - direct solar, earth's albedo, and direct earth emission, are treated with equal importance. Most of the effects are studied in a large eccentric elliptical orbit ($e = 0.56$, perigee at 200 km altitude). However, to determine relative contributions of these three radiation sources, numerical results are obtained for circular orbits at two altitudes- 200 km and

35900 km from the earth's surface. Thermal effects for the general case and for the four special orientations (cases) are studied. In addition, dependence of thermal effects on the surface area to mass ratio (A_{sf}/m) is also studied for three values of the ratio. Table 2(b) gives the summary of the values of these parameters and initial conditions selected for the computer runs.

Equilibrium temperature. Maximum and minimum equilibrium values of the temperature have been computed at three altitudes-one, at 200 km; two, at 35900 km; and three, at 23483 km (apogee of the elliptical orbit with e = 0.56). A computer program (Computer Program III) which is written for this purpose using Equations (2.40) is listed in Appendix E along with sample input data, sample run session, and sample output data.

Differential Gravitation and Radiation Pressure Forces

The equations of motion (2.14) together with Equations (2.131), which give radiation pressure forces and moments and Equation (2.16) which gives strain energy are computer programmed in order to determine the effects of the differential gravitational and radiation pressure forces on the space structure. The step size and total duration of time considered for carrying out the integration are the same as in the thermal analysis described in the sub-section

above for the elliptical orbit. A listing of a sample computer program (Computer Program IV), sample input data, a sample run session, and sample output data are presented in Appendix E.

As in the case of thermal effects, here too, the sun lies in the orbit plane along the x_I axis. The effects of the radiation pressure forces are investigated in an elliptical orbit of large eccentricity ($e = 0.56$, perigee at 200 km altitude). The radiation pressure effects greatly differ from one kind of structural surface to another. In this study, the effects of radiation pressure are determined for completely absorbing structural surface. The general case and Special Case 1 (i.e, $\theta + \emptyset = \pi/2$) are considered to study the contribution from direct solar radiation. For earth's albedo and direct earth's radiation pressure effects, only Special Case 2 has been considered. This orientation gives maximum effects due to these sources. The impact of A_{sf}/m is also studied for three values of the ratio. Also, the effects of positive and negative values of the distance l_p between the centre of mass (C) and the center of radiation pressure (P) of the structure are studied. The magnitude and sign of l_p depend on the m_1/m_2 ratio (see Equation (2.94)). The largest value of this distance (l_p) is expected to be one-quarter of the total length of the structure. The values of these parameters and initial conditions

selected for the computer runs are summarized in Table 2(c). The solution is obtained for duration of more than one orbit period.

Earth's Shadow Entry and Exit Points

The points at which the space structure enters and exits the earth's shadow has been determined by evaluating the function

$$(r_c - r_{sb})$$

systematically, for a set of closely spaced values of t. Here, r_c defines the orbit and r_{sb} the shadow boundary. The shadow entry or exit point lies in the interval at which the function changes sign. These intervals can be subdivided, and the procedure repeated to determined the shadow boundary more precisely. Of course, no matter how fine the step size (t), the shadow boundary can still wholly lie between two successive trial values of t. Therefore, to avoid unnecessary lengthy computation time, a fairly reasonable step interval of 0.1 minutes is selected.

A glossary of terms used in the computer programs is given in Appendix F.

CHAPTER IV

RESULTS AND DISCUSSION

The purpose of this chapter is to present the results from the computer solution of the complete equations of motion of an axially flexible dumbbell-shaped space structure executing planar motion under the influence of various external dynamic and thermal causes, and to analyze the results. The results, in general, are presented in the form of self-explanatory plots. However, some of them are presented in tabulated form. It has been attempted to support most of the results stated here by graphs and/or data tables, but in some cases less important and more or less obvious results are simply noted without any supporting plots or data tables. The figures, tables and accompanying discussion in this chapter give a quantitative as well as qualitative description of the effects of various external disturbances on a space structure.

The results are presented under three broad categories: 1. Differential gravitational force effects, 2. Combined thermal and differential gravitational force effects, and 3. Combined radiation pressure and differential gravitational force effects. In all three categories the results and discussion are presented so as to delineate the

effects of these factors on the axial deformation, attitude motion, and orbital motion of the space structure. The various initial conditions chosen to exemplify the effects of the above three major sources of external disturbances found in space environments are given in Table 2(a), (b), and (c), respectively. The orbit characteristics (altitudes, types, and periods) of the orbits considered in the present analysis are shown in Table 3.

Differential Gravitational Force Effects

At a given altitude, the differential gravitational force depends on the mass ratio (m_1/m_2) of the dumbbells and the length (x) and the libration (attitude) angle ($\emptyset$) of the space structure (Equation 2.14). The variation of the differential gravitational force (F_g) along an orbit has been obtained and its effects on the space structure's axial deformation, attitude motion, and orbital motion have been studied. Under the sole influence of the earth's gravitational attraction, we obtain results to see the effects on the space structure's axial deformation and motions due to change in the m_1/m_2 ratio, static length (x_s), initial length (x_0), initial libration angle ($\emptyset_0$) and total mass (m) of the structure, as well as the eccentricity and altitude of the orbit. The step size for the computations is equal to 0.2 minutes for all the computer runs reported below.

Ideal Initial Conditions

Initial conditions for this run are given under Example No. 1 in Table 2(a). The principal purpose of the first run is to verify the stability of the equations of motion and the equibilibrium value of x used for x_0. The initial conditions for this run are selected by satisfying the

steady state equilibrium configuration of the space structure (Appendix D). The orbit is circular at an altitude of 200 km (Figure 14(a), and the structure is released from perigee (i.e., $\theta_0 = 0$, $\dot{r}_0 = 0$). The initial misalignment is zero (i.e., $\phi_0 = \dot{\phi}_0 = 0$). The static length of the dumbbell structure is one kilometer. The dumbbell mass ratio (m_1/m_2) is unity. Each dumbbell mass is 1800 metric tons (5.0×10^5 N-min^2/km). The solution is run for about 4.5 orbits (t = 400 minutes in the computation). The step size for the numerical integration is 0.2 minutes. The orbit remains perfectly circular at the altitude of 200 km for all time (Figure 14(a)). The period of the orbit is found to be approximately 88.4 minutes (Table 3).

For the perfect initial conditions selected, the flexible dumbbell space structure stays aligned with the local vertical (i.e., $\phi = \dot{\phi} = 0$) and has no oscillation in the axial length (i.e., $x = x_0$, $\dot{x} = 0$) (Figure 14(b). The computer data, however, shows a slight oscillation in ϕ which reached a maximum amplitude of approximately 0.155×10^{-6} radians in the four and one-half orbit run. A plot of ϕ versus time is shown in Figure 17(a) for one orbit duration. Due to the round off and truncation error while computing the initial value of x (x_0 = 1.000023 km) by satisfying the equilibrium state, the computer data also show a slight oscillation in x. The amplitude of

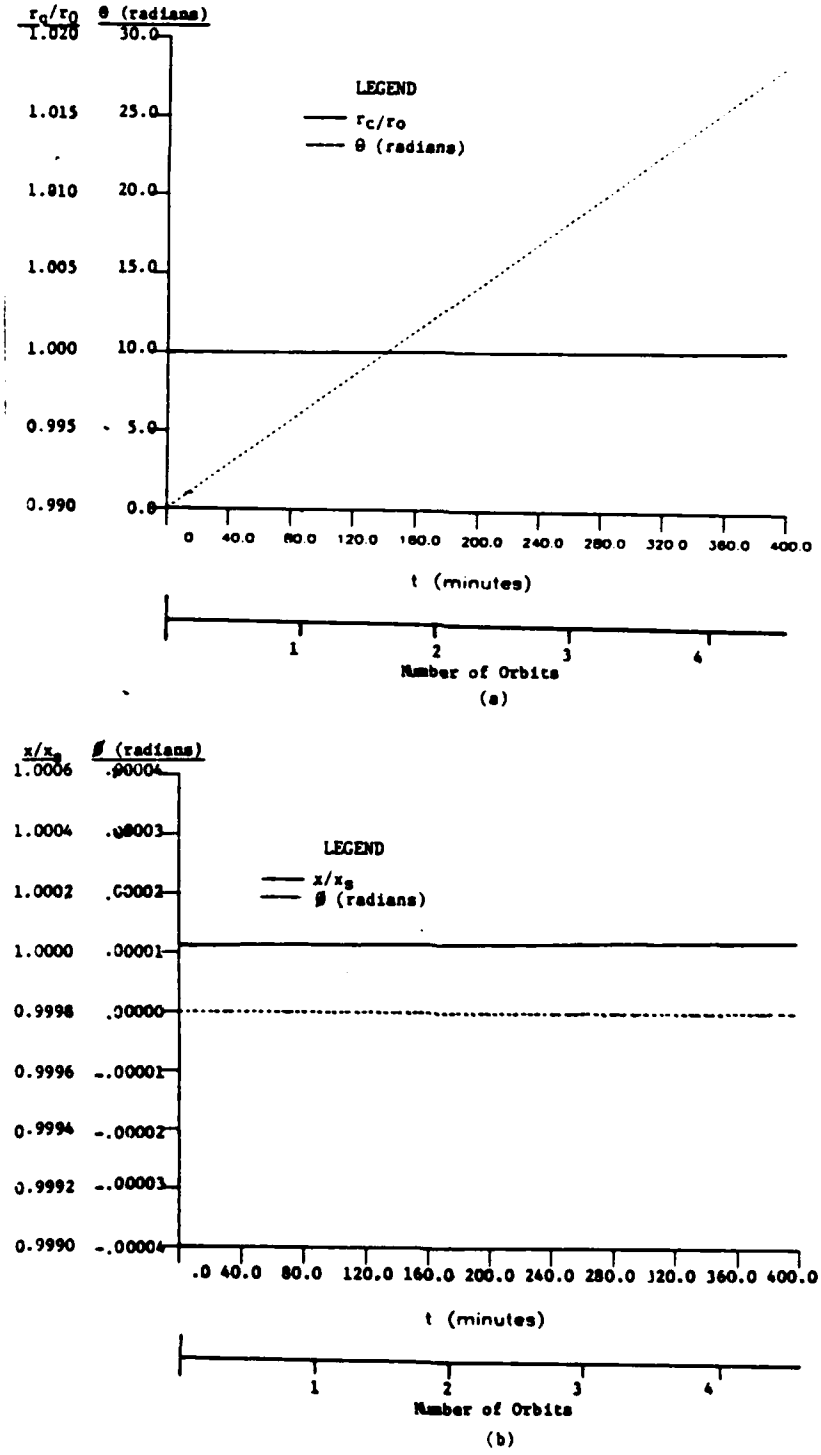

Figure 14. Circular orbit at 200 km altitude: Variations of (a) the orbit parameters (r_c and θ), (b) structural axial length (x) and attitude (Ø)

oscillation in x increases as time increases. The maximum amplitude of fluctuation in x is never greater than 4.7 x 10^{-4} percent of the initial x during the 4.5 orbit duration. A plot of x versus time is shown in Figure 16(a) for one orbit period. Figure 18(a) (x_s = 1 km) shows that the differential gravitational force (ΔF_g) in the structure also remains constant at a magnitude of approximately 5.046 x 10^3 N. A slight oscillation in ΔF_g is observed which is mainly due to the slight oscillation in x and Ø. Except for these small librations, the nature of the solution agrees with that given by Stocker and Vachino for a rigid dumbbell [47] and by Hall and Smith for a non-rigid dumbbell.

Effects of Differential Dumbbell Masses (m_1/m_2 Ratios)

A complete set of initial conditions for these runs is presented in Example No. 2 through 4 in Table 2(a). Keeping all the initial conditions as above, computer runs are made for three additional values of m_1/m_2 (1.5, 3.0 and 1/3). The total mass ($m = m_1 + m_2$) of the structure is kept constant at 3600 tons (i.e., 1.0 x 10^6 N-min^2/km). The values of m_2 have been changed accordingly to obtain the desired values of the ratio m_1/m_2. This insures that the total initial gravitational forces on the system are the same for all values of m_1/m_2 ratios. The step

size chosen for the computations is 0.2 minutes. The larger the difference between the values of m_1 and m_2, the higher is the value of differential gravitational force (ΔF_g). Figure 15(a) clearly shows this result, where plots of $\Delta F_g/F_{g0}$ versus time are shown for four values of m_1/m_2 for approximately 4.5 orbits (t = 400 minutes) duration. The $\Delta F_g/F_{g0}$ values remain constant over the duration considered: at -0.152110×10^{-3} for m_1/m_2 = 1.0, at 0.19985397 for m_1/m_2 = 1.5, at 0.4998859 for m_1/m_2 = 3.0, and at -0.50015156 for m_1/m_2 = 1/3. The magnitudes of $\Delta F_g/F_{g0}$ are equal for m_1/m_2 = 3 and 1/3 because one configuration can be obtained from the other by replacing m_1 by m_2 and vice versa. The computer data show that there is small fluctuation in $\Delta F_g/F_{g0}$ values from the seventh place after the decimal point. This is a very insignificant fluctuation and may have occurred due to computer round off and truncation error.

For m_1/m_2 = 1.5, the orbit remains perfectly circular at the initial altitude of 200 km (r_0 = 6574.3300 km), and the orbital period remains unchanged at 88.4 minutes. On the other hand, a slight perturbation in the orbit has been noticed for m_1/m_2 = 3 and 1/3. The orbit now becomes slightly eccentric with apogee point at a distance 6574.3301 km from the center of the earth and with perigee point at a distance 6574.3300 km from the center of

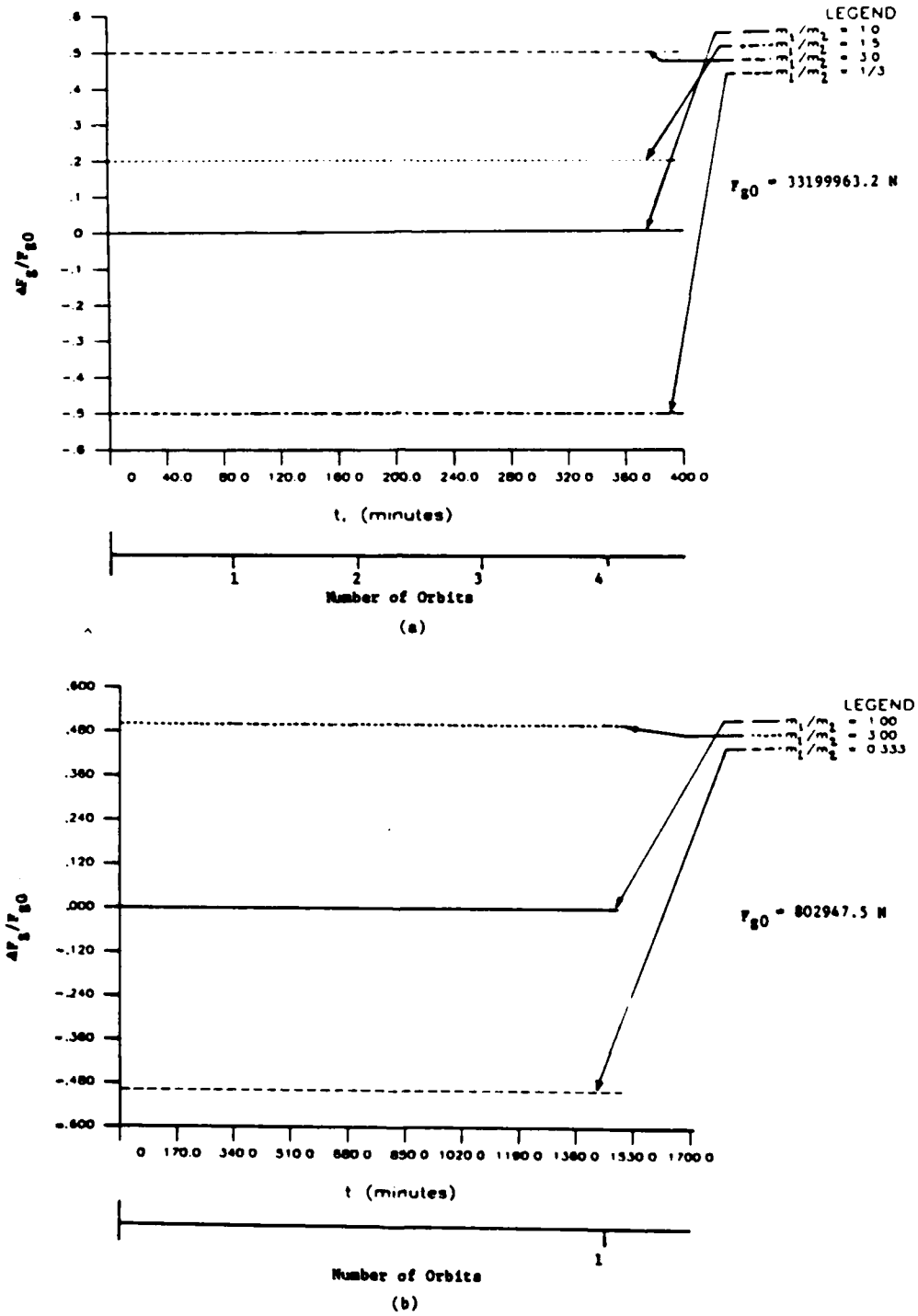

Figure 15. Dependency of differential gravitational force (ΔF_g) on dumbbell mass ratio m_1/m_2: Circular orbit at altitude (a) 200 km, (b) 35900 km

the earth which is the initial value of r_c. The orbit period remains unaltered.

Increased oscillations in x have been noticed with larger differences in the values of m_1 and m_2 (Figure 16(a)). However, the maximum magnitude of amplitude of the oscillation is still very small, - only 0.00122 percent of the initial length (x_0) even for m_1/m_2 = 3 and 1/3. The general trend of the oscillation in x is to reduce the length of the structure. The ratios m_1/m_2 = 3 and 1/3 follow the identical oscillation pattern in x. The period of oscillation in x is approximately 3.4 minutes for both values of m_1/m_2 during the 400 minute run. For m_1/m_2 = 1.5, the maximum value of the amplitude of oscillation in x is small, 0.0005 percent of x_0, and the period of oscillation is approximately 1.2 minutes.

Similarly, there is an increased effect of differential mass of the dumbbell structure in the attitude motion (Ø). Again, the larger the difference between the values of m_1 and m_2, the greater is the libration in Ø. Figure 17(a) shows a plot of Ø versus t for m_1/m_2 = 1, 1.5, 3.0, and 1/3 during a 100 minute duration. The ratios m_1/m_2 = 3 and 1/3 have identical effects on Ø also. The maximum values of amplitude of libration in Ø are approximately 0.66 x 10^{-5} radians for m_1/m_2 = 3 and 1/3, and 0.995 x 10^{-6} radians for m_1/m_2 = 1.5 during the 400 minute run. The period of libration in Ø is the same for all

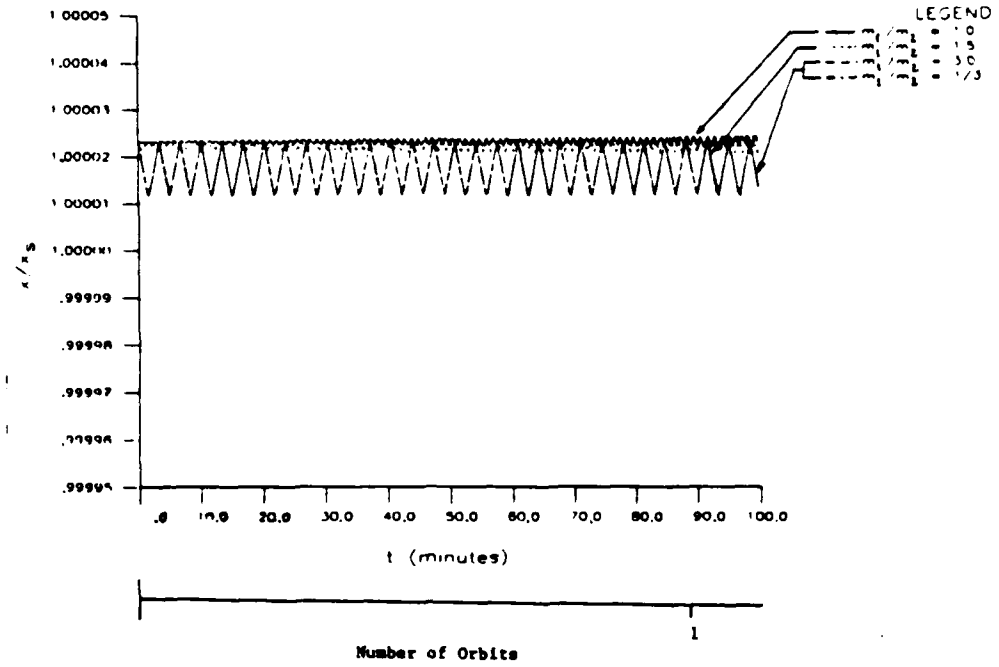

(a)

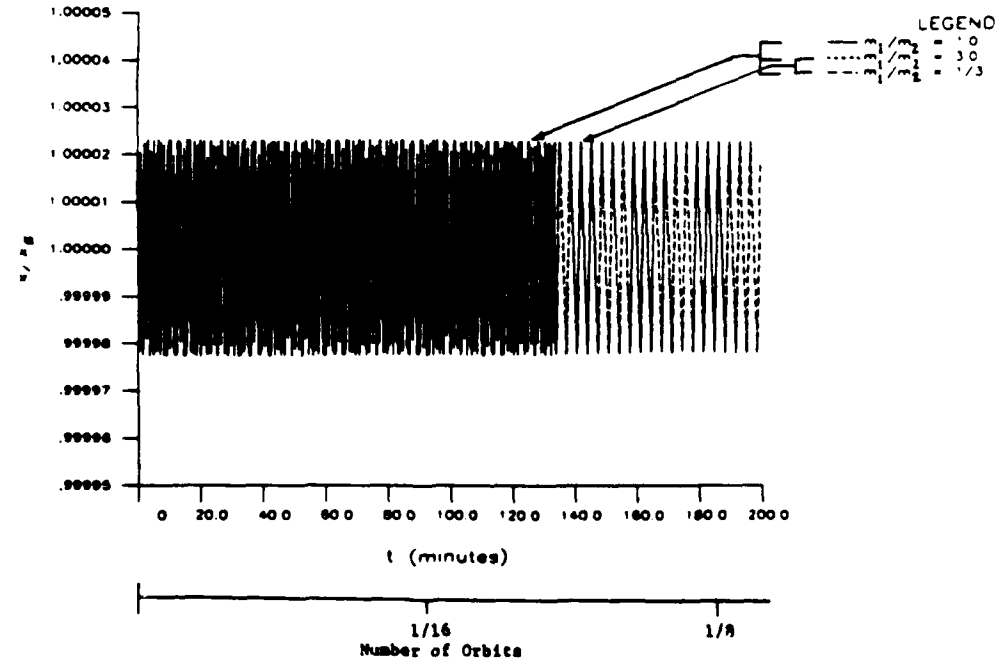

(b)

Figure 16. Effect of dumbbell mass ratio m_1/m_2 on axial deformation (x): Circular orbit at altitude (a) 200 km, (b) 35900 km

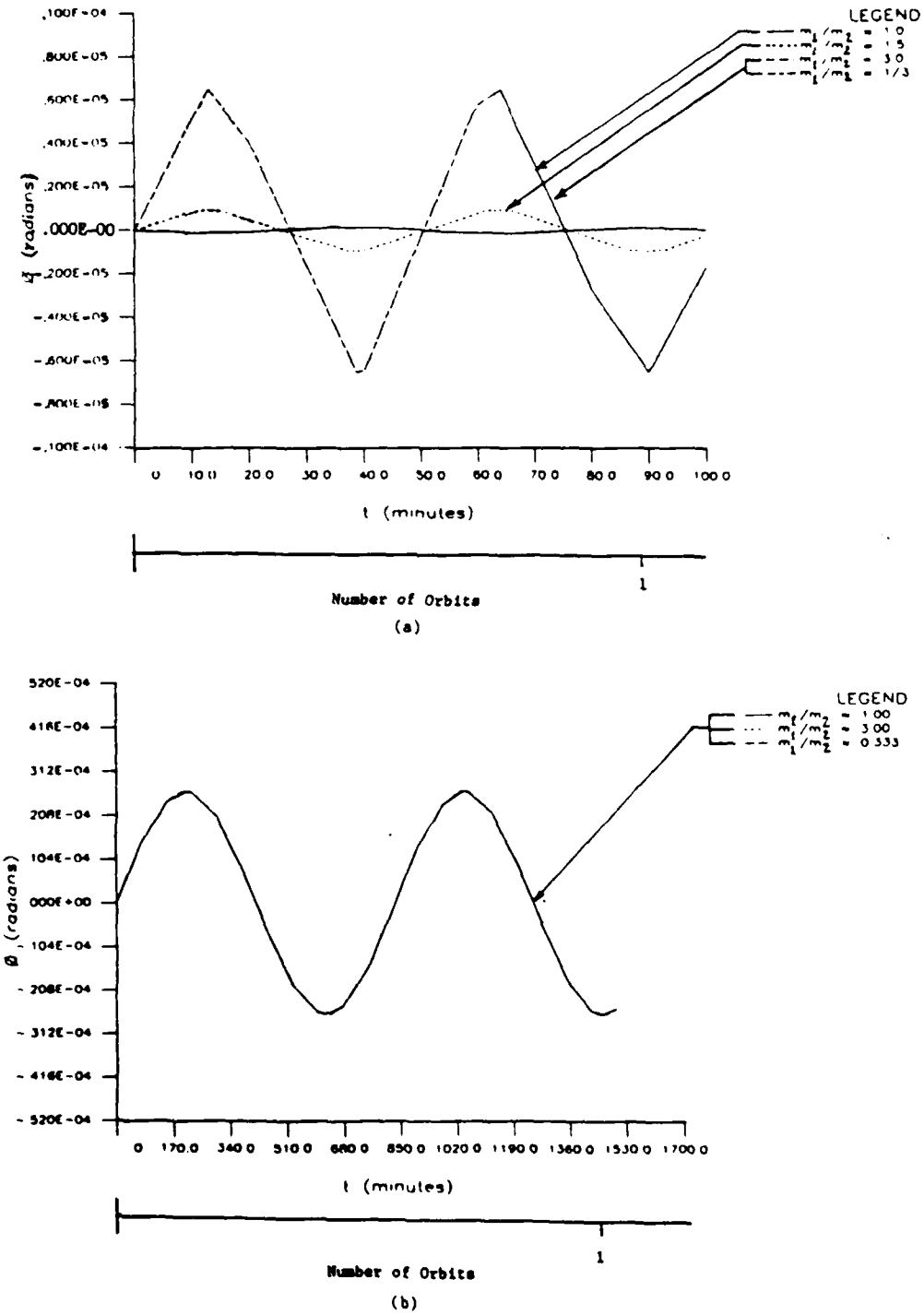

Figure 17. Effects of dumbbell mass ratio m_1/m_2 on attitude motion (Ø): Circular orbit at altitude (a) 200 km, (b) 35900 km

m_1/m_2 values which is approximately 51.11 minutes. The amplitude of oscillation in x and Ø remains constant throughout the duration considered.

From these results, we can conclude that the differential gravitational forces as induced by the change in the value of the m_1/m_2 ratio do produce some oscillations in x and Ø, the exact magnitudes of which are very small. An accurate determination of such a small oscillations has been difficult mainly due to the presence of other small amplitude oscillation caused by the truncation and rounding off of the initial value of x while computing it from the equilibrium state.

Effects of Length

Example No. 5 through 7 in Table 2(a) correspond to the initial conditions of these runs. Here, computer runs are obtained for three additional values of the static length (x_s) equal to 3 km, 5 km, and 0.5 km of the dumbbell space structure. The initial value (x_0) of x has been accordingly changed to 3.000069 km, 5.000115 km, and 0.5000115 km, respectively, to make sure that the equilibrium configuration will be maintained and that only the effects of changing the values of x_s could be observed. As before all runs are made for approximately a 4.5 orbit duration (t = 400 minutes with step size for the

computations equal to 0.2 minutes). Figure 18(a) shows a plot of $\Delta F_g/F_{gO}$ versus time for x_s = 1 km, 3 km, 5 km, and 0.5 km. The plot shows that the values of the differential gravitational force increase with increasing x_s. The magnitude of $\Delta F_g/F_{gO}$ remains constant throughout the duration of 400 minutes at -0.15211×10^{-3} for x_s = 1 km, at -0.45633×10^{-3} for x_s = 3.0, at -0.76055×10^{-3} for x_s = 5 km, and at 0.76055×10^{-4} for x_s = 0.5 km. The computer data show a slight oscillation in these values from the fifth place after the decimal point (i. e., from the seventh significant figure after the decimal point). This is mainly due to the oscillations in x and Ø and a slight perturbation of the orbit. B comparing these values of F_g with those obtained while studying the effects of the ratio m_1/m_2, we can say that the dependency of the differential gravitational force on x_s is thus not as strong as that on the m_1/m_2 ratio.

Increased perturbation of the orbit is noticed with the increasing difference in values between the equilibrium x_s (equal to 1 km) and x_s selected arbitrarily (3 km, 5 km, and o.5 km). For x_s = 0.5 km, the orbit apogee point is seen to be located at r_c = 6574.3302 km and $\theta = \pi$ whereas the perigee remains at the initial value of r_c (r_O = 6574.3300 km) and θ = 0 or 2π. On the other hand, for both x_s = 3 km and 5 km, the point r_O = 6574.3300 km and

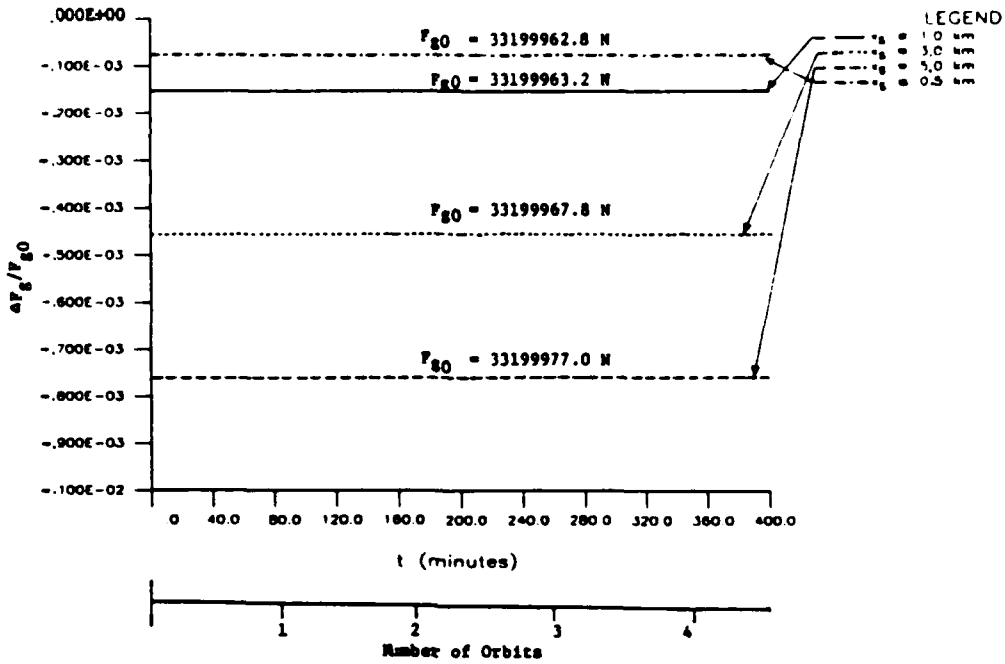

(a)

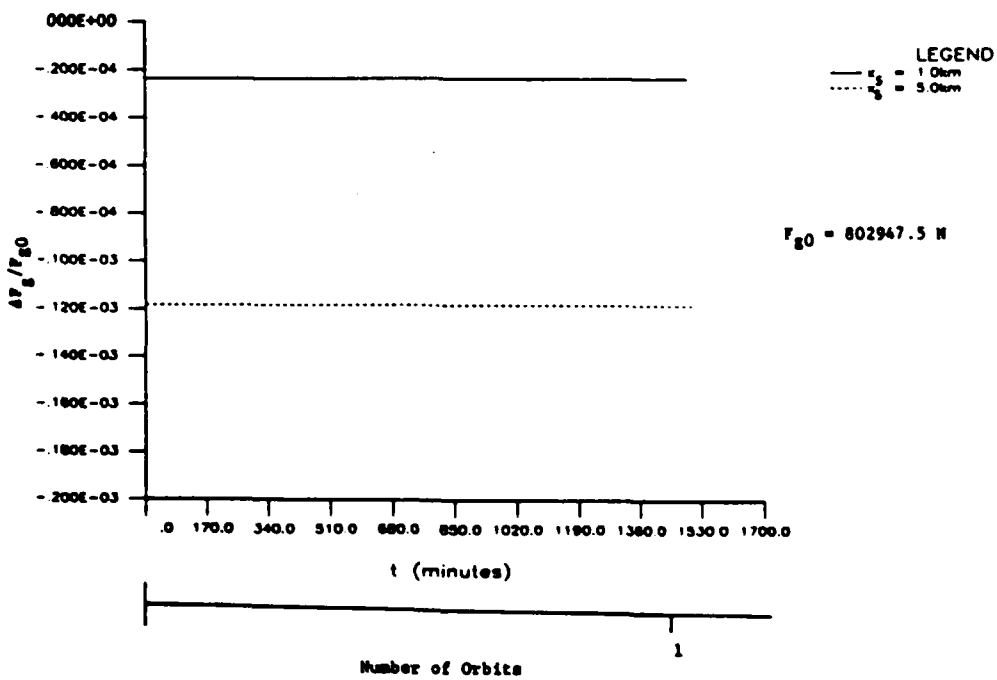

(b)

Figure 18. Dependency of differential gravitational force (ΔF_g) on static length (x_s) : Circular orbit at altitude (a) 200 km, (b) 35900 km

$\theta_0 = 0$ selected initially becomes the apogee point. Perigee points are at $r_c = 6574.3282$ km and $\theta = \pi$ for $x_s = 3$ km, and at $r_c = 6574.3245$ km and $\theta = \pi$ for $x_s = 5$ km.

The effect of x_s on the axial length (x) of the space structure is very insignificant. The oscillations in x are similar for all x_s values with the only difference being that the amplitude of oscillation increases with time in a different proportion from one x_s value to the other. Figure 19(a) shows a plot of x/x_s versus time for $x_s = 1$ km, 5 km and 0.5 km. For all x_s values, the amplitudes of oscillation in x start with zero value at t = 0 and keep increasing as time increases, and the difference in the amplitude values of the oscillation corresponding to various x_s become more and more distinct. In any case, the maximum amplitudes among all cases occur for $x_s = 5$ km which is no more than 0.00009 percent of the initial length. The period of oscillation in x is 1.0 minutes for all cases. The time step considered for the numerical computations is 0.2 minutes. The effects of x_s are also negligible on attitude motion (Ø) of the space structure. As can be seen in Figure 20(a), the oscillations in Ø for $x_s = 0.5$ km is the same as that for $x_s = 1$ km (equilibrium state), of which the maximum amplitude and period of oscillation are approximately 0.156×10^{-6} radians and 50.3 minutes, respectively. These values remain

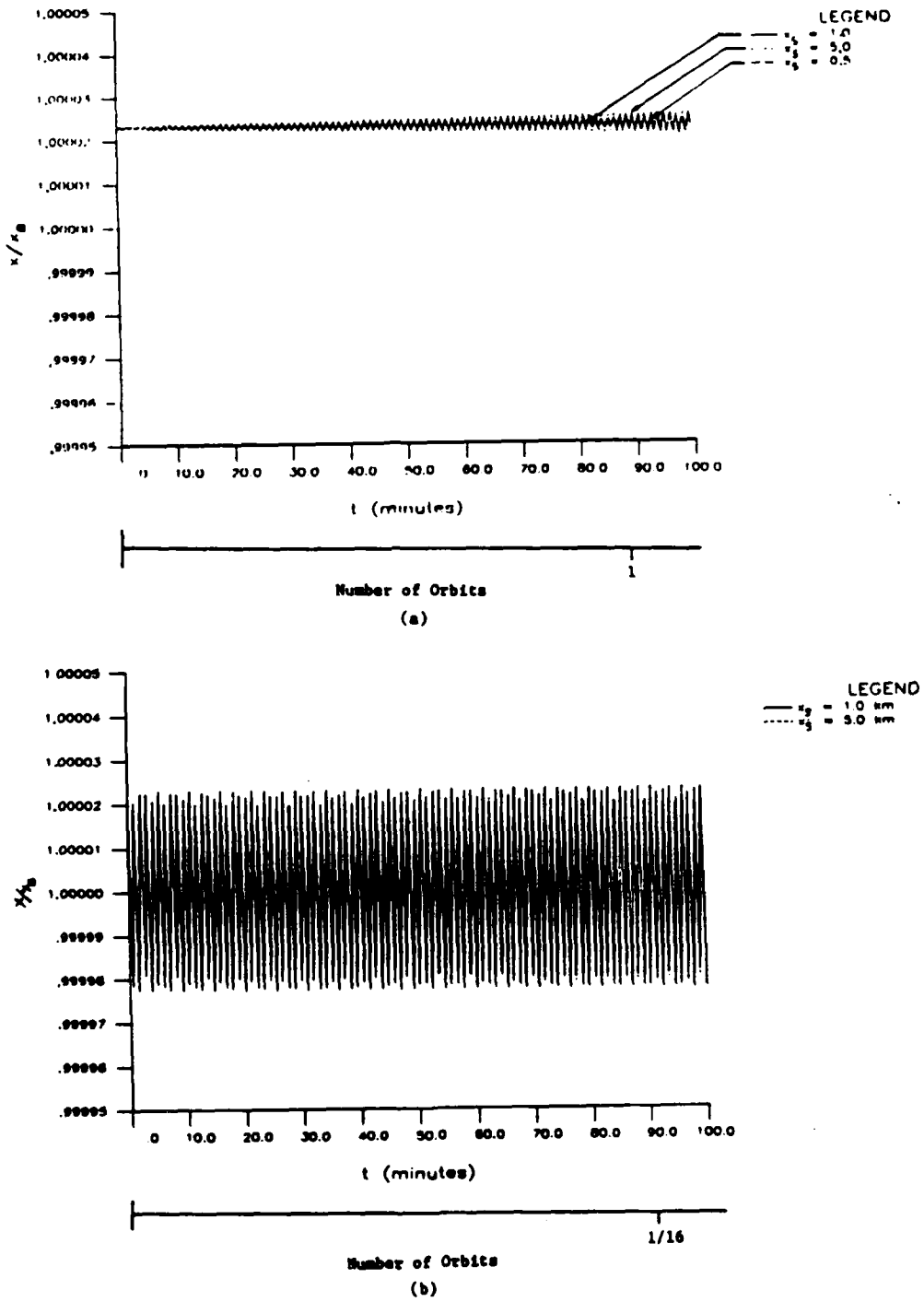

Figure 19. Effects of static length (x_s) on axial deformation (represented by x/x_s): Circular orbit at altitude (a) 200 km, (b) 35900 km

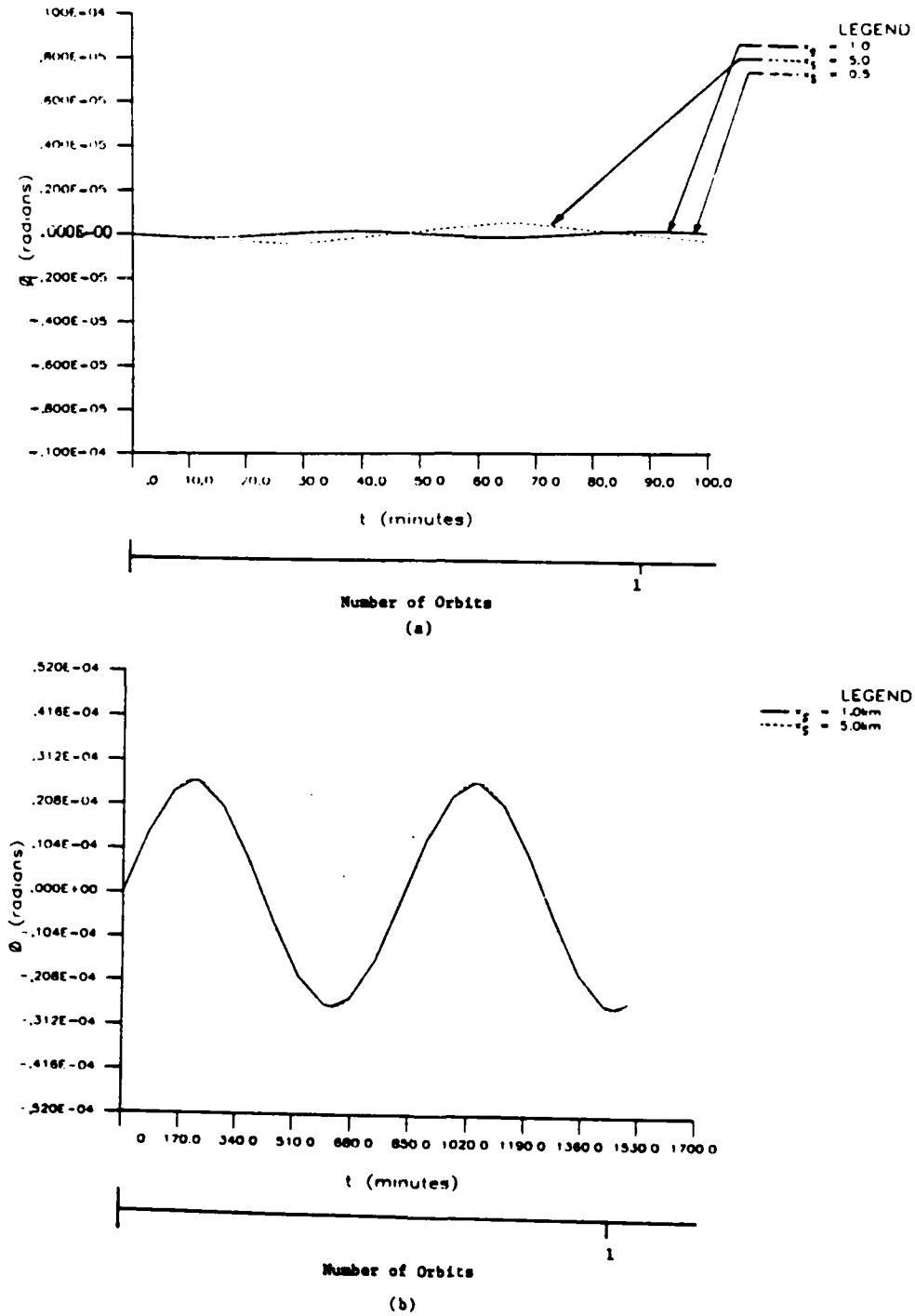

Figure 20. Effects of static length (x_s) on attitude motion (Ø): Circular orbit at altitude (a) 200 km, (b) 35900 km

approximately constant throughout the duration considered. For x_s = 5 km, the amplitude of oscillation in $\emptyset$ is approximately constant at 0.53×10^{-6} radians, but the period of libration is not constant. For the first oscillation the period is 85.2 minutes. For the second, third and fourth oscillations, they are respectively 92.2 minutes, 91.6 minutes and 82.2 minutes.

Effects of Initial Attitude

The additional values of the initial attitude ($\emptyset_0$) selected are 0.1 radians and 1.5707963 (equal to $\pi/2$) radians. Example No. 8 and 9 in Table 2(a) show the complete initial conditions for these runs. Figure 21(a) shows a plot of $\Delta F_g/F_{g0}$ versus time for $\emptyset_0$ = 0 radians, 0.1 radians, and 1.5707963 radians for a duration of 400 minutes. The step size chosen for numerical integration is again 0.2 minutes. The differential gravitational force (expressed as $\Delta F_g/F_{g0}$) oscillates between an amplitude of approximately -0.13135×10^{-3} and -0.15211×10^{-3} for $\emptyset_0$ = 0.1 radians and between approximately 0 and 0.15211×10^{-3} for $\emptyset_0$ = 1.5707963 radians. As mentioned earlier, $\Delta F_g/F_{g0}$ remains constant at -0.15211×10^{-3} for $\emptyset$ = 0 radians at all time. It should be noted that for the larger value of $\emptyset_0$ (equal to 1.5707963 radians), the amplitude of oscillation

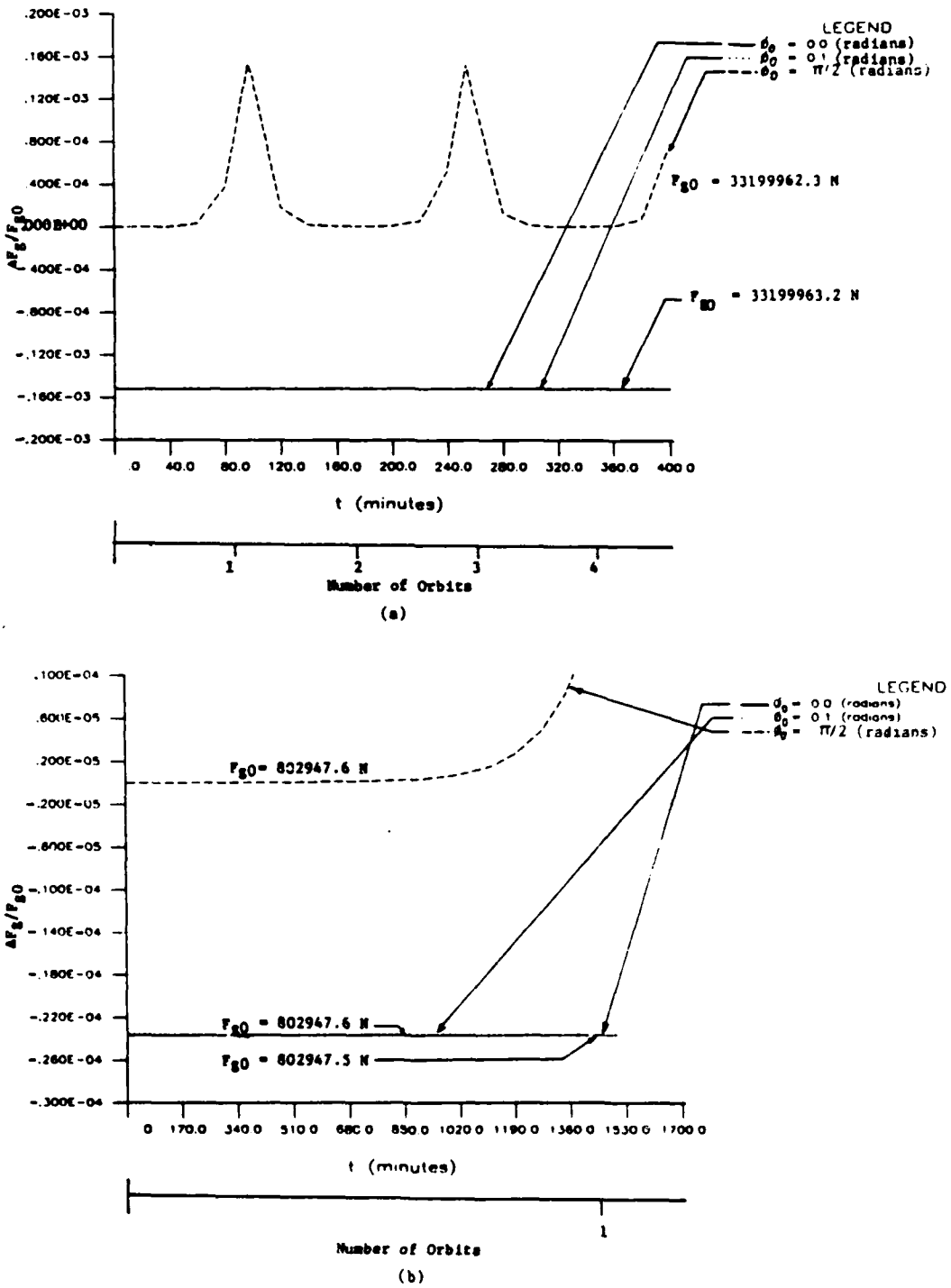

Figure 21. Dependency of differential gravitational force (ΔF_g) on initial libration angle (ϕ_0): Circular orbit at altitude (a) 200 km, (b) 35900 km

in $\Delta F_g/F_{g0}$ occurs as spikes near the perigee points. The period of oscillation in $\Delta F_g/F_{g0}$ is approximately 25.5 minutes for $\emptyset_0$ = 0.1 radians and 157.2 minutes for $\emptyset_0$ = 1.5707963 radians.

As far as the perturbation of orbit is concerned the small value of $\emptyset_0$ (equal to 0.1 radians) does not perturb the orbit at all. However, the larger value of $\emptyset_0$ equal to $\pi/2$ radians perturbs the orbit. In this latter case the largest variation in the value of r_c in one orbit is seen to be from 6574.3299 km to 6574.3305 km during the 400 minutes run. The orbital period can be taken to be the same as earlier (88.4 minutes). Thus, the perturbation of orbit due to $\emptyset_0$ is still very insignificant.

Figure 22(a) shows the plot of x/x_s versus time for $\emptyset_0$ = 0, 0.1 and $\pi/2$ radians. The oscillation in x for $\emptyset_0$ = 0.1 radians is seen to be sinusoidal about the initial value of x (x_0 = 1.000023 km). The maximum value of amplitude of oscillation in x is only 0.0004 percent of the initial length (x_0). For $\emptyset_0 = \pi/2$ radians except in the vicinity of t = 96.2 minutes where the peak value (equal to 1.0000953 km) occurs, x/x_s oscillates about the static length (x_s = 1 km) with amplitudes between 1.000023 km and 0.999977 km. It is noteworthy that the value of x goes below the static length (x_s) for the first time. The maximum value of amplitude of oscillation is still very small, only approximately 0.00072 percent of the initial

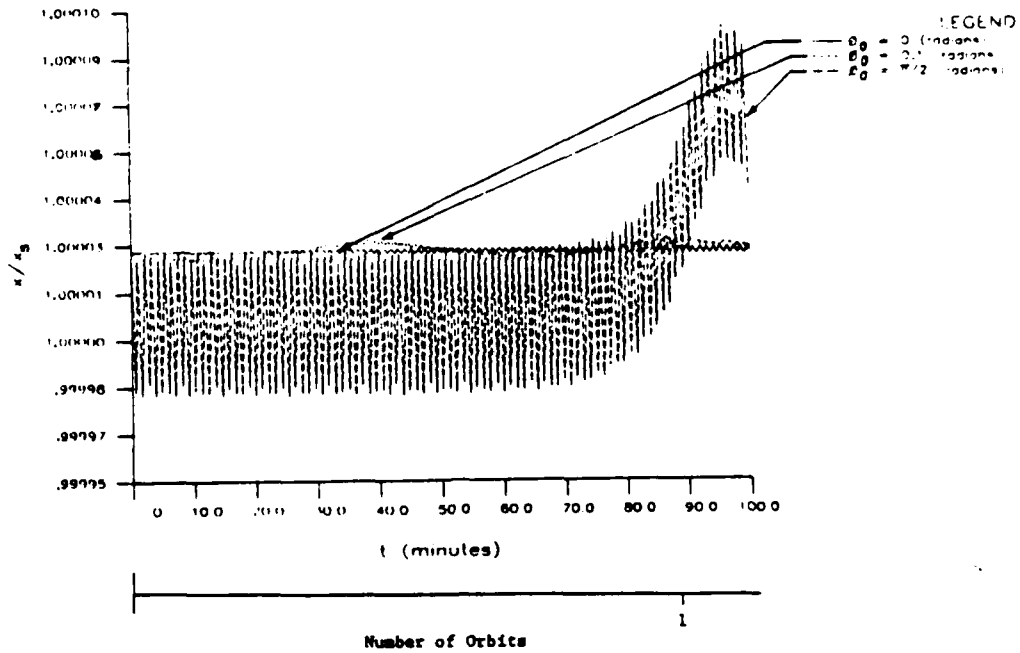

(a)

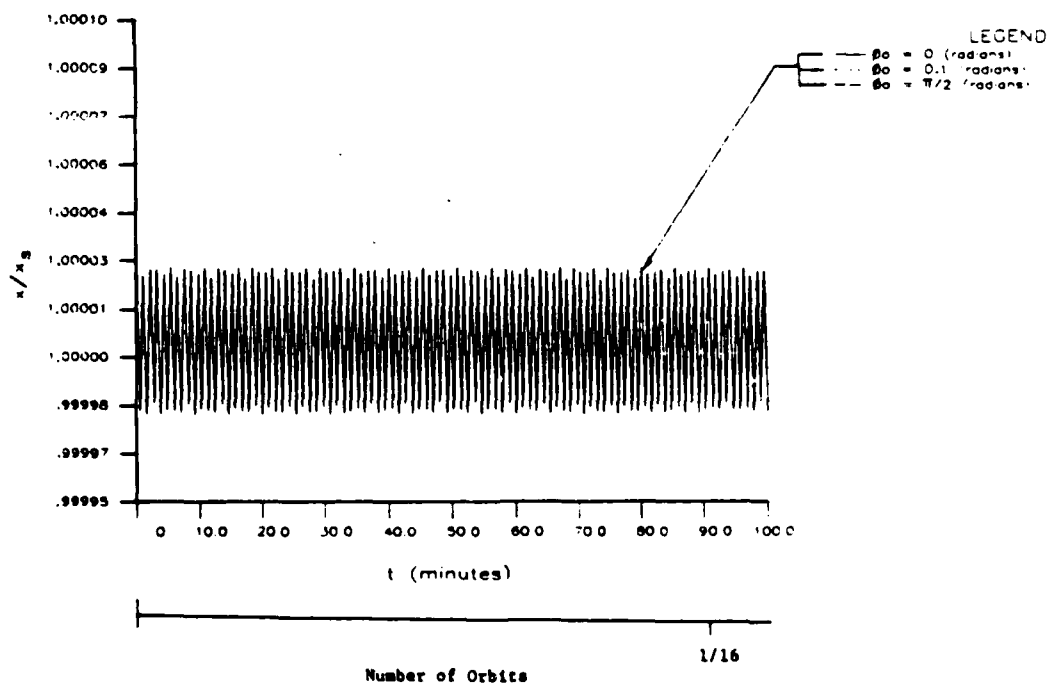

(b)

Figure 22. Effects of initial libration angle (ϕ_0) on axial length (x): Circular orbit at altitude (a) 200 km, (b) 35900 km

length. The period of vibration in x is approximately 1.1 minutes. The step size used for the computations is 0.2 minutes. The plots in Figure 22(a) are shown for only 100 minutes whereas the computer data are obtained for 400 minute duration. The trend of oscillation in x remains the same as shown in the plot for duration after 100 minutes, too.

The initial libration angle ($\emptyset_0$) has very significant effects on the attitude motion ($\emptyset$) of the space structure. When $\emptyset_0$ = 0.1 radians, $\emptyset$ oscillates about the r_c vector (local vertical) sinusoidally with a constant period and with a constant amplitude equal to its initial amplitude (Figure 23(a) and (c)). The angular rates ($\dot{\emptyset}$) of the dumbbell vary from zero to nearly 0.205×10^{-3} radians per second. The orbital period for this run is 88.4 minutes, and the period of libration is 51.2 minutes, the ratio of these periods being 1.7266 (approximately $\sqrt{3}$). The small difference between this value and the value of $\sqrt{3}$ (1.73205) is mainly due to the approximation made in intrapolation to obtain the orbital period and libration period from the computer run. It can therefore be concluded that the ratio of orbital to libration period is indeed $\sqrt{3}$ as predicted by Klemperer and Baker for a rigid dumbbell [45], and by Hall and Smith for an axially flexible dumbbell [79]. For a larger initial libration angle ($\emptyset_0$) equal to $\pi/2$, the variation of $\emptyset$ with time is seen to have nearly a

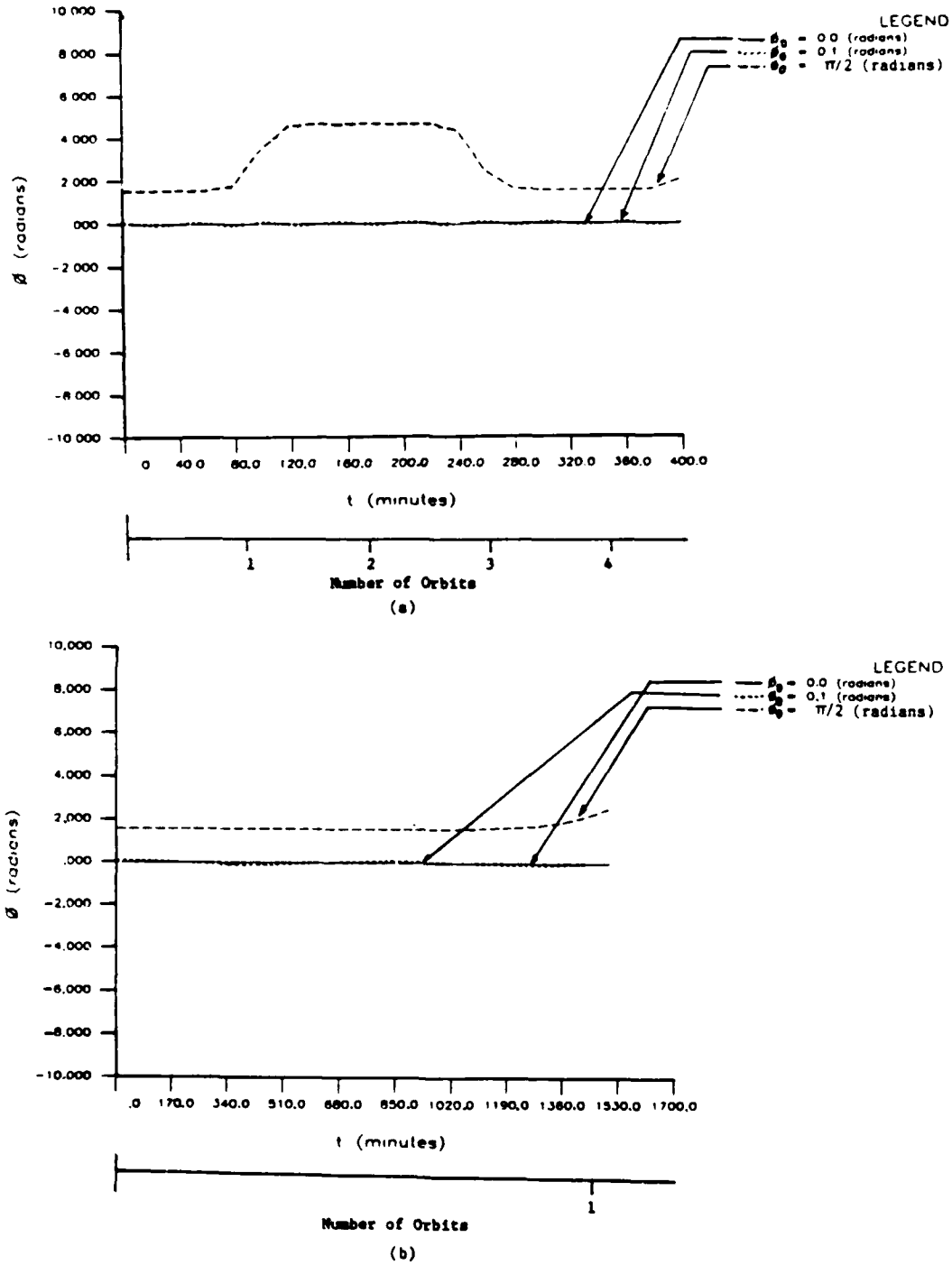

Figure 23. Effects of initial attitude angle (ϕ_0) on attitude (ϕ): Circular orbit at altitude (a) 200 km, (b) 35900 km, (c) 200 km (scale in ϕ enlarged), (d) 35900 km (scale in ϕ enlarged)

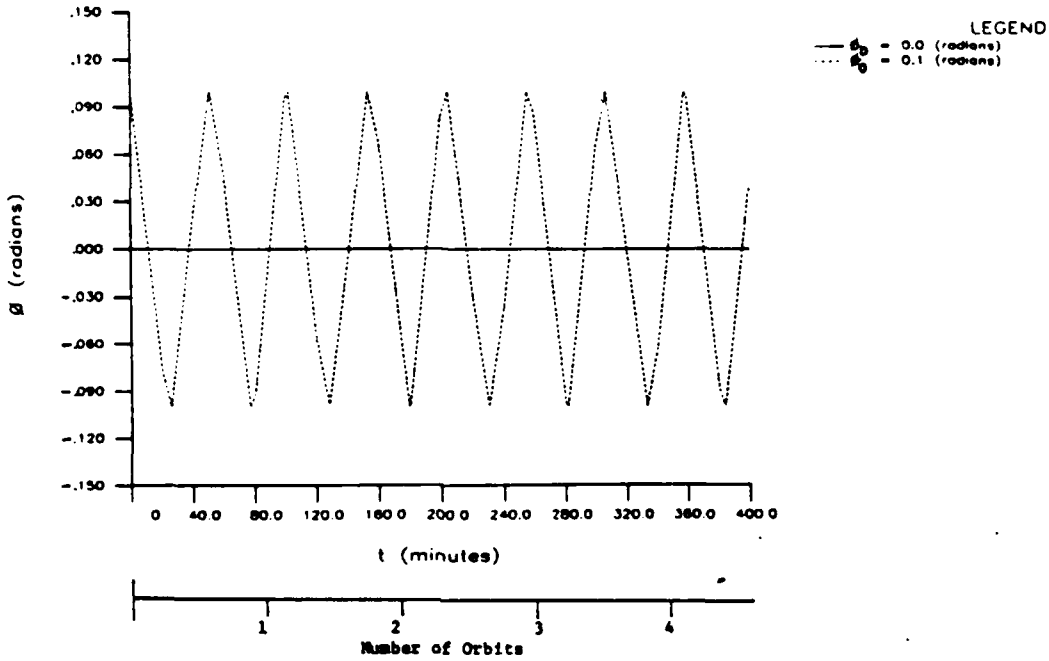

(c)

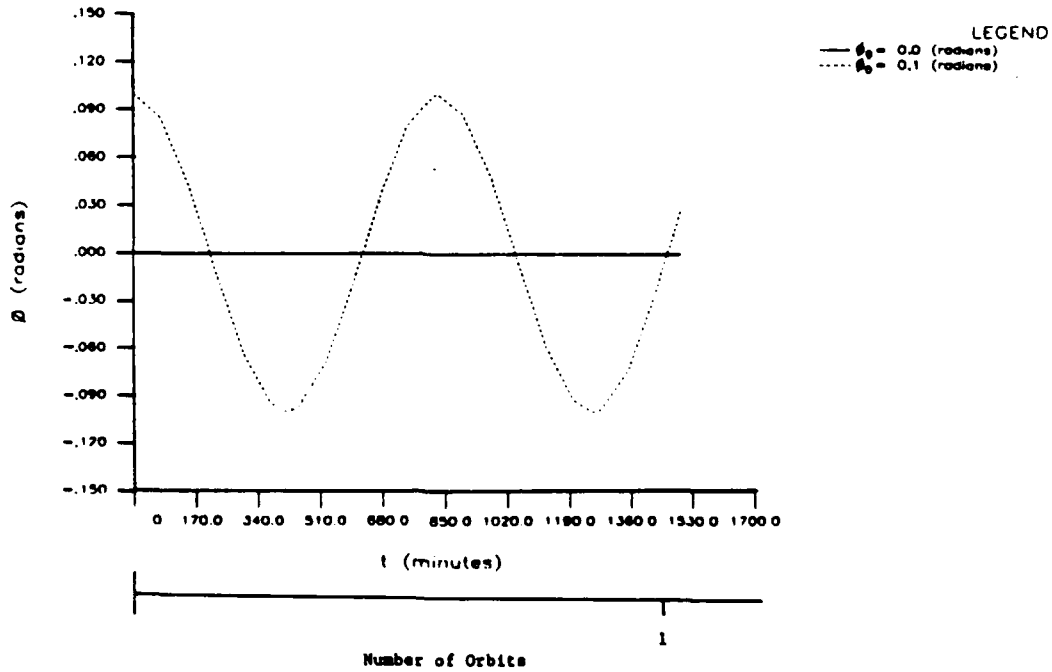

(d)

Figure 23. (Continued ...)

rectangular distribution (Figure 23 (a)). Figure 23(a) shows that Ø for the structure now essentially remains constant at either of two values, one at the minimum value of approximately $\pi/2$ radians, and the other at the maximum value of approximately $3\pi/2$. The transition from one position to the other takes place in a relatively short period of time (approximately 40 minutes) compared to the total period of libration in Ø (approximately 260 minutes). This total period of libration in Ø is greater than twice the orbital period. The dumbbell is thus found to be oscillating very slowly about the r_c-vector in the $Ø = \pi$ position.

Effects of Initial Axial Deformation

The simultaneous equations of motion are solved for three additional initial values of x (x_0/x_s = 1.01, 1.05, and 0.975). Example No. 10 through 12 in Table 2(a) give the complete initial conditions for these runs. The computer runs are made for approximately 4.5 orbits (400 minutes) with step size for numerical integration equal to 0.2 minutes. Figure 24(a) shows a plot of $\Delta F_g/F_{g0}$ versus time for x_0/x_s equal to 1.000023 (equilibrium value), 1.01, and 1.05 the during first 100 minute period. The same oscillation pattern continues for the rest of the run. This plot shows that ΔF_g oscillates about its

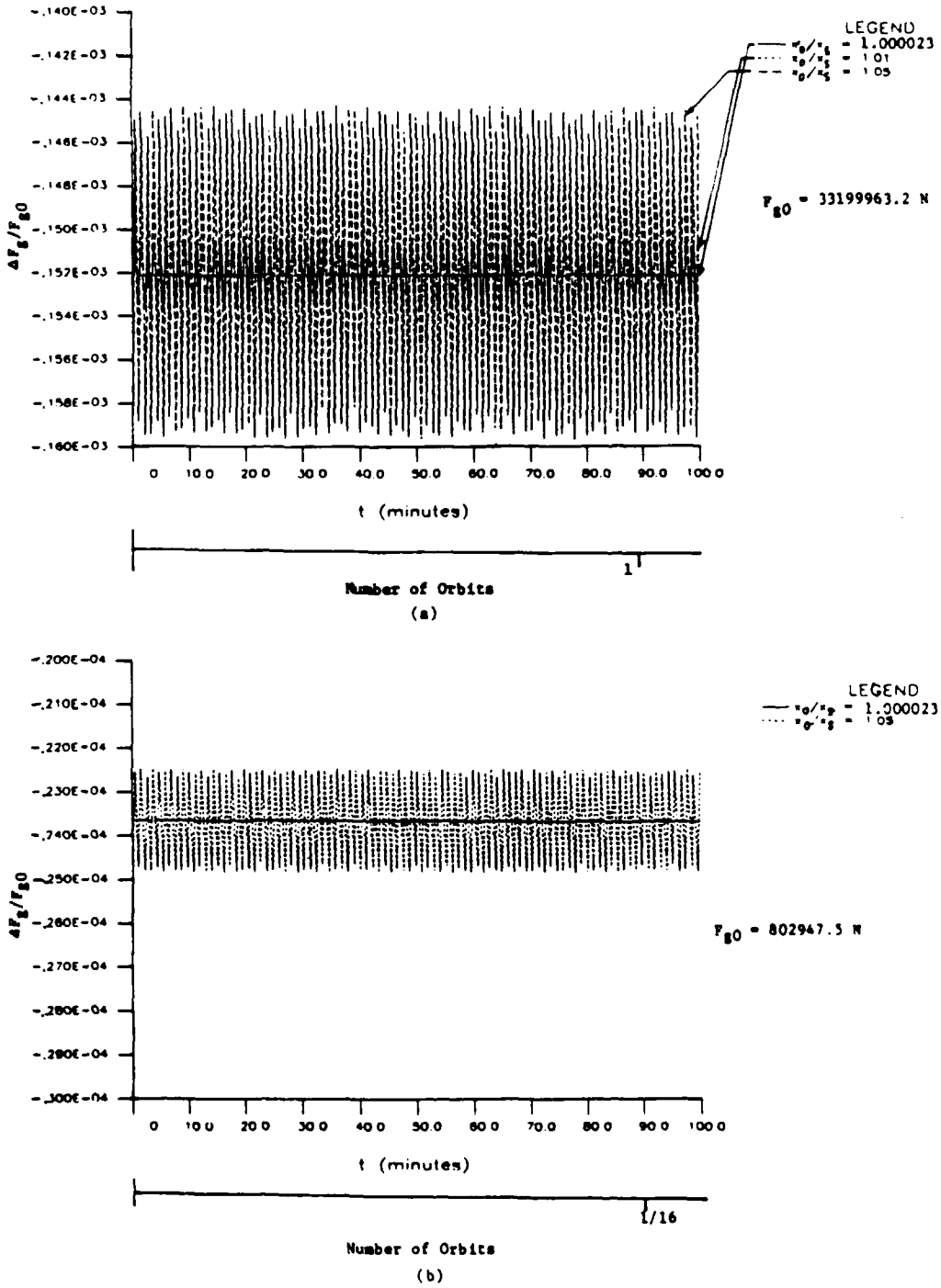

Figure 24. Dependency of differential gravitational force (ΔF_g) on initial axial deformation (x_0/x_s): Circular orbit altitude (a) 200 km, (b) 35900 km

equilibrium value equal to (when x_0/x_s = 1.000023) as a larger initial axial deformation is introduced. The larger the initial axial deformation, the larger becomes the amplitude of oscillation of $\Delta F_g/F_{g0}$. The oscillation in $\Delta F_g/F_{g0}$ is of approximately constant amplitude of magnitude 0.0015 x 10^{-3} for x_0/x_s = 1.01, and 0.00789 x 10^{-3} for x_0/x_s = 1.05 relative to the equilibrium value. The periods of oscillation are approximately 1.1 minutes for all values of x_0/x_s. For x_0/x_s = 0.975 (which is below the equilibrium value), the oscillation pattern is similar to when x_0/x_s is above the equilibrium values (x_0/x_s = 1.01 and 1.05), but these two oscillations are out of phase.

The computer results show that the orbit remains unperturbed in all respects for all values of initial axial deformation (x_0-x_s) of the structure. The orbit is circular at 200 km altitude and has a period approximately 88.4 minutes.

The contributions of x_0 are quite significant in perturbing the axial length (x) of the space structure. Figures 25(a), 25(b), and 26(a) show the plots of x/x_s versus time for x_0/x_s = 1.01, 0.975, and 1.05, respectively. All of these figures also contain a plot of x/x_s versus time for x_0/x_s = 1.000023 representing the equilibrium (steady state) configuration. These plots show that x oscillates sinusoidally with a constant period of 1.1

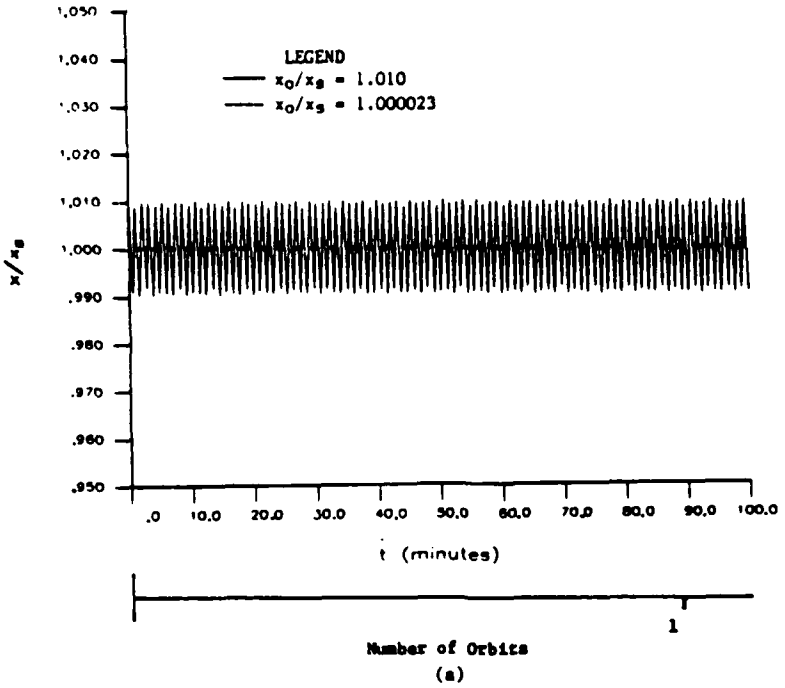

(a)

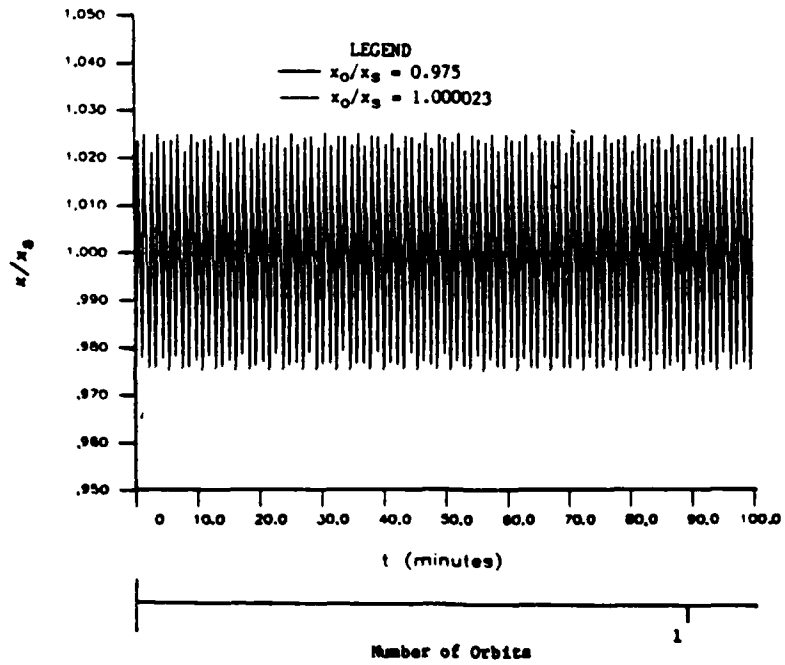

(b)

Figure 25. Effects of initial axial deformation (x_0/x_s) on oscillation of axial length (x): Circular orbit at altitude 200 km (a) x_0/x_s = 1.01, (b) x_0/x_s = 0.975

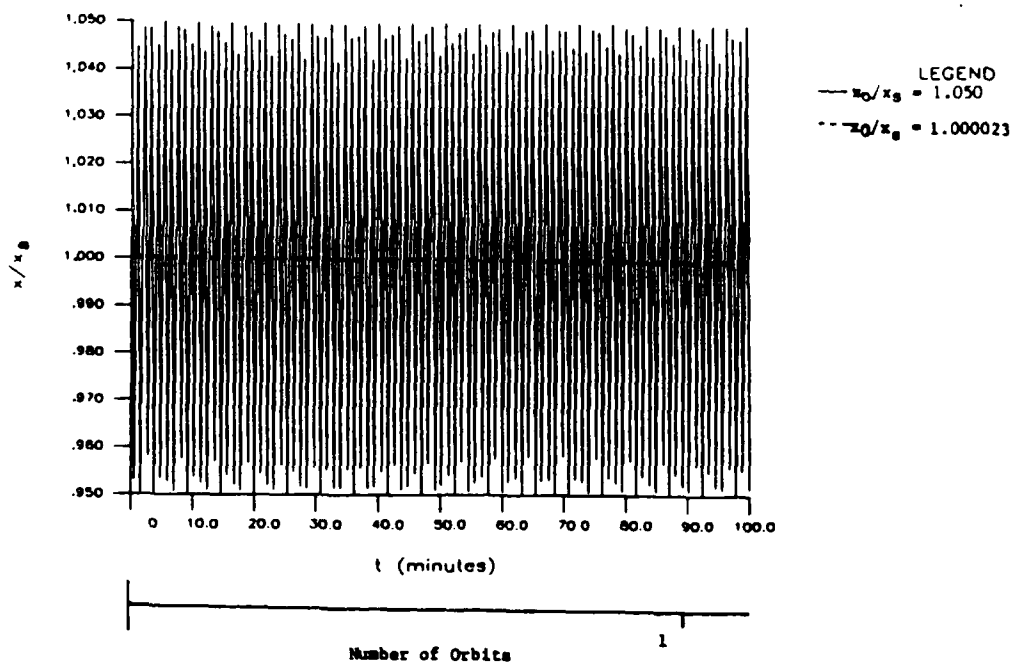

(a)

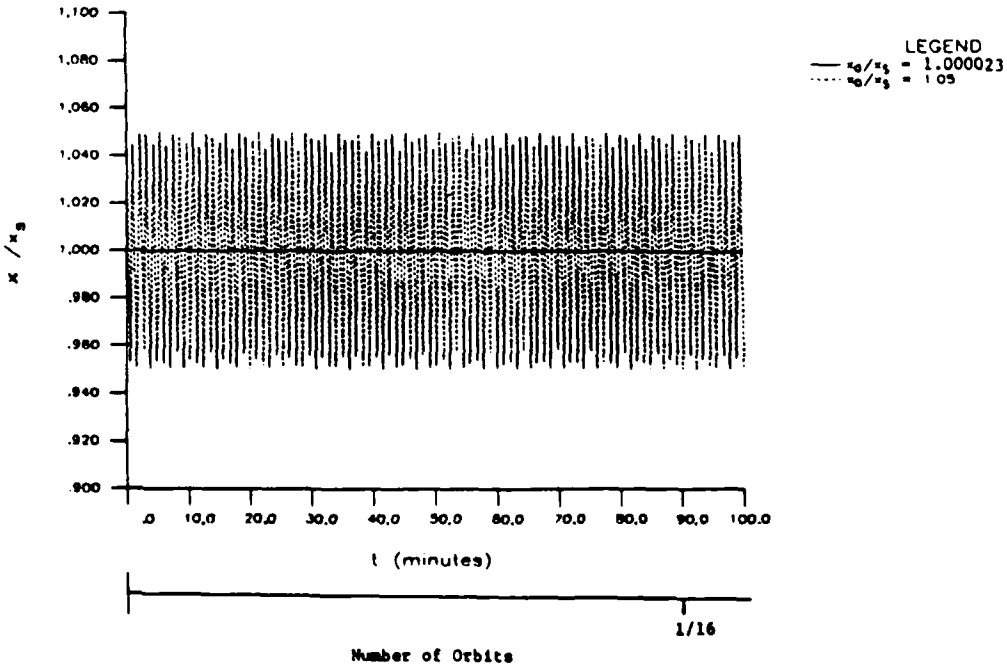

(b)

Figure 26. Effects of initial axial deformation (x_0/x_s) on oscillation of structural axial length (x): Circular orbit at altitude (a) 200 km, (b) 35900 km

minutes and with a constant amplitude of initial deformation (x_0-x_s). The rate of deformation ($\dot{x}$) of the axial length (x) of the dumbbell varies from zero to 1.28, 0.256, and 0.66 kilometer per minutes for x_0/x_s equal to 1.05, 1.01 and 0.975 respectively.

Figure 27(a) shows the plot of Ø versus time for x_0/x_s = 1.00023, 1.01, 1.05, and 0.975. That figure shows that the larger initial deformation produces a larger magnitude of oscillation in Ø. The dumbbell oscillates sinusoidally about the radial vector (local vertical). The periods of oscillation in Ø are the same for all values of x_0/x_s, approximately 51.0 minutes. The amplitudes of oscillation are constant at values of approximately 0.0616 radians for x_0/x_s = 1.05, at 0.0117 radians for x_0/x_s = 1.01, and at 0.028 radians for x_0/x_s = 0.975. The angular rates ($\dot{Ø}$) of the dumbbell about the local vertical vary from zero to nearly 0.015, 0.0028, and 0.0066 radians per minute for x_0/x_s = 1.05, 1.01 and 0.975, respectively.

Effects of Orbit Eccentricity

In addition to the circular orbit, two more elliptical orbits are now considered to study the effects of orbit eccentricity. In the first case, $\dot{\theta}_0$ is slightly increased

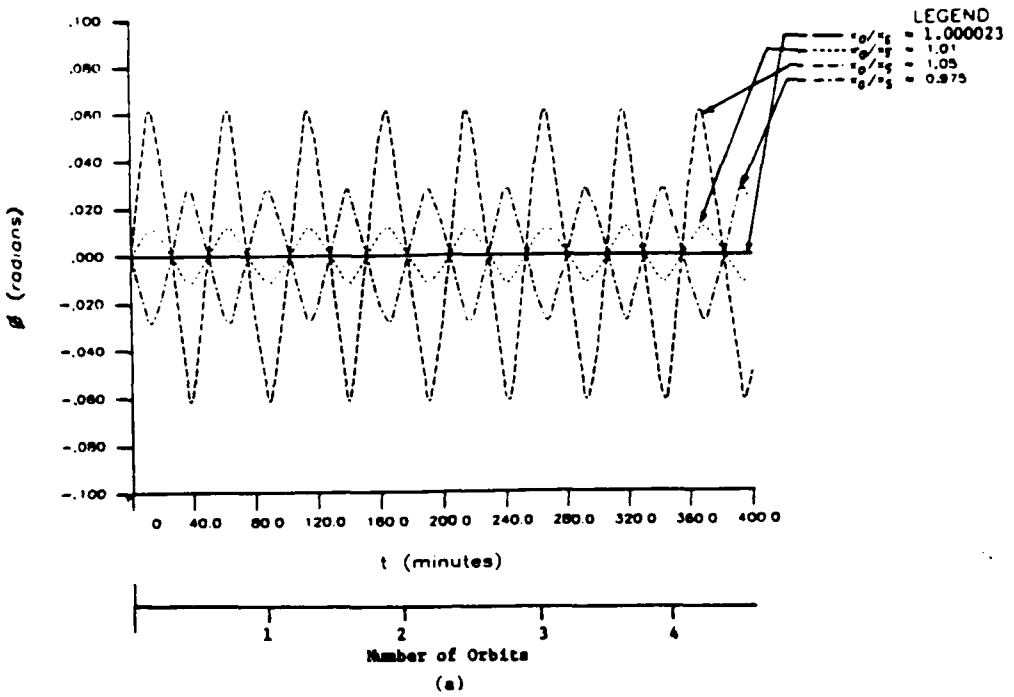

(a)

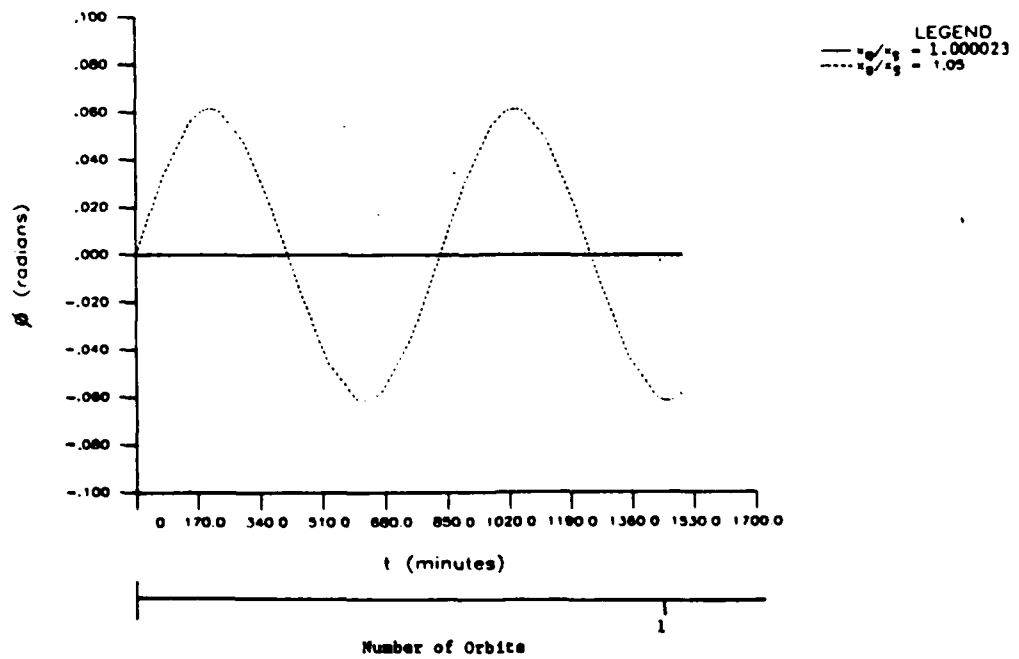

(b)

Figure 27. Effects of initial axial deformation (x_0/x_s) on oscillation of attitude motion (Ø): Circular orbit at altitude (a) 200 km, (b) 35900 km

to a value of 0.0738 radians per minute to obtain an elliptical orbit with small eccentricity ($e \approx 0.0785$). The period of such orbit is approximately 100 minutes (Table 3). The distance from the center of the earth to the apogee of the orbit is approximately 7694.6759 km, and to perigee is 6574.3300 km, which is the initial value of r_c. In the second case, to obtain a fairly large eccentric orbit ($e \approx 0.56$), the value of $\dot{\theta}_0$ is further increased to 0.08883 radians per minute. The period of the orbit is approximately 305.6 minutes (Table 3). The perigee of the orbit is at $r_c = 6574.33$ km, and apogee is at $r_c =$ 23,483.013 km. The complete set of initial conditions for these runs is indicated by Example No. 14 and 15 in Table 2(a). Figures 28(a), 28(b), and 30(a) show the plots of r_c/r_0, θ, and $\dot{\theta}$ versus time, respectively for these elliptical orbits along with the ideal circular orbit at $r_c = 6574.33$ km (200 km altitude). The solution of the complete equations of motion is obtained for 400 minutes. The step size chosen for the computations is 0.2 minutes.

By increasing the eccentricity (e) of an orbit, we are increasing the value of r_c. The differential gravitational force (ΔF_g) therefore will be reduced with an increase in e. Figure 31(a) shows a plot of $\Delta F_g/F_{g0}$ versus time during the 400 minute journey of the space structure into orbit. The magnitude of $\Delta F_g/F_{g0}$ is minimum at the apogee point for both elliptical orbits as the value of r_c

Table 3 : Orbit Characteristics and Earth's Shadow Entry and Exit Locations

The space structure starts its motion in an orbit from perigee altitude at $\theta = 0$

Orbit Characteristics				Earth Shadow Entry and exit points			
Perigee Altitude (km) *	Apogee Altitude (km)	Orbit Period (minutes)	Orbit Type	Altitude (km)	θ measured from Perigee (radians)	Time (minutes)	Entry/Exit
200.00 (LEO)	200.00	88.4	circular (e = 0)	200.00	1.8192107 4.4698577 8.108279 10.7518199 14.3902414 17.033782 20.6722 23.31572	25.6 62.9 114.1 151.3 202.5 239.7 290.9 328.1	entry exit entry exit entry exit entry exit
35900.0 (GEO)	35900.0	1441.7	circular (e = 0)	35900.0	2.990583 3.293041	686.2 755.6	entry exit
200.00	1320.35	100.0	elliptical (e = .0785)	-	-	-	-
200.00	17108.7	305.6	elliptical (e = .56)	15913.2 15907.3 15914.4	2.851831 3.432198 9.135086	112.6 193.1 418.2	entry exit entry
35900.0	43102.1	1629.8	elliptical (e = .0785)	-	-	-	-

LEO Low Earth Orbit (at an altitude of 200 km from the surface of the earth)
GEO Geosynchronous Earth Orbit (at an altitude of 35900 km from the surface of the earth)
* Distance of the space structure from the surface of the earth

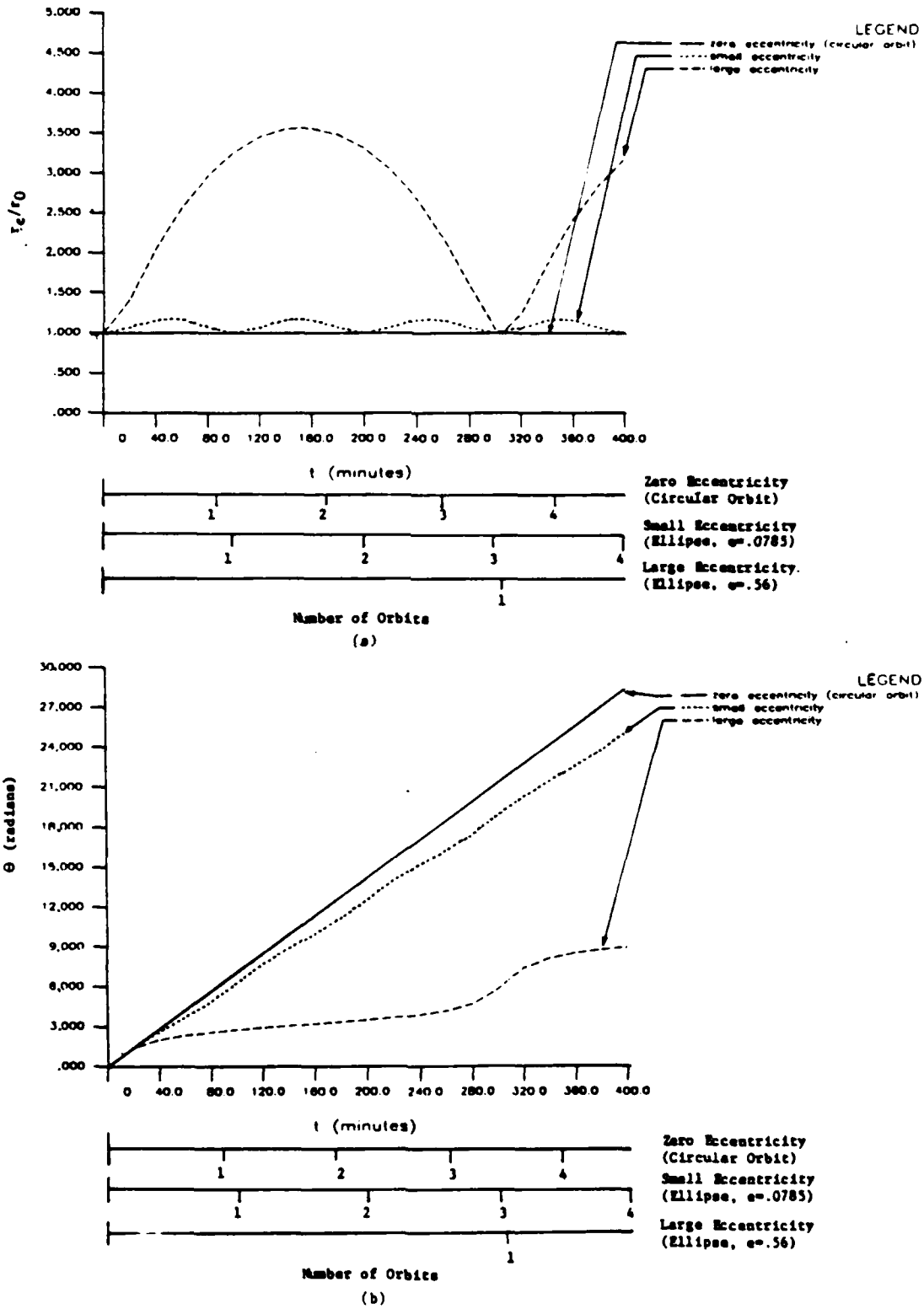

Figure 28. Variation of (a) r_c, (b) θ_0: Circular and elliptical orbits at perigee altitude 200 km

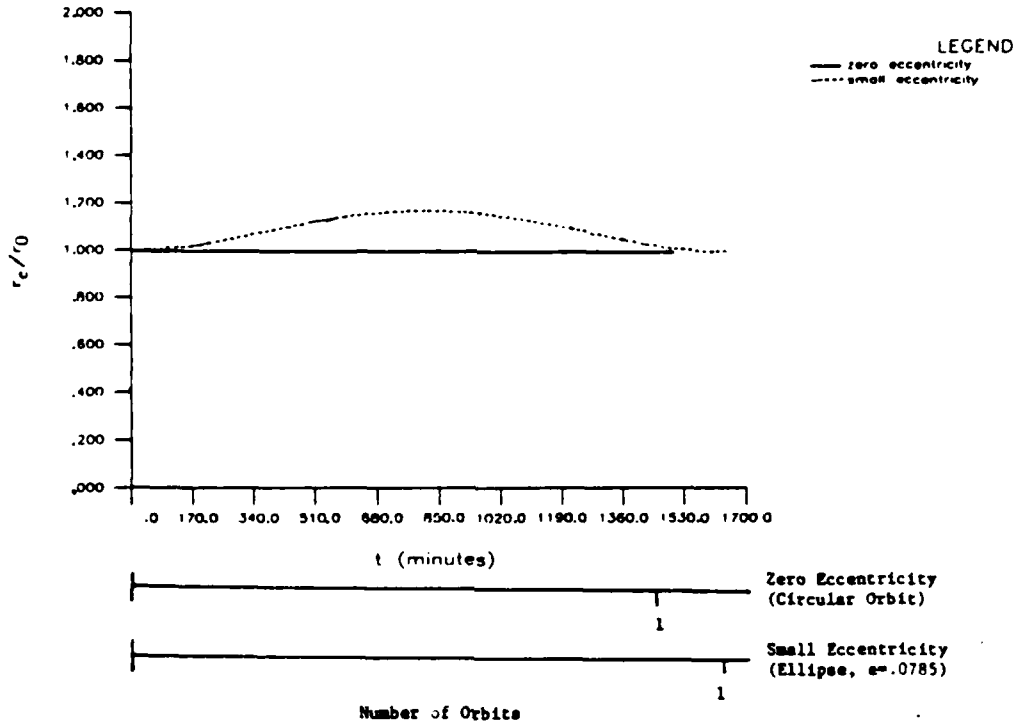

(a)

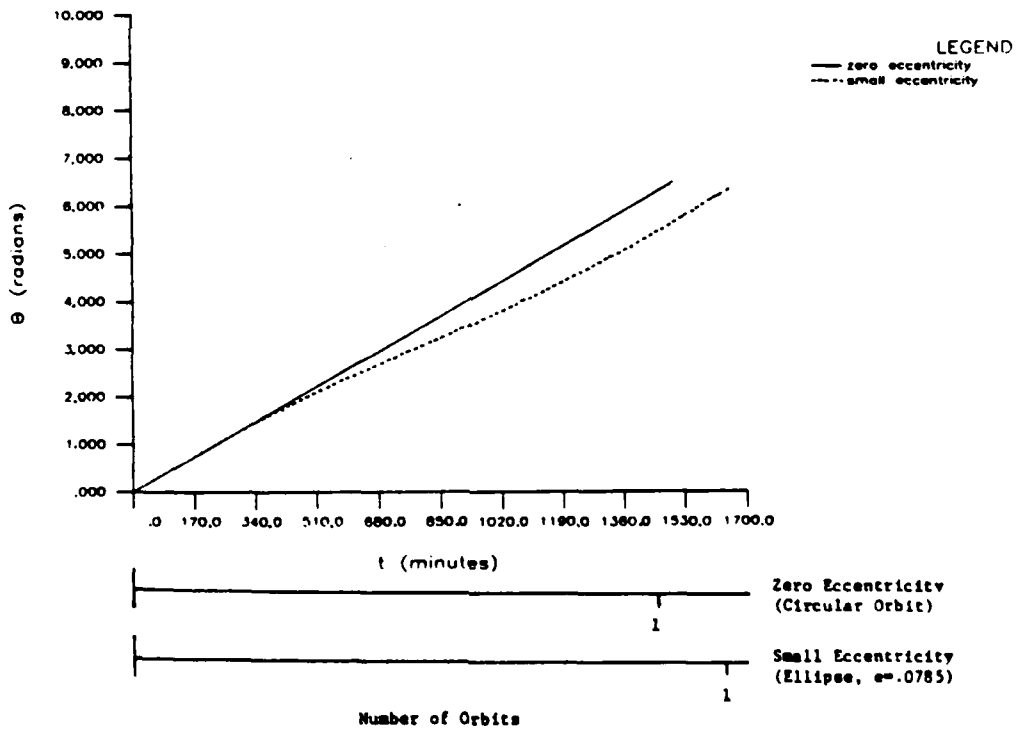

(b)

Figure 29. Variation (a) r_c, (b) θ: Circular and elliptical orbits at altitude 35900 km

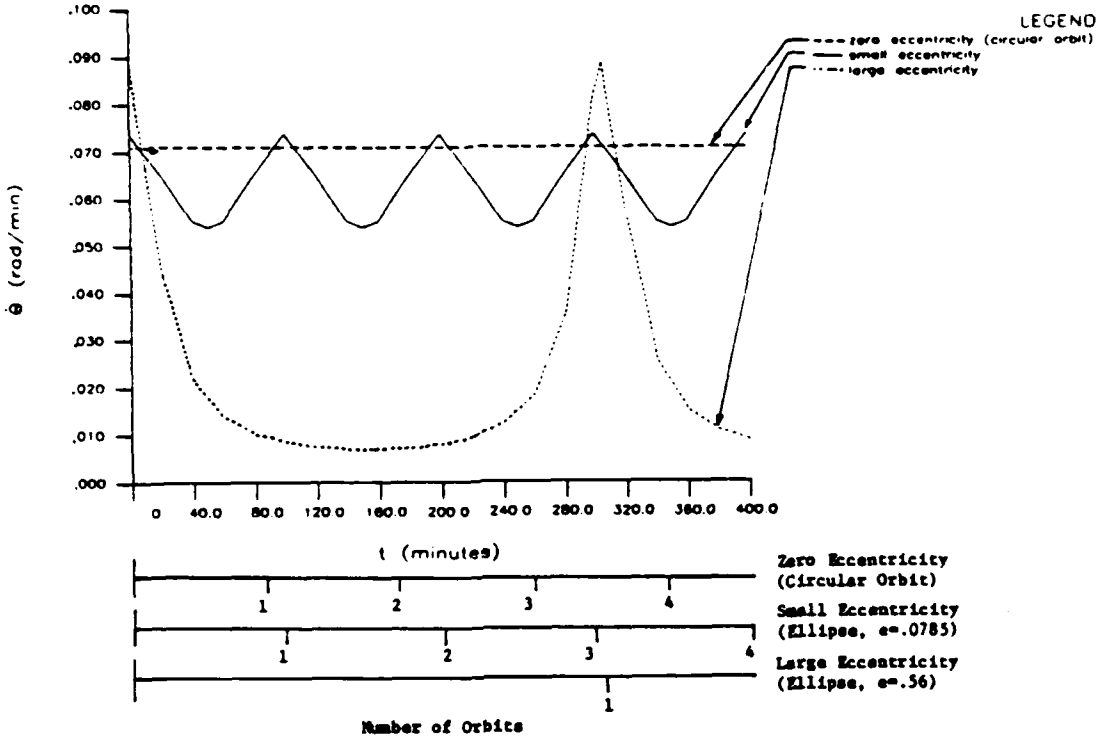

(a)

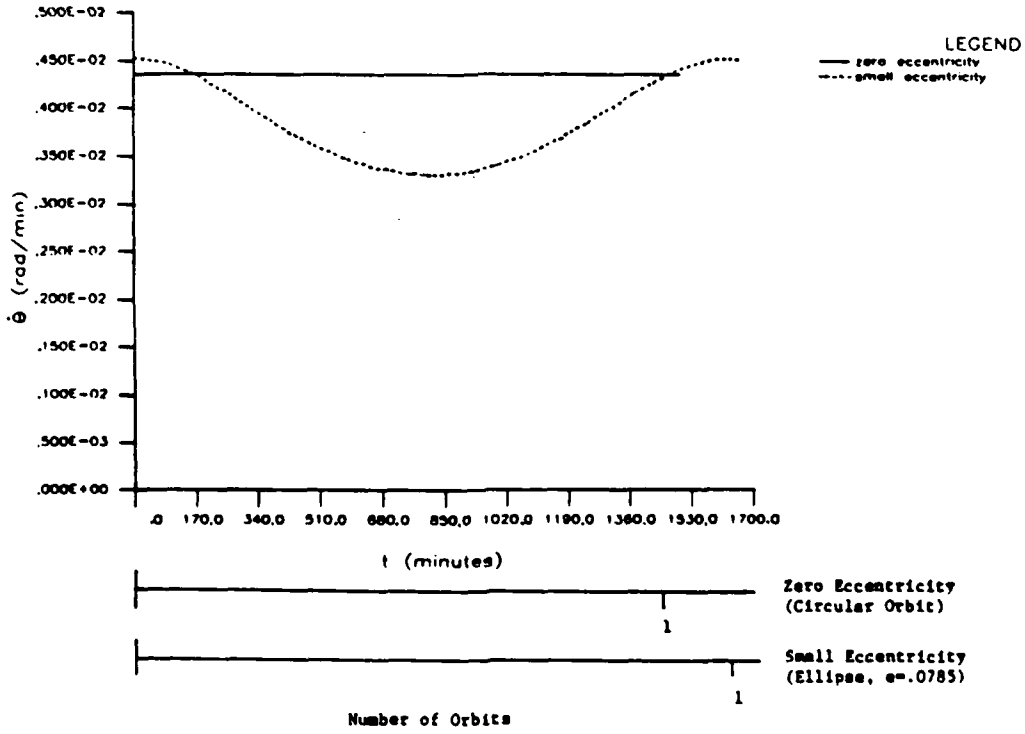

(b)

Figure 30. Variations of angular velocity ($\dot{\theta}$) at altitude (a) 200 km, (b) 35900 km: Circular and elliptical orbits

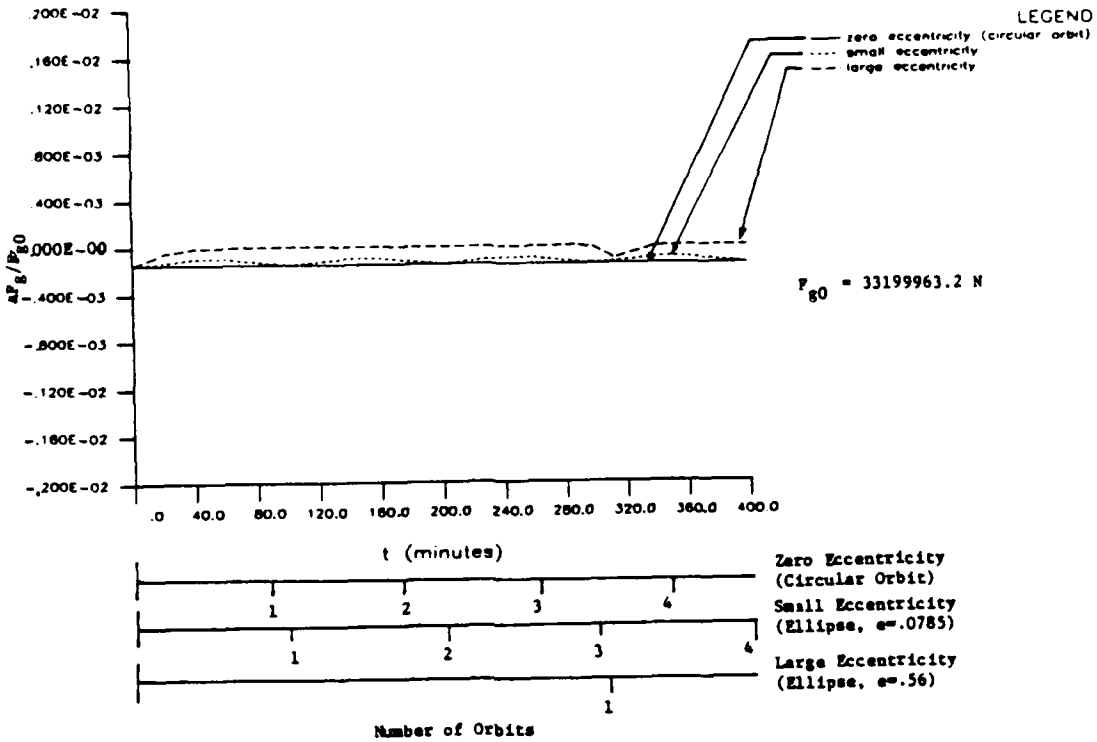

(a)

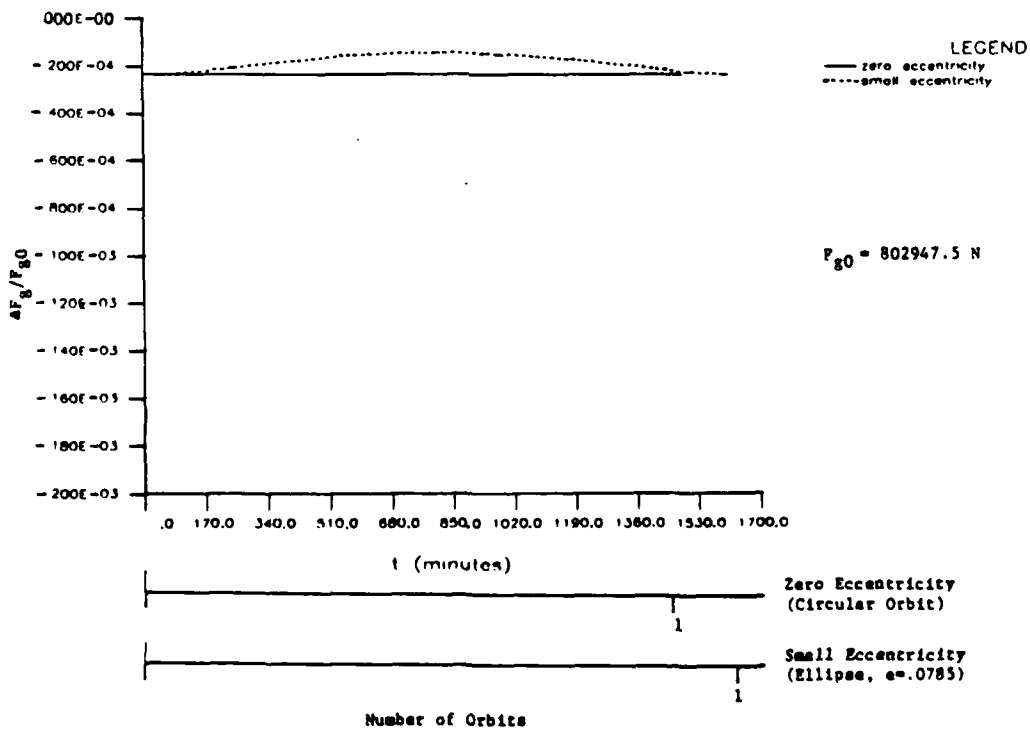

(b)

Figure 31. Dependency of differential gravitational force (ΔF_g) on orbit eccentricity (e) at altitude (a) 200 km, (b) 35900 km

is maximum at this point. For the larger eccentric orbit (e = 0.56), $\Delta F_g/F_{g0}$ is nearly zero around the orbit except near the perigee points. For the smaller eccentric orbit (e = 0.0785), the magnitude of $\Delta F_g/F_{g0}$ is 0.9782×10^{-4} at apogee. The value of $\Delta F_g/F_{g0}$ equal to 0.15211×10^{-3} at the perigee points is the same as that for an ideal circular orbit at 200 km altitude.

Figure 32(a) shows the plot of x/x_s versus time for both the elliptical orbits and the ideal circular orbit. The effects of the orbit eccentricity are quite apparent from the figure in which two different types of oscillation in x/x_s can be seen. One is the fine, closely spaced, small amplitude oscillation in x, which is due to the fact that the value of x_0 (equal to 1.000023 km) used in the computations is not the exact value of x_0 which satisfies the equilibrium steady state but an approximation within the rounding off and truncation of numbers after sixth significant figure after the decimal point. In subsequent time, this error produces some oscillation in Ø. This oscillation in Ø, in turn, causes larger amplitude of oscillation in x/x_s. Such small oscillation in x/x_s exits in alleven in zero eccentric orbit (circular orbit) (Figure 32(a)). The period of such oscillation in x/x_s is about 1.1 minutes. For circular and near circular (small eccentric) orbits, the amplitudes of the oscillation increase with time. However, for a large eccentricity orbit

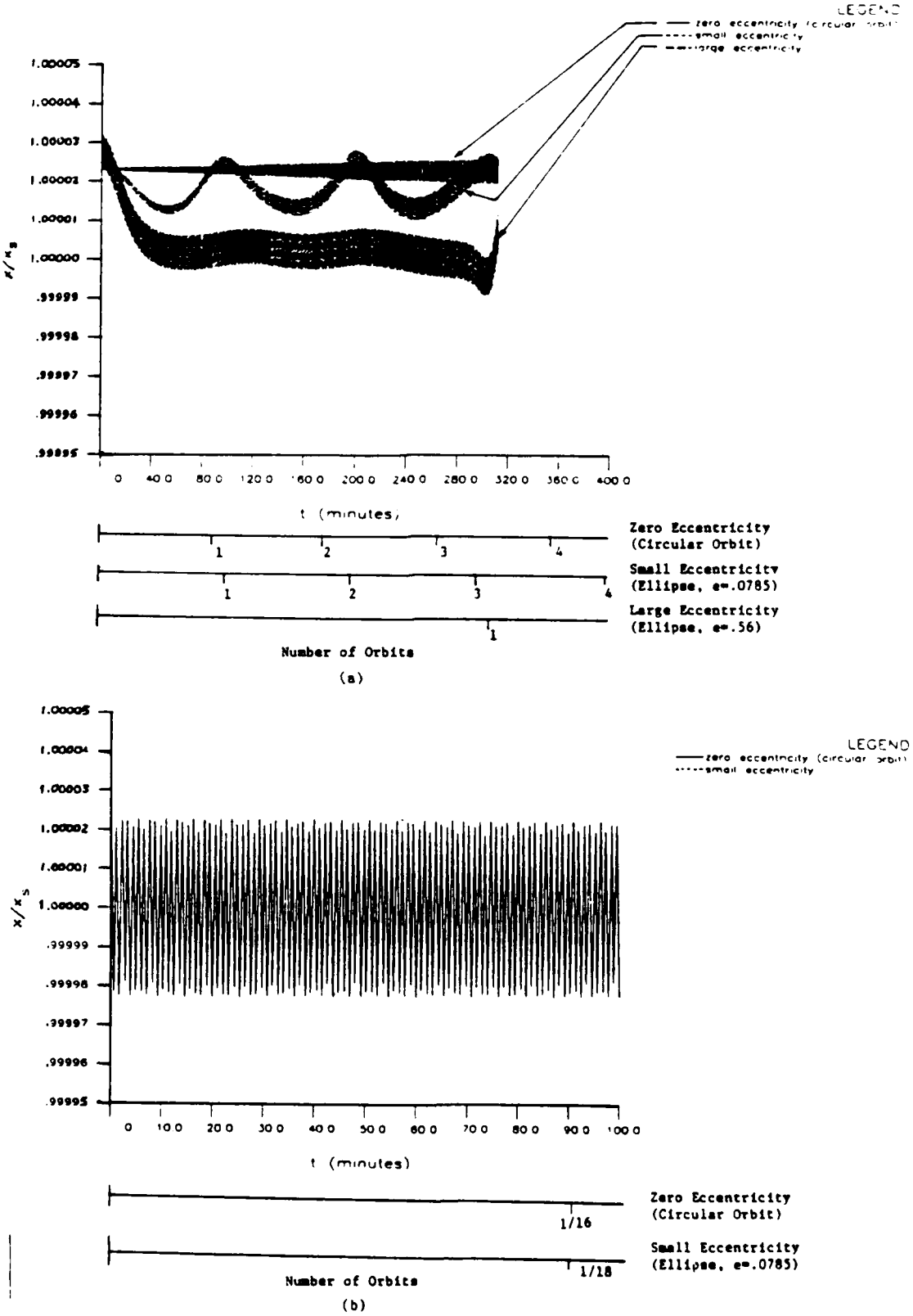

Figure 32. Effects of orbit eccentricity (e) on oscillation of axial length (x) at altitude (a) 200 km, (b) 35900 km

(e = 0.56), the maximum amplitudes of vibration remain almost constant with time. The increase in orbit eccentricity increases the amplitudes of such oscillation in x/x_s, but it does not affect the period of oscillation. The second kind of oscillation in x/x_s, which has larger amplitude and longer period of oscillation, is mainly due to the orbit eccentricity. For small eccentricity (e = 0.0785), x/x_s oscillates between approximately 1.000028 and 1.000010 with period approximately 100 minutes. For the larger eccentricity (e = 0.56), the structural length decreases quickly to its static length (x_s = 1.0 km) and remains at this value until it approaches the next perigee point in the orbit at which the structural length increases quickly to exceed its initial value. The period of this kind of oscillation in x is more than the orbital period (305.6 minutes). The maximum change in length of the structure in any case is still not significant being only 0.0028 percent of the initial x.

More significant is the effect of the orbit eccentricity (e) on the attitude motion (Ø) of the space structure. Increasing the eccentricity means introducing larger libration in Ø. Figure 33(a) shows a plot of Ø versus time for the circular orbit (e = 0), and the elliptical orbits with e = 0.0785 and e = 0.56. Figure 33(c) shows the same plot in enlarged scale for Ø. Eccentricity of an orbit causes the same kind of effects on

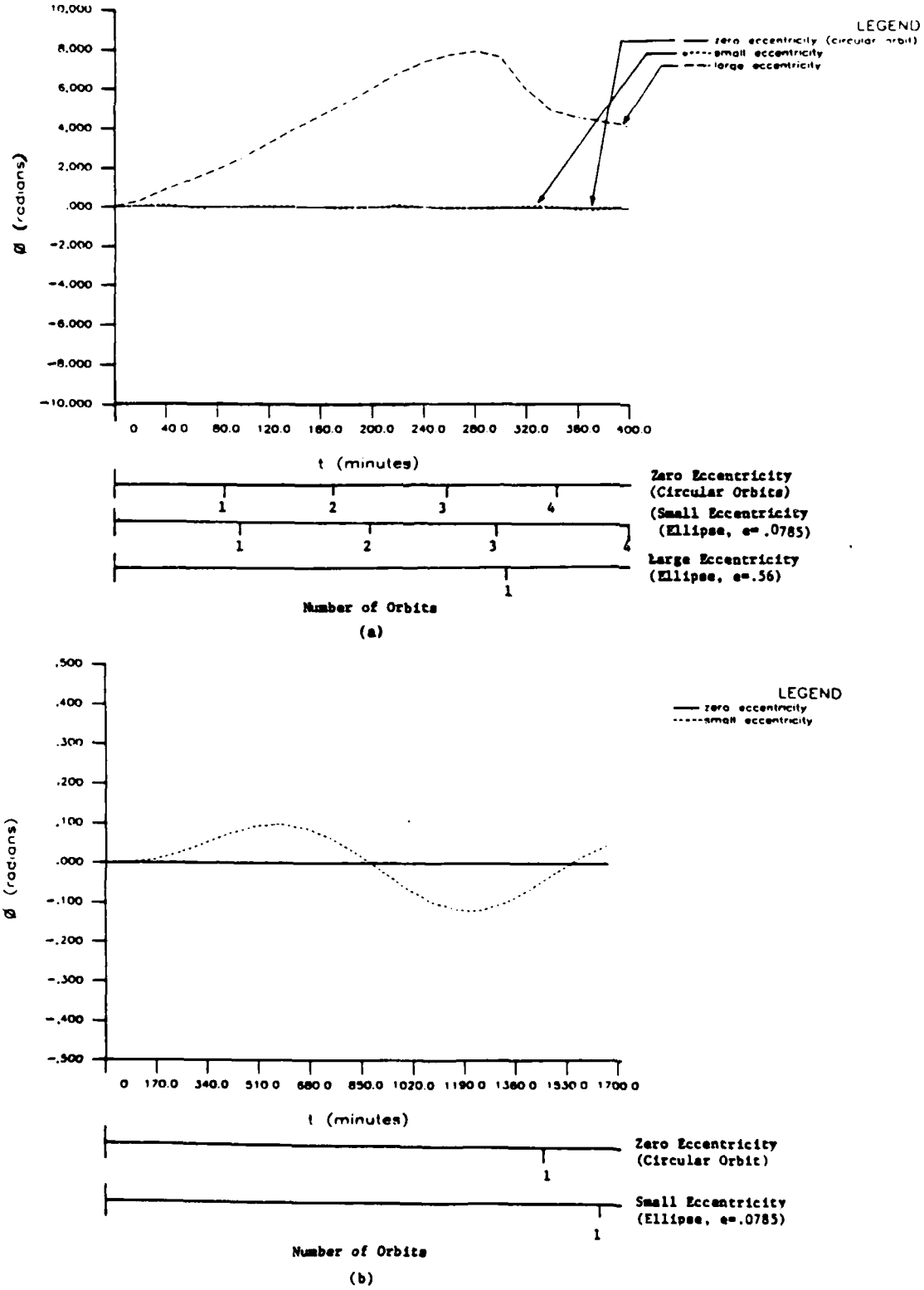

Figure 33. Effects of orbit eccentricity (e) on attitude (Ø) at altitude (a) 200 km, (b) 35900 km, (c) 200 km (scale in Ø enlarged)

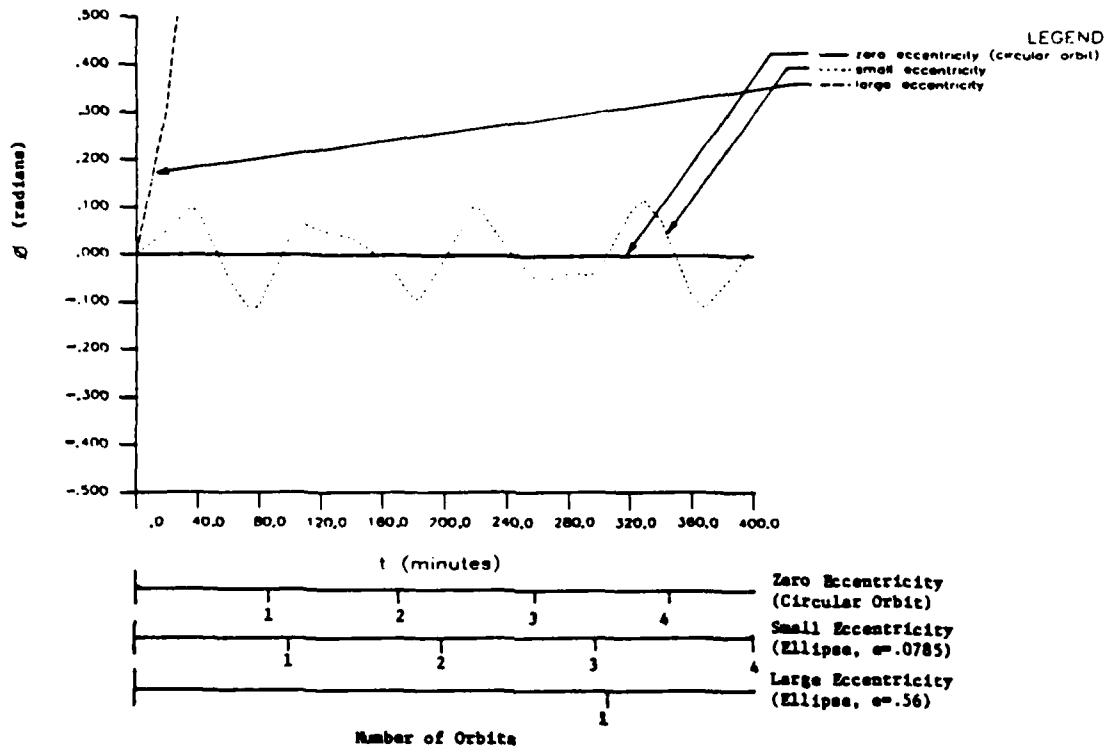

(c)

Figure 33. (continued ...)

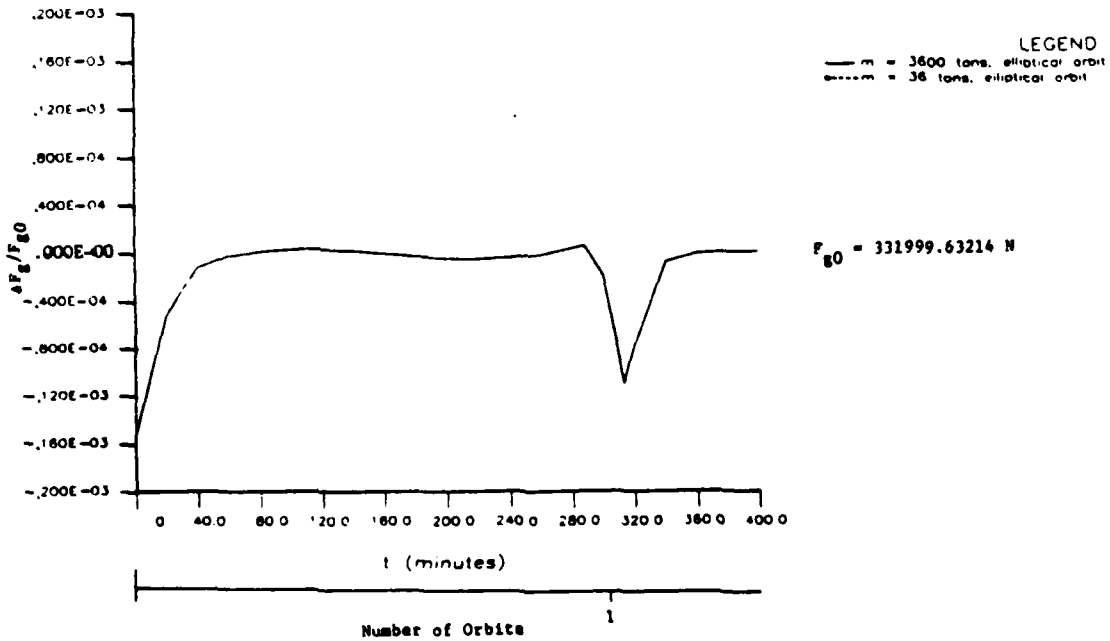

Figure 34. Dependency of differential gravitational force (ΔF_g) on total dumbbell mass (m): Elliptical orbit with eccentricity (e = 0.56) and perigee altitude = 200 km

$\emptyset$ as does increasing the initial libration angle ($\emptyset_0$). For the slightly eccentric orbit, $\emptyset$ oscillates about the local vertical. The amplitudes and period of oscillation in $\emptyset$ do not remain constant however. For example, in the first orbit, the dumbbell oscillates between $\emptyset$ equal to approximately 0.09760 radians and -0.12051 radians with period equal to 94.4 minutes; whereas in the third orbit, it oscillates between $\emptyset$ equal to approximately 0.1082 radians and -0.05674 radians with period equal to 105.4 minutes. For the large eccentricity orbit (e = 0.56), the dumbbell keeps rotating about its center of mass continuously up to the maximum value of $\emptyset$ equal to 7.9889 radians at time, t = 282.4 minutes. After reaching this value, $\emptyset$ is seen to decrease (Figure 33(a)). The dumbbell may therefore tumble continuously if the orbit eccentricity is increased above some critical value.

Effects of Altitudes

To this point the analysis has been carried out in a low earth orbit (LEO) at an altitude of 200 km from the surface of the earth (r_0=6574.33km). To study the effects of the altitudes on the space structure's motion and deformation, the solution of the equations of motion has been obtained by deploying the structure in the geosynchronous orbit (GEO) at an altitude of 35900 km from

the surface of the earth (i. e., r_0 = 42274.33 km) for various initial conditions and values of the physical parameters as was done for the LEO. The initial value ($\dot{\theta}_0$) of $\dot{\theta}$ is accordingly changed to 0.00435818 radians per minute to obtain a circular orbit at the higher altitude of r_0 = 42274.33 km. For the first computer run at this higher altitude (GEO) all other initial conditions and the values of the physical parameters (Example No. 16, Table 2(a)) remain the same as in LEO (Example No. 1, Table 2(a)). The solution is obtained for 1500 minutes with time step for computations equal to 0.2 minutes. The orbit remains perfectly circular at the altitude of 35900 km with orbital period approximately 1441.7 minutes (Table 3).

Since the gravitational force is inversely proportional to the square of the distance of the space structure from the center of the earth, the total gravitational force (F_{g0}) on the structure is far less at this altitude than that in LEO. The value of F_{g0} is 8.029475×10^5 N in GEO, whereas it is 3.319996×10^7 N in LEO, the ratio of these values being equal to the ratio $r_c^2(\text{LEO})/r_c^2(\text{GEO})$ as expected. The value of the differential gravitational force (ΔF_g) is accordingly much smaller in GEO, and is approximately 19 N, whereas it is 5.046×10^3 N in LEO. However, the magnitude of $\Delta F_g/F_{g0}$ remains constant along the orbit as in LEO (Figure 15(b), m_1/m_2 = 1.0).

The value of x_0 (1.000023 km) is not an equilibrium

value for this altitude. Hence, the axial length of the structure now oscillates about its static length (x_s = 1 km) with constant amplitude equal to the initial deformation (0.000023 km) and with period equal to 1.1 minutes (Figure 16(b), m_1/m_2 = 1.0). Since any change in altitude disturbs the equilibrium configuration and gives rise to different values of ΔF_g and different variations in x, it is obvious that due to these changes the attitude motion (Ø) will be affected. Figure 17(b) shows a plot for Ø versus time for m_1/m_2 = 1.0. The dumbbell oscillation about its local vertical is very distinct now. This same plot gives a nearly horizontal straight line distribution in the case of the orbit at the lower altitude. The amplitude of oscillation in Ø is approximately 0.265×10^{-4} radians, and the period of oscillation is about 832.3 minutes. The larger amplitude of oscillation in Ø of the dumbbell may have been caused also because of the weaker restoring torque developed owing to the smaller gravitational pull at the higher altitude. The ratio of orbital period and liberation period is 1.7322 which is again approximately equal to $\sqrt{3}$.

<u>Influence of mass ratio and length.</u> At the altitude of GEO, the ratio x_s/r_0 is very small. (For x_s = 5 km, $x_s/r_0 = 0.118 \times 10^{-3}$). This may be the main reason that the effects of differential masses (the m_1/m_2 ratio) and the length (x_s) have no noticeable influence on Ø and x of the space structure. The complete initial conditions are

given under Example No. 16 through 19 in Table 2(a). Figures 15(b), 16(b), and 17(b) show respectively the plots of $\Delta F_g/F_{g0}$, x/x_s, and $\emptyset$ versus time for m_1/m_2 = 1, 3, and 1/3. Figures 18(b), 19(b), and 20(b) show respectively the plots of $\Delta F_g/F_{g0}$, x/x_s, and $\emptyset$ versus time for x_s = 1.0km and 5.0km. The differential gravitational force ΔF_g increases with increase in the (m_1-m_2) value. However, the distribution of ΔF_g again remains constant throughout the one orbit run for all m_1/m_2 ratios. Dependency of ΔF_g on x_s can be seen in Figure 18(b). A comparison of the plots in Figures 15(b) and 18(b) shows that the dependency of ΔF_g on x_s is not as sigificant as in the case of the m_1/m_2 values.

The length (x) of the space structure oscillates about its static length (x_s) for all m_1/m_2 ratios and x_s values with maximum amplitudes approximately equal to the initial axial deformation, that is, the (x_0-x_s) value (Figures 16(b) and 19(b)). However, in the case of the effects of x_s, the period of oscillation in x is about 1.1 minutes, which is the same as in the first run at this altitude where x_s = 1.0 km and m_1/m_2 = 1.0, whereas the period of oscillation in x is approximately equal to 3.4 minutes for each of the other values of the ratio m_1/m_2 (3 and 1/3). As far as the effects of the m_1/m_2 ratio and of x_s on $\emptyset$ are concerned, the effects are almost zero. In all cases, the amplitudes and period of oscillation in $\emptyset$

remain the same as mentioned for the first run (Example No. 16, Table 2(a)) above in GEO. For all these situations, the orbit remains completely circular at 35900 km altitude with the same orbital period of approximately equal to 1441.7 minutes.

Influence of initial attitude motion. As in LEO the computer results are obtained for two more values of ϕ_0 (0.1 and $\pi/2$ radians). Example No. 20 and 21 in Table 2(a) give the initial conditions used in these runs. The variation of $\Delta F_g/F_{g0}$ with time in GEO is similar to LEO (Figure 21 (b)). Here also, when ϕ_0 = 0.1 radians, $\Delta F_g/F_{g0}$ oscillates about the $\Delta F_g/F_{g0}$ value of -0.23656×10^{-4} corresponding to ϕ_0 = 0 radians. The amplitude of the oscillation lies between the two maximum values of approximately -0.2354×10^{-4} and -0.23656×10^{-4}. The period of oscillation is approximately 426.3 minutes. As in LEO for ϕ_0 = $\pi/2$ (Figure 21(b)), $\Delta F_g/F_{g0}$ remains almost constant for approximately the first 1106.0 minutes, the change in $\Delta F_g/F_{g0}$ in this period being from 0 to 0.9369×10^{-6}. The increase in $\Delta F_g/F_{g0}$ is more rapid toward the end of one orbit period and reaches a maximum value of approximately 0.1994×10^{-4} at t = 1500 minutes. As far as the perturbation of orbital motion due to ϕ_0 is concerned, the orbit is circular throughout the duration considered at the altitude of 35900km and with orbit time the same as before (1441.7 minutes), whereas in

LEO, a slight perturbutaion in orbital radius (r_c) when $\emptyset_0 = \pi/2$ radians has been noticed.

Exactly as in the case of the LEO, for small values of $\emptyset_0$ (0.1 radians), the dumbbell oscillates here too about the local vertical sinusoidally with a constant period and with a constant amplitude equal to its initial value ($\emptyset_0$) (Figures 23(b) and (d)). The period of libration is 834.4 minutes, the ratio of orbital to libration periods being 1.72783 which is approximately equal to $\sqrt{3}$. This result agrees with the prediction of Klemperer and Baker [45] for the rigid dumbbell, and of Hall and Smith [79] for an axially flexible dumbbell. For large value of $\emptyset_0$ (1.5707963 radians which is equal to $\pi/2$ radians), the attitude angle $\emptyset$ keeps on increasing very slowly for most of the time in one orbit (for example, from 1.5707963 radians at t = 0 minutes to 1.6325 radians at t = 1190 minutes). Toward the end of the first orbit, the increase in $\emptyset$ becomes more rapid. During the duration of the 1500 minutes run, the maximum value of $\emptyset$ is equal to about 2.573272 radians at t = 1500 minutes. The minimum value of $\emptyset$ is equal to $\emptyset_0$.

Figure 22(b) shows a plot of x/x_s versus time for the three different values of $\emptyset_0$ (0, 0.1, and 1.5707963 radians) during the first 100 minutes. Exactly the same trend of oscillation in x/x_s has been observed throughout the duration of 1500 minutes considered for the computer solution. It is clearly seen that there is no effect of

$\emptyset_0$ on x in GEO. The computer results show some differences in the x values from the sixth place (or sixth significant figure) after the decimal for these $\emptyset_0$. For all values of $\emptyset_0$, the dumbbell length (x) oscillates about the static length (x_s) with almost constant value of amplitude equal to the initial axial deformation (x_0-x_s) and with constant period of oscillation equal to approximately 1.1 minutes. Although the amplitude of oscillation is still very small (only 0.0023 percent of x_s), the trends of oscillation in x when $\emptyset$ equal to 0 and 0.01 radians clearly differ from those obtained for LEO (see Figures 22(a) and 22(b)).

Influence of initial axial deformation. The effects of the initial axial deformation are studied by obtaining computer results for one more value of x_0 equal to $1.05x_s$ (Example No. 22, Table 2(a)). Here again, the effects of x_0 are similar to those obtained for LEO. The value of the differential gravitational force ($\Delta F_g/F_{g0}$) for x_0/x_s equal to 1.05 fluctuates between the peak values approximately equal to -0.2484×10^{-4} and -0.225×10^{-4} with period equal to about 1.1 minutes. Figure 24(b) shows a plot of $\Delta F_g/F_{g0}$ versus time for the first 100 minutes of the 1500 minute duration. The variation of $\Delta F_g/F_{g0}$ continues in the same fashion throughout the total duration. For x_0/x_s = 1.000023, $\Delta F_g/F_{g0}$ remains almost constant at approximately

-0.2365×10^{-4}.

As in LEO, the dumbbell length (x) oscillates about its static length (x_s) with almost a constant amplitude of initial axial deformation and with a constant period equal to approximately 1.1 minutes. Figure 26(b) shows a representative plot of x/x_s versus time for x_0/x_s = 1.000023 and also for 1.05 during the first 100 minutes of the one orbit period. The initial axial displacement causes the structure to oscillate about the local vertical (r_c vector) with a constant amplitude. Figure 27(b) shows a plot of ϕ versus time. For x_0/x_s = 1.05, the maximum amplitude of oscillation in ϕ is equal to approximately 0.06148 radians, and the period of oscillation in ϕ is about 831.1 minutes. It has been seen from the computer data that the orbit remains completely unperturbed in all respects.

<u>Influence of orbit eccentricity</u>. Only an orbit with small eccentricity is selected here. An orbit with large eccentricity ($e = \pi/2$ radians) is not considered at this higher perigee altitude of 35900 km. This is mainly because such an orbit gives altitudes much higher than contemporary concern and also because the computer time required for the numerical solution is large, (of the order of a few hours). The value of $\dot{\theta}_0$ is increased from 0.00435818 radians per minute to 0.004526 radians per minute to obtain an orbit of eccentricity (e) equal to approximately 0.0785 (the same as in the case of LEO). The initial conditions used here are

given under Example No. 24 in Table 2(a). The period of orbit is approximately 1629.8 minutes and the apogee of the orbit is at a distance of approximately 49476.436km from the center of the earth (i. e., at an altitude of 43102.1 km from the surface of the earth), and the perigee is at a distance of 42274.33 km from the center of the earth (i. e., at an altitude of 35900 km from the surface of the earth) (Table 3). Plots of r_c/r_0, θ, and $\dot{\theta}$ versus time are shown respectively in Figures 29(a), 29(b), and 30(b).

The variations of the differential gravitational force along the circular and elliptical orbits are given in Figure 31(b). For the elliptical orbit, the value of $\Delta F_g/F_{g0}$ decreases from 0.23656×10^{-4} at perigee to 0.147482×10^{-4} at apogee and increases back to 0.23656×10^{-4} at perigee again. No effect has been observed on the axial length (x) of the structure due to the orbit eccentricity (Figure 32(b)). The oscillations in x are the same for the circular and the slightly eccentric orbit. As in LEO, the orbit eccentricity makes the dumbbell structure oscillate about its local vertical with amplitudes of Ø between peak values of approximately 0.097549 radians and -0.12044 radians and with libration period equal to about 1539.9 minutes for the 2000 minute duration run. The amplitudes and period of oscillation in Ø are thus increased with increasing orbit eccentricity.

Effects of Attractive Forces Between the Dumbbell Masses

The general equations of motion of the space structure include the attractive forces between the two end dumbbell masses, m_1 and m_2. Although this attractive force may be negligible in comparision with the gravitational pull at lower altitudes, it may be quite significant at higher altitudes where the gravitational attractive force is relatively small. To obtain a satisfactory answer to this question, the solution to the complete equations of motion is obtained by neglecting the attractive force term (Gm_1m_2/x^2) between the masses m_1 and m_2 in Equation 2.14(c). The solution is obtained for circular orbits at 200 km and 35900 km altitudes separately. The complete initial conditions for these runs are given in Example No. 13 and 23 in Table 2(a). The results thus obtained are compared with the respective results obtained earlier (Example No. 1, and 16, Table 2(a)) for the same initial conditions and physical parameter values with the attractive force term included in the equations of motion.The step size used for the computations is 0.2 minutes.

The computer data show that, for both the altitudes, the orbit and the length (x) of the structure remain completely unaffected. The values of r_c, $\dot{r}_c$, θ, $\dot{\theta}$, x,

and $\dot{x}$ remain identical up to eighth place after the decimal. (The data read out is to 8 places after the decimal). Similarly, $\Delta F_g/F_{g0}$ remained exactly the same. A slight difference in read out occurs for ϕ from the fifth place after the decimal at the 200 km altitude orbit and from the seventh place after the decimal at the 35900 km altitude orbit. However, the maximum values of ϕ are very small, of the order of 10^{-7} radians at 200 km altitude and of the order of 10^{-5} radians at 35900 km altitude. We can therefore conclude that the attraction between the two dumbbell masses has no effect on the orbital motion, attitude motion, or the axial deformation of the space structure.

Effects on Controlled Orientations

The truss-like space structure is now required to have a certain fixed orientation with respect to the sun or the earth at all time in the orbital journey. The orbit selected here is the elliptical one with large eccentricity ($e = 0.56$). Figures 28(a), (b), and 30(a) show the plots of r_c, θ and $\dot{\theta}$ versus time, respectively for such elliptical orbit when the structure takes a general orientation (Example No. 15, Table 2(a)). The term general orientation (case) means that the structure is free to take any orientation (i.e., any value of ϕ) during its travel in the

orbit. For such a case, the first perigee is at r_0 = 6574.3300 km, and the second perigee occurs at r_c = 6574.3309 km at t = 305.6 minutes. The apogee of the orbit is at r_c = 23483.013 km at t = 152.8 minutes. These values are noted here once again to compare with the corresponding results obtained in the various special cases (orientations). Four special orientations (as defined in Chapter III) of the structure are considered, and results are obtained for each of them for a time of 400 minutes with the 0.2 minute step size for the computations. The initial conditions and physical parameter values associated with these runs are given by Example No. 25 through 28 in Table 2(a). These controlled orientations of the space structure may not be of any significance as far as the effects of differential gravitational force are concerned, but they are of greater importance while studying thermal and radiation pressure effects on the space structure. Results obtained for each special case are presented below in comparison with those obtained for the general case.

<u>Special Case 1 ($\theta + \phi = \pi/2$)</u>. Figures 42 shows a plot of θ and ϕ versus time for Special Case 1 during a period of 400 minutes. There is a very insignificant effect on the apogee and perigee heights of the orbit. Apogee is at r_c = 23483.014 km at t = 152.8 minutes, and the second perigee is at r_c = 6574.3308km at t = 305.6 minutes. The first perigee is at r_0 and θ_0. The orbital period can be

considered to be 305.6 minutes which is the same as in the general case. Since $\Delta F_g/F_{gO}$ depend on $\emptyset$ and r_c, its magnitude varies from zero at perigee at t = 0 to nearly -0.7726×10^{-4} at t = 102.0 minutes, then is zero at apogee at t = 152.8 minutes, is 0.77263×10^{-4} at t = 295.4 minutes, and is finally again zero at the second perigee point at t = 305.6 minutes. Thus, the period of oscillation in $\Delta F_g/F_{gO}$ is equal to the orbital period of 305.6 minutes. The length (x) of the structure oscillates about its static length (x_s = 1.0 km) from the very beginning with maximum amplitude of x equal to approximately 0.0045 percent of x_s and with period about 1.1 minutes. A plot of x/x_s versus time is show in Figure 43(b) (G only).

Special Case 2 ($\emptyset = \pi/2$). Figure 44 shows a plot of θ and $\emptyset$ versus time for special case 2. The effects on orbital motion are negligible. The apogee and perigee points and orbital period remain the same as in Special Case 1. Since m_1 is equal to m_2, and $\emptyset$ is always $\pi/2$, the differential gravitational force ΔF_g is zero at all times. However, the computer data shows $\Delta F_g/F_{gO}$ equal to approximately 0.51×10^{-12}. This small numerical value is due to round-off and truncation errors. The length (x) of the structure oscillates about its static length (x_s) from the very beginning with a constant amplitude equal to its initial axial deformation (0.000023 km). The period of oscillation in x is again about 1.1 minutes. A plot of

x/x_s versus time is shown in Figure 45(b) (G only). For an enlarged scale of x/x_s the oscillation pattern of x would be seen similar to that in Figure 22(b).

Special Case 3 ($\emptyset = 0$). In this case also, there is no noteworthy perturbation in the orbital motion of the structure. Perigee and apogee points and the orbital period can be taken the same as in the general case. Since $\emptyset$ is zero at all time, the differential gravitational force (ΔF_g) in this configuration has the maximum values of all four special cases. This is because the masses, m_1 and m_2, are farthest apart with respect to the earth. $\Delta F_g/F_{gO}$ has maximum amplitude equal to 0.15211×10^{-3} at perigee at t = 0 and 305.6 minutes and minimum amplitude equal to 0.333766×10^{-5} at the apogee point at t = 152.8 minutes. The variation of $\Delta F_g/F_{gO}$ with time will be similar to that shown in Figure 31(a) (large eccentricity). The oscillation in x with time is of the same kind as shown in Figures 32(a) (large eccentricity) for the general case. Two distinct kinds of oscillation in x can be observed as can be seen for the general case. One is about its initial length (x_O) with larger amplitude (maximum amplitude equal to 0.0028 percent of x_O) and greater period of oscillation (approximately equal to one orbital period of 305.6 minutes). The other kind of oscillation in x can be considered about its static length (x_s) with small amplitude (only 0.0009 percent of x_s) and closely spaced

(period about 1.1 minutes). A plot of x/x_s versus time is shown in Figure 46(b) (G only).

Special Case 4 ($\theta + \phi = 0$). Figure 47 shows a plot of θ and ϕ versus time for Special Case 4. Again, there is no noteworthy perturbation in the orbital motion of the structure. As both the parameters r_c and ϕ are changing, $\Delta F_g/F_{gO}$ changes along the orbit. However, since m_1 is equal to m_2, $\Delta F_g/F_{gO}$ is expected to take zero values when $\theta = \pi/2$, $3\pi/2$ and $5\pi/2$ radians. Also, $\Delta F_g/F_{gO}$ decreases with increase in r_c. Some critical values of $\Delta F_g/F_{gO}$ are shown below:

t (minutes)	$\Delta F_g/F_{gO}$	
0	-0.15211×10^{-3}	(perigee, $\theta = 0$)
24.8	0.11699×10^{-6}	($\theta = \pi/2$)
41.8	0.74749×10^{-5}	
152.8	0.33764×10^{-5}	(apogee, $\theta = \pi$)
264.0	0.7475×10^{-5}	
281.0	-0.15747×10^{-6}	($\theta = 3\pi/2$)
305.6	-0.15211×10^{-3}	(perigee, $\theta = 2\pi$)

As far as the effects of this special orientation on the length (x) of the dumbbell is concerned, the instantaneous length oscillates about its static length (x_s) from the very beginning with a constant maximum amplitude equal to the initial axial deformation ($x_0 - x_s = 0.000023$ km) and with a constant period approximately 1.1 minutes. The plot

of x/x_s versus time is shown in Figure 48(b) (G only).

Effects of Total Mass

Until this point the total mass (m) of the space structure selected is 3600 metric tons (1.0×10^6 N-min^2/km). A relatively light-weight structure of total mass (m) equal to 36 metric tons (1.0×10^4 N-min^2/km) has been selected next. The mass of 36 metric tons is greater than the value of 24 metric tons which is the mass of the one kilometer long truss-like structure (Appendix C). The additional mass above the 24 metric tons may be due to the payload and any smaller structures erected on the main structure. The orbit selected is elliptical with large eccentricity (e = 0.56). All the inital conditions and physical parameter values (Example No. 29, Table 2(a)) are the same as in the previous case where m = 3600 metric tons (Example No. 1, Table 2(a)). The computer data show that the decrease in the value of m does not affect the orbit in any respect. This confirms the result which can be inferred from the equations of motion (2.14) with $m_1 = m_2$ (i.e. $m_1/m_2 = 1$) and only gravitational force acting on the structure. As can be seen in Figure 35(b), the decrease in the value of m does not have any appreciable effect in Ø either.

The variation of $\Delta F_g/F_{gO}$ with time (Figure 34) here

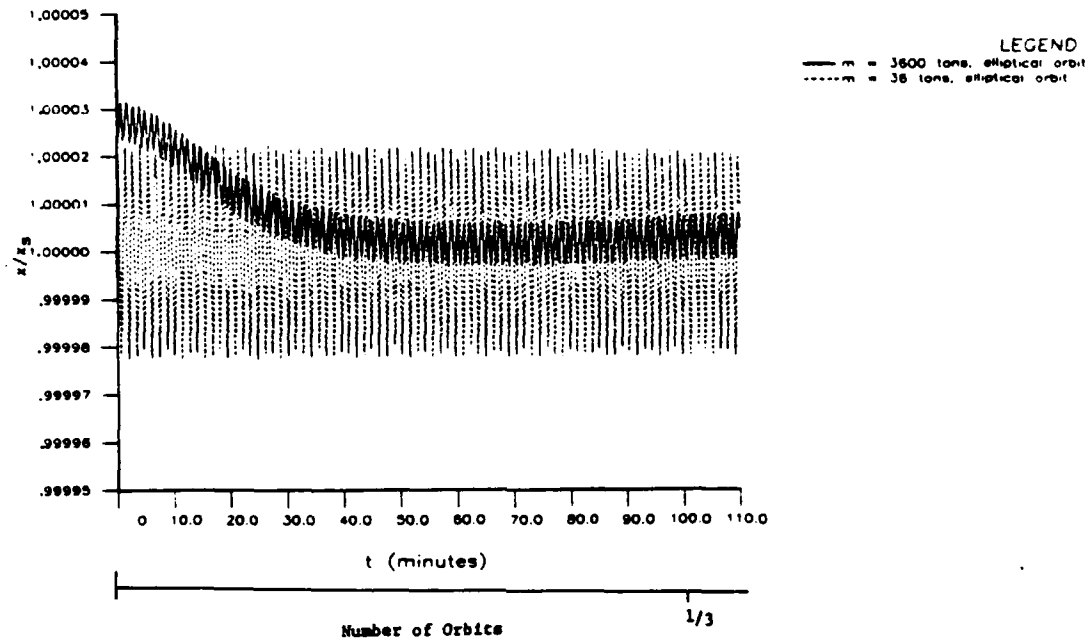

(a)

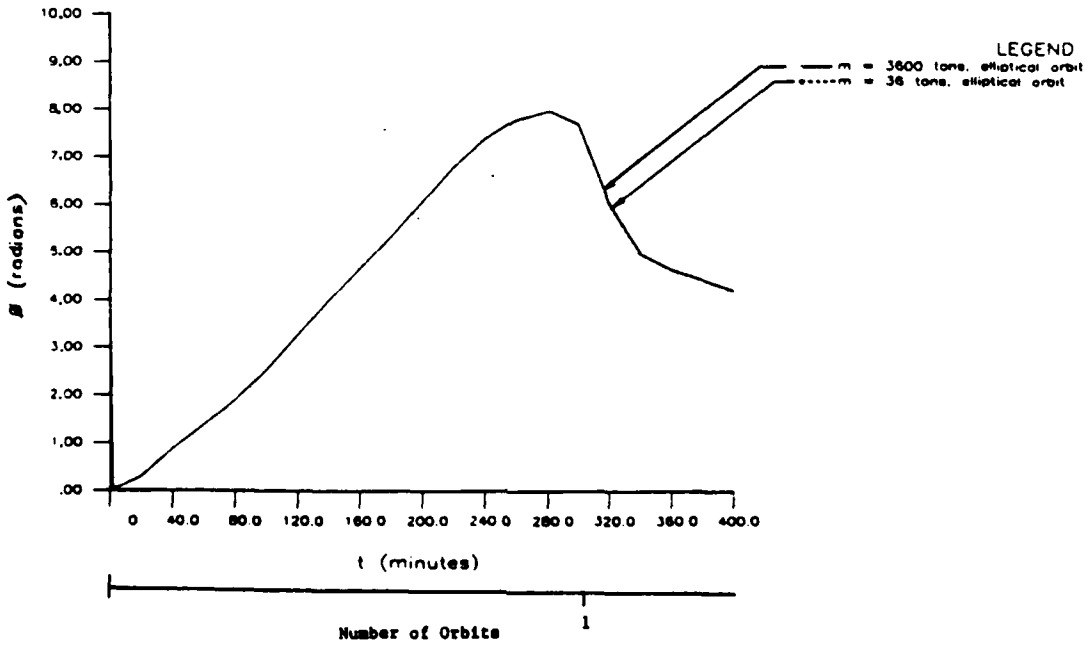

(b)

Figure 35. Effects of total dumbbell mass (m) on oscillation of (a) axial length (x), (b) attitude (Ø): Elliptical orbit with eccentricity (e = 0.56) and perigee attitute = 200 km

is similar to that obtained for the higher value of m. The magnitude of ΔF_g is almost two orders of magnitude smaller in this case because m is decreased by two orders of magnitude. Similarly, the value of F_{g0} is equal to 331999.63214 N which is two orders of magnitude smaller than that for m = 3600 metric tons. Figues 35(a) shows a plot of x/x_s versus time for both the values of m (3600 metric tons and 36 metric tons) during the first 110 minutes of the 400 minute total duration. As is clear from the figure, the dumbbell length (x) for m = 36 metric tons oscillates about x_s from the beginning with a constant maximum amplitude equal to the initial axial deformation (x_0-x_s = 0.000023 km) and with a constant period equal to approximately 1.3 minutes. Not only the amplitude of oscillation in x but also the period of oscillation are different here from those for m = 3600 metric tons.

Keeping m constant at 36 metric tons, the m_1/m_2 ratio is changed from 1.0 (case above) to 3, and the solution of the equations of motion is obtained again (Example No. 30, Table 2(a)). The computer data do not show any significant changes in any parameters except the expected change in the value of amplitude of $\Delta F_g/F_{g0}$. The only other significant difference here is the oscillation in x. The amplitude of oscillation in x remains almost as that for m_1/m_2 = 1.0, but its period of oscillation in x is now decreased from 1.3 minutes to 0.6 minutes.

Thermal Effects

The combined effects of radiation heating and differential gravitational force on the truss-like rectangular space structure is studied next. The dumbbell masses, m_1 and m_2 are considered as point masses; and therefore, they do not have any areas to absorb radiation. The solutions for the complete equations of motion of the space structure are obtained in order to examine the effects of the radiation heating on its orbital and attitude motions and axial deformation simultaneously. Results are obtained to observe the relative contributions of the various possible radiation heat sources, namely, direct solar, earth's albedo, and earth's direct radiation.

The influences of altitude (r_c), orientation of the structure with respect to the sun and the earth (θ and $\emptyset$), and the structure's surface area-to-mass ratio (A_{sf}/m) on the thermal responses of the structure have been studied. The orbits selected for these studies are circular and elliptical. The static length (x_s) of the space structure is the same for all cases, and is equal to 1 km. As the space structure goes around the earth in an orbit, it passes through the earth's shadow. The locations of the space structure's entry into, and exit from, the earth's shadow for various orbits and altitudes are given in Table 3. The initial temperature (T_0) is taken to be equal to 290 °K.

Effects due to the combined thermal and differential gravitational force versus time are plotted along with those due to the differential gravitational force for comparison of the results. The step sizes considered for the computations are 0.2 minutes when $|\theta| \leq \pi/2$ and 0.1 when $|\theta| \geq \pi/2$

Maximum and Minimum Equilibrium Temperature

The equilibrium temperature is heavily dependent on the altitude and the orientation of the space structure with respect to the sun and the earth. Figure 36 shows the space structure's orientations and its locations in an orbit giving maximum and minimum equilibrium temperatures at a given altitude. Table 4 represents the maximum and minimum equilibrium temperatures at three altitudes of contemporary concern taking into account all three possible sources of radiation heating (direct solar, earth's albedo, and its direct radiation) separately and then jointly. The effect of direct solar radiation remains constant with altitude, but the effects of the earth's albedo and its direct radiation decrease with increasing altitudes with respect to the earth. It can also be seen from the results that in the geosynchronous orbit (GEO) the contributions of the earth's albedo and its direct radiation are virtually zero. In the earth's shadow in a given orbit, the contribution to

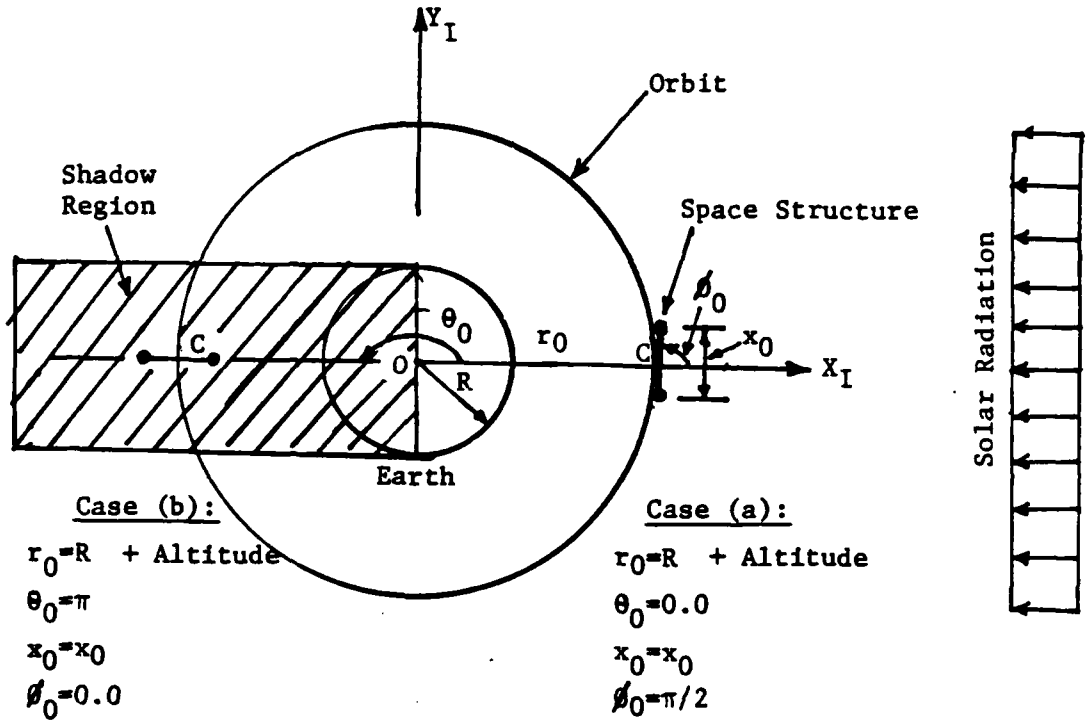

Figure 36 . Configurations of a Space Structure Giving Maximum (Case a) and Minimum (Case b) Equilibrium Temperature

Table 4 : Maximum and Minimum Equilibrium Temperature

Altitude (km)	Radiation Heat Source	Case (a): Maximum Temperature (θ_0=0, x_0=1.0km, ϕ_0=π/2) (°K) (Computed values)	Case (b): Minimum Temperature (θ_0=π, x_0=1.0km, ϕ_0=0) (°K) (Computed values)
200.000 (Low Earth Orbit)	D.S.	330.500	0.0
	D.E.	210.536	194.975
	ALB	240.848	0.0
	D.S. + ALB	351.678	0.0
	D.S. + ALB + D.E.	362.465	194.975
35900.0 (Geosynchronous Orbit)	D.S.	330.500	0.0
	D.E.	83.026	41.8310
	ALB	94.980	0.0
	D.S. + ALB.	331.062	0.0
	D.S. + ALB + D.E.	331.390	41.8310
17108.7 (Apogee of an orbit with e=.56 & perigee at 200 km)	D.S.	330.500	0.0
	D.E.	111.397	65.2699
	ALB	127.436	0.0
	D.S. + ALB	332.311	0.0
	D.S. + ALB + D.E.	333.355	65.2699

D.S. Direct Solar Radiation
D.E. Direct Earth Radiation
ALB Albedo Radiation

temperature change comes solely from the direct earth radiation and decreases with increasing altitudes.

The temperatures given in Table 4 are the absolute maximum (sunlight side) and minimum (earth shadow side) at a given altitude. In the present study, we consider a linear relationship between the temperature difference and the axial deformation of the structure. It can therefore be concluded that the amount of axial deformation of the space structure is controlled by these temperatures and the initial temperature (T_0). Thus, it is possible now to estimate the maximum relative contributions to the axial deformation of the structure from the direct solar, earth's albedo, and earth's direct radiation when the space structure attains radiation equilibrium. For example, in low earth orbit (LEO) at the altitude of 200 km when the structure is in the sunlight side and attains thermal radiation equilibrium, the maximum contribution from direct solar radiation is approximately 56.0 percent of the total radiation effect; that from the earth's albedo radiation is about 29.0 percent of the total radiation effect; and that from the earth's direct radiation is 15.0 percent of the total effect. These relative contributions from the various radiation sources to the structural deformation vary greatly with the initial temperature (T_0).

Thermal Effects in General Orientation

The maximum and minimum equilibrium temperatures computed above are independent of time. The orientation of the space structure with respect to the sun and the earth is also restricted by the simple fact that we require the temperature to be a maximum or minimum. Results are presented below for a general situation. Mass and surface area of the structure exposed to radiation come into the picture now for the evaluation of the temperature at a time t. The mass (M) of the one kilometer long plate-like space structure (link structure connecting the two dumbbell masses, m_1 and m_2) is approximately 24 tons, and the ratio (A_{sf}/A_{sd}) of the total surface area to the surface area of one side of the rectangular structure is 2.0 (Table 1 and Appendix C). The total mass (m) of the complete system is still 3600 tons (1.0×10^6 N-min^2/km). The ratio of the total surface area (A_{sf}) to the total mass (m) of the space system is 0.000486 m^2/kg. Complete initial conditions and physical parameter values for these runs are given under Example No. 31 through 33 in Table 2(b). In these cases the space structure is permitted to assume any orientation as related to the sun and the earth with respect to time (general case). Results are obtained for all three sources of radiation.

Circular orbits in LEO and GEO (Effects of Altitude).

First of all, we study the relative contributions from the three major sources of radiation. For a better illustration of the influence of the altitude on the thermal effects of these three sources on the space structure motion and deformation, circular orbits are selected at two altitudes - one at 200 km (LEO, r_0 = 6574.33 km) and two at 35900 km (GEO, r_0 = 42274.33 km) - from the surface of the earth. Figures 37(a), 38(a), and 39(a) show the plots of temperature (T), x/x_s, and Ø versus time, respectively for the circular orbit at the altitude of 200 km. Figures 37(b), 38(b), and 39(b) give the plots of T, x/x_s, and Ø versus time respectively for the circular orbit at the altitude of 35900 km. The computer data are obtained for about a 297 minute duration (more than 3 orbits) in LEO and for about 1679 minutes (more than 1 orbit) in GEO.

At a given altitude (r_c) and size (x) of the space structure, the temperature (T) is a function of the orientation of the structure with respect to the earth and the sun and its location in the orbit (i.e., θ and Ø). The temperature increases in the sunlight and decreases in the earth shadow side. Figure 37(a) shows that in LEO the minimum temperature occurs just befor the structure exits from the earth's shadow, and the max.mum temperature at the point where it is about to enter the shadow. It also shows that except in the first orbit, the temperature is due to only direct solar radiation is always below the initial value

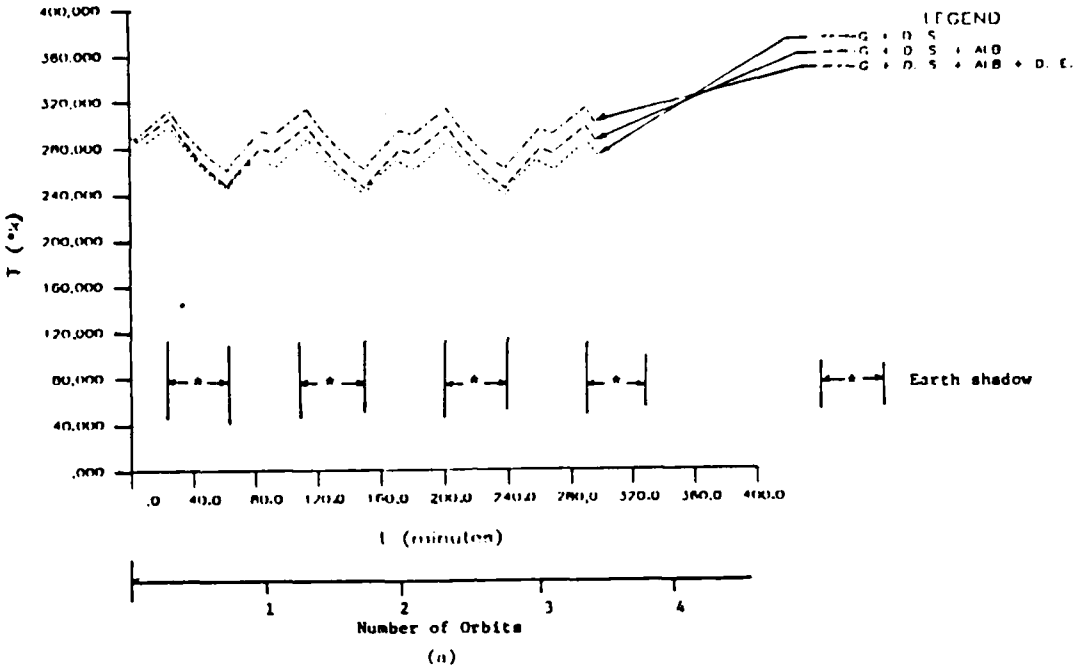

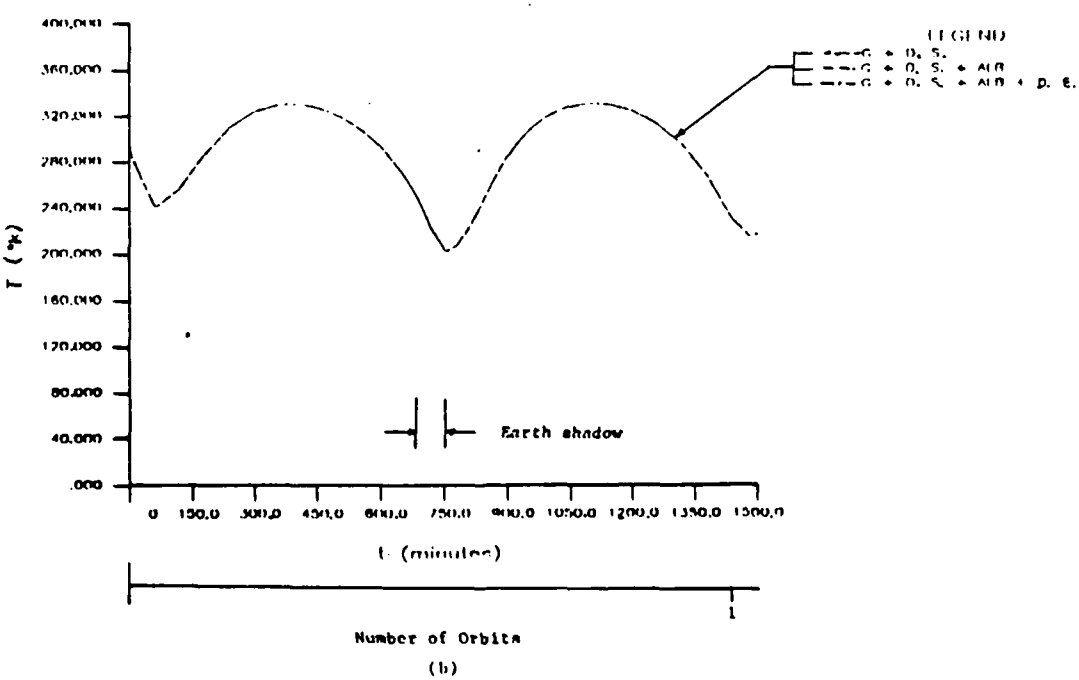

Figure 37. Variation of temperature (T) in a circular orbit at altitude (a) 200 km, (b) 35900 km, for general orientation (case)

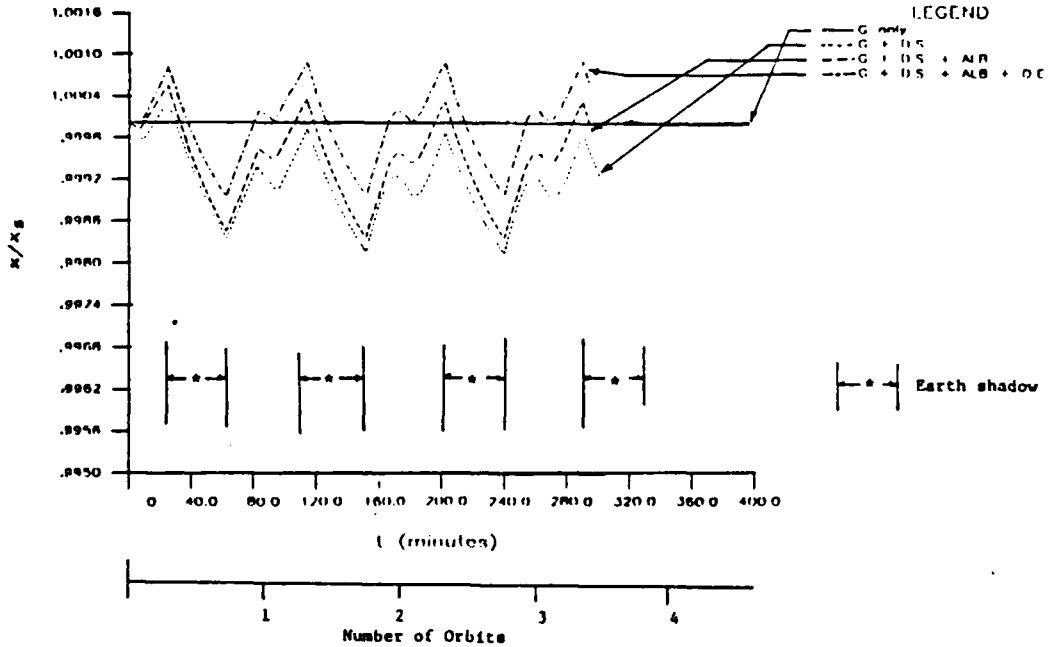

(a)

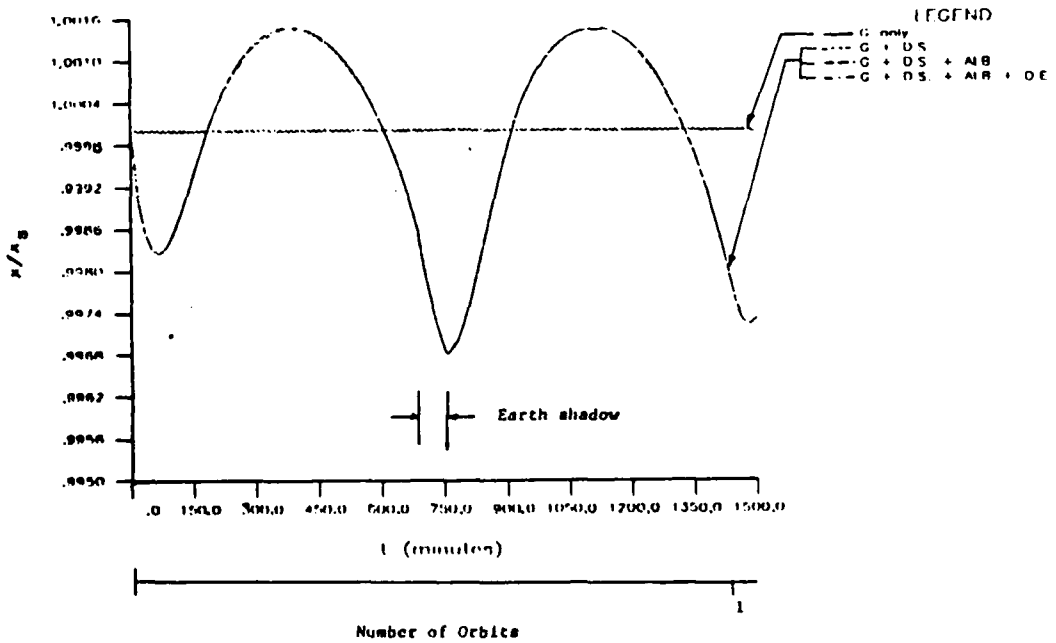

(b)

Figure 38. Thermal effects on axial length (x): Circular orbit at altitude (a) 200 km, (b) 35900 km, for general orientation (case)

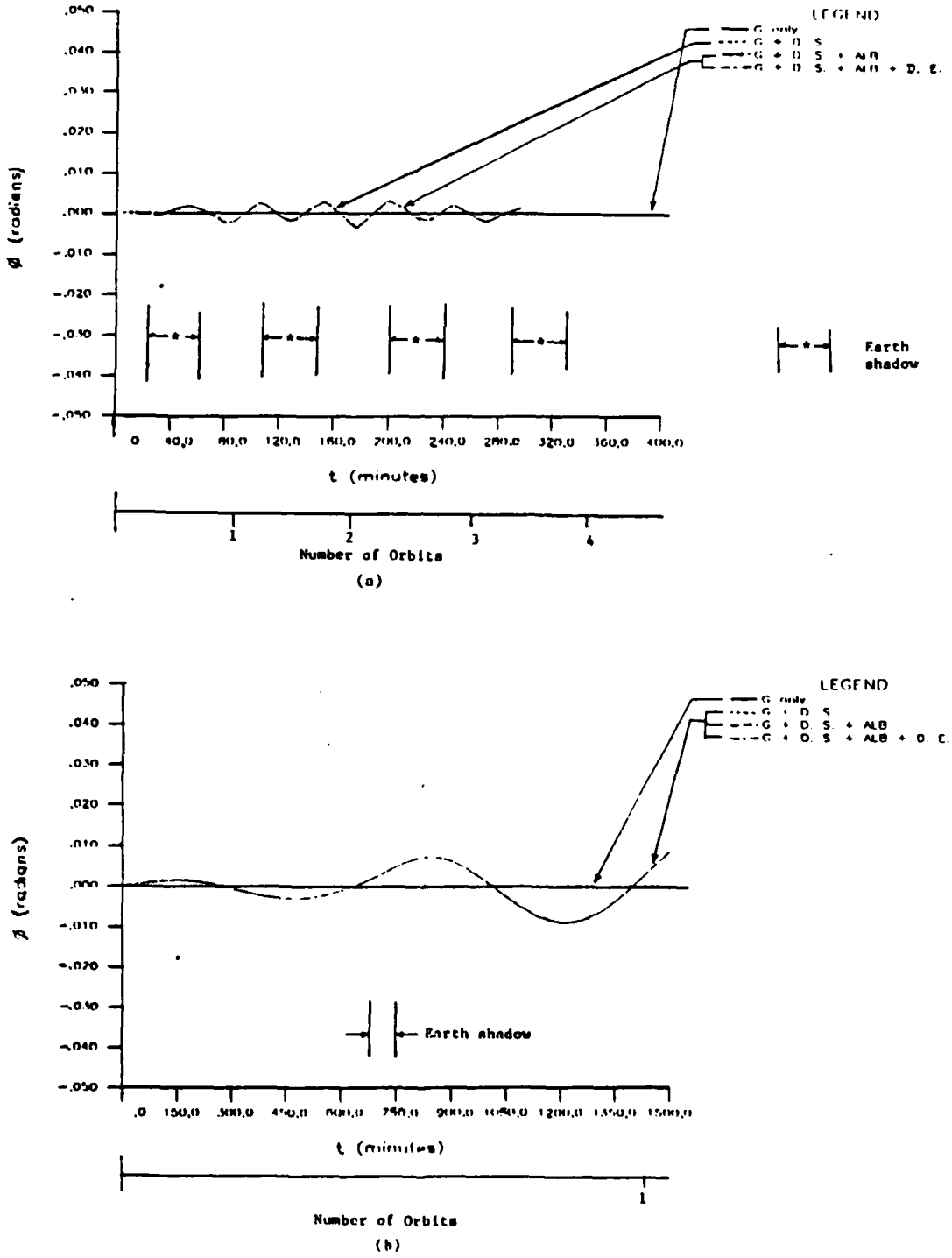

Figure 39. Thermal effects on attitude (Ø): Circular orbit at altitude (a) 200 km, (b) 35900 km when Ø = Ø (general orientation (case))

(290 °K). In LEO during the 3 orbit duration, the maximum (sunlight side) and minimum (earth's shadow side) temperatures due to all three sources of radiation combined are respectively 313.59 °K and 259.90 °K. Due to direct solar and earth's albedo radiations combined, these are respectively 305.27 °K and 243.51 °K. Due to direct solar radiation alone, these values are respectively 299.33 °K and 237.68 °K. The greatest contribution from the earth's albedo radiation in the time considered is to increase the temperature by approximately 14 °K and that from the direct earth radiation is to further increase the temperature by approximately 17 °K. These maximum contributions occur at time equal to 270.8 minutes where the temperature due to only direct solar radiation is 260.06 °K.

In GEO, the maximum value of the temperature in the sunlight portion is 330.031 °K and the minimum temperature which occurs in the earth's shadow is 201.570 °K. Figure 37(b) shows that at this higher altitude the distributions of temperature with time due to direct solar radiation alone, due to direct solar and the earth's albedo radiations combined, and due to all three radiation sources (direct solar, earth's albedo and earth's direct radiations) combined, coincide with each other. From this it can be concluded that the relative contributions from the earth's albedo and its direct radiations are zero. All thermal effects at such high altitudes can therefore be considered

to be due to only direct solar radiation.

There can be seen three important differences between temperature histories in LEO and GEO. First, in LEO the space structure is never at radiation equilibrium. Radiation equilibrium is not achieved because the shorter orbital period causes the heating rates to change much faster. Thus the transient term in Equations (2.26) has a much greater effect in LEO than in GEO. Second, the much greater heating from the earth increases the magnitude of the temperature but it also moderates temperature excursions. Third, the contributions from the earth's albedo and its direct radiation heating are much greater in LEO than in GEO.

The structural responses of the very large space structure, i. e. the typical axial deformation of a one kilometer long continuum model of a tetrahedral truss, are shown in Figures 38(a) and 38(b) in LEO and GEO, respectively. The change in length of the structure follows the temperature histories given in Figures 37(a) and (b). In LEO and GEO alike, the axial length (x) fluctuates according to the temperature histories. As for length, although there are no contributions from the earth's albedo and its direct radiations in GEO (Figure 38(b)), these contributions are seen to be quite significant in LEO (Figure 38(a)). In LEO, due to only direct solar radiation the maximum increase and decrease in the length (x) are

respectively 0.039 percent and 0.1918 percent of the initial length (x_0 = 1.000023 km). Due to combined direct solar and earth's albedo radiations, the highest increase and decrease in x are respectively 0.0557 percent and 0.1704 percent of x_0. During the same three orbit duration in LEO, the values of maximum increase and decrease in x due to all three radiation sources combined are respectively 0.0872 percent and 0.109 percent of x_0. In all cases the highest increase in x occurs in the sunlight side of the orbit, whereas the greatest decrease in x occurs in the earth's shadow side of the orbit.

In GEO during the 1500 minute duration (more than one orbit), the largest increase in length (x) of the structure is approximately 0.1454 percent of the initial length (x_0). The largest decrease in x, is approximately 0.326 percent of x_0. The maximum increase of x occurs in the sunlight side, and the maximum decrease of x occurs on the shadow side of an orbit. It should be mentioned here that the change in length of the structure due to thermal effects is seen to be of much more significance than that due to only the differential gravitational force.

Figures 39(a) and (b) respectively show the plots of the attitude (Ø) of the space structure versus time in LEO and GEO under the influence of various radiation sources and the differential gravitation force. These plots show that the radiation heating has caused increased effects on Ø.

Both in LEO and GEO the dumbbell oscillates about its local vertical with increased amplitude. The amplitude and period of libration now do not remain constant. Even in LEO, the contributions from the earth's albedo and its direct radiation heating to change the values of Ø are negligible compared to the direct radiation heating. In LEO during the three orbit run, the amplitude of oscillation in Ø varies between approximately 0.3683×10^{-4} radians and 0.36566×10^{-2} radians. The period of libration varies between approximately 36.5 minutes and 57 minutes. In GEO during the one orbit period, the amplitude of oscillation in Ø varies from approximately 0.142577×10^{-2} radians to 0.91768×10^{-2} radians, and the period of libration varies between approximately 638.8 minutes and 761.3 minutes.

Regarding the effects of the radiation heating on the structure's orbital motion, the computer data indicate that the orbit remains perfectly circular for all values of time at both altitudes (200km and 35900km). As before, for LEO and GEO, the orbital periods are respectively 88.4 minutes and 1441.7 minutes.

<u>Elliptical orbits</u>. Radiation thermal effects on the structure are obtained next by requiring the one kilometer long space structure to travel in an elliptical orbit as considered in earlier sections. The perigee of the elliptical orbit is at an altitude of 200 km (r_0 = 6574.33 km) and the apogee at an altitude of 17108.68 km (r_0 =

23,483.013 km) i.e., the orbit has eccentricity (e) approximately equal to 0.56. The orbital period of this configuration is 305.6 minutes. The thermal effect on the space structure is now dependent not only on the orientation of the structure with respect to the sun or the earth and its location in the orbit, i.e., on $\emptyset$ and θ, but also on its distance from the earth i.e. on r_c. The inital conditions and physical parameter values for these runs are indicated under Example No. 33 in Table 2(b). The solution of the equations of motion is obtained for a duration of more than one orbit (400 minutes).

Figure 40 shows a plot of temperature distribution (T) with time in such a general orbit. The contribution from direct solar radiation remains constant with altitude whereas the contributions from the earth's albedo and its direct radiation heating decrease with increasing altitudes. These latter contributions are highest near the perigee point. Due to the total radiation heating during the 400 minute period considered, the maximum temperature is 317.210 °K, and the minimum temperature is equal to 212.954 °K. The structural response i.e, the change in length (x) of the structure, follows the temperature distribution. A plot of x/x_s versus time is shown in Figure 41(a). The maximum increase and decrease in x due to the total thermal effects in the 400 minute duration are respectively about 0.0978 percent and 0.283 percent of the initial length

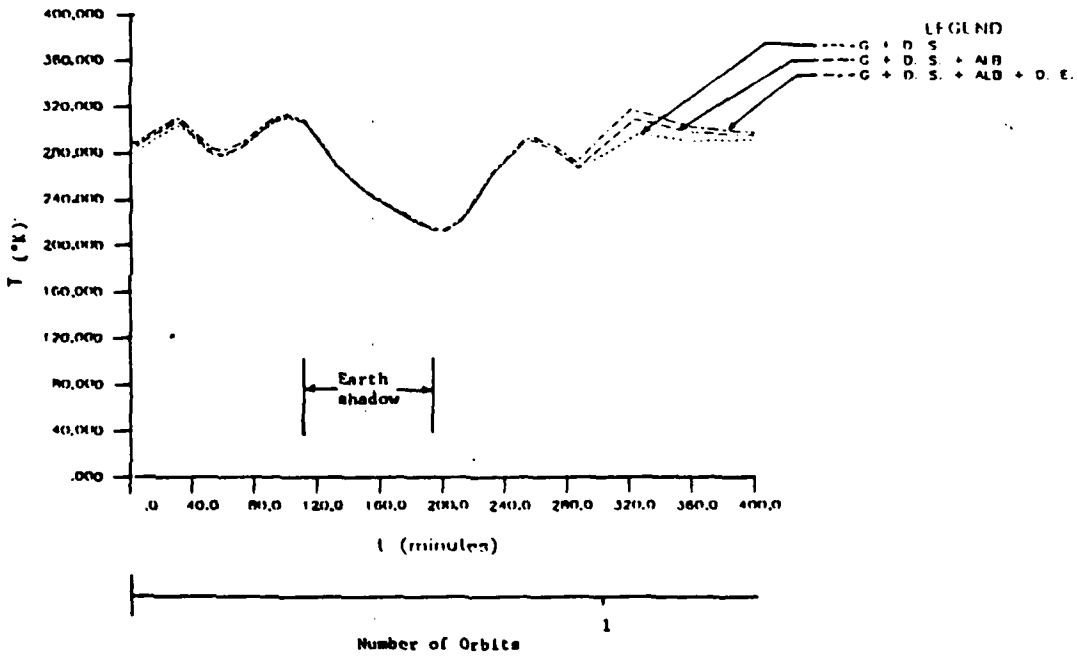

Figure 40. Temperature variation (T) in an elliptical orbit (e = 0.56, perigee height = 200 km) for general orientation (case)

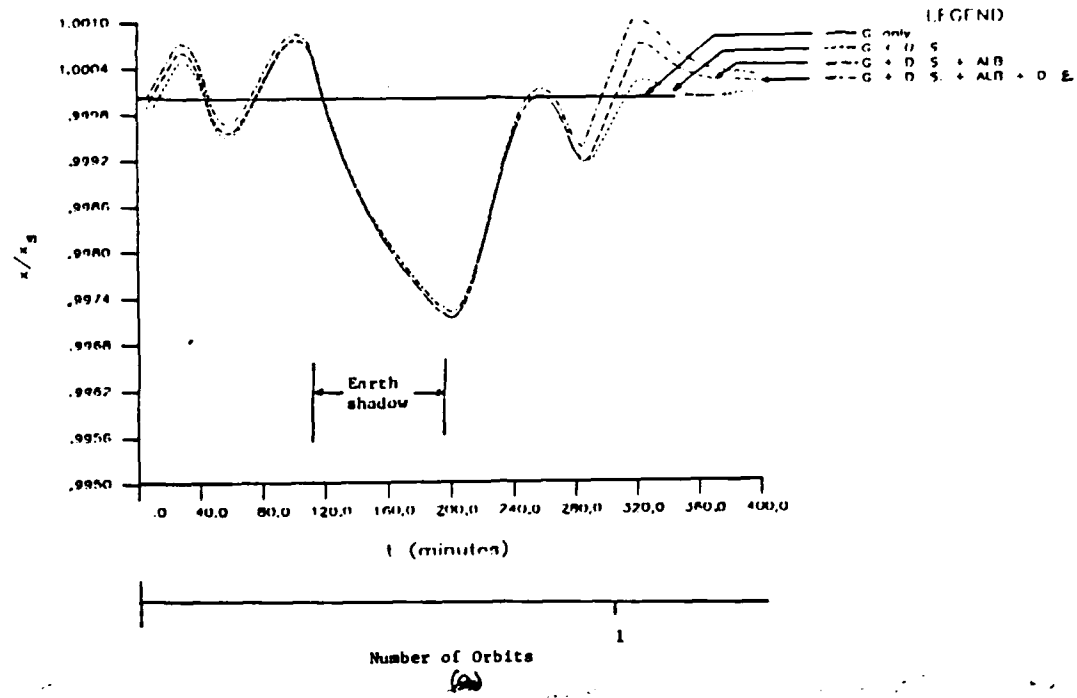

(a)

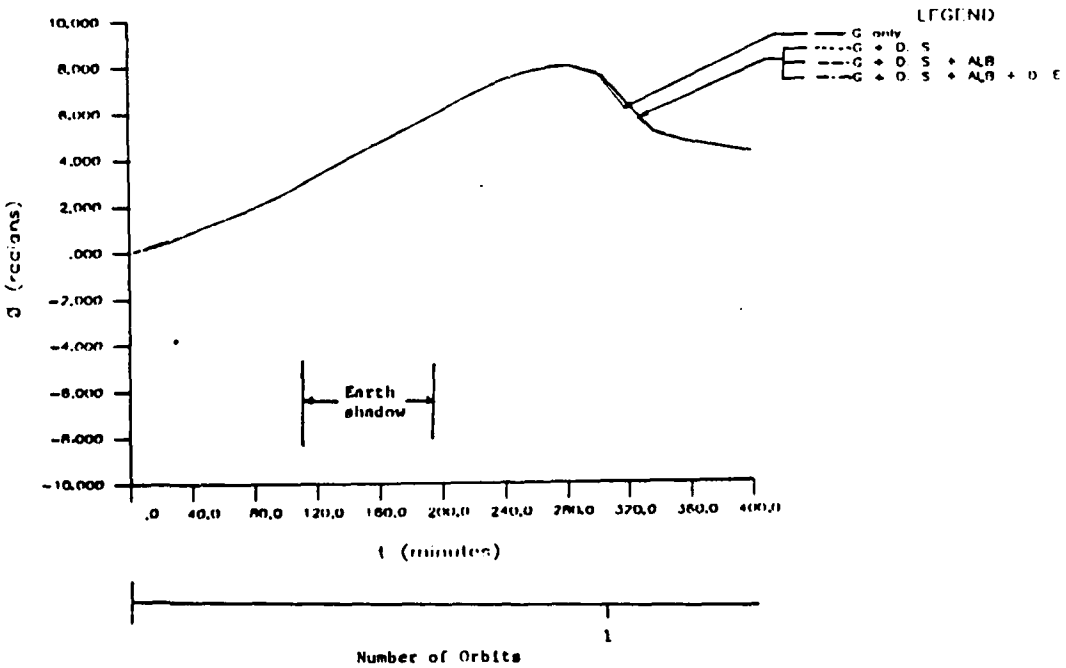

(b)

Figure 41. Thermal effects on (a) axial length (x), (b) attitude (Ø): Elliptical orbit (e = 0.56 and perigee altitude = 200 km) for general orientation (case)

(x_0).

Figure 41(b) shows a plot of Ø versus time. Unlike the circular orbit, the attitude motion (Ø) of the structure is seen to be undisturbed by the radiation thermal effect in the elliptical orbit. The computer data however show a slight difference between the values of Ø due to the differential gravitational force alone and due to the combined effects of radiation heating and gravitational force. For example, the maximum Ø due to the gravitational force alone is 7.9888049 radians while it is 7.9927713 radians due to the total radiation thermal and gravitational effects combined. This may be because the orbit eccentricity is much more influential than the thermal effects changing the attitude motion of the space structure. The computer data also indicate that radiation heating has small or negligible effects in changing the orbital motion of the structure.

Thermal Effects in Controlled Orientations

Four special cases are selected as shown in Figure 13. In these cases as described in Chapter III and in an earlier section in this chapter, the space structure is required to have a fixed orientation with respect to the sun or the earth for all time. The importance of such controlled orientations is outlined in Chapter III. The orbit selected

is the elliptical one as above. The complete initial conditions and parameter values are presented in Example No. 34 through 37 in Table 2(b). Results delineating the thermal effects of various radiation sources on each special case are presented below. Although in some instances the solution of the complete equations of motion is obtained for more than the 400 minute duration, the results and discussion presented here are based on the 400 minute duration only. In all cases, the computer data show that perturbation of orbital motion of the structure is either zero or negligible.

Special Case 1. Since the structure is always perpendicular to the sun vector (i.e. $\theta + \phi = \pi/2$) in this case, the space structure gets maximum direct solar radiation heat. Therefore, by allowing the space structure to be in such an orientation we expect to get the maximum thermal effect on the structure due to direct solar radiation. The distributions of θ and ϕ with time to achieve such an orientation are shown in Figure 42. In this case, the thermal effects due to the radiation sources depend only on the distance of the structure from the earth, location of the structure in the orbit, and its orientation with respect to the earth. The structure's orientation with respect to the sun is fixed. A plot of T versus time is shown in Figure 43(a). The maximum and minimum temperatures during the 400 minute period due to the total radiation

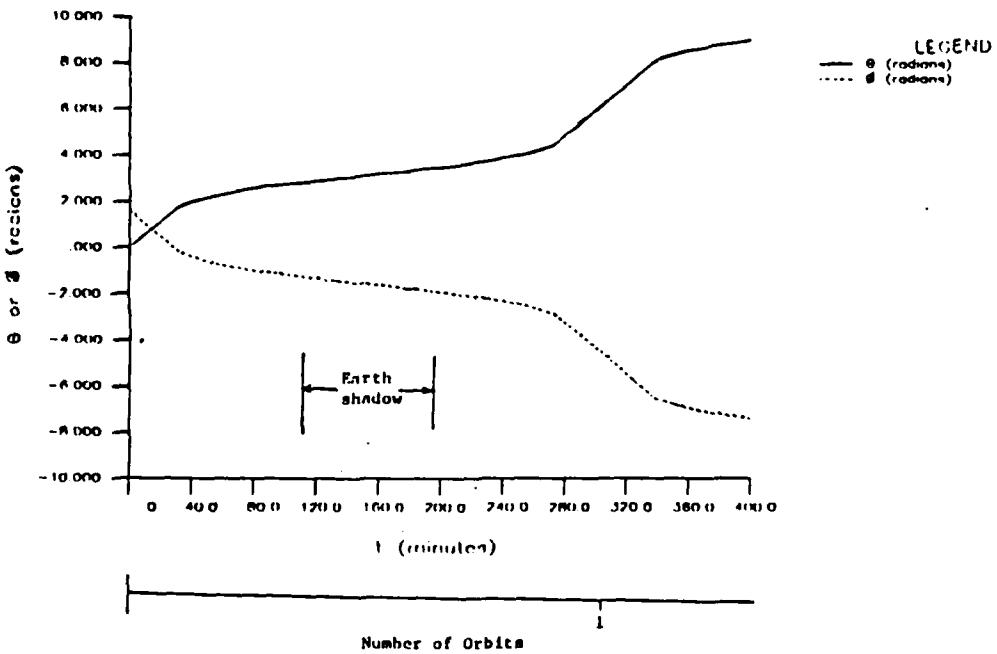

Figure 42. Variations of θ and Ø: Elliptical orbit (e = 0.56 and perigee height = 200 km), Special Case 1 (orientation θ + Ø = π/2: Maximum direct solar heating)

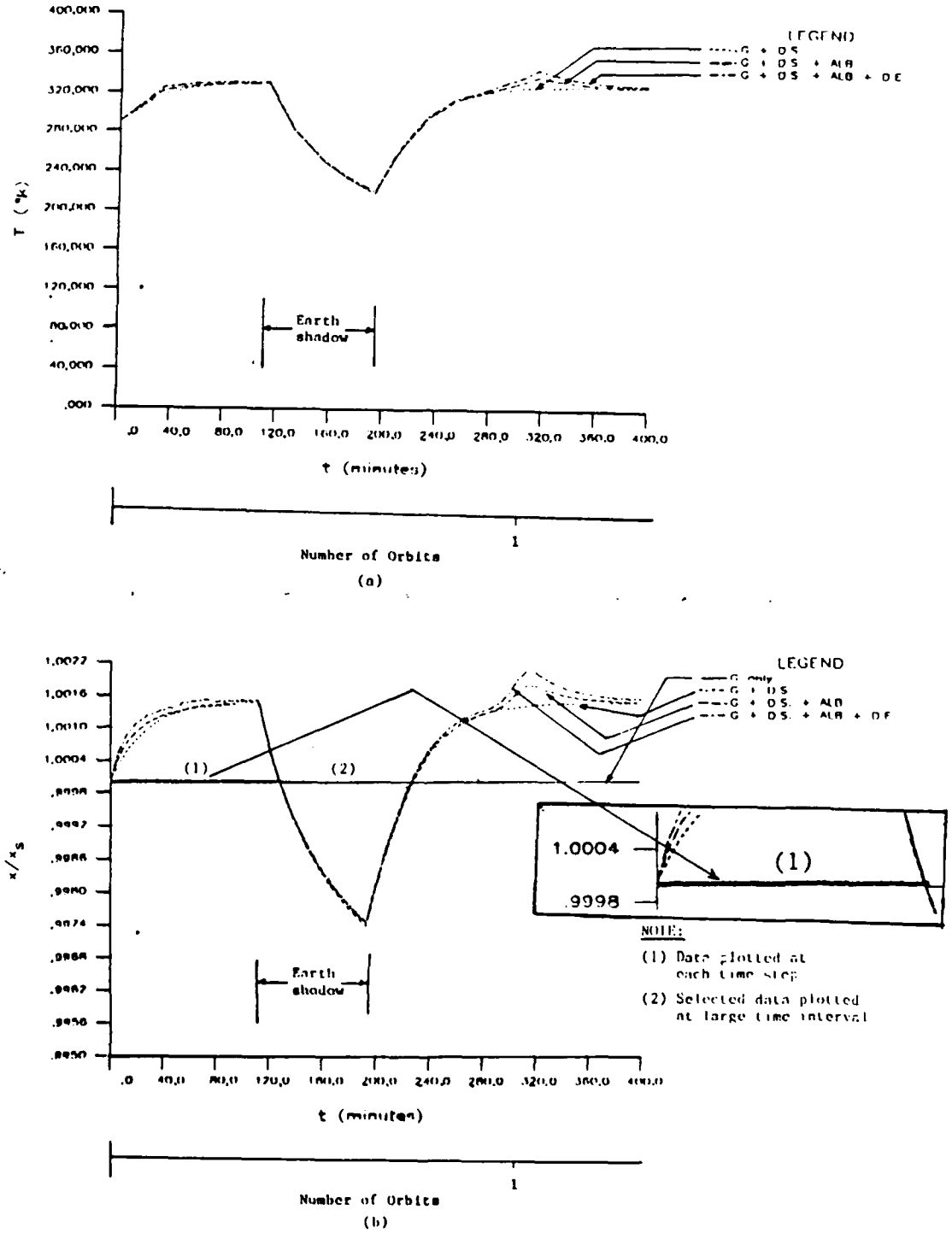

Figure 43. (a) Temperature variation (T) and (b) thermal effects on axial length (x): Elliptical orbit (e = 0.56 and perigee altitude = 200 km), Special Case 1 ($\theta+\phi = \pi/2$: Maximum direct solar heating)

heating are respectively 346.509 °K and 220.657 °K. Due to only direct solar heating, these are respectively 330.445 °K and 218.352 °K. On the sunlight side, the temperature due to direct solar radiation thus reaches the equilibrium value (Table 4). Figure 43(b) shows a plot of x/x_s versus time. The largest increase and decrease in the length (x) due to the total radiation thermal effect are respectively 0.2067 percent and 0.2577 percent of the initial length (x_0). Due to direct solar heating alone these values are respectively 0.1479 percent and 0.2659 percent of x_0. Due to the earth's albedo and its direct radiation heating the maximum increases in x are respectively 0.0371 percent and 0.0263 percent of x_0. It is noteworthy that the distributions of T and x/x_s in most part of the sunlight side remain almost uniform.

Special Case 2. The structure is required to be at right angles to the earth-space structure vector at all times (i.e. $\emptyset = \pi/2$). The structure thus gets maximum radiation from the earth (albedo and direct earth radiation). The distributions of θ and $\emptyset$ with respect to time for such an orientation are shown in Figure 44. The temperature distribution and structural response now depend on the altitude, location in the orbit, and orientation with respect to the sun, of the space structure. The structure has a fixed orientation with respect to the earth. A plot of temperature (T) versus time is given in Figure 45(a).

AD-A172 080 PARAMETRIC INVESTIGATION OF FACTORS INFLUENCING THE MECHANICAL BEHAVIOR O..(U) MASSACHUSETTS UNIV AMHERST DEPT OF CIVIL ENGINEERING W A WASH ET AL. 30 MAY 86 3/5

UNCLASSIFIED AFOSR-TR-86-0058 AFOSR-83-0025 F/G 22/2 NL

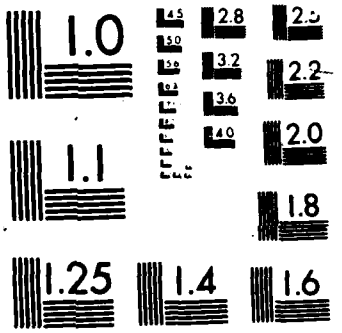
1.0
2.8
2.2
3.2
3.6
4.0
2.0
1.1
1.8
1.25
1.4
1.6

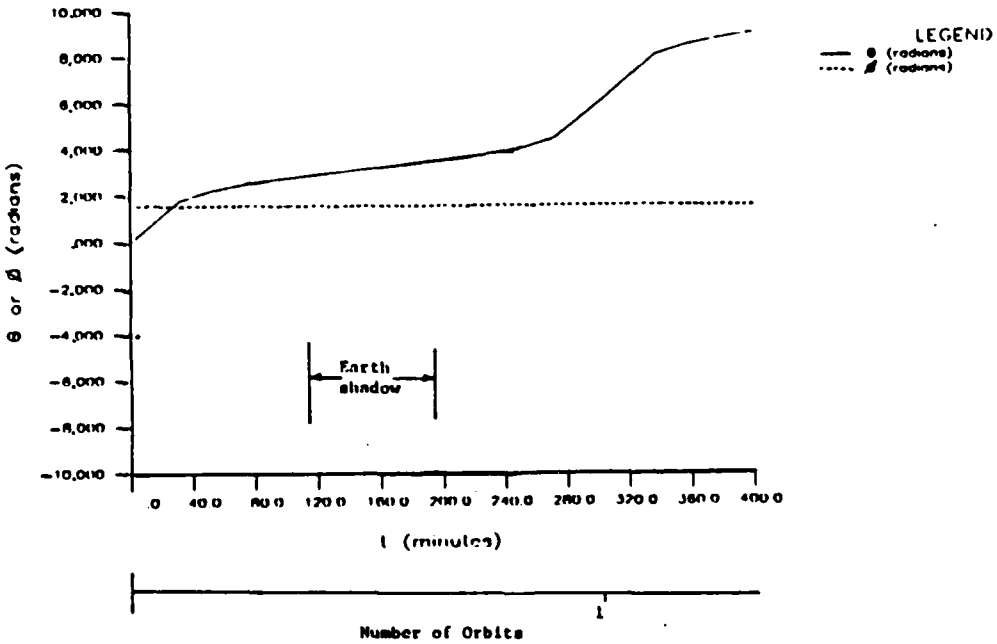

Figure 44. Variations of θ and ø: Elliptical orbit (e = 0.56 and perigee altitude = 200 km), Special Case 2 (orientation ø = π/2: Maximum direct earth and albedo heating)

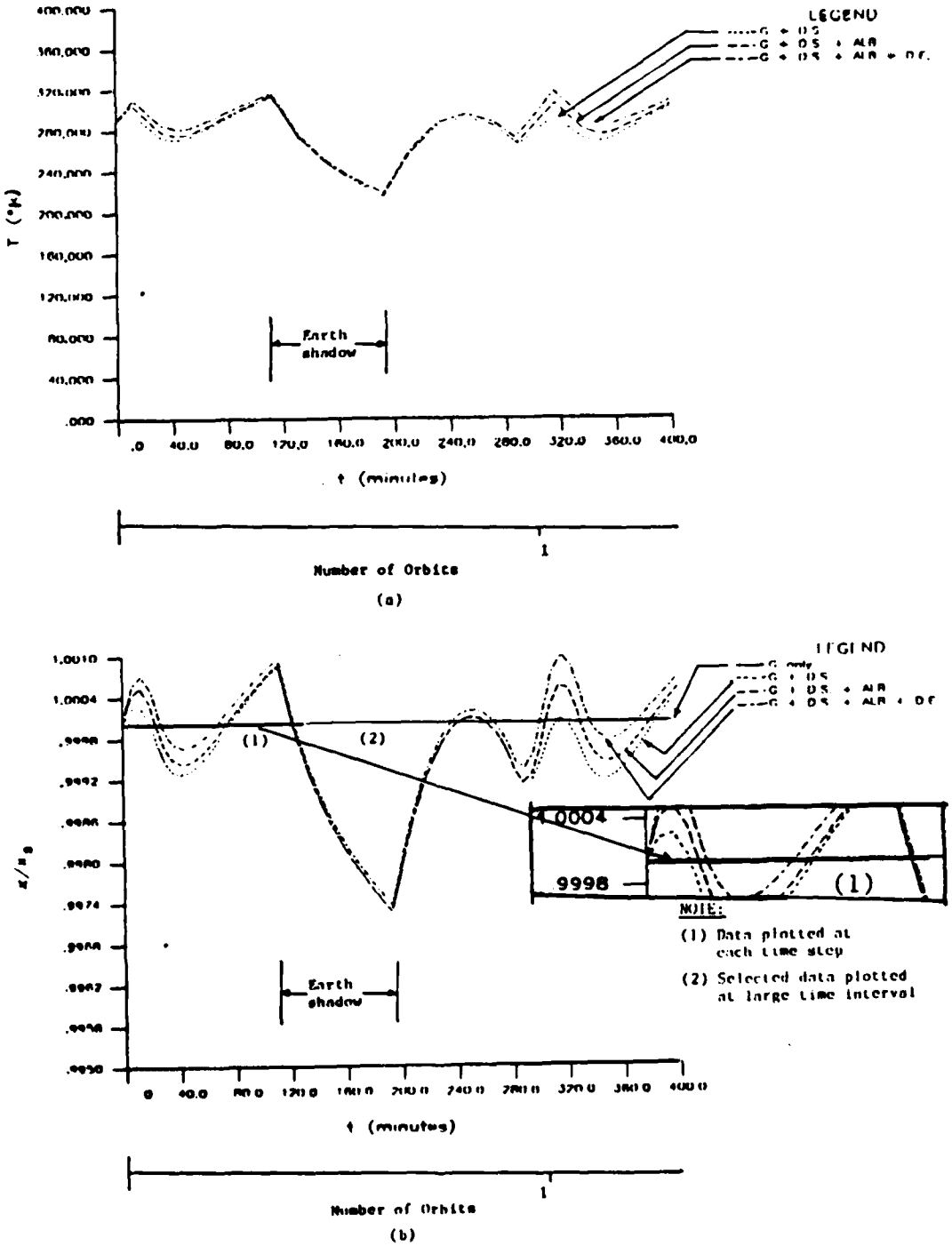

Figure 45. (a) Temperature variation (T), (b) thermal effects on axial length (x): Elliptical orbit (e = 0.56 and perigee altitude = 200 km), Special Case 2 (Ø = π/2: Maximum direct earth and albedo heating)

The maximum and minimum temperatures due to the total radiation heating are respectively 317.49 °K and 217.76 °K. The values of the temperature due to direct solar radiation only are, respectively 313.572 °K and 214.968 °K. Figure 45(b) shows a plot of x/x_s versus time for this special case. The greatest extension and shortening of the length (x) of the structure due to the total radiation heating are 0.09981 percent and 0.2672 percent of the initial length (x_0), respectively. Due to direct solar radiation alone, these quantities are respectively 0.08496 percent and 0.2773 percent of x_0. Due to the earth's albedo and its direct radiation heating the maximum increases in x are 0.0495 percent and 0.04248 percent of x_0, respectively.

Special Case 3. In this orientation the structure experiences the least radiation heating from the earth. The structure's longitudinal axis is always aligned with the local vertical (r_c-vector) i.e., $\emptyset = 0$ for all t. As in Special case 2, the temperature and structural response depend on the altitude, location in the orbit, and the orientation with respect to the sun. The maximum temperature due to the total radiation heating during the 400 minute period is 321.326 °K, and the minimum temperature is 207.130 °K (Figure 46(a)). The maximum and minimum temperatures of the structure due to direct solar radiation heating only are 315.445 °K and 206.640 °K, respectively.

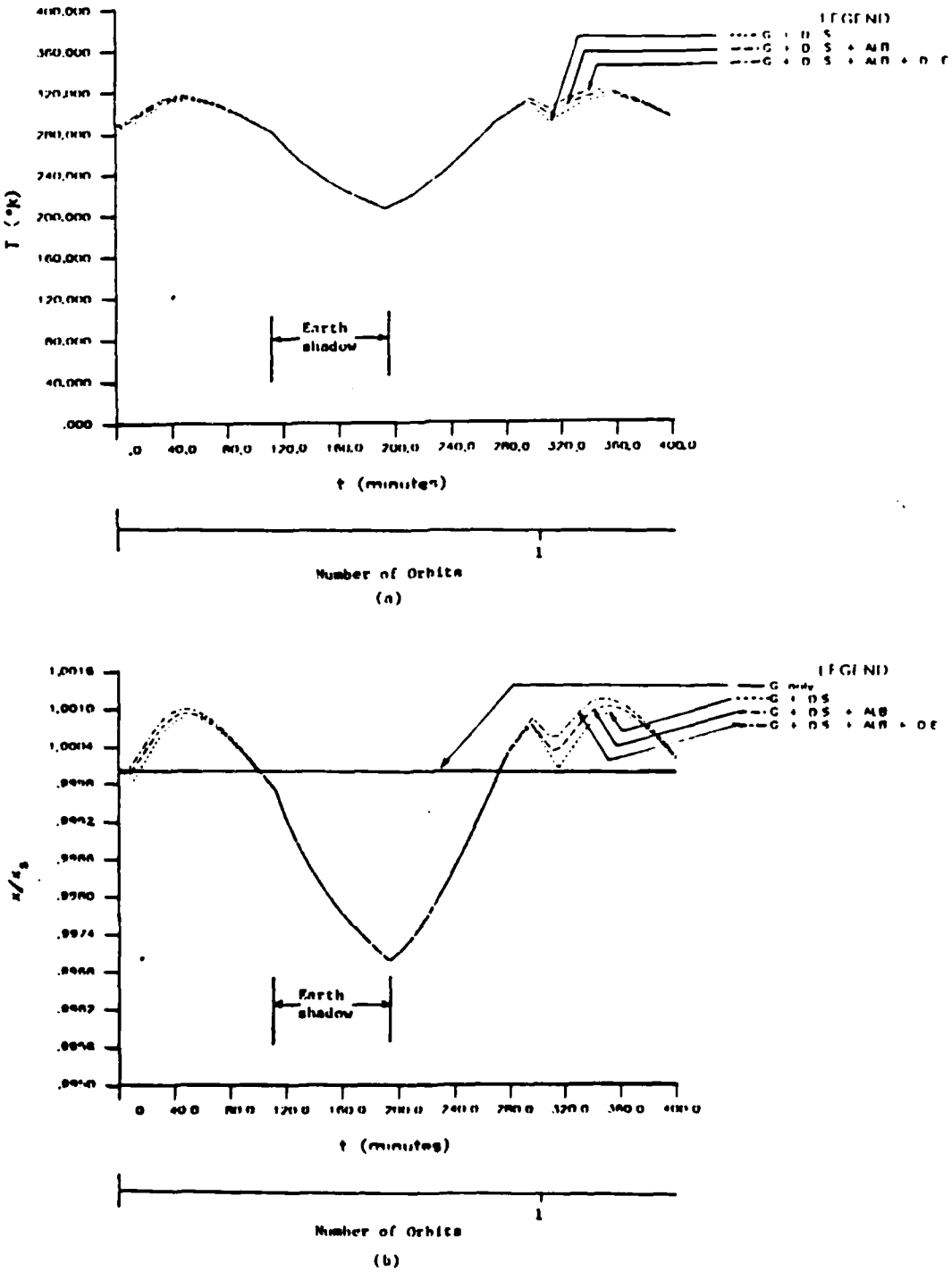

Figure 46. (a) Temperature variation (T), (b) thermal effects on axial length (x): Elliptical orbit (e = 0.56 and perigee altitude = 200 km), Special Case 3 (ϕ = 0: minimum direct earth and albedo heating)

The distribution of x/x_s with respect to time is shown in Figure 46(b). The contributions from the earth's albedo and its direct radiation are smaller, compared to the direct solar radiation effect. The greatest elongation of the length (x) of the structure due to the total radiation heating is 0.1124 percent of the initial length (x_0), and the peak shortening in x due to this effect is 0.3043 percent of x_0. The greatest elongation of x due to the direct solar radiation only is 0.091 percent of x_0, and the largest contraction in x due to the direct solar radiation heating alone is 0.3062 percent of x_0. On the sunlight side of the orbit the largest increase in x due to the earth's albedo and its direct radiation heating are 0.0292 percent and 0.0214 percent of x_0 respectively. In the earth shadow region, contributions from these terrestrial radiations are nearly zero.

Special Case 4. The structure is made to align with the sun vector (i.e., $\theta + \phi = 0$) and so, it receives a zero amount of direct solar radiation. The structure is thus under the influence of only the terrestrial radiation. The distributions of θ and ϕ with respect to time are show in Figure 47. Figure 48(a) shows a plot of T versus time. The temperature drops continuously with time except for a small increase near perigee due to the strongest intensity of the earth's albedo and its direct radiation at this region. As in Special Case 1, the structure has a fixed orientation

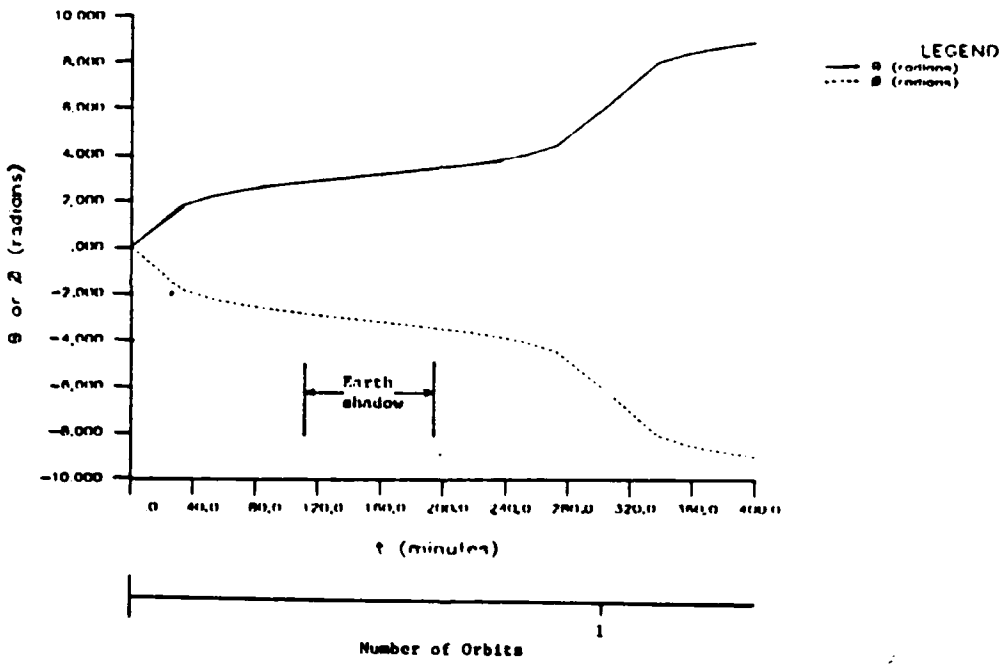

Figure 47. Variations of θ and Ø: Elliptical orbit (e = 0.56 and perigee altitude = 200 km), Special Case 4 (orientation θ + Ø = 0: Minimum direct solar heating)

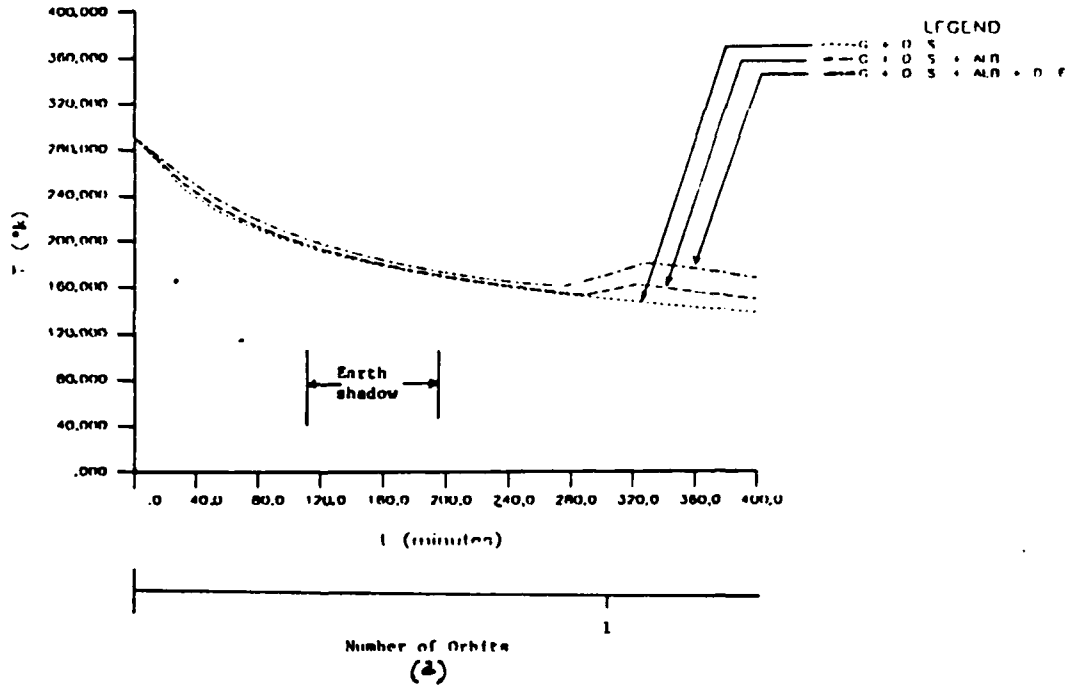

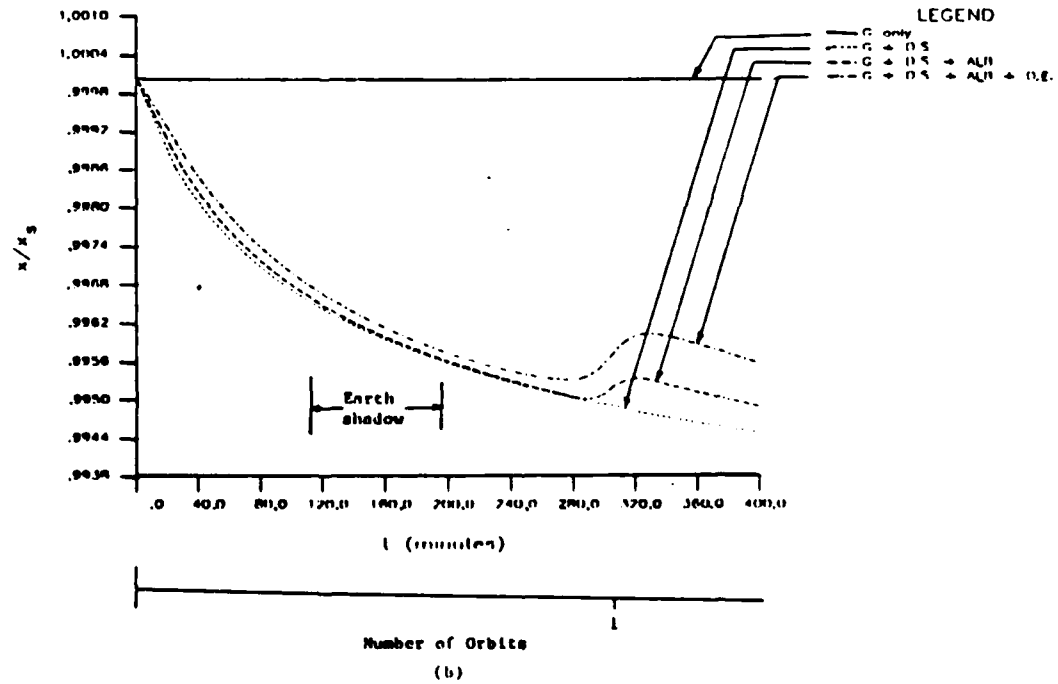

Figure 48. (a) Temperature variation (T), (b) thermal effects on axial length (x): Elliptical orbit (e = 0.56 and perigee altitude = 200 km), Special Case 4 ($\theta + \phi = 0$: Minimum direct solar heating)

with respect to the sun. Therefore, the temperature and structural response of the system depend on its distance from the earth, its location in the orbit, and its orientation with respect to the earth. The extreme temperatures of the structure due to the total radiation heating in the 400 minute duration are the initial temperature (290 °K), and the minimum temperature of 161.123 °K. Figure 48(b) shows a plot of x/x_s versus t. At any time greater than zero the structure is in compression. The largest decrease in length (x) due to the total radiation heating is 0.4722 percent of the initial length (x_0). If only direct solar radiation is considered, x decreases by 0.5546 percent of x_0. The largest change in x due to the earth's albedo and its direct radiations are 0.055 percent and 0 0714 percent of x_0, respectively.

Effects of Surface Area-to-Mass Ratio

Material properties including surface properties are of great importance regarding the thermal response of a structure. Reliable material data are a prerequisite to an accurate thermal structural response prediction of a space structure. Another fundamental quantity upon which the thermal response of a space-structure is greatly dependent is the surface area-to-mass ratio (A_{sf}/m). In this study, three values of A_{sf}/m ratio 0.000486 m^2/kg, 0.0486 m^2/kg and 2.778 m^2/kg, are

selected. The thermal effects on the structure due to the total radiation for these three values of the A_{sf}/m ratio are compared to each other considering the space structure in the elliptical orbit (e = 0.56, and perigee at 200Km altitude) described above. The complete set of initial conditions and the physical parameter values for these runs are given in Example No. 33, 38, and 39 in Table 2(b). The results and discussion presented below are based on the 400 minute duration.

Figures 49, 50(a) and (b) show plots of T, x/x_s, and Ø versus time for the three values of the A_{sf}/m ratio under the influence of the total radiation heating. These plots show that T, x/x_s, and Ø do not undergo any appreciable change when the A_{sf}/m value is changed from 0.000486 m^2/kg to 0.0486 m^2/kg. For an A_{sf}/m ratio equal to 0.000486 m^2/kg, the radiation thermal effects on these variables have already been discussed (Figures 40, 41(a) and (b)). On the other hand, for the higher value of the A_{sf}/m ratio (equal to 2.778 m^2/kg), the distributions of T, x/x_s, and Ø with respect to time are very different from those for the other two values of the A_{sf}/m ratio. The temperature in the case of A_{sf}/m equal to 2.778 m^2/kg changes much faster with the change in heat load. There are sudden drops and rises in the temperature variation while entering into, and exiting from, the earth's shadow, respectively. As before, the maximum temperature occurs when the space structure is in the sunlight side, and the minimum temperature occurs when it is in the earth's shadow region of

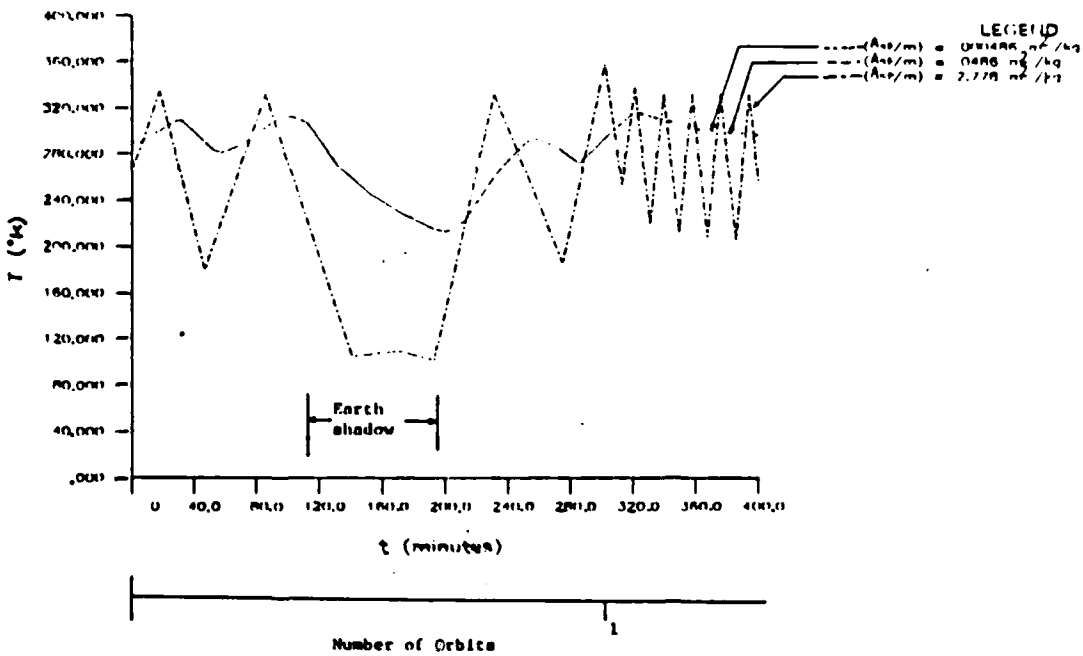

Figure 49. Effects of surface area to mass ratio (A_{sf}/m) on temperature (T): Elliptical orbit (e = 0.56, and perigee altitude = 200 km), general orientation (case)

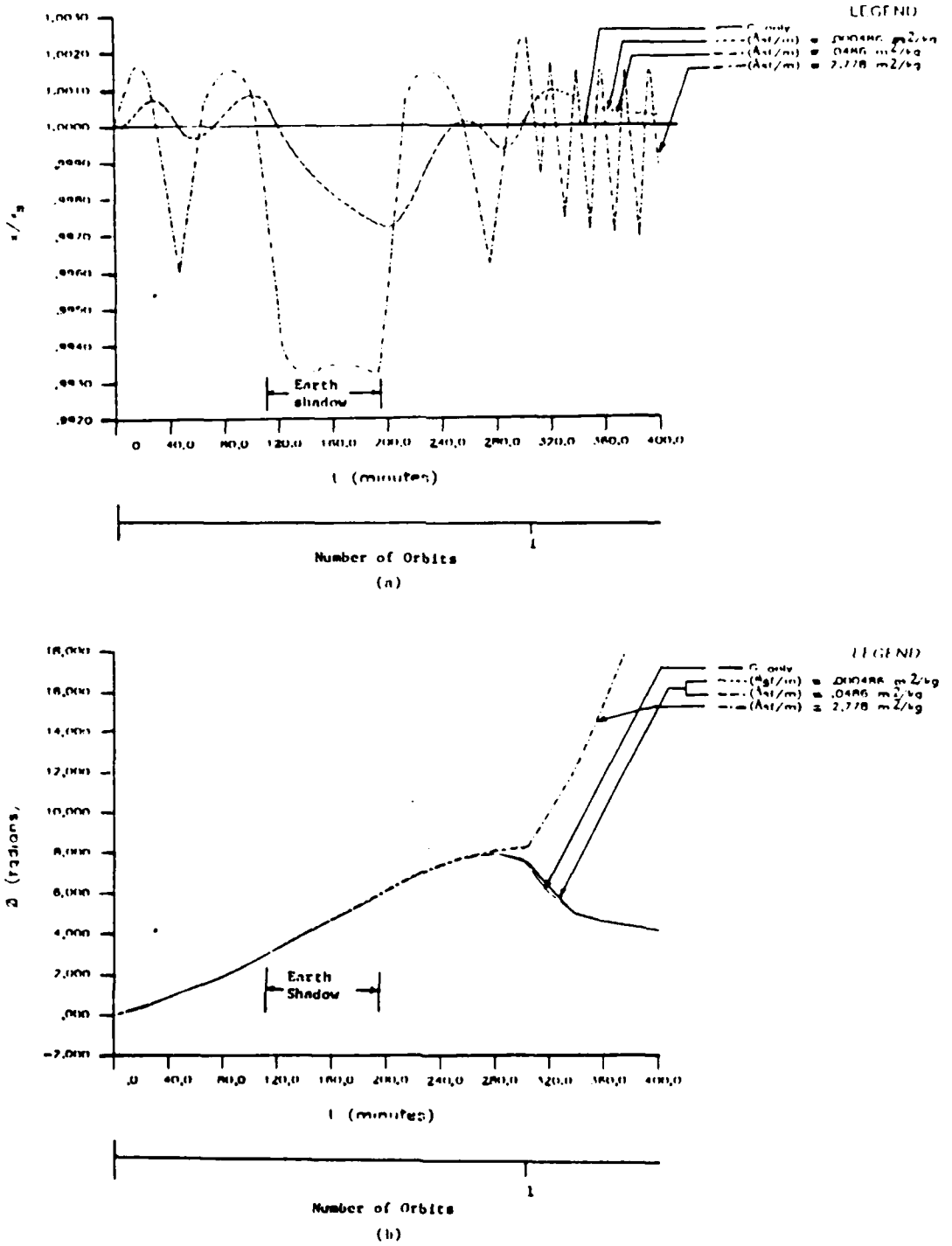

Figure 50. Influence of surface area to mass ratio (A_{sf}/m) on total thermal effects on (a) axial length (x), (b) attitude (Ø): Elliptical orbit (e = 0.56 and perigee altitude = 200 km), general orientation (case)

the orbit. The structural response (x/x_s vs. t) follows the temperature history (Figure 50(a)). The maximum increase in the length (x) of the space structure is approximately equal to 0.2454 percent of the initial length (x_0), whereas the largest decrease in x is approximately equal to 0.6758 percent of x_0.

More remarkable is the influence of thermal effects on the attitude (Ø) of the space structure with A_{sf}/m equal to 2.778 m^2/kg (Figure 50(b)). The Ø versus t curve in this case closely follows those obtained for the previous two values of the A_{sf}/m ratio until the end of one orbit period. From that point onward, instead of decreasing as is the case for the other two values of the A_{sf}/m ratio, Ø now keeps continuously increasing at a much more rapid rate. The value of Ø at the end of the duration considered here (400 minutes) is approximately 21.914 radians. The structure is thus seen to tumble continuously. This continuous rotation of the space structure about its center of mass causes the radiation heat load to change accordingly. This is the main reason behind the faster oscillation in T and x/x_s after t equal to 313.1 minutes in the sunlight side of the orbit (Figure 50(a) and (b)).

As we saw above, the total thermal effect on the structure which has a large value of the A_{sf}/m ratio is very significant. The relative contributions from the earth's albedo and its direct radiation heating are studied next in such a structure. We are interested in the maximum contributions from these radiation sources. Therefore, the orbit selected is a

circular one at 200 km altitude (LEO), and the structure is considered to be always perpendicular with respect to the earth (Special Case 2, $\emptyset = \pi/2$). The solution of the equations of motion is obtained for an almost 4 orbit duration (352 minutes). A complete set of initial conditions and values of physical parameters are given in Example No. 40 in Table 2(b). The structure has the A_{sf}/m ratio equal to 2.778 m^2/kg.

It can be observed in Figure 51(a) that the temperature reaches values of radiation equilibrium even in LEO, where the orbital period is short (88.4 minutes). In the sunlight portion the maximum temperatures are 330.405 °K, 351.650 °K, and 362.443 °K respectively due to direct solar, direct solar plus the earth's albedo, and all three sources of radiation heating (Direct solar, earth albedo and its direct radiation). In the earth's shadow part, the minimum temperatures due to these three combinations of radiation sources considered are 80.427 °K, 80.427 °K, and 210.536 °K, respectively. Figure 51(b) shows a plot of x/x_s versus time. For total radiation heating, the maximum increase and decrease in x are, respectively 0.2635 percent and 0.29022 percent of x_0. If only direct solar radiation is considered the maximum increase and decrease in x are 0.12462 percent and 0.7642 percent of x_0, respectively. In the sunlight part, the largest change in x due to the earth's albedo and its direct radiation considered separately are 0.0778 percent and 0.0397 percent of x_0 respectively. In the earth's shadow side, the contribution from the earth's albedo radiation

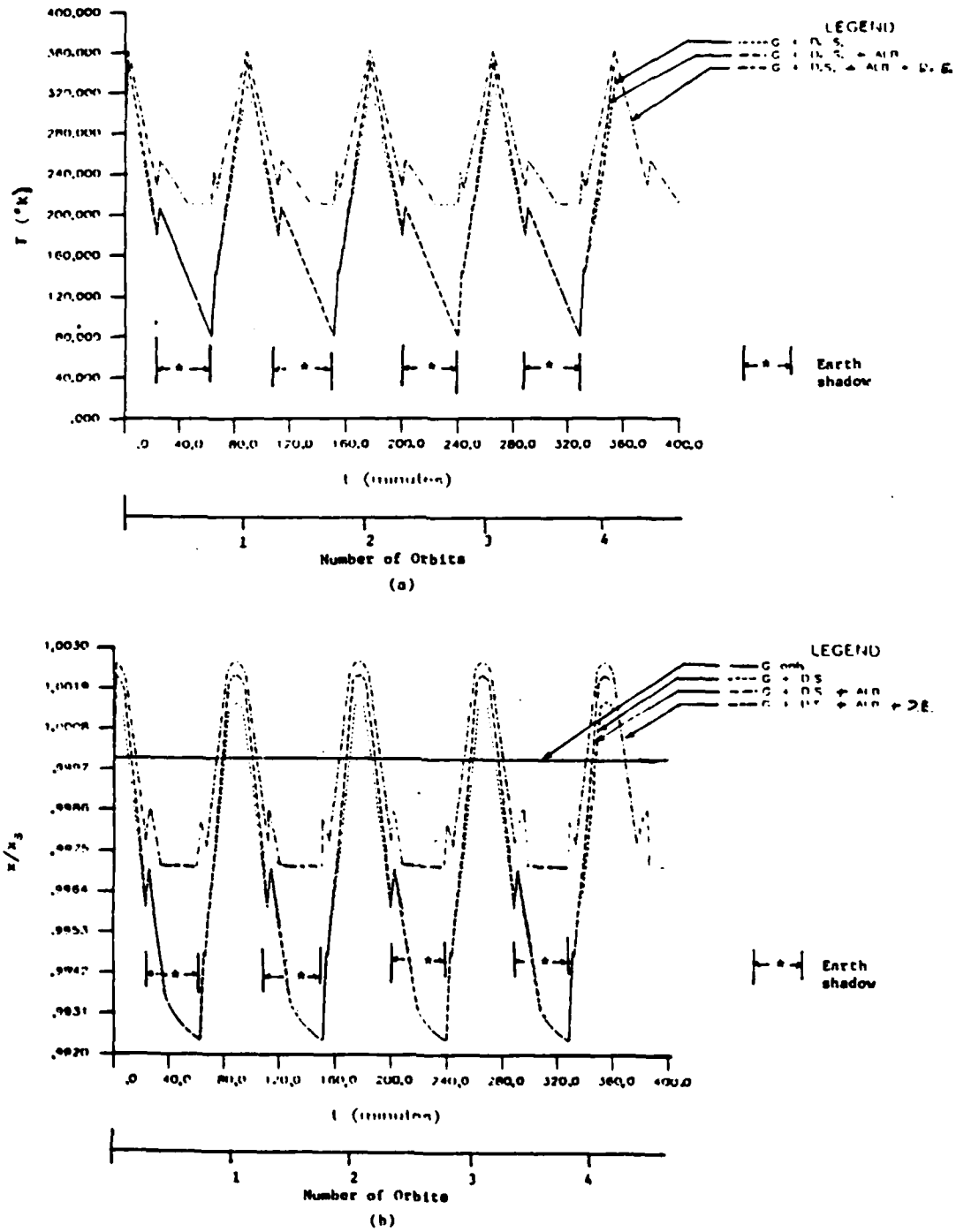

Figure 51. (a) Temperature variation (T), (b) thermal effects on axial length (x): Circular orbit at altitude 200 km, $A_{sc}/m = 2.778\ m^2/kg$, Special Case 2 ($\emptyset = \pi/2$: Maximum direct earth and albedo heating)

is zero, while the largest change in x due to direct earth radiation alone is 0.474 percent of x_0.

Radiation Pressure Effects

Lastly, in order to delineate the effects of the radiation pressure on a space structure's axial deformation and motions, orbital as well as attitude, the complete equations of motion are solved taking into account the various external forcing functions due to the radiation pressure. First, effects of direct solar radiation pressure have been studied considering the structure in a general and in a special (Special Case 1) orientation with respect to the sun and/or the earth. The direct solar radiation pressure effects are obtained simultaneously with the structure's orbital motion, attitude motion, and axial deformation. The dependency of these effects on the surface area to mass ratio (A_{sf}/m) and on the location of the center of pressure (point P) with respect to the center of mass (point C) of the structure defined by the l_p parameter (see Figure 9), has been investigated. Second, computer results are obtained to study the effects of total radiation pressure (including direct solar, earth's albedo and its direct radiation) on the space structure's axial length and its orbit considering the space structure in a special orientation (Special Case 2) which experiences maximum contribution from the terrestrial radiation pressure.

The elliptical orbit with perigee at 200 km altitude

(r_c = 6574.33 km) and apogee at 17108.68km altitude (r_c = 23483.014 km) (i.e., orbit eccentricity equal to 0.56) is considered. The static length (x_s) is kept the same (1 km) for all runs. The locations of the space structure's entry into, and exit from, the earth's shadow in such an elliptical orbit are given in Table 3. For the purpose of comparing the results, the distribution of various basic parameters in the presence of combined effects of the radiation pressure and the differential gravitational force as a function of time are shown with those in the presence of the differential gravitational force alone on the same plot. The surface of the structure is considered to be completely absorbing. The solution of the equations of motion is obtained for a duration of more than one orbit period (305.6 minutes). The step sizes considered for the computations are 0.2 minutes when $|\theta| \leq \pi/2$ and 0.1 minutes when $|\theta| \geq \pi/2$.

Direct Solar Radiation Pressure Effects

The complete sets of initial conditions and the physical parameter values corresponding to these runs are given in Table 2(c), Example no. 41 through 50. As in the radiation thermal effects, the radiation pressure effects are also very much dependent on the surface area to mass ratio (A_{sf}/m) of the structure. It has been indicated in

Chapter II that the concept of solar sailing is possible for large A_{sf}/m values. Besides this quantity, other quantities which may significantly affect the attitude (Ø) and other variables dependent on Ø, of the structure are the magnitude and sense of the distance (l_p) between the center of pressure (P) and the center of mass (C) of the structure (Figures 8 and 9). Results and discussion presented in the subsection below demonstrate the effects of the direct solar radiation pressure on the structure taking these factors into account.

Effects of surface area-to-mass ratio and position of the center of pressure with respect to the center of mass. To investigate the effects of the surface area-to-mass (A_{sf}/m) ratio on the radiation pressure effects, three values of A_{sf}/m are chosen. They are 0.000486 m^2/kg, 0.0486 m^2/kg, and 2.778 m^2/kg. It is assumed that the maximum magnitude of the distance (l_p) between the center of pressure (point P) and the center of mass (point C) is one-quarter of the one kilometer long space structure. Since the structure selected has uniform rectangular cross section, the point P always lies at the mid-length. However, the point P can be on either side of the point C depending on the value of the m_1/m_2 ratio. For example, when $m_1/m_2 = 1$, points C and P coincide to each other. If $m_1/m_2 > 1$, P is nearer to mass m_2 than C (i.e., P

lies toward m_2 from C). On the other hand, for $m_1/m_2 < 1$, P is nearer from mass m_1, than C (i.e., P lies toward m_1 from C). Since our positive x-axis is directed toward m_1 from C, l_P is negative when $m_1/m_2 > 1$, and it is positive when $m_1/m_2 < 1$. The sign of l_P is important as it determines the sign of the moment ($Q_\emptyset$) of the radiation pressure about point C. Thus, the structure may rotate about C in opposite directions depending on the sign of l_P. Three values of l_P are chosen for the computer runs. These are zero (corresponding to $m_1/m_2 = 1$), $-0.25x_s$ (corresponding to $m_1/m_2 = 3$), and $+0.25x_s$ (corresponding to $m_1/m_2 = 1/3$). The structure is permitted to take a general orientation with respect to the sun and the earth.

Figures 53(a), 53(b), 54(a), and 54(b) show the plots of the external forcing functions (Q_r, Q_θ, Q_x, and $Q_\emptyset$) due to direct solar radiation pressure versus time respectively for A_{sf}/m equal to 0.000486 m^2/kg and for the three values of l_P. These quantities are seen to be complicated functions of r_c, θ, and $\emptyset$ for the given set of the values of x, m, and l_P (m_1/m_2 ratio). All of these parameters are zero while the space structure is inside the earth's shadow as the structure does not then experience direct solar radiation pressure.

For small values of the A_{sf}/m ratio (0.000486 m^2/kg, and 0.0486 m^2/kg), the computer results show that

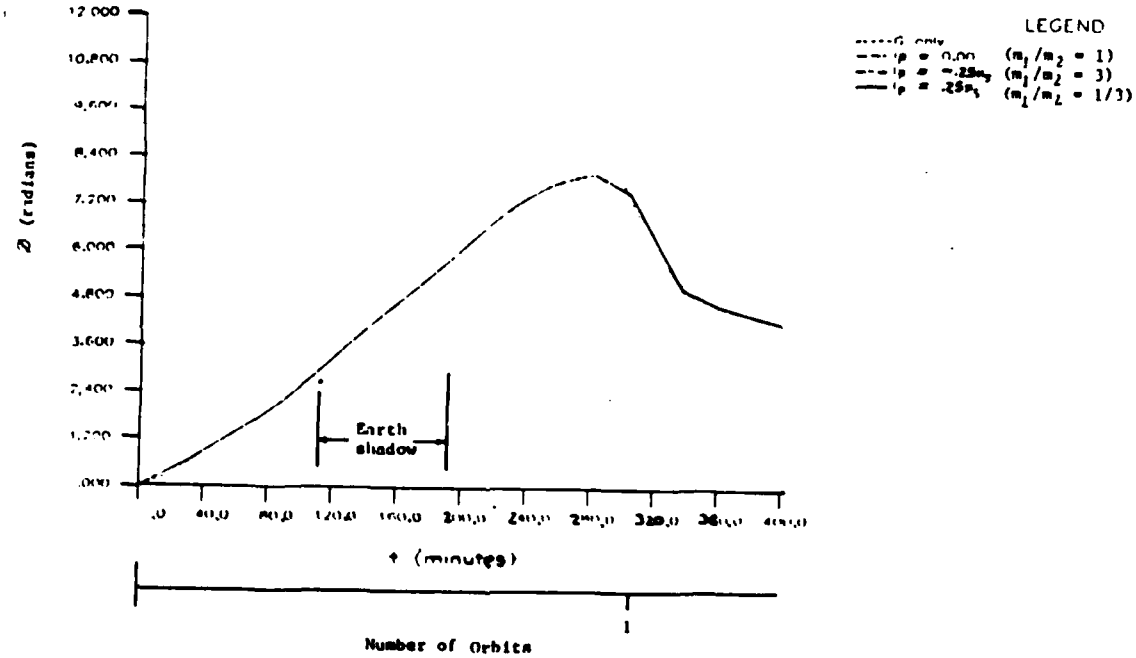

Figure 52. Effects of direct solar radiation pressure on attitude (Ø): Elliptical orbit (e = 0.56 and perigee altitude = 200 km), A_{sr}/m = 0.000486m^2/kg, general orientation (case)

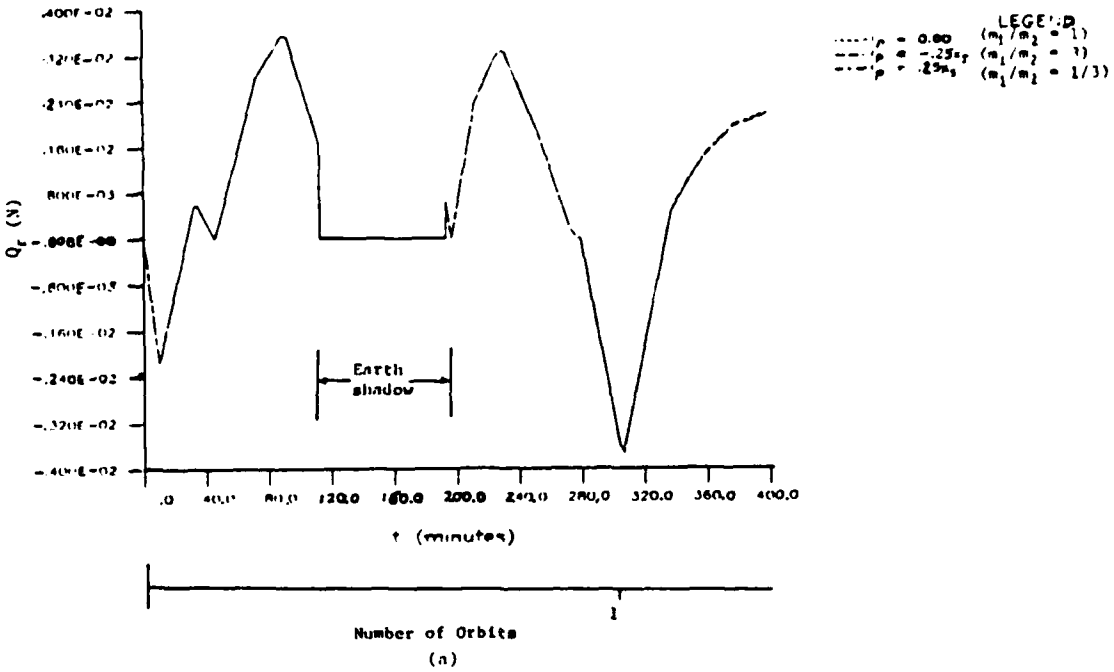

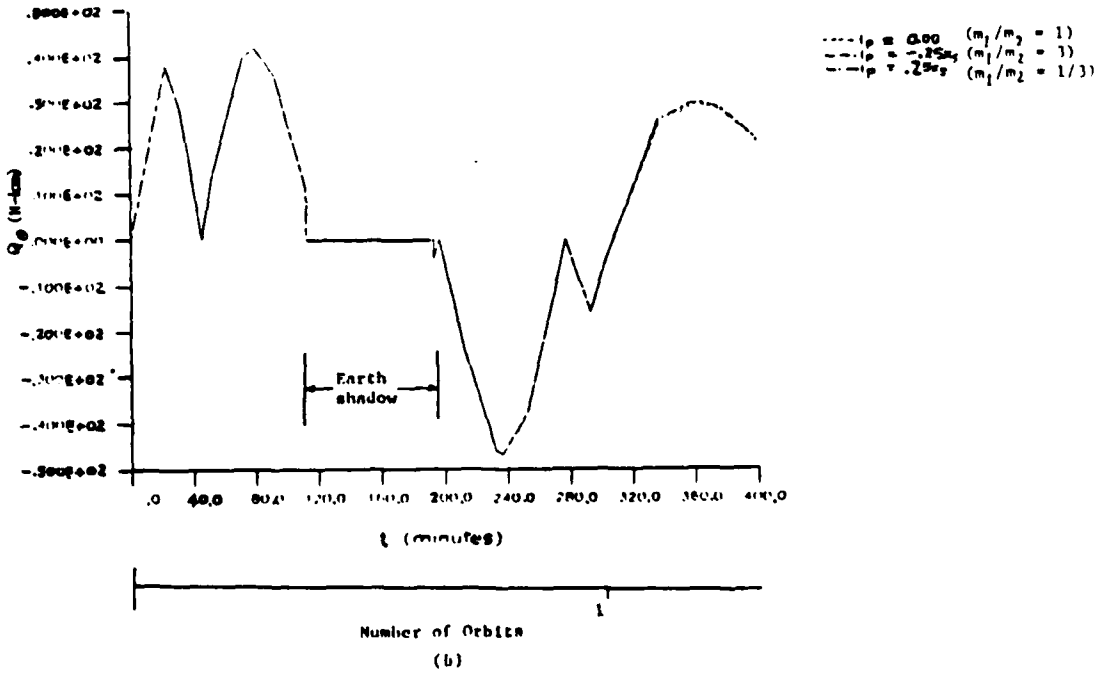

Figure 53. Variation of (a) Q_r, (b) Q_θ, under influence of direct solar radiation pressure: Elliptical orbit (e = 0.56 and perigee altitude = 200 km), $A_{sf}/m = 0.000486\ m^2/kg$, general orientation

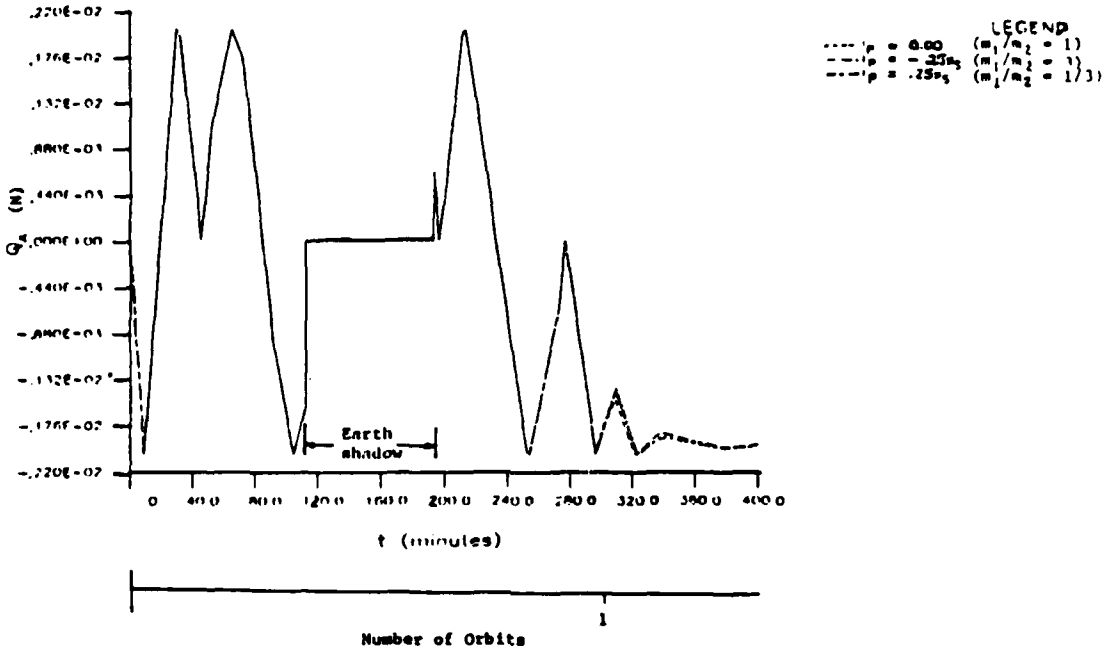

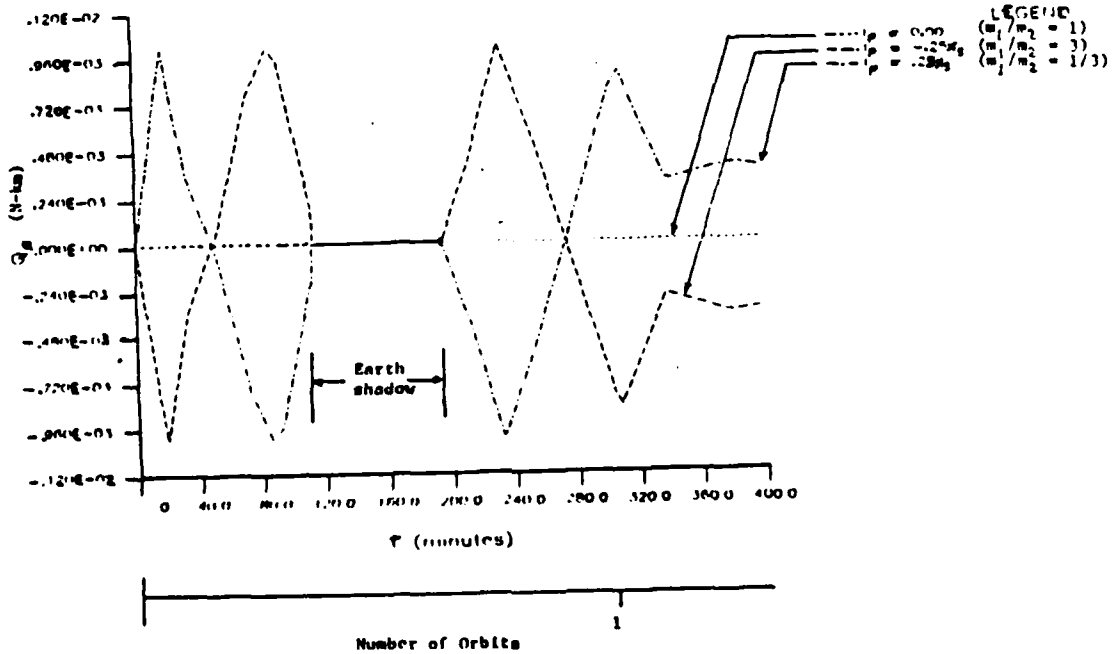

Figure 54. Variations of (a) Q_x, (b) Q_g, under influence of direct solar radiation pressure: Elliptical orbit (e = 0.56 and perigee altitude = 200 km), A_{sf}/m = 0.000486 m^2/kg, general orientation

the perturbations of orbit (r_c, θ), attitude ($\emptyset$), and length (x) of the space structure due to the direct solar radiation pressure are negligible for all lp values. For example, the radius of the orbit is perturbed by only a few meters, and the orbital period may be considered unaltered. $\emptyset$ changes at the most by 1×10^{-5} radians, and the change in x is within a few centimeters for the one kilometer long structure. A plot of $\emptyset$ versus t for A_{sf}/m equal to 0.000486 m^2/kg is shown in Figure 52 during the 400 minute period.

The effects of direct solar radiation pressures are significant when the A_{sf}/m ratio is large. The variations of Q_r, Q_θ, Q_x, and $Q_\emptyset$ with time for all lp values, when A_{sf}/m is large (2.778 m^2/kg), are shown in Figures 56(a), 56(b), 57(a) and 57(b) respectively. These plots also indicate that Q_r, Q_θ, Q_x, and $Q_\emptyset$ are affected by lp values. This gives us a hint that for larger values of the A_{sf}/m ratio, lp values play a much greater role in effecting the magnitude of the radiation pressure effects on the structure. The computer data show that the effects of the radiation pressure on the length (x) of the structure is again negligible. For all lp values, the change in x is only a few centimeters. The pattern of oscillation in x is observed to be similar to that of the differential gravitational force effect alone.

Increased perturbation of orbital motion is noticed at

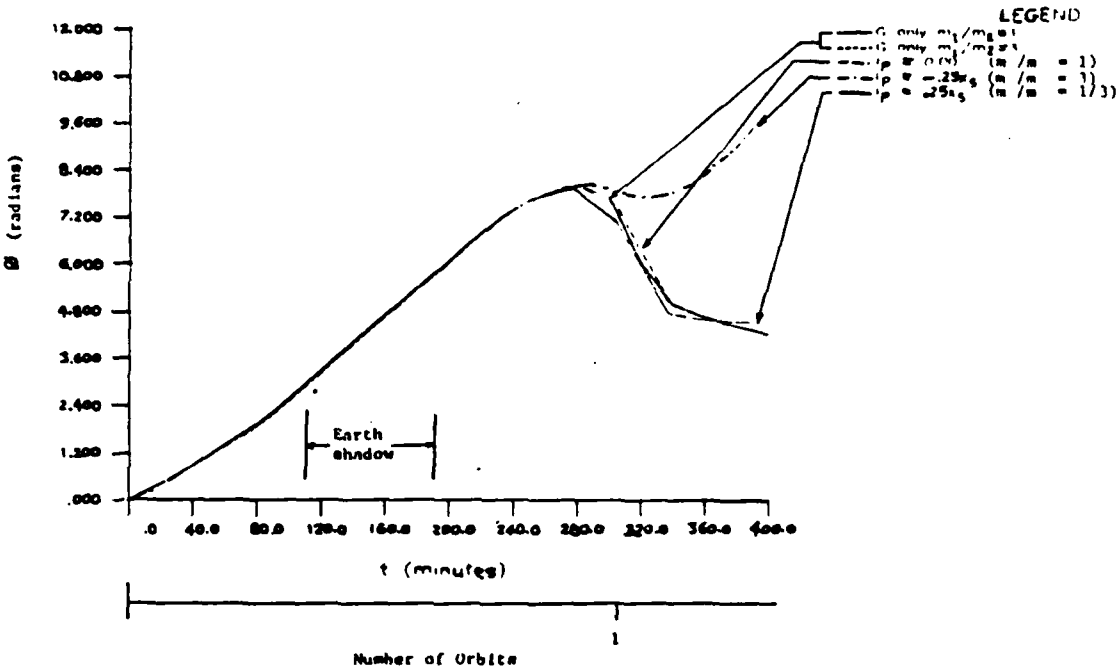

Figure 55. Effects of direct solar radiation pressure on attitude (Ø): Elliptical orbit (e = 0.56 and perigee altitude = 200 km), A_{sf}/m = 2.778 m^2/kg, general orientation (case)

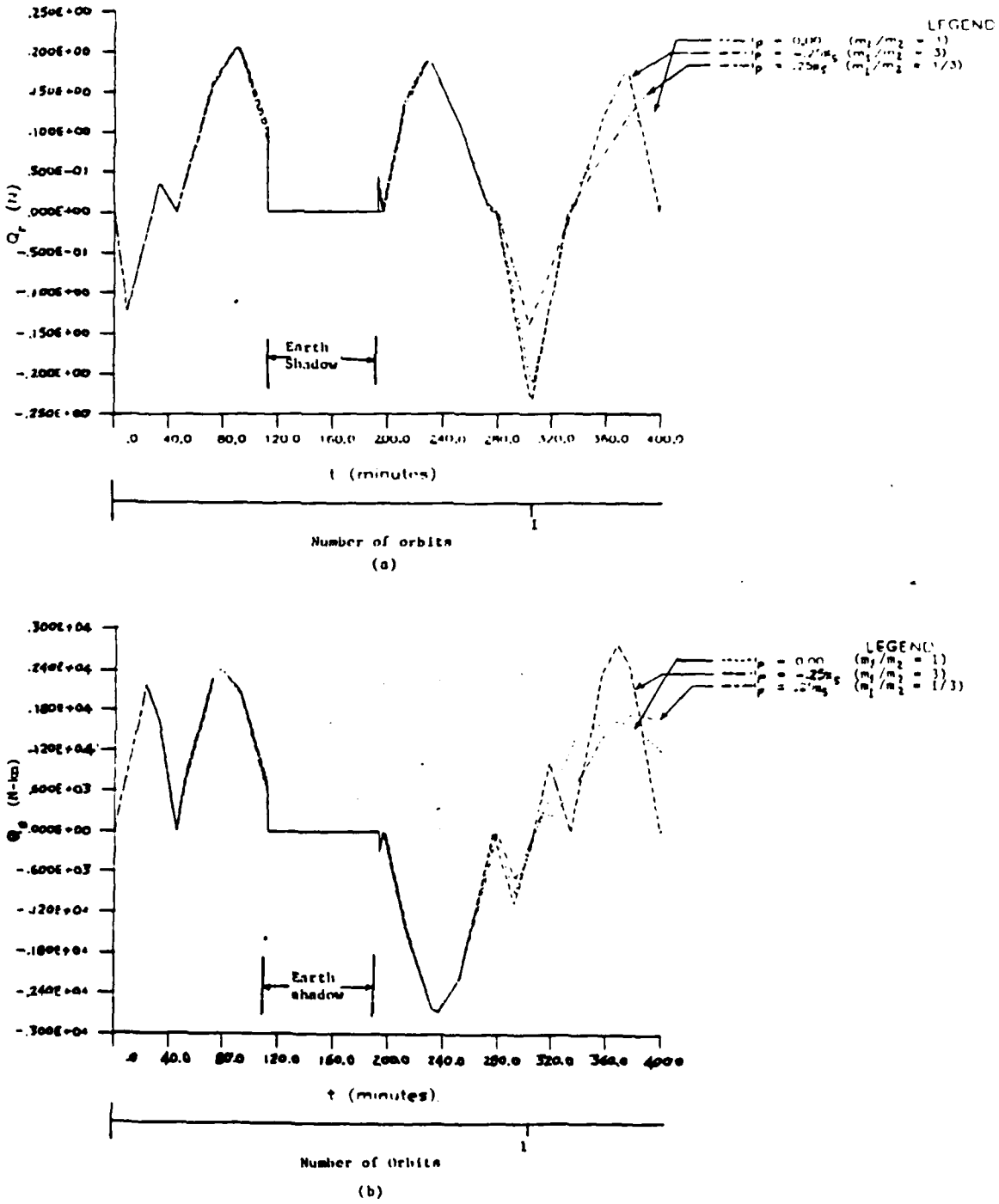

Figure 56. Variation of (a) Q_r, (b) Q_θ under influence of direct solar radiation pressure: Elliptical orbit (e = 0.56 and perigee altitude = 200 km), A_{sf}/m = 2.778 m^2/kg, general orientation

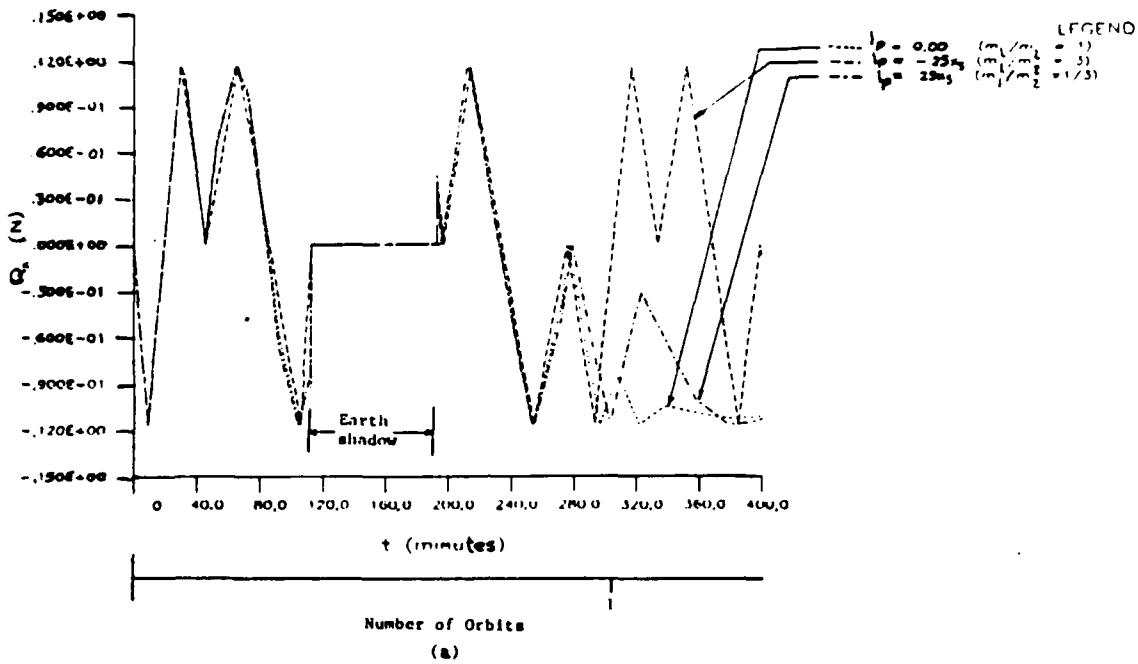

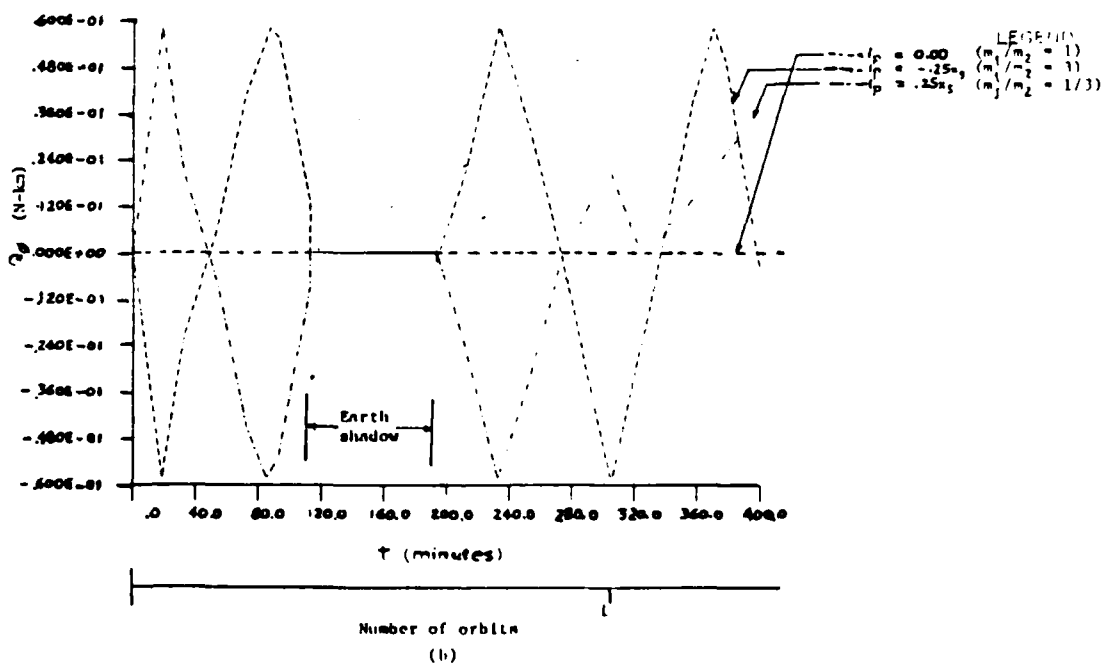

Figure 57. Variation of (a) Q_x, (b) Q_ϕ under influence of direct solar pressure: Elliptical orbit, (e = 0.56 and perigee altitude = 200 km), A_{sf}/m = 2.778 m^2/kg, general orientation (case)

this higher value of the A_{sf}/m ratio. For all three l_p values (0, -0.25 km, and 0.25 km), the variations of r_c and θ with time are the same. Therefore, l_p values do not perturb the orbit. The orbital period may still be considered to be the same as in earlier cases (305.6 minutes). Some magnitudes of the increase and decrease in r_c are presented below for A_{sf}/m = 2.778 m^2/kg, l_p = -0.25 km, and a general orientation of the structure.

t (minutes)	θ (radians)	Change in r_c due to D.S. with respect to G only (meter)	
0 (perigee)	0	0	
22.2	1.47418	-0.6	
158.2 (apogee)	3.14162	+213.0	+ increase
200.0	3.48866	+404.0	- decrease
281.0	4.71705	+947.0	D.S. Direct
290.0	5.1196	+892.4	solar
305.6 (perigee)	6.28399	+4.5	radiation
331.0	7.87874	-943.0	
400.0	8.98593	-339.0	

Figure 55 shows a plot for Ø versus t for the three l_p values when A_{sf}/m = 2.778 m^2/kg during 400 minute period. The plot shows that at this higher value of A_{sf}/m, Ø is greatly affected by l_p values. For all three values of l_p, the distribution of Ø with respect to time is approximately the same from 0 to 278 minutes. This distribution is the same as in the case of gravitational

force only. During the period 0 to 278 minutes, the radiation pressure again does not affect Ø. The magnitide of Ø in this period increases continuously from zero to 7.91663 radians. After 278 minutes, Ø decreases for l_p equal to zero and +0.25km for the rest of the time. The variation of Ø in this period is again very close to that obtained for the gravitational force effect only. At t = 400 minutes, Ø equals 4.494324 radians for l_p = +0.25 km, and 4.206196 radians for l_p = 0 and G only cases. Most of this second period, the distribution of Ø for l_p = +0.25km is less than that for l_p = 0 or G only. The largest difference in the values of Ø between l_p = +0.25km and l_p = 0 or G only is about 0.075 radians (at t = 281.8 minutes, θ = 4.7468 radians). On the other hand, for l_p equal to -0.25km (or m_1/m_2 = 3), the variation of Ø with time after 278 minutes is quite different. Ø in this case increases from 7.91663 radians at t = 278 minutes to 8.0604 radians at t = 286.3 minutes. It then decreases to 7.675698 radians at t = 322.9 minutes after which it increases very rapidly to a value of 9.91195 radians at t = 400 minutes. This means that the space structure is tumbling continuously.

Special Case 1. As mentioned earlier, in this orientation the space structure experiences maximum direct solar radiation pressure because the structure is always at a right angle to the sun vector (θ + Ø = π/2). The

variations of θ and $\emptyset$ with time for such an orientation are given in Figure 42. The A_{sf}/m ratio considered in this case is 2.778 m^2/kg. The values of l_p chosen are zero ($m_1/m_2 = 1$) and -0.25 km ($m_1/m_2 = 3$). In this orientation we expect that the structure will be affected by the direct solar radiation to a maximum extent. The plots of Q_r, Q_θ, Q_x, and $Q_\emptyset$ versus time are shown in Figures 58(a), 58(b), 59(a) and 59(b), respectively. Again, the computer data show that the length (x) of the structure is hardly effected even by the largest radiation pressure. The change in x is within a few centimeters for the one kilometer long structure. The oscillation in x remains very close to that for G only case.

The orbital period of the elliptical orbit may again be considered unaltered at 305.6 minutes (although there is a very slight change). Due to the direct solar radiation pressure, r_c is expected to decrease when $|\theta| < \pi/2$ and increase for $|\theta| > \pi/2$ in the same orbit. The changes in the r_c value at some points in the orbit are given below for $A_{sf}/m = 2.778$ m^2/kg, $l_p = -0.25$km and Special Case 1. As seen earlier, the l_p values do not seem to effect the orbit.

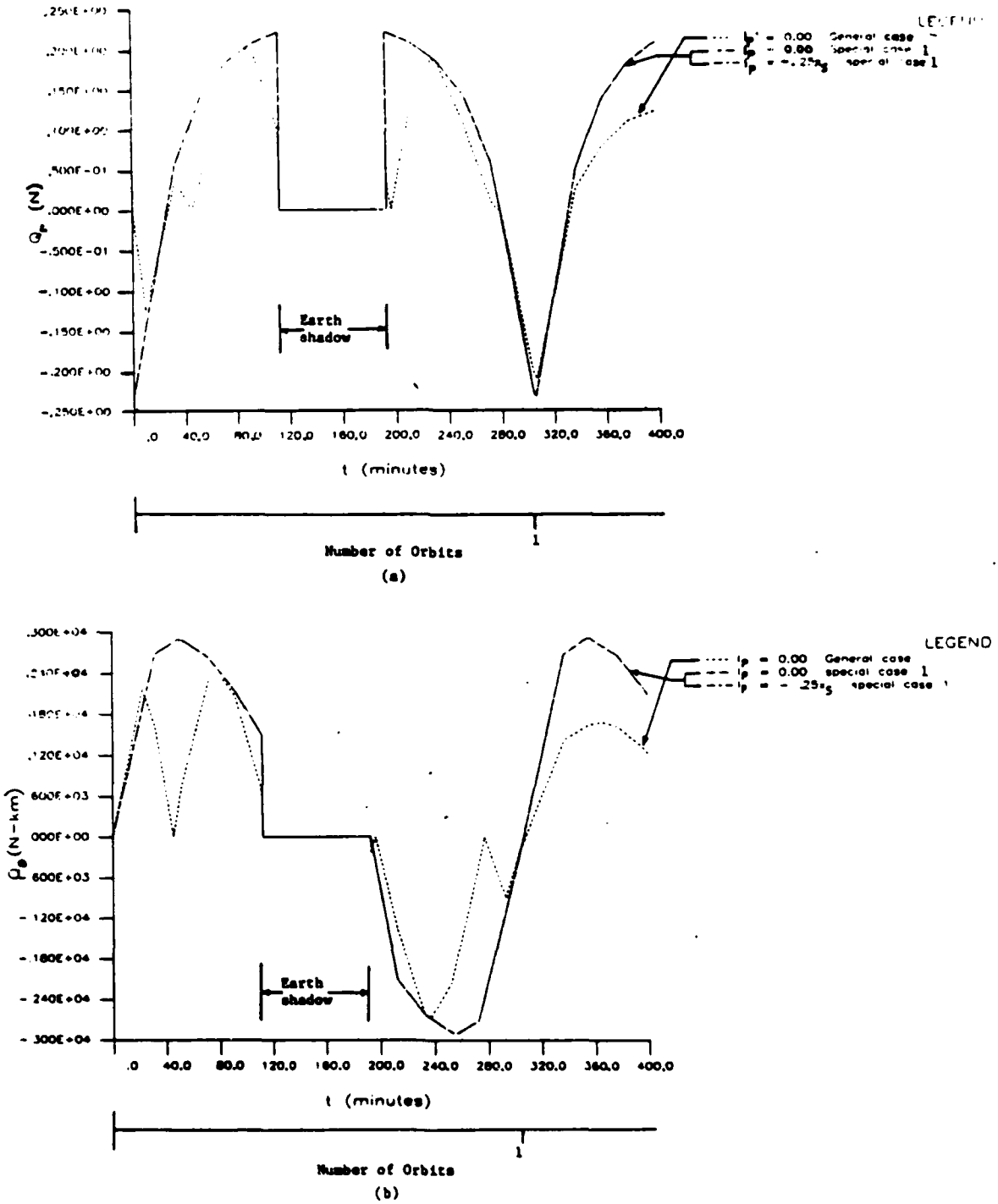

Figure 58. Variation of (a) Q_r, (b) Q_θ under influence of direct solar radiation pressure: Elliptical orbit (e = 0.56 and perigee altitude = 200 km), A_{sf}/m = 2.778 m^2/kg, general case and Special Case 1 ($\theta + \phi = \pi/2$: Maximum direct solar effect)

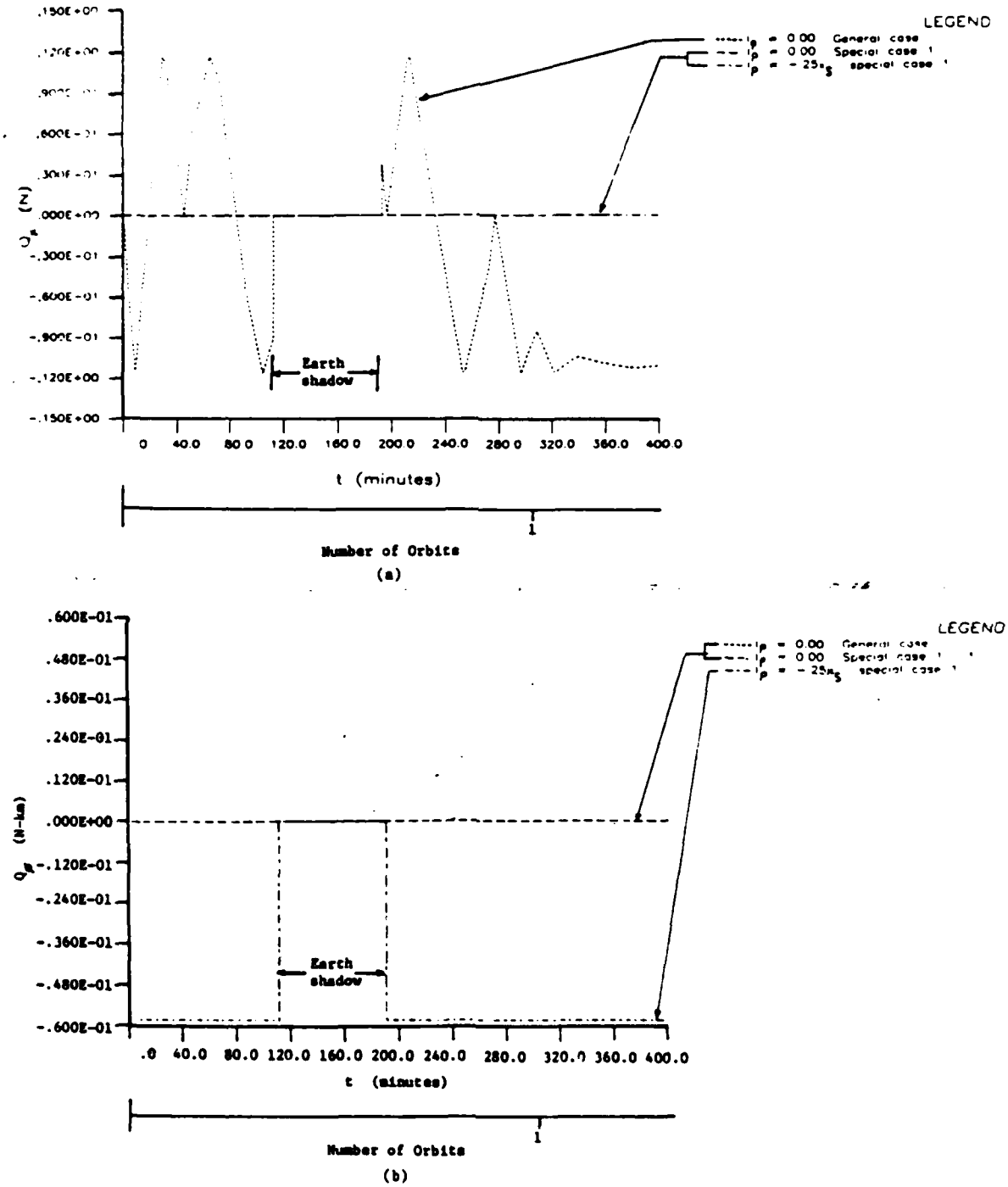

Figure 59. Variation of (a) Q_x, (b) Q_ϕ, under influence of direct solar radiation pressure: Elliptical orbit ($e = 0.56$ and perigee altitude = 200 km), A_{sf}/m = 2.778 m^2/kg, general case and Special Case 1 ($\theta + \phi = \pi/2$: Maximum direct solar effect)

t (minutes)		θ (radians)	Change in r_c due to D.S. with respect to G only (meter)	
0	(perigee)	0	0	
22.2		1.47418	-1.4	+ Increase
152.8	(apogee)	3.141624	+325.0	- Decrease
200.0		3.486635	+615.0	
281.0		4.71705	+1444.0	
290.0		5.1196	+1348.6	
305.6	(perigee)	6.28399	- 6.0	
331.0		7.87874	-1447.0	
400.0		8.98593	-523.0	

Combined Effects of Direct Solar and Terrestrial Radiation Pressures

The main purpose here is to investigate the maximum effects of the earth's albedo and its direct radiation pressure on the deformation of the structure. For this reason the structure is considered to be always perpendicular to the radial vector (r_c) (Special Case 2, $\emptyset = \pi/2$). The attitude motion ($\emptyset$) of the structure is restricted now. However, we can still investigate the maximum terrestrial radiation pressure effects on the structure's length (x) and its orbit (r_c, θ). The structure is considered to have a high A_{sf}/m ratio (2.778 m^2/kg). The initial conditions and physical parameter

values for the computer runs are given in Table 2(c), Example no. 50. The value of l_P chosen here is zero.

Figure 60(a), 60(b), 61(a), and 61(b) show the plots of Q_r, Q_θ, Q_x, and Q_ϕ versus time due to direct solar radiation only, direct solar and the earth's albedo combined, and direct solar, earth's albedo and its direct radiation combined for the period of 400 minutes. All of these cases include the effect of the gravitational force. Since the value of l_P is zero, the moment (Q_ϕ) of the radiation pressure about the point C remains zero throughout. Also since only a normal component of the terrestrial radiation pressure is effective (total transverse component is zero due to symmetry), the force (Q_x) along the length of the structure due to the terrestrial radiation pressure is zero. So, the Q_x versus t curve shown in Figure 61(a) is solely due to the contribution of direct solar radiation pressure. The plot in Figure 60(b) shows that the terrestrial radiation pressures also do not change the value of the moment (Q_θ) about the center of the earth. A very small change in the value of Q_r (force along r_c) is noticed due to the terrestrial radiation pressure when the structure is in the earth's shadow. Since the earth's albedo is zero here, all the contribution comes from the direct earth radiation alone. The terrestrial radiation pressure acts outward, which is opposite to the direct solar radiation pressure in

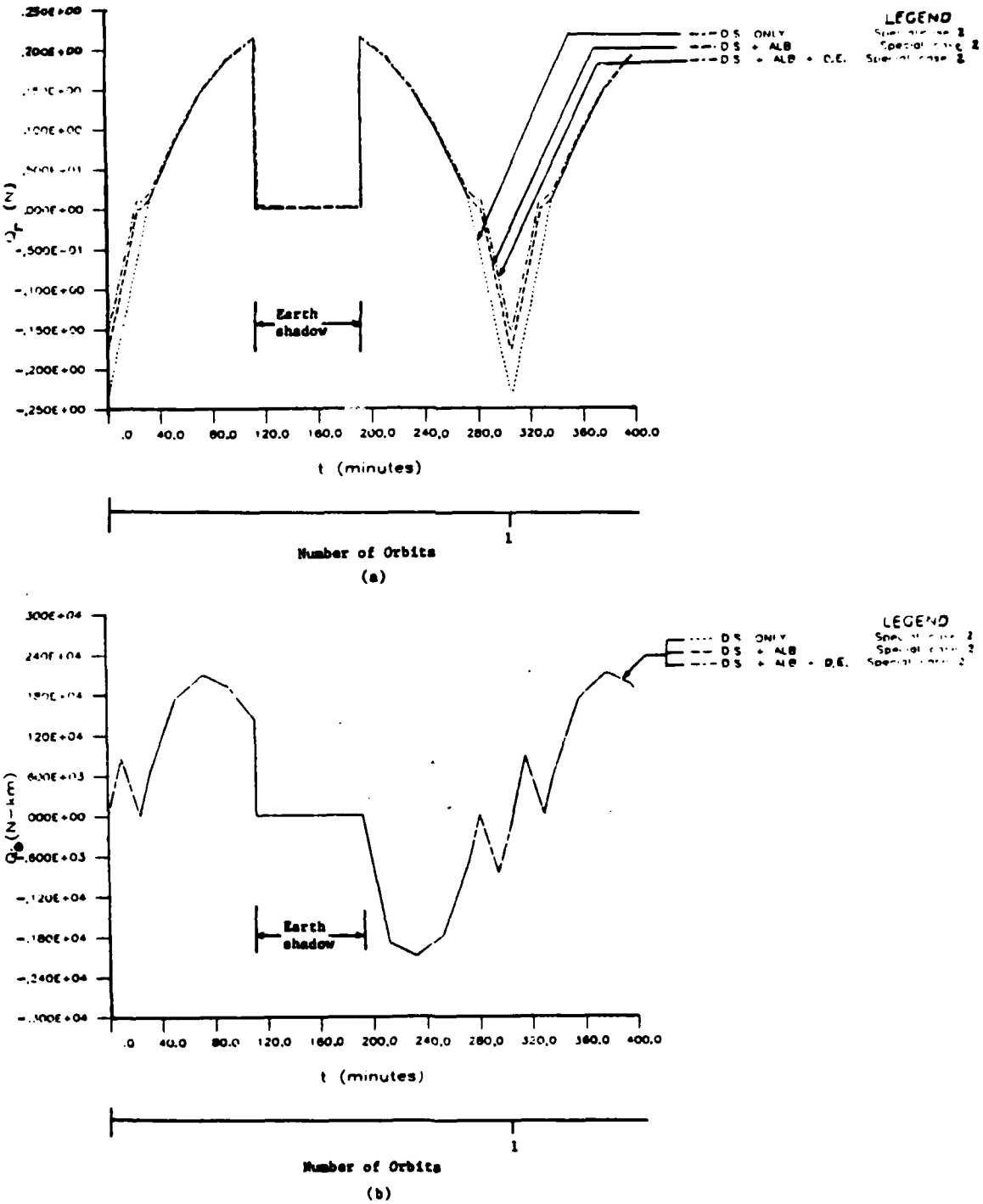

Figure 60. Variation of (a) Q_r, (b) Q_θ, under influence of all three radiation pressures: Elliptical orbit (e = 0.56 and perigee altitude = 200 km), A_{sf}/m = 2.778 m^2/kg, Special Case 2 ($\emptyset = \pi/2$: Maximum direct earth and albedo effects)

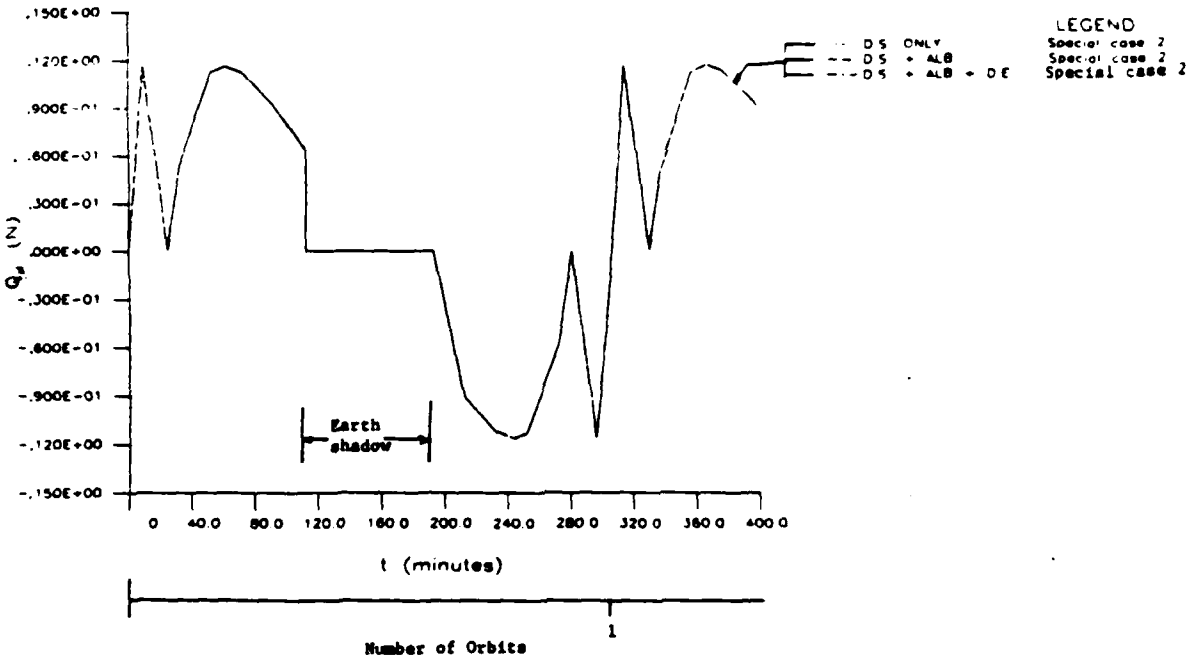

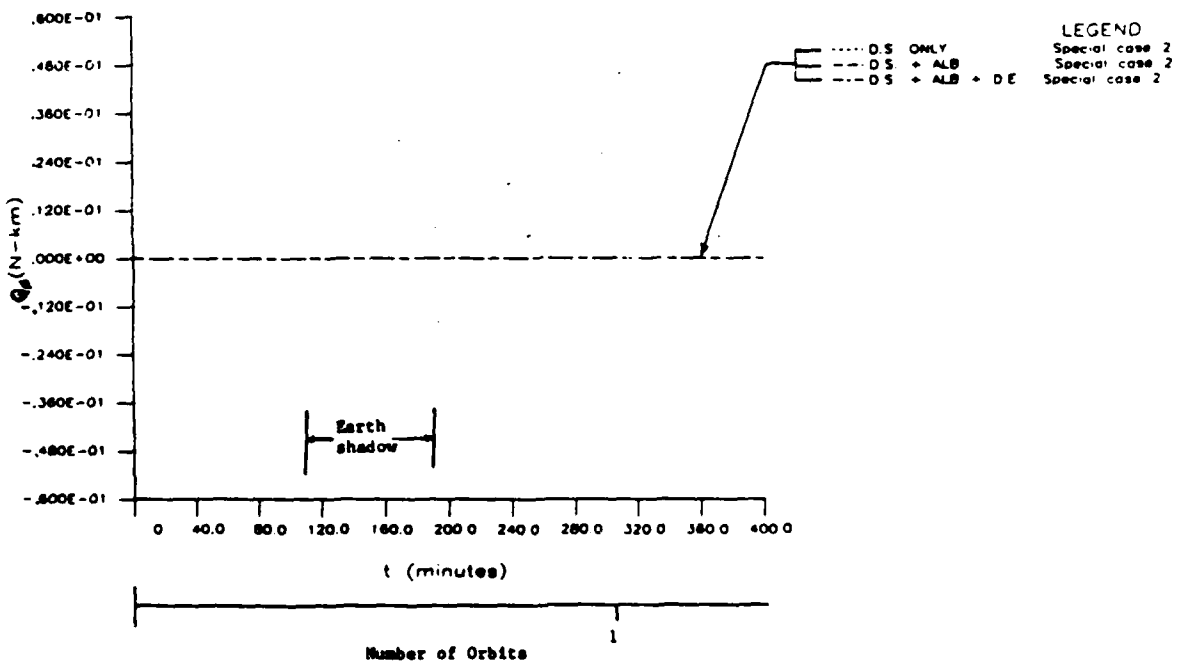

Figure 61. Variation of (a) Q_x, (b) Q_ϕ, under influence of all three radiation pressures: Elliptical orbit ($e = 0.56$ and perigee altitude = 200 km), A_{sf}/m = 2.778 m^2/kg, Special Case 2 ($\phi = \pi/2$: Maximum direct earth and albedo effects)

the region $|\theta| < \pi/2$. Hence, in this part of the orbit the terrestrial radiation tends to reduce the value of Q_r obtained for direct solar radiation (Figure 60(a)). The highest contribution (decrease in the value of Q_r due to direct solar radiation) from the terrestrial radiation pressure occurs in the vicinity of the perigee point where the altitude is lowest. The maximum decrease in Q_r due to the earth's albedo radiation and its direct radiation pressure are respectively 24.5 percent and 8.1 percent of the direct solar radiation pressure Q_r.

The computer data shows that there is no added effect in the length of the structure due to terrestrial radiation pressure. As far as the perturbation of orbit is concerned, the orbital period remains virtually uneffected. The terrestrial radiation pressures have a tendency to increase the value of r_c as they act outward from the center of the earth. Therefore, in the region $|\theta| < \pi/2$, the terrestrial radiation pressure tries to moderate the decrease in r_c due to the direct solar radiation pressure, whereas in the region $|\theta| > \pi/2$, both types of radiation pressures tend to increase r_c. The extend of the terrestrial radiation pressure effects on r_c became quite clear from the data presented below.

t (minutes)	θ (radians)	Change in r_c due to radiation pressures with respect to G only (m)		
		D.S.	D.S.+ALB	D.S.+ALB+D.E.
0 (perigee)	0	0	0	0
22.2	1.47418	-1.3	-0.6	-0.2
100.0	2.75063	+50.0	+53.0	+56.0
152.8 (apogee)	3.14162	+174.00	+179.00	+186.0
200.0	3.48663	+341.0	+348.0	+361.0
281.0	4.71705	+829.0	+842.5	+870.0
305.6 (perigee)	6.28399	-0.40	-0.45	-0.45

These results show that the effects of the radiation pressures on r_c are very small, because r_c is of the order of more than 6.5×10^3 km whereas the change in r_c due to the radiation pressures is at most of the order of a few hundred meters.

CHAPTER V

SUMMARY

These conclusions are based on the limited number of short computer solutions. The conclusions are made within the limitations imposed by the assumptions and approximations stated in the preceding chapters. Recommendations are made for future study in various aspects of the problem which warrant additional research. Reference should be made to Table 2 again for a listing of the cases treated.

Conclusions

The study of the dynamic and thermal effects of three major external disturbances, namely, the differential gravitational forces, radiation heating and radiation pressure forces on the axial length, attitude motion, and orbital motion of a very large space structure has led to the following conclusions:

1. The differential gravitational force does not have any significant effect on the length, attitude, and orbit of a very large space structure.

2. The radiation heating is very significant in causing structural deformation and in producing libration in

attitude motion of a large space structure. However, the effect on the orbital parameters due to radiation thermal effects is negligible.

3. The radiation pressure has negligible effect on changing the axial dimensions of the structure, but it can disturb the attitude and orbital motion of a large space structure significantly. Of all the three external disturbing sources, namely, the differential gravitational force, radiation heating, and radiation pressure, the radiation pressure causes the largest perturbation in the orbital parameters of the orbit of a large space structure.

4. In low earth orbit (LEO), effects of the earth's albedo and its direct radiation should be included in an analysis investigating the radiation thermal and pressure effects. At high altitude geosynchronous-like orbits (GEO), albedo and direct earth radiation effects may be neglected completely, and only direct solar radiation need be considered.

5. A change in the differential value of the end masses of a large dumbbell space structure causes a change in the differential gravitational force, but the effect due to this on the space structure is negligible.

6. Change in the length of a space structure does not produce any appreciable change in the effect of the differential gravitational force on the structure. But the dimensions of a space structure are of great importance in

the radiation thermal and pressure effect analysis, because increasing the dimensions of the structure leads to an increase in the surface area exposed to radiation.

7. Increasing the value of the initial attitude angle causes an increase in the libration of the large space structure about its center of mass. An initially imposed attitude misalignment however does not produce noticeable changes in the length and the orbit of the structure.

8. Initially induced axial deformation of a large space structure has considerable effect in changing the length and attitude of the structure, but is has zero or negligible effect on perturbing the parameters of the orbit of the structure.

9. The increase in initial angular velocity (θ_0) induces a greater eccentricity of the orbit of a space structure, and it greatly disturbs the attitude motion of a very large space structure. For highly eccentric orbits, the structure may tumble continuously. The orbit eccentricity however has a very insignificant effect in producing structural deformation.

10. Altitude from the earth of the orbit of a large space structure has negligible influence on the differential gravitational force effect, but the altitude can be more influential in radiation thermal and pressure effects since in lower altitudes, the terrestrial radiation in addition to direct solar radiation should be considered in the analysis.

11. For all practical purposes at the altitudes concerned, the attractive forces among the remote masses (dumbbells) in the space system may be ignored completely from the analysis.

12. The radiation thermal and pressure effects are greatly enhanced by the increased area-to-mass ratio of the structure. The area-to-mass ratio of the structure is found to be one of the most important physical parameters leading to an increase in the thermal and radiation pressure effects on a large space structure.

13. For all practical purposes, a change in the value of total mass of the space system does not produce any noteworthy change in the differential gravitational force effect. However, it produces significant changes in the thermal and radiation pressure effects because a decrease in the total mass means an increase in the area to mass ratio of the structure.

Recommendation for Future Research

The following recommendations are made:

1. Computer runs with a smaller integration time step should be made to show the dynamic and thermal effects in the space structure. The computations in the present study were single precision. The step size considered here for the computations are accurate enough for studying the orbital

motion and attitude motion. However, finer step sizes for the computations need to be considered for a more accurate analysis of structural deformation with a more flexible and lighter structure.

2. In order to establish an accurate criteria to achieve a practical range of the effects under consideration and to establish the effect of possible resonance with orbital or perturbation frequencies, computer runs should be made for a larger range of initial conditions and physical parameter values pertaining to a space system .

3. The study of dynamic and thermal effects on a very large space structure should be extended to include general bodies with arbitrary shape, three-dimensional motion, and an oblate, non-homogeneous earth.

4. While considering the thermal and radiation pressure effects on a large space structures, a detailed investigation should be carried out to check for the possible thermal vibration, buckling, and anomalous body motion due to thermal and pressure gradients which may exist because of a part of the structure being in the sunlight side and other part being in the earth's shadow, and/or because one part is farther away from the sun than the other, and/or because of the shadowing effect of one component on another in the large space structure.

5. A refinement of the radiation thermal and pressure analysis should be carried out by releasing the restrictions

imposed by the assumptions made here. For example, such a refinement can be achieved by taking into account the slight motion of the sun in right ascension and declination, type of orbit (polar, equatorial, etc.), slight change in the solar distance, possible variations of the solar constant, general (real life) structural surfaces possessing various optical and thermal properties simultaneously and variable specific heat.

REFERENCES

1. Bova, Ben, The High Road, Houghton Mifflin Company, Boston, 1981.

2. Clemmons, D. L., Jr., "The Echo I Inflation System," NASA TND - 2194, June 1964.

3. Teichman, L. A., "The Fabrication and Testing of PAGEOS I," NASA TND - 4596, June 1968.

4. Hedgepeth, J. M., "Survey of Future Requirements for Large Space Structures," NASA CR - 2621, January 1976.

5. Brodsky, R. F. and B. G. Morais, "Space 2020 - The Technology, The Missions Likely 20-40 Years from Now," Aeronautics and Astronautics, May 1982, pp 54-73.

6. Bush, H. G. and M. M. Mikulas, "A Nestable Tapered Column Concept for Large Space Structures," NASA TMX-73927, 1976.

7. Bush, H. G., M. M. Mikulas, and W. L. Heard, Jr.,"Some Design Considerations for Large Space Structures," AIAA Journal, Vol. 16, No. 4, April 1978, pp 352-359.

8. Noor, A. K.,"Assesment of Current State of the Art in Modeling Techniques and Analysis Methods for Large Space Structures," NASA CP-2258, May 13-14, 1982, pp 5-32.

9. Park, K. C. and J. M. Wingel,"The Potential of Non-periodic Truss Structures for Space Applications," NASA CP-2215, Part I, 1981, pp 133-143.

10. Woods, A. A., Jr.,"Offset Wrap Rib Concept and Development (LMSC)," NASA CP-2118, 1979, pp 5.

11. Archer, J. S.,"Advanced Sunflower Antenna Concept Development (TRW)," NASA CP-2118, 1979, pp 33.

12. Montgomery, D. C. and L. D. Skides,"Development of Maypole (Hoop/Column) Deployable Reflector Concept for Large Space Systems Applications (Harris Corp.)," NASA CP-2118, 1979, pp 115.

13. Vaughan, D. H.,"Modular Reflector Concept Study," NASA CP-2168 Vol. II, 1980, pp 145.

14. Agan, W. E.,"Erectable/Deployable Concepts for Large

Space System Technology (Vought Corp.)," NASA CP-2118, 1979.

15. Stokes, J. W. and E. C. Pruett,"Structural Assembly in Space," NASA CP-2118, 1979.

16. Wright, Robert, (ed) The Microwave Radiometer Spacecraft, NASA Reference Publication No. 1079, December 1981.

17. Garwin, R. L.,"Solar Sailing-A Practical Method of Propulsion Within the Solar System," Jet Propulsion, Vol. 28, No. 3, March 1958, pp 188-190.

18. Tsu, T. C.,"Interplanetary Travel by Solar Sail," ARS Journal, Vol. 29, June 1959, pp 422-427.

19. Rodriguez, G., E. L. Marsh, and S. M. Gunter,"Solar Sail Attitude Dynamics and Control,"Dynamics and Control of Large Flexible Spacecraft, AIAA symposium, June 1977, Proceedings edited by Meirovitch, L., pp 287-302.

20. Trubert, M. and M. Blount,"Thurst and Moments on the Square Sail," Solar Sail Study 662-34, October 1, 1977, JPL, CALTECH, Pasadena, CA.

21. Kraus, H.,"Thermally Induced Vibrations of Thin Non-shallow Spherical Shells," AIAA Journal, March 1966, No. 4, PP 500-505.

22. Schmidt, C. M. and A. J. Hanawalt,"Skin Temparature of a Satellite," Jet Propulsion, Vol. 27, No. 10, October 1957, pp 1079-1083.

23. Graham, J. D.,"Solar Induced Bending Vibrations of a Flexible Member," AIAA Journal, Vol. 8, No. 11, November 1970, pp 2031-2036.

24. Tsuchiya, K.,"Thermally Induced Nutational Body Motion of a Spinning Spacecraft with Flexible Appendages," AIAA Journal, Vol. 13, No. 4, April 1975.

25. Tsuchiya, K.,"Thermally Induced Vibrations of a Flexible Appendages attached to a Spacecraft," AIAA Journal, Vol. 15, No. 4, April 1977, pp 505-510.

26. Frisch, H. P.,"Thermal Bending plus Twist of a Thin-walled Cylinder of Open Section with Application to Gravity Gradient Booms," NASA TN D-4069, August 1967.

27. Donohue, J. H. and H. Frisch,"Thermoelastic Instability

of Open-Section Booms," NASA TN D-5310, December 1969.

28. Frisch, H.,"Coupled Thermally-Induced Transverse plus Torsional Vibrations of a Thin-walled Cylinder of Open Section," NASA TR R-333, March 1970.

29. Meirovitch, L. (ed),"Dynamics and Control of Large Flexible Spacecraft," AIAA Symposium Proceedings, June 1977, June 1979, and June 1981 Published by VPI & SU, Blacksburg, Virginia.

30. Moran, J. P.,"Effects of Planar Librations on the Orbital Motion of a Dumbbell Satellite," ARS Journal, Vol. 31, 1961, pp 1089-1096.

31. Reiter, G. S.,"Dynamics of Flexible Gravity-Gradient Satellites," NASA CR-64731, 1965.

32. Ashley, H.,"Observations on the Dynamic Behavior of Large Flexible Bodies in Orbit," AIAA Jornal, Vol. 5, 1967, pp 460-469.

33. Robe, T. R. and T. R. Kane,"Dynamics of an Elastic Satellite, I, II, III," Int. J. of Solids and Structures, Vol. 3, 1967, pp 333-352, 691-703,1031-1051.

34. Musen, P.,"The Influence of the Solar Radiation Pressure on the Motion of an Artificial Satellite," J. of Geophysical Research, Vol. 65, No. 5, May 1960, pp 1391-1396.

35. Bryant, R.,"A Comparision of Theory and Observation of the Echo I Satellite," J. of Geophysical Research, Vol. 66, September 1961, pp 3066-3069.

36. Flanagan, R. C. and V. J. Modi,"Attitude Dynamics of a Gravity Oriented Satellite Under the Influence of Solar Radiation Pressure," The Aeronautical J. of the Royal Aeronautical Society, Vol. 74, 1970, pp 835-841.

37. Modi, V. J. and K. C. Pande,"Solar Pressure Induced Librations of Spinning Axisymmetric Satellites," J. Spacecraft, Vol. 10, No. 9, September 1973, pp 615-617.

38. Pande, K. C., V. J. Modi, and A. K. Misra,"Solar Pressure Induced Perturbations of Orbital Elements for the Communication Technology Satellite," AAS, 1975, pp 1-25.

39. Van Der Ha, J. C. and V. J. Modi,"Orbital Perturbations and Control by Solar Radiation Forces," J. Spacecraft, Vol. 15, No. 2, March-April 1978, pp 105-112.

40. Patterson, W. B. and K. E. Kissell,"Comparision of the Theoretical Solar Radiation Effects and the Observed Accelerations of the PAGEOS Satellite," J. Spacecraft, Vol. 12, No. 9, September 1975, pp 539-543.

41. Zerbini, S.,"Direct Solar and Earth-Albedo Radiation Pressure Effects on the Orbit of PAGEOS I," Celestial Mechanics, 22, 1980, pp 307-334.

42. Cunningham, F. G.,"Power Input to a Small Flat Plate from a Diffusely Radiating Sphere, with Application to Earth Satellites," NASA TN D-710, 1961.

43. Cunningham, F. G.,"Earth Reflected Solar Radiation Input to Spherical Satellite," NASA TN D-1099, 1961.

44. Lautman, D. A.,"Perturbations of a Close-Earth Satellite due to Sunlight Diffusely Reflected from the Earth," I: Uniform Albedo, Celestial Mechanics, 15, 1977, pp 387-420; II: Variable Albedo, Celestial Mechanics, 16, 1977, pp 3-25.

45. Klemperer, W. B. and R. M. Baker, Jr.,"Satellite Librations," Astronautica Acta, Vol. 3, 1957, pp 16-27.

46. Davis, W. R.,"Determination of a Unique Attitude for an Earth Satellite," Advances in the Astronautical Sciences, Vol. 2, 1958, pp 10-1 to 10-15.

47. Stoker, T. A. J. and R. F. Vachino,"The Two-Body Librations of a Dumbbell-Shaped Satellite in a Uniform Gravitational Field," Thesis, USAF Inst. of Tech., Wright-Patterson Air Force Base, Ohio, March 1958.

48. Schindler, G. M.,"On Satellite Librations," ARS Journal, Vol. 29, May 1959, pp 368-370.

49. Klemperer, W. B.,"Satellite Librations of Large Amplitude," ARS Journal, Vol. 30, January 1960, pp 123-124.

50. Baker, R. M. L., Jr.,"Libration on a Slightly Eccentric Orbit," ARS Journal, Vol. 30, January 1960, pp 124-126.

51. Ordway, D. E.,"Coupled Planar Motion of a Dumbbell Satellite," Paper presented at the IAS 29th.

Annual Meeting, Aerospace Forum II, January 1961 (TAR-TN 611 , June 1961, TAR Project No. 014-0007, Internal Memo).

52. Rosner, R. H.,"Motion of a Dumbbell Satellite," Advances in the Astronautical Sciences, Vol. 7, 1961, pp 125-137.

53. Schechter, H. B.,"Dumbbell Librations in Elliptical Orbits," AIAA Journal, Vol. 2, No. 6, June 1964, pp 1000-1003.

54. Fischell, E.,"The TRAAC Satellite," APL Digest, Vol. 1, No. 3, February 1962, pp 3-9.

55. Paul, B.,"Planar Librations of an Extensible Dumbbell Satellite," AIAA Journal, Vol. 1, No. 2, February 1963, pp 411-418.

56. Pringle, R. Jr.,"Exploitation of Nonlinear Resonance in an Elastic Dumbbell Satellite," AIAA Journal, Vol. 6, No. 7, July 1968, pp 1217-1222.

57. Grote, P. B., J. C. McMunn, and R. Glunk, "Equations of Motion of Flexible Spacecraft," J. Spacecraft & Rockets, Vol. 8, 1971, pp 561.

58. Likins, P. W.,"Dynamics and Control of Flexible Space Vehicles," TR32-1329, Revision 1, January 1970, JPL.

59. Santini, Paolo,"Stability of Flexible Spacecrafts," Acta Astronautica, Vol. 3, 1977, pp 685-713.

60. Misra, A. K. and V. J. Modi,"The Influence of Satellite Flexibility on Orbital Motion," AIAA Symposium, June 1977, pp 59-74 (see Ref. 29 above).

61. Lips, K. W. and V. J. Modi,"Transient Attitude Dynamics of Satellites with Deploying Flexible Appandages," Acta Astronautica, Vol. 5, 1978, pp 797-815.

62. Bainum, P. M., V. K. Kumar, and P. K. James,"The Dynamics and Control of Large Flexible Space Structures," Part A: Discrete Model and Control, NASA CR-156975, May 1978, Part B: Development of Continuum Model and Computer Simulation, NASA CR-156976, May 1978.

63. Kane, T. R. and D. A. Levinson,"Large Motions of Unrestrained Space Trusses," J. of Astronautical Sciences, Vol. XXVIII, No. 1, January-March 1980, pp 49-88.

64. Levinsion, D. A. and T. R. kane,"Simulation of Large Motions of Nonuniform Beams in Orbit, Part I - The Cantilever Beam, Part II - The Unrestrained Beam," J. of Astronautical Sciences, Vol. XXIX, No. 3, July - September 1981, pp 213-244, and pp 245-275.

65. Nayfeh, A. H. and M. S. Hefzy,"Continuum Modeling of the Mechanical and Thermal Behavior of Discrete Large Structures," AIAA Journal, Vol. 19, No. 6, June 1981, pp 766-773.

66. Aswani, Mohan,"Development of an Analytical Model for Large Space Structures," Report SD-TR-82-59, March 15, 1982, Space Division, Air Force System Command, Los Angeles, CA.

67. Fitzpatrick, P. M., Principles of Celestial Mechanics, Academic Press, New York, 1970, pp. 287.

68. Timoshenko, S. and D. H. Young, Advanced Dynamics, McGraw-Hill Book Co., Inc., New York, 1948.

69. Clough, R. W. and J. Penzien, Dynamics of Structures, McGraw-Hill Book Co., 1975, Ch. 16.

70. Modest, m. F., "Solar Flux Incident on an Orbiting Surface After Reflection from a Planet," AIAA Jour., June 1980,pp. 727-730.

71. Wyatt, S. P., "The Effect of Radiation Pressure on the Secular Acceleration of Satellites," Smithsonian Contribution to Astrophysics, Vol. 6, 1963, pp. 109-112.

72. London, H. S., "Some Exact Solutions of the Equations of Motion of a Solar Sail with Constant Sail Setting," ARS Jour., Vol. 30, Feb. 1960, pp 198-200.

73. Clancy, T. F. and T. P. Mitchell, "Effects of Radiation Forces on the Attitude of an Artificial Earth Satellite," AIAA Jour., Vol. 2, No. 3, March 1964, pp. 517-524.

74. Mills, S. et al, "Earth Albedo and Emitted Radiation," NASA SP - 8067, July 1971.

75. Haffner, J. W., Handbook of Near Earth (Sea Level to Geosynchronous Altitude) Environments, April 1973, Rockwell Internatinal Satellite System Division, Los Angeles, CA.

76. Levin, E. " Reflected Radiation Received by an Earth Satellite," ARS Jour., Vol. 32, 1962, pp. 1328-1331.

77. Flanagan, R. C. and V. J. Modi, "Radiation Forces on a Flat Plate in Ecliptic Near-Earth Orbits," Transactions of the Canadian Aeronautics and Space Institute, Vol. 3, September 1970, pp. 147-158.

78. Yu, E. Y. "Long Term Coupling Effects Between the Librational and Orbital Motions of a Satellite," AIAA Jour., Vol. 2, no. 3, March 1964, pp. 553-555.

79. Hall, J. H. and J. H. Smith,"Passive Damping of the Two - Dimensional Librations of a dumbbell-shaped Satellite," M. S. Thesis, Air Force Inst. Tech., Wright-Patterson Air Force Base, Ohio, 1959.

80. Carslaw, H. S., and J. C. Jaeger, Conduction of Heat in Solids, Oxford, Clarendron Press, 1959.

81. Whittaker, E. T., Treatise on the Analytical Dynamics of Particles and Rigid Bodies, Cambridge Univ. Press, 1960.

82. Greenberg, M. D., Foundations of Applied Mathematics Printice-Hall, 1978.

83. Boley, B. A. and J. H. Weiner, Theory of Thermal Stresses, John Wiley & Sons, Inc., Publishers, U. S. A., 1960.

84. Wyatt, S. P., "The Effect of Terrestrial Radiation Pressure on Satellite Orbits," IUTAM Symposium, Dynamics of Satellites (Ed. Roy, M.), Academic Press, Inc., Publishers, New York, 1963, pp 180-196.

85. Shapiro, I. I., "The Prediction of Satellite Orbits," Dynamics of Satellites (Ed. Roy, M.), Academic Press, Inc., Publishers, New York, 1963, pp 257-312.

86. Sehnal, L., "The Effect of Re-Radiation of the Sunlight from the Earth on the Motion of Artificial Satellites," The Use of Artificial Satellites for Geodesy, Amsterdam: North-Holland Publishing Co., 1963.

87. Chapman, A. J., Heat Transfer, Macmillan Publishing Co., Inc., New York, Third Edition, 1974.

88. Prior, E. J. "Earth Albedo Effects on the Orbital Variations of Echo I and PAGEOS I."Dynamics of

Satellites (Ed. Morando, B.), Springer-Verlag, Berlin / Heidelberg / New York, 1970, pp 303-312.

89. Modi, V. J. and R. C. Flanagan, "Effects of Environmental Forces on the Attitude Dynamics of Gravity Oriented Satellites - Part I, Part II, and Part III," The Aeronautical Journal of the Royal Aeronautical Soceity, Vol. 75, Nov. 1971, pp 783-793; Vol. 75, Dec. 1971, pp846-849; and Vol. 76. Jan. 1972, pp 34-40.

90. Krishna, R. and P. M. Bainum, "Orientation and Shape-Control of an Orbiting Flexible Beam under the Influence of Solar Radiation Pressure," Advances in the Astronautical Sciences - Astrodynamics 1983. Vol. 54, part I, pp 221-238.

91. Shrivastava, S. K. and H. B. Hablani, "Analysis of Solar Radiation Pressure Induced Coupled Librations of a Gravity Stabilized Axisymmetric Satellite," Celestial Mechanics, 20 (1979), pp 297-313.

92. Pande, K. C. "Parametric Excitation of a High Altitude Gravity-Gradient Satellite," Celestial Mechanics, Vol. 29, 1983, pp 101-106.

93. Modi, V. J. and K. C. Pande, "On the Periodic Solutions and Resonance of Spinning Satellite in Near - Circular Orbit," Celestial Mechanics, 11 (1975), pp 195-212.

94. Modi, V. J. and K. Kumar, " Coupled Librational Dynamic and Attitude Control of Satellites in Presence of Solar Radiation Pressure," Proceedings of the XXII Congress of the International Astronautical Federation, Editor L. G. Napolitano, D. Reidel Publishing Co., Dordrecht-Hollad/Boston, U. S. A., 1973, pp 37-52.

95. Modi, V. J. and C. Tschann, "On the Attitude and Libration Control of a Satellite Using Solar Radiation Pressure," Proceedings of the XXI Congress of the International Astronautical Federation, (Constance, Oct. 1970), Ed. L. G. Napolitano, D. Reidel Publishing Co., Dordrecht - Holland / Boston, U. S. A., 1972, pp 84-100.

96. Wertz, J. R. (Editor), Spacecraft Attitude Determination and Control, published by D. Reidel Publishing Co., 1978.

97. Accord, J. D. and J. C. Nicklas, "Theoretical and Practical Aspects of Solar Pressure Attitude Control for Interplanetary Spacecraft," Progress in Astronautics and Aeronautics, Vol. 13, (AIAA Series), Guidance and Control - II, 1964.

98. Evans, W. J., "Aerodynamics and Radiation Disturbance Torques in Satellite Having Complex Geometry," Jour. of Astronautical Sciences, Vol. 9, pp. 93, 1962.

APPENDIX A

DERIVATION OF EQUATIONS OF MOTION

A detail derivation of the equations of motion of a dumbbell- shaped space structure (Figure 1) executing coplanar motion (structure moving in orbital plane) in a general orbit will be presented below.

Kinetic Energy

The total kinetic energy of the system can be expressed as the summation of (i) the kinetic energy of the center of mass (C) of the system (Figure 2) with respect to the origin (O) of the inertial reference frame and (ii) the kinetic energy of masses m_1 and m_2 with respect to the center of mass (C) of the system [68]. In vectorial notation, it can be written as:

$$K_E = \frac{m}{2} \dot{\underline{r}}_C \cdot \dot{\underline{r}}_C + \frac{1}{2} \sum_{i=1}^{2} m_i (\dot{\underline{x}}_i \cdot \dot{\underline{x}}_i) \qquad \text{(A-1)}$$

where $$m = \sum_{i=1}^{2} m_i = m_1 + m_2 \qquad \text{(A-2)}$$

$\underline{r}_C$ is the position vector of point C with respect to O, $\underline{x}_1$ and $\underline{x}_2$ are the position vectors of masses m_1 and m_2 with respect to point C.

The velocity of a moving point, say C, with respect to

cylindrical coordinates is given by [82]

$$\dot{\underline{r}}_c = \dot{r}_c \, \underline{i}_o + r_c\dot{\theta} \, \underline{j}_o \qquad \text{(A-3)}$$

Where $\underline{i}_o$ and $\underline{j}_o$ are the units vectors along $\underline{r}_c$ and θ directions. Similarly, for points m_1 and m_2, we can write

$$\dot{\underline{x}}_1 = \dot{x}_1 \, \underline{i} + x_1 \, (\dot{\theta} + \dot{\emptyset}) \, \underline{j} \qquad \text{(A-4)}$$

$$\dot{\underline{x}}_2 = \dot{x}_2 \, (-\underline{i}) + x_2 \, (\dot{\theta} + \dot{\emptyset}) \, (-\underline{j}) \qquad \text{(A-5)}$$

where $\underline{i}$ and $\underline{j}$ are the unit vectors along $\underline{x}_1$ and the perpendicular to the $\underline{x}_1$ the direction in the same plane.

Equation (A-1) gives on expanding

$$K_E = \left(\frac{1}{2}\right) [m(\dot{\underline{r}}_c \cdot \dot{\underline{r}}_c) + m_1(\dot{\underline{x}}_1 \cdot \dot{\underline{x}}_1) + m_2(\dot{\underline{x}}_2 \cdot \dot{\underline{x}}_2)] \qquad \text{(A-6)}$$

Substituting Equations (A-3), (A-4), and (A-5) into Equation (A-6), we get

$$K_E = \left(\frac{1}{2}\right) \{m[\dot{r}_c^2 + (r_c\dot{\theta})^2] + m_1[\dot{x}_1^2 + x_1^2(\dot{\theta} + \dot{\emptyset})^2] + m_2[\dot{x}_2^2 + x_2^2(\dot{\theta} + \dot{\emptyset})^2]\} \qquad \text{(A-7)}$$

Substitution of values of x_1 and x_2 given below

$$\text{(a)} \quad x_1 = \frac{m_2}{m} x$$

$$\text{(b)} \quad x_2 = \frac{m_1}{m} x$$

$$\text{(c)} \quad x = x_1 + x_2 \qquad \text{(A-8)}$$

into Equation (A-7) yields

$$K_E = \frac{m}{2}\left[\dot{r}_c^2 + (r_c\dot{\theta})^2\right] + \frac{m_1}{2}\left[\left(\frac{m_2}{m}\dot{x}\right)^2 + \left(\frac{m_2}{m}x\right)^2(\dot{\theta} + \dot{\phi})^2\right]$$

$$+ \frac{m_2}{2}\left[\left(\frac{m_1}{m}\dot{x}\right)^2 + \left(\frac{m_1}{m}x\right)^2(\dot{\theta} + \dot{\phi})^2\right] \qquad \text{(A-9)}$$

Noting $\bar{m} = \dfrac{m_1 m_2}{m}$ (A-10)

which we define as a "Reduced Mass,"

we get

$$K_E = \left(\frac{m}{2}\right)\left[\dot{r}_c^2 + (r_c\dot{\theta})^2\right] + \left(\frac{m}{2}\right)\left[\dot{x}^2 + x^2(\dot{\theta} + \dot{\phi})^2\right] \qquad \text{(A-11)}$$

<u>Potential Energy</u>

The total potential energy of the dumbbell system in space consists of that due to the earth's gravitational pull, attraction between the point masses, m_1 and m_2, and strain energies, i.e.,

$$P_E = V_g + V_m + U_e \qquad \text{(A-12)}$$

where

V_g = earth's gravitation potential function

V_m = potential function governing the attractive forces between the point masses m_1 and m_2

U_e = strain energy of the system.

According to Newton's law of gravitation, the attractive force, $\underline{F}_{gi}$ exerted by a body of mass m_i moving around the earth of mass M_e at a distance, r_i from m_i, at that location, is given by:

$$\underline{F}_{gi} = - \frac{GM_e m_i}{r_i^2} \underline{e}_r \qquad \text{(A-13)}$$

where $\underline{e}_r$ is a unit vector along r_i line.

Since the gravitational force ($\underline{F}_{gi}$) is conservative, we can express it as the gradient (∇) of the gravitational potential (V_{gi})

$$\underline{F}_{gi} = \nabla V_{gi} \qquad \text{(A-14)}$$

Hence, it follows that

$$V_{gi} = - GM_e \frac{m_i}{r_i} \qquad \text{(A-15)}$$

The total gravitational potential (energy) can be written as

$$V_g = - GM_e \sum_{i=1}^{N} \frac{m_i}{r_i} \qquad \text{(A-16)}$$

For point masses m_1 and m_2, we get

$$V_g = - GM_e \left(\frac{m_1}{r1} + \frac{m_2}{r2}\right) \qquad \text{(A-17)}$$

where the Law of cosines gives,

$$\text{(a)} \quad r_1^2 = r_c^2 + x_1^2 + 2r_c\, x_1 \cos\emptyset$$

$$\text{(b)} \quad r_2^2 = r_c^2 + x_2^2 - 2r_c\, x_2 \cos\emptyset \qquad \text{(A-18)}$$

Noting $\mu = GM_e = gR^2$ (A-19)

we can write,

$$V_g = -\mu\left(\frac{m_1}{r_1} + \frac{m_2}{r_2}\right) \qquad \text{(A-20)}$$

Similarly, for the attraction between masses m_1 and m_2, we can write

$$V_m = -G\,\frac{m_1 m_2}{x} \qquad \text{(A-21)}$$

Thus substituting Equations (A-20) and (A-21) into Equation (A-12), we obtain

$$P_E = -\mu\left(\frac{m_1}{r_1} + \frac{m_2}{r_2}\right) - G\,\frac{m_1 m_2}{x} + U_e \qquad \text{(A-22)}$$

Substituting for r_1 and r_2 from Equations (A-18) and then for x_1 and x_2 from Equations (A-8), we find the total potential energy expression:

$$P_E = -\mu\left[\frac{m_1}{\left\{r_c^2 + \left(\frac{m_2}{m}x\right)^2 + 2\frac{m_2}{m}r_c\,x\,\mathrm{Cos}\emptyset\right\}^{1/2}} + \frac{m_2}{\left\{r_c^2 + \left(\frac{m_1}{m}x\right)^2 - 2\frac{m_1}{m}r_c\,x\,\mathrm{Cos}\emptyset\right\}^{1/2}}\right] - G\,\frac{m_1 m_2}{x} + U_e \qquad \text{(A-23)}$$

Equations of Motion

The general Lagrange's equations of motion [69, page 273] are as below:

$$(a)\quad \frac{\partial}{\partial t}\left(\frac{\partial K_E}{\partial \dot{r}_c}\right) - \frac{\partial K_E}{\partial r_c} + \frac{\partial P_E}{\partial r_c} = Q_r$$

$$(b)\quad \frac{\partial}{\partial t}\left(\frac{\partial K_E}{\partial \dot{\theta}}\right) - \frac{\partial K_E}{\partial \theta} + \frac{\partial P_E}{\partial \theta} = Q_\theta$$

$$(c)\quad \frac{\partial}{\partial t}\left(\frac{\partial K_E}{\partial \dot{x}}\right) - \frac{\partial K_E}{\partial x} + \frac{\partial P_E}{\partial x} = Q_x$$

$$(d)\quad \frac{\partial}{\partial t}\left(\frac{\partial K_E}{\partial \dot{\phi}}\right) - \frac{\partial K_E}{\partial \phi} + \frac{\partial P_E}{\partial \phi} = Q_\phi \qquad \text{(A-24)}$$

where Q_r, Q_θ, Q_x and Q_ϕ are generalized forcing functions corresponding to r_c, θ, x, and ϕ respectively.

We substitute for K_E and P_E respectively from Equations (A-11) and (A-23) into above equations of motion, and carry out the indicated differentiation with respect to time.

The first of Equations (A-24) gives

$$m(\ddot{r}_c - r_c\dot{\theta}^2) + \mu\left[\frac{m_1\{r_c + (m_2/m)\,x\,\mathrm{Cos}\phi\}}{\{r_c^2 + (m_2/m)^2x^2 + 2r_c(m_2/m)\,x\,\mathrm{Cos}\phi\}^{3/2}} + \frac{m_2\{r_c - (m_1/m)\,x\,\mathrm{Cos}\phi\}}{\{r_c^2 + (m_1/m)^2x^2 - 2r_c(m_1/m)\,x\,\mathrm{Cox}\phi\}^{3/2}}\right] = Q_r \qquad \text{(A-25)}$$

The second of Equations (A-24) gives

$$m(\ddot{\theta}r_c^2 + 2\dot{\theta}\dot{r}_c r_c) + m(\ddot{\theta} + \ddot{\phi})x^2 + 2\bar{m}x\dot{x}(\dot{\theta} + \dot{\phi}) = Q_\theta \qquad \text{(A-26)}$$

The third of Equations (A-24) gives

$$\bar{m}[\ddot{x} - x(\dot{\theta} + \dot{\phi})^2]$$

$$+ \bar{m}\,\mu\left[\frac{\{(m_2/m)\,x + r_c\,\mathrm{Cos}\phi\}}{\{r_c^2 + (m_2/m)^2x^2 + 2r_c(m_2/m)\,x\,\mathrm{Cos}\phi\}^{3/2}}\right.$$

$$\left. + \frac{\{(m_1/m)\,x - r_c\,\mathrm{Cos}\phi\}}{\{r_c^2 + (m_1/m)^2x^2 - 2r_c(m_1/m)\,x\,\mathrm{Cox}\phi\}^{3/2}}\right]$$

$$+ \frac{Gm1m2}{x^2} + \frac{\partial Ue}{\partial x} = Q_x \qquad \text{(A-27)}$$

The last of Equations (A-24) gives

$$\bar{m}[(\ddot{\theta} + \ddot{\phi})x^2 + 2x\dot{x}(\dot{\theta} + \dot{\phi})]$$

$$+ m\,\mu\left[\frac{\{-\,r_c\,x\,\mathrm{Sin}\phi\}}{\{r_c^2 + (m_2/m)^2x^2 + 2r_c(m_2/m)\,x\,\mathrm{Cos}\phi\}^{3/2}}\right.$$

$$\left. + \frac{\{r_c\,x\,\mathrm{Sin}\phi\}}{\{r_c^2 + (m_1/m)^2x^2 - 2r_c(m_1/m)\,x\,\mathrm{Cox}\phi\}^{3/2}}\right]$$

(A-28)

Making note of Equations (A-8) and (A-18), we find that Equations (A-25) to (A-28) can be expressed in more compact form as below:

$$\text{(a)}\quad m\ddot{r}_c - mr_c\dot{\theta}^2 + \mu\left[\frac{m_1(r_c + x_1\mathrm{Cos}\phi)}{r_1^3} + \frac{m_2(r_c - x_2\mathrm{Cos}\phi)}{r_2^3}\right] = Q_r \quad .$$

$$\text{(b)}\quad mr_c(r_c\ddot{\theta} + 2\dot{\theta}\dot{r}_c) + \bar{m}(\ddot{\theta} + \ddot{\phi})x^2 + 2\bar{m}x\dot{x}(\dot{\theta} + \dot{\phi}) = Q_\theta$$

$$\text{(c)}\quad \bar{m}\ddot{x} - \bar{m}x(\dot{\theta} + \dot{\phi})^2 + \bar{m}\,\mu\left[\frac{(x_1 + r_c\mathrm{Cos}\phi)}{r_1^3} + \frac{(x_2 - r_c\mathrm{Cos}\phi)}{r_2^3}\right] + \frac{Gm_1m_2}{x^2} + \frac{\partial U_e}{\partial x} = Q_x$$

$$(d)\ \bar{m}[x^2(\ddot{\theta} + \ddot{\phi}) + 2x\dot{x}(\dot{\theta} + \dot{\phi})] + \bar{m}\ \mu[\frac{(-1)}{r_1^3} + \frac{1}{r_2^3}]x r_c \sin\phi = Q_\phi \qquad \text{(A-29)}$$

Upon substitution of the last relation (d) into the second relation (b) of above Equation (A-29), we get

$$m r_c(r_c\ddot{\theta} + 2\dot{\theta}\dot{r}_c) - \bar{m}\ \mu[\frac{(-1)}{r_1^3} + \frac{1}{r_2^3}]x r_c \sin\phi = (Q_\theta - Q_\phi) \qquad \text{(A-30)}$$

The motion of the space structure now can be defined completely by Equations (A-29a), (A-30), (A-29c) and (A-29d). These equations are found in Chapter II (Equations (2.14)).

APPENDIX B

GEOMETRY OF SPACE STRUCTURE AND ORBIT

The main purpose here is to derive the expressions which show the geometric relationships of the incident and reflected solar light vectors with the orbital and body coordinate systems. Consider a structure in space (Figure 1). X_I, Y_I, Z_I form a geocentric fixed inertial rectangular coordinate system with center at O. x_o, y_o, z_o describe the the rotating orthogonal orbital coordinate system with Cx_o, Cy_o, Cz_o along the local vertical, local horizontal, and the orbit normal, respectively. Cx, Cy, Cz are the rotating orthogonal bcdy coordinates axes fixed at the center of mass (C) of the structure. The space structure is assumed to execute coplanar motion. That is, the inertial coordinate axes OX_I and OY_I, the orbital cordinate axes Cx_o and Cy_o, and the structural cordinate axes Cx and Cy, all lie on the same plane. The coordinate axes OZ_I, Cz_o, and Cz are normal to the orbital plane.

Arbitrary Sun Position

At first a general case where the sun is at an arbitrary position defined by the parameters σ (angle between

the earth-sun line and the X_I axis) and i (inclination of the ecliptic plane, which contains the sun, with respect to the orbital plane) is considered.

Relation between the incident solar light vector and the orbital coordinate system. Let $\underline{i}_o$, $\underline{j}_o$, and $\underline{k}_o$ be the unit vectors along the orbital coordinate axes, x_o, y_o, and z_o, respectively (Figure 62). The unit vector ($\underline{S}_s$) along the structure (or earth)-sun vector (opposite to the Incident light vector) can be expressed as

$$\underline{S}_s = S_{o1}\underline{i}_o + S_{o2}\underline{j}_o + S_{o3}\underline{k}_o \qquad \text{(B-1)}$$

where, S_{o1}, S_{o2}, and S_{o3} denote the components of $\underline{S}_s$ along the orbital coordinate axes, x_o, y_o, and z_o, respectively. Geometric consideration of the spherical triangle formed by Cx_o, CS, and CX_I (Figure 62) gives [see ref. 67, page 118-121]

(a) $S_{o1} = [\text{Cos}\theta\ \text{Cos}\sigma + \text{Sin}\theta\ \text{Cos}i\ \text{Sin}\sigma]$

(b) $S_{o2} = -[\text{Sin}\theta\ \text{Cos}\sigma - \text{Cos}\theta\ \text{Cos}i\ \text{Sin}\sigma]$

(c) $S_{o3} = -[\text{Sin}i\ \text{Sin}\sigma]$

(B-2)

Upon substitution of the above relations (B-2) into Equation (B-1), we obtain

$$\underline{S}_s = [\text{Cos}\theta\ \text{Cos}\sigma + \text{Sin}\theta\ \text{Cos}i\ \text{Sin}\sigma]\underline{i}_o - [\text{Sin}\theta\ \text{Cos}\sigma - \text{Cos}\theta\ \text{Cos}i\ \text{Cos}\sigma]\underline{j}_o - [\text{Sin}i\ \text{Sin}\sigma]\underline{k}_o \qquad \text{(B-3)}$$

Relation between the incident solar light vector and the body coordinate system. Let $\underline{i}$, $\underline{j}$, and $\underline{k}$ be the unit vectors

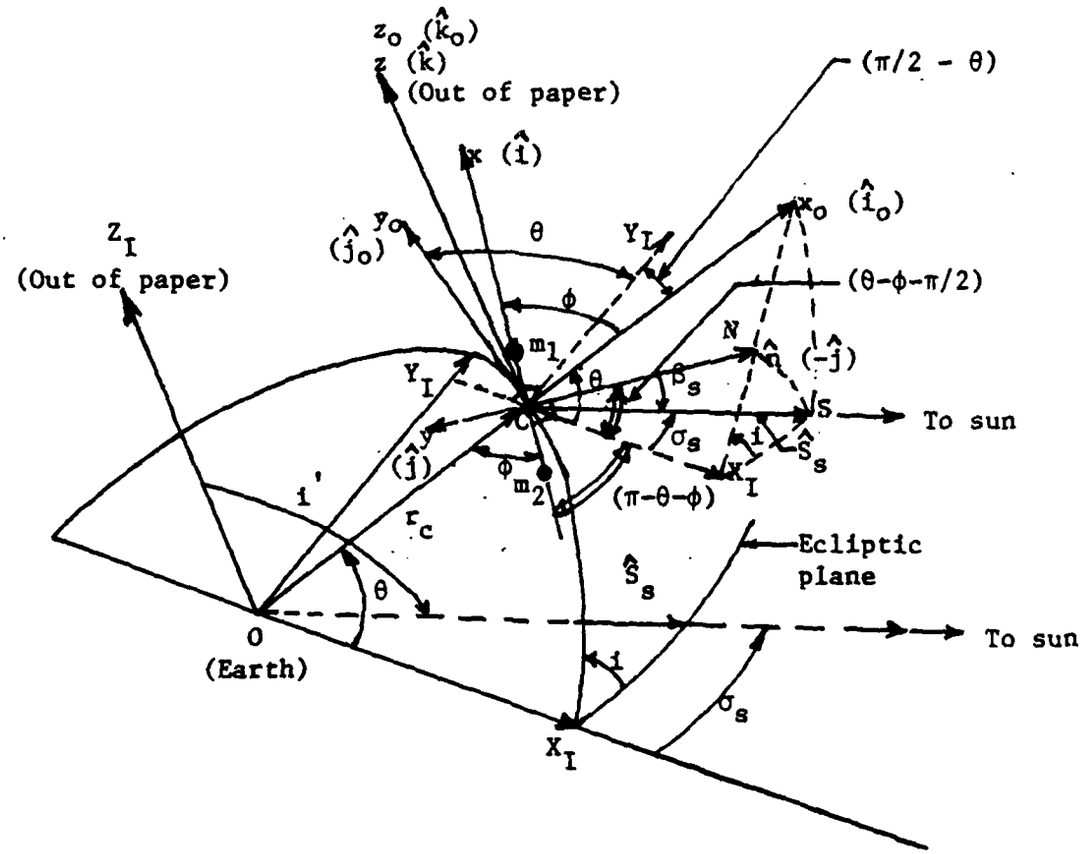

Figure 62. Relation Among Incident Solar Light vector, Orbital Coordinate System, and Body Coordinate System

along x, y, and z axes, respectively (Figure 62). The unit vector $\underline{S}_s$ may also be expressed in terms of body coordinates:

$$\underline{S}_s = S_1\underline{i} + S_2\underline{j} + S_1\underline{k} \qquad \text{(B-4)}$$

where, S_1, S_2, and S_3 are the components of $\underline{S}_s$ along the body coordinates axes, x, y, and z, respectively.

For the spherical triangle formed by the lines CN, CX_I, and CS in Figure 62, we can write [ref. 67, Equation (6.2.4)]

$$\begin{aligned} \text{Cos}\beta_s &= \text{Cos}\sigma\ \text{Cos}(\theta+\emptyset-\pi/2) + \text{Sin}\sigma\ \text{Sin}(\theta+\emptyset-\pi/2)\ \text{Cos}i \\ &= \text{Cos}\sigma\ \text{Sin}(\theta+\emptyset) - \text{Sin}\sigma\ \text{Cos}(\theta+\emptyset)\ \text{Cos}i \end{aligned} \qquad \text{(B-5)}$$

where β_s is the angle between the structure normal and the structure - sun line.

Noting that $S_2 = \underline{S}_s \cdot \underline{j} = -\underline{S}_s \cdot \underline{n} = -\text{Cos}\beta_s$ (B-6)

we can write,

$$S_2 = -[\text{Cos}\sigma\ \text{Sin}(\theta+\emptyset) - \text{Sin}\sigma\ \text{Cos}(\theta+\emptyset)\ \text{Cos}i] \qquad \text{(B-7)}$$

Similarly, we can write

$$S_1 = [\text{Cos}\sigma\ \text{Cos}(\theta+\emptyset) + \text{Sin}\sigma\ \text{Sin}(\theta+\emptyset)\ \text{Cos}i] \qquad \text{(B-8)}$$

and

$$S_3 = -[\text{Sin}\sigma\ \text{Sin}i] \qquad \text{(B-9)}$$

Hence, after making use of the above expressions for S_1, S_2, and S_3 in Equation (B-4), we get

$$\begin{aligned} \underline{S}_s = {} & [\text{Cos}\sigma\ \text{Cos}(\theta+\emptyset) + \text{Sin}\sigma\ \text{Sin}(\theta+\emptyset)\ \text{Cos}i]\ \underline{i} \\ & - [\text{Cos}\sigma\ \text{Sin}(\theta+\emptyset) - \text{Sin}\sigma\ \text{Cos}(\theta+\emptyset)\ \text{Cos}i]\ \underline{j} \\ & - [\text{Sin}\sigma\ \text{Sin}i]\ \underline{k} \end{aligned} \qquad \text{(B-10)}$$

Relation between the reflected solar light vector and the body coordinate system. In terms of body coordinates axes, the unit vector ($\underline{S}_r$) along the direction of the reflected solar light may be expressed as

$$\underline{S}_r = S_{r1}\underline{i} + S_{r2}\underline{j} + S_{r3}\underline{k} \tag{B-11}$$

where, S_{r1}, S_{r2}, and S_{r3} are the direction cosines of $\underline{S}_r$ with respect to x, y, and z axes. We note that the vectors $\underline{S}_s$, $\underline{S}_r$, and $\underline{n}$ lie in the same plane.

We observe that (see Figure 63)

$$\underline{S}_r \cdot \underline{n} = \cos\beta_s \ (= -S_{r2}) \tag{B-12}$$

Also, we have

$$\underline{S}_s \cdot \underline{n} = \cos\beta_s \ (= -S_2) \tag{B-13}$$

Comparing Equation (B-12) with Equation (B-13), we get

$$S_{r2} = S_2 \tag{B-14}$$

Similarly, we see that

$$S_{r1} = -S_1 \tag{B-15}$$

and

$$S_{r3} = -S_3 \tag{B-16}$$

Making use of Equations (B-14) through (B-16) in Equation (B-11), we find that S_r, in the body coordinates, can be written as

$$\underline{S}_r = -S_1\underline{i} + S_2\underline{j} - S_3\underline{k} \tag{B-17}$$

where, S_1, S_2, and S_3 are given by Equations (B-8), (B-7), and (B-9), respectively.

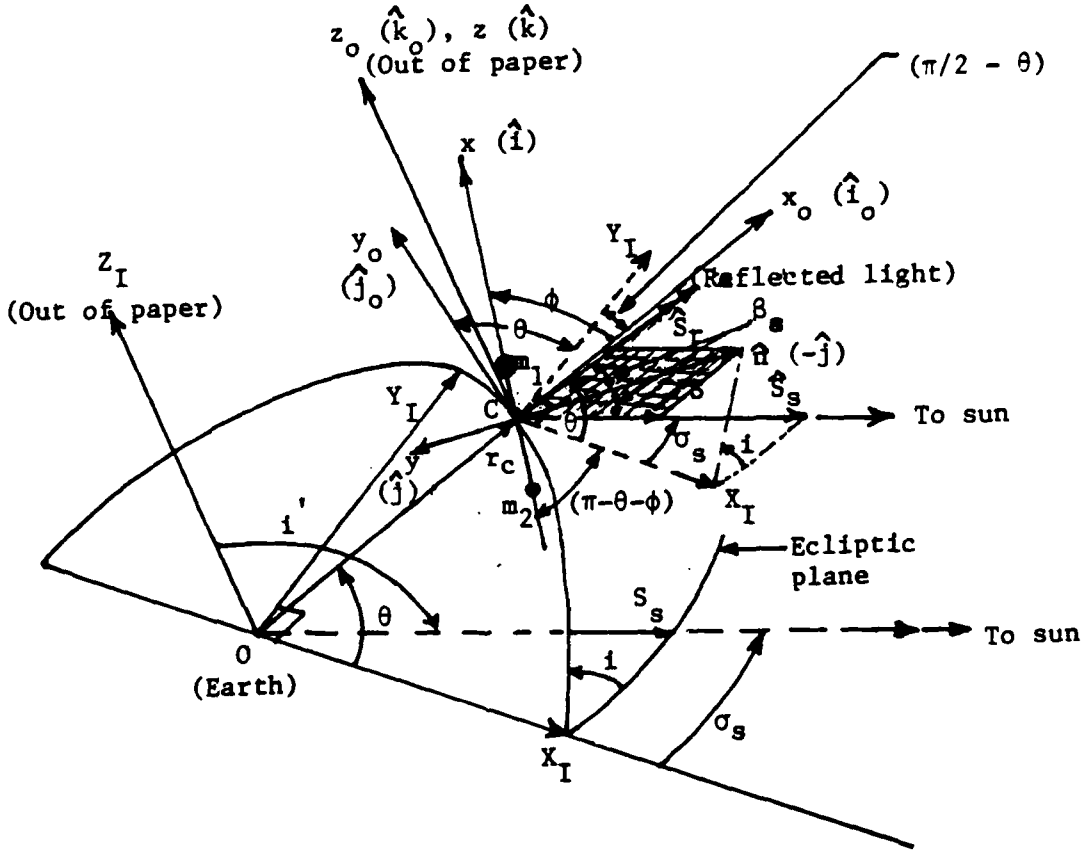

Figure 63. Relation Among Reflected Solar Light Vector, Orbital Coordinate System, and Body Coordinate System

Relation between the reflected solar light vector and the orbital coordinate system. The unit vector ($\underline{S}_r$) along the direction of reflected solar light can be written in terms of the orbital coordinate axes as

$$\underline{S}_r = S_{ro1}\underline{i}_o + S_{ro2}\underline{j}_o + S_{ro3}\underline{k}_o \qquad \text{(B-18)}$$

where, S_{ro1}, S_{ro2}, and S_{ro3} are the direction cosines of $\underline{S}_r$ with respect to the orbital axes x_o, y_o, and z_o, respectively. It can be readily seen that the following relations exist between the body and orbital coordinate systems (see Figure 62 or 63)

(a) $\underline{i} = \text{Cos}\emptyset\,\underline{i}_o + \text{Sin}\emptyset\,\underline{j}_o$

(b) $\underline{j} = -[\text{Sin}\emptyset\,\underline{i}_o - \text{Cos}\emptyset\,\underline{j}_o]$

(c) $\underline{k} = \underline{k}_o$

(B-19)

Substituting for $\underline{i}$, $\underline{j}$, and $\underline{k}$ from the above relations into Equation (B-17), we obtain

$$\begin{aligned}\underline{S}_r = &-[S_1\text{Cos}\emptyset + S_2\text{Sin}\emptyset]\underline{i}_o \\ &+ [-S_1\text{Sin}\emptyset + S_2\text{Cos}\emptyset]\underline{j}_o \\ &- [S_3]\underline{k}_o\end{aligned} \qquad \text{(B-20)}$$

Comparing Equations (B-18) and (B-20), we get the following relations:

(a) $S_{ro1} = -[S_1\text{Cos}\emptyset + S_2\text{Sin}\emptyset]$

(b) $S_{ro2} = -[S_1\text{Sin}\emptyset - S_2\text{Cos}\emptyset]$

(c) $S_{ro3} = -[S_3]$

(B-21)

Particular Sun Position

Now, by imposing the condition that the sun lies in the $X_I - Z_I$ plane as in the thermal effect analysis (i. e., $i = \pi/2$ and $\sigma = \pi/2 - i'$, where i' is the inclination of the sun from the orbit normal), we find from Equations (B-2)

(a) $S_{o1} = \cos\theta \sin i'$

(b) $S_{o2} = -\sin\theta \sin i'$

(c) $S_{o3} = -\cos i'$

(B-22)

These equations are given in Chapter II as Equations (2.104). Similarly, Equations (B-8), (B-7), and (B-9) respectively yield

(a) $S_1 = \cos(\theta+\emptyset) \sin i'$

(b) $S_2 = -\sin(\theta+\emptyset) \sin i'$

(c) $S_3 = -\cos i'$

(B-23)

These equations are given in Chapter II as Equations (2.102). Corresponding expressions for the direction cosines of the reflected solar light vector ($\underline{S}_r$) are given by Equations (B-15), (B-14), and (B-16) in the body coordinates (Equations (2.103) in Chapter II), and by Equations (B-21) in the orbital coordinates (Equations (2.105) in Chapter II). The expression for $\cos\beta_s$ given by Equation (B-5) now becomes

$$\cos\beta_s = \sin(\theta+\emptyset) \sin i' \qquad \text{(B-24)}$$

which is rewritten in Equation (2.106) in Chapter II. Finally, by assuming that the sun lies on the X_I-axis, i.e., $i' = \pi/2$, we get the following trigonometrical relations:

Equations (B-22) reduce to

(a) $S_{o1} = \cos\theta$

(b) $S_{o2} = -\sin\theta$

(c) $S_{o3} = 0$

(B-25)

Equations (B-23) reduce to

(a) $S_1 = \cos(\theta+\emptyset)$

(b) $S_2 = -\sin(\theta+\emptyset)$

(c) $S_3 = 0$

(B-26)

Equation (B-24) reduces to

$$\cos\beta_s = \sin(\theta + \emptyset) \qquad \text{(B-27)}$$

APPENDIX C

SELECTION OF PHYSICAL PARAMETER VALUES

Computation of Equivalent Properties of the Truss-like Structure

Consider the space structure to be an equivalent continuum representation of an hypothetical space platform composed of an assembly of tetrahedral truss (Figure 11). The equivalent continuum model of the large truss-like platform can be viewed as a plate.

Equivalent Mechanical Properties

Elastic modulus and mass density. The equivalent extensional elastic modulus (E) of the continuum model is given by [65, 66]:

$$E = \frac{3\sqrt{3}}{4\,lh}\left(E_1A_1 + E_2A_2 + \frac{1}{9}\,\frac{l^3}{d^3}\,E_dA_d\right) \qquad \text{(C-1)}$$

where

l is the length of the members in the top and bottom layers

d is the length of bracing members which is given by

$$d = \sqrt{[h^2 + (l^2/3)]} \qquad \text{(See Figure 12)} \qquad \text{(C-2)}$$

h is the height of the truss

E_1 and A_1 are respectively the modulus of elasticity and cross-sectional area of the top layer,

E_2 and A_2 are respectively the modulus of elasticity and cross-sectional area of bottom layer, and

E_d and A_d are respectively the modulus of elasticity and cross-sectional area of the bracing bars.

The equivalent mass density (ρ) is given by

$$\rho = \frac{2\sqrt{3}}{lh} \left(\rho_1 A_1 + \rho_2 A_2 + \frac{1}{d} \rho_d A_d \right) \qquad \text{(C-3)}$$

where ρ_1, ρ_2, and ρ_d are the mass densities of the top layer, bottom layer, and bracing members, respectively. Assume that all members are identical in all respects. Then,

(a) $A_1 = A_2 = A_d = A_1$

(b) $E_1 = E_2 = E_d = E_1$

(c) $l = d$

(d) $\rho_1 = \rho_2 = \rho_d = \rho_1$

(C-4)

h is now given by Equation (C-2) as

$$h = \sqrt{(2/3)}\,l \qquad \text{(C-5)}$$

With these simplifications, the equivalent mechanical properties of the truss become

$$E = \left(\frac{57\sqrt{3}}{36\ lh}\right) E_1 A_1 \qquad \text{(C-6)}$$

$$\rho = \left(\frac{6\sqrt{3}}{lh}\right) \rho_1 A_1 \qquad \text{(C-7)}$$

Consider the truss material made of aluminum, for which

$$E_1 = 71.7 \times 10^9\ N/m^2 \qquad \text{(C-8)}$$

$$\rho_1 = 2768\ kg/m^3 \qquad \text{(C-9)}$$

For each member, let the

area of cross section, $A_1 = 100 \times 10^{-6}\ m^2$ (C-10)

(diameter, D = 1.13 cm)

length, $l = 6$ m (C-11)

Therefore, from Equation (C-5)

$$h = 4.899\ m \qquad \text{(C-12)}$$

Now, from Equations (C-6) and (C-7)

$$E = 6.689496 \times 10^5\ N/m^2 = 6.689496 \times 10^{11}\ N/km^2 \qquad \text{(C-13)}$$

$$\rho = 0.0978632\ kg/m^3 = 2.71843 \times 10^7\ N\text{-}min^2/km^4 \qquad \text{(C-14)}$$

Equivalent Geometrical Properties

Area of cross-section. We assume that the width (z_s) of the structure to be 0.05 times the length (x_s) of the structure, i.e.,

$$z_s = 0.05\ x_s \qquad \text{(C-15)}$$

Hence, the area of the cross section (A_{cs}) is given by

$$A_{cs} = 0.05\ x_s\ h \qquad \text{(C-16)}$$

For a 1 km long structure (x_s = 1 km) with height (h) as given by Equation (C-12),

$$A_{cs} = 0.00024495\ km^2 \qquad \text{(C-17)}$$

Total mass of the truss structure. The total mass (M) of the truss structure now is

$$M = 0.05\ \rho h\ x_s^{\ 2} \qquad \text{(C-18)}$$

For a 1 km long structure (x_s = 1 km) with h and ρ as given by Equations (C-12) and (C-14), respectively,

$$M = 6658.768\ (N\text{-}min^2)/km = 23.9715\ ton \qquad \text{(C-19)}$$

Surface areas effective to radiation. In order to study the effects of radiation disturbances on the space structure, we need to know the area of the truss-like structure effective to radiation influx. For this purpose, we compute the area of each member of the truss projected onto the x - z plane.

The inclination of a bracing (diagonal) bar from x-z plane (top or bottom layer) is given by (Figure 11)

$$\text{Sin}u = (h/d) = \sqrt{(2/3)} \qquad \text{(C-20)}$$

$$\text{Then, Cos}u = 1/\sqrt{3} \qquad \text{(C-21)}$$

The length of a bracing (diagonal) member projected onto the x - z plane is

$$l_{bp} = d \cos u = (1/\sqrt{3})\, l \qquad (\text{since } d = l) \qquad \text{(C-22)}$$

The area (A_{pu}) of a unit repeating element of the tetrahedral truss projected onto the x - z plane is given below.

For a repeating unit surrounded by other units in all sides,

$$(A_{pu})_c = 6(Dl) + 3(D_b l_{bp}) \qquad \text{(C-23)}$$

For a repeating unit on the edge of the structure (no element on one side),

$$(A_{pu})_e = 7(Dl) + 4(D_b l_{bp}) \qquad \text{(C-24)}$$

where D is the diameter of the bars in top or bottom layer

D_b is the diameter of the bracing members.

Let all members have equal diameters, i.e., $D = D_b = D$

Then,

$$\text{(a)} \quad (A_{pu})_c = 3D(2\, l + l_{bp})$$

$$\text{(b)} \quad (A_{pu})_e = D(7\, l + 4\, l_{bp})$$

$$\text{(C-25)}$$

We have,

number of bays along the length (x_s) of the structure,

$$N_l = (x_s/l) \qquad \text{(C-26)}$$

number of bays along the width (z_s) of the structure,

$$N_w = \frac{2}{\sqrt{3}} \left(\frac{z_s}{l}\right) \qquad \text{(C-27)}$$

The total numbers of repeating truss elements

$$N_T = N_l N_w = \frac{2}{\sqrt{3}} \left(\frac{x_s z_s}{l^2}\right) \qquad \text{(C-28)}$$

The numbers of repeating truss elements in the edges along the length is equal to twice the number of bays along the length (assuming $N_w \geq 2$). That is,

$$N_e = 2N_l = 2(x_s/l) \qquad \text{(C-29)}$$

Therefore, the numbers of repeating truss elements surrounded by other truss elements,

$$N_c = (N_T - N_e) = 2\left(\frac{x_s}{l}\right)\left(\frac{z_s}{\sqrt{3}\, l} - 1\right) \qquad \text{(C-30)}$$

Hence, the total area of one side of the plate-like structure effective to radiation is (from Equations (C-25), (C-29), and (C-30)) given by

$$A_{sd} = 3N_c D\ (2\ l + l_{bp}) + N_e D\ (7\ l + 4\ l_{bp}) \qquad \text{(C-31)}$$

The total surface area of the rectangular plate effective to radiation is

$$A_{sf} = 2\ A_{sd} \qquad \text{(C-32)}$$

For a 1 km long structure (x_s = 1 km) with values of D and z_s as given earlier in Equation (C-10) and (C-15), respectively,

(a) $A_{sd} = 0.00087518\ km^2$, and

(b) $A_{sf} = 2\ A_{sd} = 0.00175036\ km^2$

(C-33)

In a case where the structure is covered on all sides with

thin aluminum foil, then

$$A_{sd} = x_s z_s = 0.05 \text{ km}^2 \tag{C-34}$$

Equivalent Thermal Properties

Thermal expansion property. The equivalent thermal expansion property (E_α) of the structure can be determined from the following relation [65].

$$E_\alpha = \frac{\sqrt{3}}{lh} [E_1 A_1 \alpha_1 + E_2 A_2 \alpha_2 + \frac{1}{3} \frac{1}{d} E_d A_d \alpha_d] \tag{C-35}$$

where α_1, α_2, α_d are the coefficient of thermal expansion or contraction of the top, bottom, and bracing members, respectively. As in earlier discussion, we consider all bars identical to each other in all respects,

$$\alpha_1 = \alpha_2 = \alpha_d = \alpha_1 \tag{C-36}$$

In such case, Equation (C-35) reduces to

$$E_\alpha = (\frac{7\sqrt{3}}{3hl}) E_1 A_1 \alpha_1 \tag{C-37}$$

For aluminum,

$$\alpha_1 = 24.7 \times 10^{-6} /°K \tag{C-38}$$

Substituting the values of h, E_1, A_1, and l from Equations (C-5), (C-8), (C-10), and (C-11), respectively and the above value of α_1, into Equation (C-37), we get

$$E_\alpha = 24.34976 \times 10^6 \text{ N/(km}^2\text{-°K)} \tag{C-39}$$

APPENDIX D

SELECTION OF INITIAL CONDITIONS

The reference set of initial conditions is selected from the equilibrium configuration of the structure in a circular orbit under the earth's gravitational pull. Let L be the Lagrangian function which is given by

$$L = K_E - P_E \tag{D-1}$$

K_E and P_E are respectively kinetic and potential energies of the system and are given by equations (A-7) and (A-23) respectively. To obtain the equilibrium configuration (steady state solution) [81, page 177], we have

$$\begin{aligned}
&(a)\ \frac{\partial L}{\partial r_c} = 0 \\
&(b)\ \frac{\partial L}{\partial \theta} = 0 \\
&(c)\ \frac{\partial L}{\partial x} = 0 \\
&(d)\ \frac{\partial L}{\partial \phi} = 0
\end{aligned} \tag{D-2}$$

In all of the above relations $\dot{r}_c$, $\dot{x}$, and $\dot{\phi}$ should be replaced by zero.

Carrying out the indicated differentiation as in Appendix A and writing in brief, we obtain,

$$\text{(a)} \quad -r_c\dot{\theta}^2 + \frac{\mu}{m}\left[\frac{m_1(r_c + x_1\cos\phi)}{r_1^3} + \frac{m_2(r_c - x_2\cos\phi)}{r_2^3}\right] = 0$$

(b) Identically satisfied

$$\text{(c)} \quad -\bar{m}x(\dot{\theta} + \dot{\phi})^2 + \bar{m}\mu\left[\frac{(x_1 + r_c\cos\phi)}{r_1^3} + \frac{(x_2 - r_c\cos\phi)}{r_2^3}\right] + G\frac{m_1 m_2}{x^2} + K_a(x - x_s) = 0$$

(Here, Equation (2.16) is used to substitute for $(\partial U_e/\partial x)$.)

$$\text{(d)} \quad \left[-\frac{1}{r_1^3} + \frac{1}{r_2^3}\right] r_c x \sin\phi = 0$$

(D-3)

Equation (D-3d) can be satisfied by

either (a) $\phi = 0$

or (b) $r_1 = r_2$

(D-4)

The latter condition may indicate unstable equilibrium [51, 52] in which we are not interested at present. Therefore, we choose the first condition, i.e., $\phi = 0$, which gives a stable equilibrium. This configuration also gives the largest possible differential gravitational force on the system.

Let us assign the following set of values for the variables at $t = 0$

(a) $r_c(0) = r_0$

(b) $\theta(0) = 0$ (Structure is released from perigee.)

(c) $x(0) = x_0$

(d) $\phi(0) = 0$

(e) $\dot{r}_c(0) = 0$

(f) $\dot{\theta}(0) = \theta_0$

(g) $\dot{x}(0) = 0$

(h) $\dot{\phi}(0) = 0$

(D-5)

With this set of values, Equation (D-3d) is satisfied identically. The first and third relations of Equations (D-3) respectively reduce to

$$\text{(a)} \quad -r_0\dot{\theta}_0^2 + \frac{\mu}{m}\left[\frac{m_1}{r_{10}^2} + \frac{m_2}{r_{20}^2}\right] = 0$$

$$\text{(b)} \quad -\bar{m}x_0\dot{\theta}_0^2 + m\mu\left[\frac{1}{r_{10}^2} - \frac{1}{r_{20}^2}\right] + G\frac{m_1 m_2}{x_0^2} + K_a(x_0 - x_s) = 0$$

(D-6)

where

$$\text{(a)} \quad r_{10} = r_0 + \frac{m_2}{m}x_0$$

$$\text{(b)} \quad r_{20} = r_0 - \frac{m_1}{m}x_0$$

(D-7)

From the first relation of Equations (D-6), we get

$$\dot{\theta}_0 = \left[\frac{\mu}{m}\frac{1}{r_0}\left(\frac{m_1}{r_{10}^2} + \frac{m_2}{r_{20}^2}\right)\right]^{1/2} \qquad \text{(D-8)}$$

Now, substituting for θ_0^2 in the second relation of (D-6), we can write

$$- \bar{m}x_0\left[\frac{\mu}{mr_0}\left(\frac{m_1}{r_{10}^2} + \frac{m_2}{r_{20}^2}\right)\right] + m\mu\left[\frac{1}{r_{10}^2} - \frac{1}{r_{20}^2}\right] + G\frac{m_1 m_2}{x_0^2} + K_a(x_0 - x_s) = 0 \qquad \text{(D-9)}$$

For a given set of values of r_0 and physical parameters (m_1, m_2, x_s, K_a, G, and μ), Equation (D-9) can be solved for x_0. Equation (D-8) gives the angular velocity (θ_0).

In the present example, we choose

(a) r_0 = 6574.33 km (200 km altitude)

(b) $m_1 = m_2$

(c) $m_2 = 5.0 \times 10^5$ N-min^2/km (1800 metric tons at the earth's surface)

(d) $E = 6.689496 \times 10^{11}$ N/km^2 (See Appendix C)

(e) x_s = 1.0 km

(D-10)

From these, we obtain

(a) $m = (m_1 + m_2) = 1.0 \times 10^6$ N min^2/km

(b) $\bar{m} = (m_1 m_2/m) = 2.5 \times 10^5$ N-min^2/km

(D-11)

For a structure with a height, $h = 4.899 \times 10^{-3}$ km (see Appendix C) and a width , $z_s = (0.05\ x_s)$ km, we get

(a) area of cross-section, $A_{cs} = 0.00024495$ km^2

(b) stiffness, $k_a = (EA_{cs}/x_s) = 163859204.52$ N/km

(D-12)

We have,

(a) Universal Gravitational Constant,

$$G = 8.64432 \times 10^{-16}\ km^4/N\text{-}min^4$$

(b) Acceleration due to gravity at the earth's surface,

$$g = 35.316\ km/min^2$$

(c) Radius of the earth, $R = 6374.33$ km

(D-13)

Therefore,

$$\mu = gR^2 = 1.434963 \times 10^9\ km^3/min^2 \qquad \text{(D-14)}$$

When equation (D-9) is solved with these values, we get

$$x_0 = 1.0000230\ km \qquad \text{(D-15)}$$

Equation (D-8) gives,

$$\dot{\theta}_0 = 0.07106292\ radian/min \qquad \text{(D-16)}$$

We have therefore the complete set of initial conditions and values of all other constant parameters associated with the equilibrium configuration.

APPENDIX E

COMPUTER PROGRAMS

Computer Program I

Listing of Sample Program to Compute Effects of Differential Gravitational Forces

```
      PROGRAM DGRVEFF (INPUT,OUTPUT,TAPE15,TAPE16,TAPE17)
C- ----------------------------------------
C  THIS PROGRAM COMPUTES R, THETA, Z AND PHI
C    AND THEIR FIRST TIME DERIVATIVES
C  FOR AN AXIALLY FLEXIBLE DUMBBELL STRUCTURE
C  ORBITING IN SPACE WITH PLANAR MOTION
C   UNDER EARTH,S GRAVITATIONAL FORCE ALONE.
C ----------------------------------------
C    SIMULTANEOUS  NONLINEAR COUPLED DIFFERENTIAL
C  EQUATIONS ARE SOLVED BY NUMERICAL ANALYSIS USING
C    5TH AND 6TH. ORDER RUNGE-KUTTA-VERNER METHOD
C    (IMSL SUBROUTINE PACKAGE: DVERK)
C-  ----------------------------------------
C    *****
      DIMENSION Y(8)
       DIMENSION C(24),W(8,9)
       REAL IGF
      COMMON XM,XM1,XM2,XMBAR,XMU,UGC,XE,XA,XS,XKA,RM
      EXTERNAL FCN1
C    ****
      WRITE (16,*) 'UNITS ARE IN NEWTON, KILOMETER AND'
      WRITE (16,*) '    MINUTES ( ANGLE IN RADIAN) '
      WRITE (17,*) 'UNITS ARE IN NEWTON, KILOMETER AND'
      WRITE (17,*) '    MINUTES ( ANGLE IN RADIAN) '
      READ (15,*) RM,XM2,GE,RE,UGC
      READ (15,*) XE,XHT,XS
      READ (15,*) R0,TH0,X0,PH0
      READ (15,*) RDOT,THDOT,XDOT,PHDOT
      READ (15,*)TOL
      XM1=RM*XM2
      XA=0.05*XS*XHT
      XKA=(XE*XA)/XS
      XMU=GE*(RE**2.)
      XM=XM1+XM2
      XMBAR=(XM1*XM2)/XM
C    ****
      WRITE (16,*)' M1= ',XM1,' M2= ',XM2,' M1/M2= ',RM
      WRITE (16,*)' ACC.GRAV.= ',GE,' RADIUS OF EARTH= ',RE
      WRITE (16,*)' ELAST MOD= ',XE,' X-AREA OF LINK= ',XA
      WRITE (16,*)' STIFFNESS= ',XKA,' REF LEGTH= ',XS
```

```
      WRITE (16,*)' UNIVERSAL GRAV. CONST.= ',UGC
      WRITE (16,*)'  GRAV. CONST.= ',XMU
      WRITE (16,*)' TOTAL MASS= ',XM,' REDUCED MASS= ',XMBAR
      WRITE (16,*)TOL
      WRITE (17,*)' M1= ',XM1,' M2= ',XM2,' M1/M2= ',RM
      WRITE (17,*)' ACC.GRAV.= ',GE,' RADIUS OF EARTH= ',RE
      WRITE (17,*)' FLAST MOD= ',XE,' X-AREA OF LINK= ',XA
      WRITE (17,*)' STIFFNESS= ',XKA,' REF LEGTH= ',XS
      WRITE (17,*)' UNIVERSAL GRAV. CONST.= ',UGC
      WRITE (17,*)'  GRAV. CONST.= ',XMU
      WRITE (17,*)' TOTAL MASS= ',XM,' REDUCED MASS= ',XMBAR
      WRITE (17,*)TOL
      NW=8
      N=8
      T=0.0
      Y(1)=R0
      Y(2)=TH0
      Y(3)=X0
      Y(4)=PH0
      Y(5)=RDOT
      Y(6)=THDOT
      Y(7)=XDOT
      Y(8)=PHDOT
      IND=1
C       ****
      A0=Y(1)**2
      B0=(Y(3)**2/XM**2)
      CC0=COS(Y(4))
      D0=2.*(1./XM)*Y(1)*Y(3)*CC0
      R10=(A0+(XM2**2)*B0+D0*XM2)**0.5
      R20=(A0+(XM1**2)*B0-D0*XM1)**0.5
      X10=(XM2/XM)*Y(3)
      X20=(XM1/XM)*Y(3)
      E0=(XM1*(Y(1)+X10*CC0))/R10**3
      F0=(XM2*(Y(1)-X20*CC0))/R20**3
      IGF=XMU*(E0+F0)
      TGF0=XMU*(E0+F0)
      DGF0=XMU*(E0-F0)
      TGFRAT=TGF0/IGF
      DGFRAT=DGF0/IGF
      XRAT=Y(3)/XS
      RRAT=Y(1)/R0
      WRITE (16,*) 'INITIAL TOTAL GRAV. FORCE (IGF)= ',IGF
      WRITE (16,*)'***                    ***'
      WRITE (17,*) 'INITIAL TOTAL GRAV. FORCE (IGF) =',IGF
      WRITE (17,*)'*****'
C     ***
      WRITE (16,5)
    5 FORMAT ('TIME',12X,'RC',10X,'THETA',12X,'X',12X,'PHI',
     +   11X,'THDOT',9X,'RC/R0',10X,'X/XS',10X,'DGF/IGF')
      WRITE (16,10)T,(Y(K),K=1,4),Y(6),RRAT,XRAT,DGFRAT
```

```
   10  FORMAT (9E14.8)
    WRITE (17,13)
    13  FORMAT ('TIME',12X,'RDOT',12X,'XDOT',12X,'PHDOT',12X,
+         'TGF/IGF')
    WRITE (17,16) TEND,Y(5),Y(7),Y(8),TGFRAT
    16  FORMAT (5E14.8)
    DO 2000 K=1,2000
    TEND=FLOAT(K)*0.20
    CALL DVERK(N,FCN1,T,Y,TEND,TOL,IND,C,NW,W,IER)
    IF (IND.LT.0.OR.IER.GT.0) GO TO 30
    A=Y(1)**2.
    B=(Y(3)**2./XM**2.)
    CC=COS(Y(4))
    D=2.*(1./XM)*Y(1)*Y(3)*CC
    R1=(A+(XM2**2.)*B+D*XM2)**0.5
    R2=SQRT(A+(XM1**2.)*B-D*XM1)
    X1=(XM2/XM)*Y(3)
    X2=(XM1/XM)*Y(3)
    E=(XM1*(Y(1)+X1*CC))/R1**3.
    F=(XM2*(Y(1)-X2*CC))/R2**3.
    TGF=XMU*(E+F)
    DGF=XMU*(E-F)
    TGFRAT=TGF/IGF
    DGFRAT=DGF/IGF
    RRAT=Y(1)/R0
    XRAT=Y(3)/XS
    WRITE (16,20)TEND,(Y(L),L=1,4),Y(6),RRAT,XRAT,DGFRAT
    20  FORMAT (9E14.8)
    WRITE (17,25) TEND,Y(5),Y(7),Y(8),TGFRAT
   25  FORMAT (5E14.8)
    50  CONTINUE
    STOP
    30  CONTINUE
    PRINT *,'IER = ',IER
    STOP
    END
C   ---------------------------------------------
C   ---  SUBROUTINE * FCN1 *  --------
C   ------------------------------------------------
    SUBROUTINE FCN1 (N,T,Y,YD)
     DIMENSION Y(N),YD(N)
    COMMON XM,XM1,XM2,XMBAR,XMU,UGC,XE,XA,XS,XKA,RM
    YD(1)=Y(5)
    YD(2)=Y(6)
    YD(3)=Y(7)
    YD(4)=Y(8)
    A=Y(1)**2.
    B=(Y(3)**2./XM**2.)
    CC=COS(Y(4))
    D=2.*(1./XM)*Y(1)*Y(3)*CC
    R1=(A+(XM2**2.)*B+D*XM2)**0.5
```

```
R2=SQRT(A+(XM1**2.)*B-D*XM1)
X1=(XM2/XM)*Y(3)
X2=(XM1/XM)*Y(3)
DUDX=XKA*(Y(3)-XS)
E=(XM1*(Y(1)+X1*CC))/R1**3.
F=(XM2*(Y(1)-X2*CC))/R2**3.
YD(5)=(Y(1)*(Y(6))**2.)-(XMU/XM)*(E+F)
G=SIN(Y(4))
BH=XMU*((1./R2**3.)-(1./R1**3.))*G
YD(6)=(-2.)*(Y(5)/Y(1))*Y(6)+(XMBAR/XM)*BH*(Y(3)/Y(1))
BI=Y(6)+Y(8)
BJ=(X1+Y(1)*CC)/(R1**3.)
BK=(Y(1)*CC-X2)/(R2**3.)
GRV=(UGC*XM1*XM2)/(Y(3)**2.)
YD(7)=Y(3)*(BI**2.)-XMU*(BJ-BK)-(DUDX/XMBAR)-(GRV/XMBAR)
BL=((XMBAR/XM)*(Y(3)/Y(1)))+(Y(1)/Y(3))
YD(8)=2.*(Y(5)/Y(1))*Y(6)-2.*(Y(7)/Y(3))*BI-(BL*BH)
RETURN
END
```

Sample Input Data

Tape 15

```
PRINT,TAPE15

1.000000000,5.000E+05,3.5316E+1,6.37433E+3,8.64432E-16
6.689496E+11,4.899E-3,1.0
6.5743300000E+3,0.0,1.0000230,0.00000000
0.0,7.1062920411420E-2,0.0,0.0
1.0E-06

 READY.
```

Sample Run Session

```
FORTRAN
 READY.
FINDLIB,IMSL
 READY.
X,LIBRARY,IMSL
 READY.
OLD,GEFF
 READY.
GET,TAPE15
 READY.
RUN

    STOP

SRU       2.171 UNTS.

 RUN COMPLETE.
```

Sample Output Data

Tape 16

```
UNITS ARE IN NEWTON, KILOMETER AND
   MINUTES ( ANGLE IN RADIAN)
 M1= 500000. M2= 500000. M1/M2= 1.
 ACC.GRAV.= 35.316 RADIUS OF EARTH= 6374.33
 ELAST MOD= 6.689496E+11 X-AREA OF LINK= .00024495
 STIFFNESS= 163859204.52 REF LEOTH= 1.
 UNIVERSAL GRAV. CONST.= 8.64432E-16
  GRAV. CONST.= 1.434962641423E+9
 TOTAL MASS= 1000000. REDUCED MASS= 250000.
 1.E-6
 INITIAL TOTAL GRAV. FORCE (IGF)= 33199963.21351
 ***          ***
TIME          RC          THETA          X           PHI          THDOT        RC/RO        X/XS         DGF/IGF
.00000000E+00 .65743300E+04 .00000000E+00 .10000230E+01 .00000000E+00 .71062920E-01 .10000000E+01 .10000230E+01-.15211025E-03
.20000000E+00 .65743300E+04 .14212584E-01 .10000231E+01-.38680514E-08 .71062920E-01 .10000000E+01 .10000231E+01-.15211026E-03
.40000000E+00 .65743300E+04 .28425168E-01 .10000232E+01-.70587591E-08 .71062920E-01 .10000000E+01 .10000232E+01-.15211028E-03
.60000000E+00 .65743300E+04 .42637752E-01 .10000232E+01-.95976157E-08 .71062920E-01 .10000000E+01 .10000232E+01-.15211029E-03
.80000000E+00 .65743300E+04 .56850336E-01 .10000231E+01-.12240822E-07 .71062920E-01 .10000000E+01 .10000231E+01-.15211027E-03
.10000000E+01 .65743300E+04 .71062920E-01 .10000230E+01-.15764742E-07 .71062920E-01 .10000000E+01 .10000230E+01-.15211025E-03
.12000000E+01 .65743300E+04 .85275504E-01 .10000230E+01-.19864992E-07 .71062920E-01 .10000000E+01 .10000230E+01-.15211025E-03
.14000000E+01 .65743300E+04 .99488089E-01 .10000231E+01-.23580872E-07 .71062920E-01 .10000000E+01 .10000231E+01-.15211027E-03
.16000000E+01 .65743300E+04 .11370067E+00 .10000233E+01-.26282200E-07 .71062920E-01 .10000000E+01 .10000233E+01-.15211029E-03
.18000000E+01 .65743300E+04 .12791326E+00 .10000233E+01-.28428603E-07 .71062920E-01 .10000000E+01 .10000233E+01-.15211029E-03
.20000000E+01 .65743300E+04 .14212584E+00 .10000231E+01-.31241574E-07 .71062920E-01 .10000000E+01 .10000231E+01-.15211026E-03
.22000000E+01 .65743300E+04 .15633842E+00 .10000229E+01-.35183387E-07 .71062920E-01 .10000000E+01 .10000229E+01-.15211024E-03
.24000000E+01 .65743300E+04 .17055101E+00 .10000230E+01-.39461236E-07 .71062920E-01 .10000000E+01 .10000230E+01-.15211025E-03
.26000000E+01 .65743300E+04 .18476359E+00 .10000232E+01-.42672275E-07 .71062920E-01 .10000000E+01 .10000232E+01-.15211029E-03
.28000000E+01 .65743300E+04 .19897618E+00 .10000233E+01-.44641553E-07 .71062920E-01 .10000000E+01 .10000233E+01-.15211030E-03
.30000000E+01 .65743300E+04 .21318876E+00 .10000232E+01-.46534305E-07 .71062920E-01 .10000000E+01 .10000232E+01-.15211028E-03
.32000000E+01 .65743300E+04 .22740135E+00 .10000229E+01-.49824611E-07 .71062920E-01 .10000000E+01 .10000229E+01-.15211024E-03
.34000000E+01 .65743300E+04 .24161393E+00 .10000229E+01-.54236686E-07 .71062920E-01 .10000000E+01 .10000229E+01-.15211023E-03
.36000000E+01 .65743300E+04 .25582651E+00 .10000231E+01-.58120315E-07 .71062920E-01 .10000000E+01 .10000231E+01-.15211027E-03
.38000000E+01 .65743300E+04 .27003910E+00 .10000233E+01-.60371658E-07 .71062920E-01 .10000000E+01 .10000233E+01-.15211030E-03
.40000000E+01 .65743300E+04 .28425168E+00 .10000233E+01-.61694545E-07 .71062920E-01 .10000000E+01 .10000233E+01-.15211030E-03
.42000000E+01 .65743300E+04 .29846427E+00 .10000231E+01-.63969092E-07 .71062920E-01 .10000000E+01 .10000231E+01-.15211026E-03
.44000000E+01 .65743300E+04 .31267685E+00 .10000228E+01-.67886419E-07 .71062920E-01 .10000000E+01 .10000228E+01-.15211023E-03
.46000000E+01 .65743300E+04 .32688943E+00 .10000229E+01-.72211650E-07 .71062920E-01 .10000000E+01 .10000229E+01-.15211024E-03
.48000000E+01 .65743300E+04 .34110202E+00 .10000232E+01-.75060938E-07 .71062920E-01 .10000000E+01 .10000232E+01-.15211029E-03
.50000000E+01 .65743300E+04 .35531460E+00 .10000234E+01-.76265744E-07 .71062920E-01 .10000000E+01 .10000234E+01-.15211031E-03
.52000000E+01 .65743300E+04 .36952719E+00 .10000232E+01-.77538086E-07 .71062920E-01 .10000000E+01 .10000232E+01-.15211028E-03
.54000000E+01 .65743300E+04 .38373977E+00 .10000229E+01-.80522440E-07 .71062920E-01 .10000000E+01 .10000229E+01-.15211024E-03
.56000000E+01 .65743300E+04 .39795235E+00 .10000228E+01-.84778239E-07 .71062920E-01 .10000000E+01 .10000228E+01-.15211023E-03
.58000000E+01 .65743300E+04 .41216494E+00 .10000231E+01-.88296044E-07 .71062920E-01 .10000000E+01 .10000231E+01-.15211027E-03
.60000000E+01 .65743300E+04 .42637752E+00 .10000234E+01-.89821677E-07 .71062920E-01 .10000000E+01 .10000234E+01-.15211031E-03
      :            :            :            :            :            :            :            :            :
```

Sample Output Data (continued ...)

Tape 17

```
UNITS ARE IN NEWTON; KILOMETER AND
   MINUTES ( ANGLE IN RADIAN)
 M1= 500000. M2= 500000. M1/M2= 1.
 ACC.GRAV.= 35.316 RADIUS OF EARTH= 6374.33
 ELAST MOD= 6.689496E+11 X-AREA OF LINK= .00024495
 STIFFNESS= 163859204.52 REF LEGTH= 1.
 UNIVERSAL GRAV. CONST.= 8.64432E-16
  GRAV. CONST.= 1.434962641423E+9
 TOTAL MASS= 1000000. REDUCED MASS= 250000.
T.E-6
 INITIAL TOTAL GRAV. FORCE (IGF) =33199963.21351
 ****
 TIME          RDOT          XDOT          PHDOT          TGF/IGF
 .00000000E+00 .00000000E+00 .00000000E+00 .00000000E+00 .10000000E+01
 .20000000E+00-.54778725E-12-.28164722E-05-.85834259E-08 .10000000E+01
 .40000000E+00-.10474281E-11-.25183446E-05-.27593335E-07 .10000000E+01
 .60000000E+00-.15436427E-11 .76772333E-06-.35017596E-07 .10000000E+01
 .80000000E+00-.21195526E-11 .35084069E-05-.20358619E-07 .10000000E+01
 .10000000E+01-.26697000E-11 .22249285E-05 .31995233E-09 .10000000E+01
 .12000000E+01-.32375689E-11-.17987042E-05 .35384895E-08 .10000000E+01
 .14000000E+01-.36559408E-11-.41041298E-05-.16891331E-07 .10000000E+01
 .16000000E+01-.41918213E-11-.17941613E-05-.38243289E-07 .10000000E+01
 .18000000E+01-.47993751E-11 .30026114E-05-.35978831E-07 .10000000E+01
 .20000000E+01-.53344691E-11 .46441393E-05-.88241688E-08 .10000000E+01
 .22000000E+01-.57903270E-11 .98965675E-06-.12349968E-07 .10000000E+01
 .24000000E+01-.64105585E-11-.43134061E-05 .17511762E-08 .10000000E+01
 .26000000E+01-.69688517E-11-.48043123E-05-.30417954E-07 .10000000E+01
 .28000000E+01-.75979221E-11-.31505779E-06-.48003003E-07 .10000000E+01
 .30000000E+01-.80780826E-11 .56624822E-05-.27733384E-07 .10000000E+01
 .32000000E+01-.86898905E-11 .44313378E-05 .87725859E-08 .10000000E+01
 .34000000E+01-.92448417E-11-.21149915E-05 .17885852E-07 .10000000E+01
 .36000000E+01-.98709260E-11-.63745439E-05-.11773793E-07 .10000000E+01
 .38000000E+01-.10391042E-10-.32650600E-05-.46487125E-07 .10000000E+01
 .40000000E+01-.10985074E-10 .39594449E-05-.44437873E-07 .10000000E+01
 .42000000E+01-.11501543E-10 .66203902E-05-.62873371E-08 .10000000E+01
 .44000000E+01-.11942016E-10 .15225344E-05 .23801208E-07 .10000000E+01
 .46000000E+01-.12574572E-10-.56470750E-05 .97117003E-08 .10000000E+01
 .48000000E+01-.13184956E-10-.62084453E-05-.32761118E-07 .10000000E+01
 .50000000E+01-.13660927E-10 .60804744E-06-.53258699E-07 .10000000E+01
 .52000000E+01-.14181601E-10-.68996178E-05-.26541944E-07 .10000000E+01
 .54000000E+01-.14755331E-10 .50750364E-05 .16918036E-07 .10000000E+01
 .56000000E+01-.15204499E-10-.28411631E-05 .25752423E-07 .10000000E+01
 .58000000E+01-.15748970E-10-.75891194E-05-.10836336E-07 .10000000E+01
 .60000000E+01-.16300118E-10-.33919317E-05-.50322665E-07 .10000000E+01
 .62000000E+01-.16929352E-10 .49566930E-05-.44920709E-07 .10000000E+01
      :             :             :             :             :
```

Computer Program II

Listing of Sample Program to Compute Combined Effects of Thermal and Differential Gravitational Forces

```
      PROGRAM THRMEFF (INPUT,OUTPUT,TAPE40,TAPE41,TAPE42)
C     ------------------------------------------
C     THIS PROGRAM COMPUTES R, THETA, Z AND PHI
C       AND THEIR FIRST TIME DERIVATIVES
C     FOR AN AXIALLY FLEXIBLE DUMBBELL STRUCTURE
C     ORBITING IN SPACE WITH PLANAR MOTION
C      UNDER DIFF. GRAVITATIONAL FORCE AND
C      TEMPERATURE EFFECTS.
C    ---------------------------------------------
C      ***
C      SIMULTANEOUS  NONLINEAR COUPLED DIFFERENTIAL
C     EQUATIONS ARE SOLVED BY NUMERICAL ANALYSIS USING
C       5TH AND 6TH. ORDER RUNGE-KUTTA-VERNER METHOD
C       (IMSL SUBROUTINE PACKAGE: DVERK)
C-    ---------------------------------------------
C        ***
      DIMENSION Y(9)
       DIMENSION C(24),W(9,9)
      REAL IPRM
      INTEGER NROT
      COMMON XM,XM1,XM2,XMBAR,XMU,UGC,XE,XA,XS,XKA,RM,
     + RE,TMPS,NDSOL,NDERT,NALBD,GS,ALBD,
     + ABSOL,ABERT,ABALB,DERAD,EPSL,SIGMA,
     +  XASDE,XASRF,XMASS,SPHT,
     +  PI,IPRM,TPROP,NDELTA,NCOUNT,RDIFF1
      EXTERNAL FCN1
C       ***
      PRINT *,'ENTER CODE FOR DIRECT SOLAR, DIRECT EARTH,'
      PRINT *,'AND ALBEDO: 1=YES, 2=NO'
      READ *,NDSOL,NDERT,NALBD
      IF (NDSOL .EQ. 1 .AND. NDERT .NE. 1 .AND. NALBD
     +   .NE. 1)THEN
      WRITE (41,*)'**DIRECT SOLAR EFFECT ONLY **'
      WRITE (42,*) '**DIRECT SOLAR EFFECT ONLY **'
      ELSE
      END IF
      IF (NDSOL .NE. 1 .AND. NDERT .EQ. 1 .AND. NALBD
     +   .NE. 1) THEN
      WRITE (41,*) '**DIRECT EARTH RADIATION EFFECT ONLY **'
      WRITE (42,*) '**DIRECT EARTH RADIATION EFFECT ONLY **'
      ELSE
      END IF
      IF (NDSOL .NE. 1 .AND. NDERT .NE. 1 .AND. NALBD
```

```
+     .EQ. 1) THEN
      WRITE (41,*) '**ALBEDO EFFECT ONLY**'
      WRITE (42,*) '**ALBEDO EFFECT ONLY**'
      ELSE
      END IF
      IF (NDSOL .EQ. 1 .AND. NDERT .EQ. 1 .AND. NALBD
+        .EQ. 1) THEN
         WRITE (41,*) '**TOTAL THERMAL EFFECTS**'
         WRITE (42,*) '**TOTAL THERMAL EFFECTS**'
      ELSE
      END IF
      IF (NDSOL .EQ. 1 .AND. NDERT .NE. 1 .AND. NALBD
+          .EQ. 1) THEN
       WRITE (41,*) '***DIRECT SOLAR AND ALBEDO HEATING***'
       WRITE (42,*) '**DIRECT SOLAR AND ALBEDO HEATING**'
      ELSE
      END IF
       PI=3.141592
C
      WRITE (41,*) 'UNITS ARE IN NEWTON, WATT, KILOMETER AND'
      WRITE (41,*)'MINUTES (ANGLE IN RADIAN, TEMP. IN KELVIN)'
      WRITE (42,*) 'UNITS ARE IN NEWTON, WATT, KILOMETER AND'
      WRITE (42,*)'MINUTES (ANGLE IN RADIAN, TEMP. IN KELVIN)'
      READ (40,*) RM,XM2,GE,RE,UGC
      READ (40,*) XE,XHT,XS,TMPS,TPROP
      READ (40,*) R0,TH0,X0,PH0,TMP0
      READ (40,*) RDOT,THDOT,XDOT,PHDOT
      READ (40,*)XMASS,SPHT
      READ (40,*)GS,ALBD
      READ (40,*)ABSOL,ABERT,ABALB,DERAD
      READ (40,*)EPSL,SIGMA
      READ (40,*)XASDE,XASRF
      READ (40,*) IPRM,NDELTA
      READ (40,*)TOL
      XM1=RM*XM2
      XA=0.05*XS*XHT
      XKA=(XE*XA)/XS
      XMU=GE*(RE**2.)
      XM=XM1+XM2
      XMBAR=(XM1*XM2)/XM
C        ***
      WRITE (41,*)' M1= ',XM1,' M2= ',XM2,' M1/M2= ',RM
      WRITE (41,*)' ACC.GRAV.= ',GE,' RADIUS OF EARTH= ',RE
      WRITE (41,*)' ELAST MOD= ',XE,' X-AREA OF LINK= ',XA
      WRITE (41,*)' STIFFNESS= ',XKA,' REF LENGTH= ',XS
      WRITE (41,*)' UNIVERSAL GRAV. CONST.= ',UGC
      WRITE (41,*)'GRAV. CONST.= ',XMU,'REF. TEMP= ',TMPS
      WRITE (41,*)' TOTAL MASS= ',XM,' REDUCED MASS= ',XMBAR
      WRITE (41,*)'***'
      WRITE (41,*)'REF. TEMP.= ',TMPS
      WRITE (41,*) 'SOLAR RADIATION CONSTANT= ',GS
```

```
      WRITE (41,*) 'AVERAGE ALBEDO= ',ALBD
      WRITE (41,*) 'AVE. EARTH EMITTED RADIATION= ',DERAD
      WRITE (41,*) 'ABSORPTANCE TO DIRECT SOLAR RADIATION= ',
     +  ABSOL
      WRITE (41,*) 'ABSORPTANCE TO ALBEDO RADIATION = ',ABALB
      WRITE (41,*) 'ABSORPTANCE TO DIRECT EARTH RADIATION=  ',
     +   ABERT
      WRITE (41,*) 'EMITTANCE TO THERMAL RADIATION= ',EPSL
      WRITE (41,*) 'STEPHAN-BOLTZMANN CONSTANT= ',SIGMA
      WRITE (41,*) '***'
      WRITE (41,*) 'SPECIFIC HEAT OF LINK-MATERIAL(AL)= ',SPHT
      WRITE (41,*)'THERMAL EXPANSION PROPERTY OF LINK-MATERIAL= '
     +  ,TPROP
      WRITE (41,*) 'TOTAL MASS OF LINK-STRUCTRE= ',XMASS
      WRITE (41,*) 'TOTAL AREA OF ONE SIDE OF LINK EFFECTIVE '
      WRITE (41,*) '   FOR THERMAL ABSORPTANCE= ',XASDE
      WRITE (41,*) 'TOTAL SURFACE AREA EFFECTIVE FOR'
      WRITE (41,*) '   THERMAL EMITTANCE= ',XASRF
      WRITE (41,*) '***'
      WRITE (41,*) 'INCLINATION OF SUN FROM NORMAL TO'
      WRITE (41,*) '   ORBIT PLANE= ',IPRM,' (RAD)'
      WRITE (41,*)TOL
      WRITE (41,*)'****'
      WRITE (42,*)' M1= ',XM1,' M2= ',XM2,' M1/M2= ',RM
      WRITE (42,*)' ACC.GRAV.= ',GE,' RADIUS OF EARTH= ',RE
      WRITE (42,*)' ELAST MOD= ',XE,' X-AREA OF LINK= ',XA
      WRITE (42,*)' STIFFNESS= ',XKA,' REF LENGTH= ',XS
      WRITE (42,*)' UNIVERSAL GRAV. CONST.= ',UGC
      WRITE (42,*)'GRAV. CONST.= ',XMU,'REF. TEMP= ',TMPS
      WRITE (42,*)' TOTAL MASS= ',XM,' REDUCED MASS= ',XMBAR
      WRITE (42,*)'***'
      WRITE (42,*)'REF. TEMP.= ',TMPS
      WRITE (42,*) 'SOLAR RADIATION CONSTANT= ',GS
      WRITE (42,*) 'AVERAGE ALBEDO= ',ALBD
      WRITE (42,*) 'AVE. EARTH EMITTED RADIATION= ',DERAD
      WRITE (42,*) 'ABSORPTANCE TO DIRECT SOLAR RADIATION= ',
     +  ABSOL
      WRITE (42,*) 'ABSORPTANCE TO ALBEDO RADIATION = ',ABALB
      WRITE (42,*) 'ABSORPTANCE TO DIRECT EARTH RADIATION=  ',
     +   ABERT
      WRITE (42,*) 'EMITTANCE TO THERMAL RADIATION= ',EPSL
      WRITE (42,*) 'STEPHAN-BOLTZMANN CONSTANT= ',SIGMA
      WRITE (42,*) '***'
      WRITE (42,*) 'SPECIFIC HEAT OF LINK-MATERIAL(AL)= ',SPHT
      WRITE (42,*)'THERMAL EXPANSION PROPERTY OF LINK-MATERIAL= '
     +   ,TPROP
      WRITE (42,*) 'TOTAL MASS OF LINK-STRUCTRE= ',XMASS
      WRITE (42,*) 'TOTAL AREA OF ONE SIDE OF LINK EFFECTIVE '
      WRITE (42,*) '   FOR THERMAL ABSORPTANCE= ',XASDE
      WRITE (42,*) 'TOTAL SURFACE AREA EFFECTIVE FOR'
      WRITE (42,*) '   THERMAL EMITTANCE= ',XASRF
```

```
      WRITE (42,*) '***'
      WRITE (42,*) 'INCLINATION OF SUN FROM NORMAL TO'
      WRITE (42,*) '   ORBIT PLANE= ',IPRM,' (RAD)'
      WRITE (42,*)TOL
      WRITE (42,*)'***'
      NW=9
      N=9
      T=0.0
      Y(1)=R0
      Y(2)=TH0
      Y(3)=X0
      Y(4)=PH0
      Y(5)=RDOT
      Y(6)=THDOT
      Y(7)=XDOT
      Y(8)=PHDOT
      Y(9)=TMP0
      IND=1
C        ***
      RCRAT=Y(1)/R0
      XRAT=Y(3)/XS
      WRITE (41,10)
   10  FORMAT ('TIME',15X,'RC',10X,'THETA',9X,'X',13X,'PHI',
     +   11X,'THDOT',9X,'RC/R0',10X,'X/XS',9X,'TEMP')
      WRITE (42,15)
   15  FORMAT ('TIME',12X,'RDOT',10X,'XDOT',10X,'PHDOT',24X,
     +   'RDIFF')
      WRITE (41,20)T,(Y(K),K=1,4),Y(6),RCRAT,XRAT,Y(9)
      20  FORMAT (9E14.8)
      WRITE (42,25)T,Y(5),Y(7),Y(8)
      25  FORMAT (4E14.8)
       NCOUNT=0
      TEND=0.0
       DTEND=0.2
         DO 50 K=1,4000
      TEND=TEND+DTEND
      CALL DVERK(N,FCN1,T,Y,TEND,TOL,IND,C,NW,W,IER)
      IF (IND.LT.0.OR.IER.GT.0) GO TO 30
      IF (Y(2) .LE. (2.0*PI)) NORB=0
      IF (Y(2) .GE. (2.0*PI)) NORB=1
      IF (Y(2) .GE. (4.0*PI)) NORB=2
      IF (Y(2) .GE. (6.0*PI)) NORB=3
      IF (Y(2) .GE. (8.0*PI)) NORB=4
      THETA1=(1.0+4.0*NORB)*PI/2.0
      THETA2=THETA1+PI
      IF (Y(2) .GT. THETA1 .AND. Y(2) .LT.THETA2) THEN
      CALL SHADOW (N,T,Y,TEND,RDIFF)
       DTEND=0.1
      ELSE
       NCOUNT=0
       DTEND=0.2
```

```
      END IF
      RCRAT=Y(1)/R0
      XRAT=Y(3)/XS
      WRITE (41,40)TEND,(Y(L),L=1,4),Y(6),RCRAT,XRAT,Y(9)
      40  FORMAT (9E14.8)
      IF (Y(2) .GT. THETA1 .AND. Y(2) .LT.THETA2) THEN
         WRITE (42,45)TEND,Y(5),Y(7),Y(8),RDIFF
     45  FORMAT (4E14.8,14X,E14.8)
      ELSE
        WRITE (42,48)TEND,Y(5),Y(7),Y(8)
      48  FORMAT (4E14.8)
      END IF
      50  CONTINUE
      STOP
      30  CONTINUE
      PRINT *,'IER = ',IER
      STOP
      END
C     ---------------------------------------------
C     ---        SUBROUTINES          --------
C     ------------------------------------------------
C         ****
      SUBROUTINE FCN1 (N,T,Y,YD)
       DIMENSION Y(N),YD(N)
       REAL IPRM
      COMMON XM,XM1,XM2,XMBAR,XMU,UGC,XE,XA,XS,XKA,RM,
     +  RE,TMPS,NDSOL,NDERT,NALBD,GS,ALBD,
     +   ABSOL,ABERT,ABALB,DERAD,EPSL,SIGMA,
     +  XASDE,XASRF,XMASS,SPHT,
     +  PI,IPRM,TPROP,NDELTA,NCOUNT,RDIFF1
      YD(1)=Y(5)
      YD(2)=Y(6)
      YD(3)=Y(7)
      YD(4)=Y(8)
      A=Y(1)**2.
      B=(Y(3)**2./XM**2.)
      CC=COS(Y(4))
      D=2.*(1./XM)*Y(1)*Y(3)*CC
      R1=(A+(XM2**2.)*B+D*XM2)**0.5
      R2=SQRT(A+(XM1**2.)*B-D*XM1)
      X1=(XM2/XM)*Y(3)
      X2=(XM1/XM)*Y(3)
      TMPEF=XA*TPROP*(Y(9)-TMPS)
      DUDX=XKA*(Y(3)-XS)-TMPEF
      E=(XM1*(Y(1)+X1*CC))/R1**3.
      F=(XM2*(Y(1)-X2*CC))/R2**3.
      YD(5)=(Y(1)*(Y(6))**2.)-(XMU/XM)*(E+F)
      G=SIN(Y(4))
      BH=XMU*((1./R2**3.)-(1./R1**3.))*G
      YD(6)=(-2.)*(Y(5)/Y(1))*Y(6)+(XMBAR/XM)*BH*(Y(3)/Y(1))
      BI=Y(6)+Y(8)
```

```
      BJ=(X1+Y(1)*CC)/(R1**3.)
      BK=(Y(1)*CC-X2)/(R2**3.)
      GRV=(UGC*XM1*XM2)/(Y(3)**2.)
      YD(7)=Y(3)*(BI**2.)-XMU*(BJ-BK)-(DUDX/XMBAR)-(GRV/XMBAR)
      BL=((XMBAR/XM)*(Y(3)/Y(1)))+(Y(1)/Y(3))
      YD(8)=2.*(Y(5)/Y(1))*Y(6)-2.*(Y(7)/Y(3))*BI-(BL*BH)
      CALL HEAT (N,T,Y,QIN,QOUT)
      YD(9)=(QIN-QOUT)/(XMASS*SPHT)
      RETURN
      END
C       ***********
C     ------------------------------------------ --------
C      SUBROUTINE TO DETERMINE EARTH SHADOW ENTRY AND EXIT
C     ------------------------------------------------------
C     ***********
       SUBROUTINE SHADOW (N,T,Y,TEND,RDIFF)
       DIMENSION Y(N)
       REAL IPRM
       COMMON XM,XM1,XM2,XMBAR,XMU,UGC,XE,XA,XS,XKA,RM,
+      RE,TMPS,NDSOL,NDERT,NALBD,GS,ALBD,
+      ABSOL,ABERT,ABALB,DERAD,EPSL,SIGMA,
+      XASDE,XASRF,XMASS,SPHT,
+      PI,IPRM,TPROP,NDELTA,NCOUNT,RDIFF1
       CSQ=(COS(Y(2)))**2
      SSQ=(SIN(IPRM))**2
      RSH=RE/SQRT(1-CSQ*SSQ)
      RDIFF=RSH-Y(1)
      IF (NCOUNT .EQ. 0) GO TO 300
       IF (RDIFF1 .GT. 0 .AND. RDIFF .LT. 0 .OR.
+          RDIFF1 .LT. 0 .AND. RDIFF .GT. 0) THEN
         NDELTA=ABS(NDELTA-1)
       PRINT *,'SHADOW ENTRY/EXIT AT ',Y(2),' (RAD)',' TIME= ',
+       TEND
       WRITE (42,*) 'SHADOW ENTRY/EXIT AT ',Y(2),' (RAD)',
+       ' TIME= ',TEND
        ELSE
       NDELTA=NDELTA
      END IF
     300  RDIFF1=RDIFF
       NCOUNT=NCOUNT+1
       RETURN
      END
C       ****
C       ____________________________ ------------------
C      SUBROUTINE TO DETERMINE HEAT IN AND HEAT OUT
C      ---------------------------------------------------
C      *****
       SUBROUTINE HEAT (N,T,Y,QIN,QOUT)
       DIMENSION Y(N)
       REAL IPRM
       INTEGER NROT
```

```
      COMMON XM,XM1,XM2,XMBAR,XMU,UGC,XE,XA,XS,XKA,RM,
+     RE,TMPS,NDSOL,NDERT,NALBD,GS,ALBD,
+     ABSOL,ABERT,ABALB,DERAD,EPSL,SIGMA,
+     XASDE,XASRF,XMASS,SPHT,
+     PI,IPRM,TPROP,NDELTA,NCOUNT,RDIFF1
C    **************
C     HEAT INPUT
C    ***************
C     ***
C     DIRECT SOLAR RADIATION HEAT INPUT (QDSOL):
C     ***
      Y4NEW=Y(4)
      IF (NDSOL .EQ. 1) THEN
      CBTS=SIN(IPRM)*SIN(Y(2)+Y4NEW)
      QDSOL=NDELTA*ABSOL*GS*XASDE*ABS(CBTS)
      ELSE
      QDSOL=0.0
      END IF
C     *****
C     VIEW FACTORS:
C     *****
      IF (Y4NEW .LT. 0.0) Y4NEW = -Y4NEW
      NROT=Y4NEW/(2*PI)
      Y4NEW=Y4NEW-NROT*(2*PI)
      IF (Y4NEW .GT. PI) Y4NEW=Y4NEW-PI
      GMMA=ASIN(RE/Y(1))
      BTR=ABS(Y4NEW-PI/2.0)
      XX=(PI/2.0) - GMMA
      IF (BTR .GE. 0.0 .AND. BTR .LE. XX) THEN
      FE1=(SIN(GMMA)**2)*(COS(BTR))
      FE2=0.0
      ELSE
      F1=1.0/(TAN(GMMA)*TAN(BTR))
      F2=COS(GMMA)/SIN(BTR)
      F3=SQRT((SIN(GMMA))**2-(COS(BTR))**2)
      PT1=(SIN(GMMA)**2)*COS(BTR)*ACOS(-F1)
      PT2=ACOS(F2)-COS(GMMA)*F3
      FE1=(PT1+PT2)/PI
      BTR=PI-BTR
      F1=1.0/(TAN(GMMA)*TAN(BTR))
      F2=COS(GMMA)/SIN(BTR)
      F3=SQRT((SIN(GMMA))**2-(COS(BTR))**2)
      PT1=(SIN(GMMA)**2)*COS(BTR)*ACOS(-F1)
      PT2=ACOS(F2)-COS(GMMA)*F3
      FE2=(PT1+PT2)/PI
      END IF
C     ***
      ASDE1=XASDE
      ASDE2=XASDE
C     ***
C     DIRECT EARTH RADIATION HEAT INPUT (QDERT):
```

```
C     ***
      IF (NDERT .EQ. 1) THEN
      ABERT1=ABERT
      ABERT2=ABERT
      QDERT=(ABERT1*FE1*ASDE1+ABERT2*FE2*ASDE2)*DERAD
      ELSE
      QDERT=0.0
      END IF
C     ***
C     EARTH'S ALBEDO RADIATION HEAT INPUT (QALBD):
C     ***
     IF (NALBD .EQ. 1) THEN
      ALBRAD=ALBD*GS
      ABALB1=ABALB
      ABALB2=ABALB
      CBETA=SIN(IPRM)*COS(Y(2))
      IF (CBETA .LT. 0.0) CBETA=0.0
      QALBD=(NDELTA)*(ABALB1*ASDE1*FE1+ABALB2*ASDE2*
+     FE2)*ALBRAD*CBETA
      ELSE
      QALBD=0.0
      END IF
C     **
C     TOTAL HEAT INPUT (QIN):
C     **
      QIN=QDSOL + QDERT +QALBD
C     **
C      ------------------------------------
C     *** HEAT OUTPUT ***
C      ----------------------------------------
      QOUT=EPSL*SIGMA*XASRF*Y(9)**4
      RETURN
      END
```

AD-A172 880 PARAMETRIC INVESTIGATION OF FACTORS INFLUENCING THE MECHANICAL BEHAVIOR O..(U) MASSACHUSETTS UNIV AMHERST DEPT OF CIVIL ENGINEERING W A NASH ET AL. 30 MAY 86 4/3

UNCLASSIFIED AFOSR-TR-86-0858 AFOSR-83-0025 F/G 22/2 NL

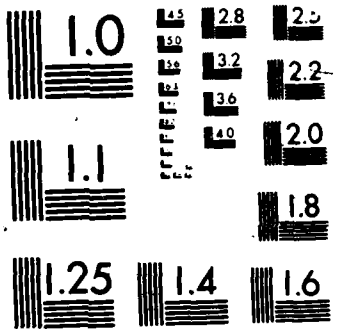
1.0
2.8
3.2
3.6
4.0
2.2
2.0
1.8
1.1
1.25
1.4
1.6

Sample Input Data

Tape 40

```
1.000000,5.000E+05,3.5316E+1,6.37433E+3,8.64432E-16
6.689496E+11,4.899E-3,1.0,290.000,24.34976E+06
6.5743300000E+3,0.000,1.0000230,0.00000000,290.000
0.0,8.8830000000E-02,0.0,0.00
6658.7678,52.75368
1353.0E+06,0.3
1.00,1.00,1.00,237.0E+06
1.00,5.670E-02
8.7518784E-04,1.75037568E-03
1.570796,1
1.0E-06
```

Sample Run Session

```
FORTRAN
 READY.
FINDLIB,IMSL
 READY.
X,LIBRARY,IMSL
 READY.
OLD,TEFF
 READY.
GET,TAPE40
 READY.
RUN

 ENTER CODE FOR DIRECT SOLAR, DIRECT EARTH,
 AND ALBEDO: 1=YES, 2=NO
? 1,1,1


     STOP


SRU        5.078 UNTS.

 RUN COMPLETE.
```

Sample Output Data

Tape 41

```
**TOTAL THERMAL EFFECTS**
UNITS ARE IN NEWTON, WATT, KILOMETER AND
MINUTES (ANGLE IN RADIAN, TEMP. IN KELVIN)
 M1= 500000. M2= 500000. M1/M2= 1.
 ACC.GRAV.= 35.316 RADIUS OF EARTH= 6374.33
 ELAST MOD= 6.689496E+11 X-AREA OF LINK= .00024495
 STIFFNESS= 143859204.52 REF LENGTH= 1.
 UNIVERSAL GRAV. CONST.= 8.64432E-16
GRAV. CONST.= 1.434942641423E+9REF. TEMP= 290.
 TOTAL MASS= 1000000. REDUCED MASS= 250000.
***
REF. TEMP.= 290.
SOLAR RADIATION CONSTANT= 1.353E+9
AVERAGE ALBEDO= .3
AVE. EARTH EMITTED RADIATION= 237000000.
ABSORPTANCE TO DIRECT SOLAR RADIATION= 1.
ABSORPTANCE TO ALBEDO RADIATION = 1.
ABSORPTANCE TO DIRECT EARTH RADIATION=  1.
EMITTANCE TO THERMAL RADIATION= 1.
STEFHAN-BOLTZMANN CONSTANT= .0567
***
SPECIFIC HEAT OF LINK-MATERIAL (CL)= 52.75368
THERMAL EXPANSION PROPERTY OF LINK-MATERIAL= 24349760.
TOTAL MASS OF LINK-STRUCTURE= 4458.7870
TOTAL AREA OF ONE SIDE OF LINK EFFECTIVE
   FOR THERMAL ABSORPTANCE= .0008751878 4
TOTAL SURFACE AREA EFFECTIVE FOR
   THERMAL EMITTANCE= .0017503756 8
***
INCLINATION OF SUN FROM NORMAL TO
   ORBIT PLANE= 1.570796 (RAD)
1.E-6
****
TIME          RC            THETA         X             PHI           THDOT         RC/RO         X/XS          TEMP
.00000000E+00 .65743300E+04 .00000000E+00 .10000230E+01 .00000000E+00 .88830000E-01 .10000000E+01 .10000230E+01 .29000000E+03
.20000000E+00 .65747035E+04 .17765327E-01 .10000183E+01 .59437069E-06 .88819907E-01 .10000568E+01 .10000183E+01 .28982829E+03
.40000000E+00 .65758239E+04 .35526618E-01 .10000175E+01 .54679686E-05 .88789645E-01 .10002272E+01 .10000175E+01 .28966925E+03
.60000000E+00 .65776904E+04 .53279844E-01 .10000146E+01 .18635835E-04 .88739260E-01 .10005111E+01 .10000146E+01 .28952250E+03
.80000000E+00 .65803022E+04 .71020986E-01 .10000067E+01 .44054675E-04 .88668832E-01 .10009084E+01 .10000067E+01 .28938801E+03
      :             :             :             :             :             :             :             :             :
.11240000E+03 .22276113E+05 .28502840E+01 .10006389E+01 .29823742E+01 .77372001E-02 .33883473E+01 .10006389E+01 .30755638E+03
.11250000E+03 .22282144E+05 .28510575E+01 .10006433E+01 .29860742E+01 .77330125E-02 .33892446E+01 .10006433E+01 .30745071E+03
.11260000E+03 .22288159E+05 .28518306E+01 .10006306E+01 .29897753E+01 .77288391E-02 .33901795E+01 .10006306E+01 .30734403E+03
.11270000E+03 .22294159E+05 .28526033E+01 .10006290E+01 .29934775E+01 .77246798E-02 .33910921E+01 .10006290E+01 .30709317E+03
.11280000E+03 .22300143E+05 .28533755E+01 .10006150E+01 .29971806E+01 .77205347E-02 .33920023E+01 .10006150E+01 .30684312E+03
.11290000E+03 .22306111E+05 .28541474E+01 .10006066E+01 .30008849E+01 .77164037E-02 .33929102E+01 .10006066E+01 .30659387E+03
      :             :             :             :             :             :             :             :             :
```

Sample Output Data (continued...)

Tape 42

```
**TOTAL THERMAL EFFECTS**
UNITS ARE IN NEWTON, WATT, KILOMETER AND
MINUTES (ANGLE IN RADIAN, TEMP. IN KELVIN)
 M1= 500000. M2= 500000. M1/M2= 1.
 ACC.GRAV.= 35.316 RADIUS OF EARTH= 6374.33
 ELAST MOD= 6.68949AE+11 X-AREA OF LINK= .00024495
 STIFFNESS= 163859204.52 REF LENGTH= 1.
 UNIVERSAL GRAV. CONST.= 8.44432E-16
GRAV. CONST.= 1.43496264142 3E+9REF. TEMP= 290.
 TOTAL MASS= 1000000. REDUCED MASS= 250000.
***
REF. TEMP.= 290.
SOLAR RADIATION CONSTANT= 1.353E+9
AVERAGE ALBEDO= .3
AVE. EARTH EMITTED RADIATION= 237000000.
ABSORPTANCE TO DIRECT SOLAR RADIATION= 1.
ABSORPTANCE TO ALBEDO RADIATION = 1.
ABSORPTANCE TO DIRECT EARTH RADIATION=  1.
EMITTANCE TO THERMAL RADIATION= 1.
STEPHAN-BOLTZMANN CONSTANT= .0567
***
SPECIFIC HEAT OF LINK-MATERIAL(AL)= 52.75368
THERMAL EXPANSION PROPERTY OF LINK-MATERIAL= 24349760.
TOTAL MASS OF LINK-STRUCTRE= 8838.7878
TOTAL AREA OF ONE SIDE OF LINK EFFECTIVE
   FOR THERMAL ABSORPTANCE= .00087518784
TOTAL SURFACE AREA EFFECTIVE FOR
   THERMAL EMITTANCE= .00175037568
***
INCLINATION OF SUN FROM NORMAL TO
   ORBIT PLANE= 1.570796 (RAD)
1.E-6
***
TIME            RDOT            XDOT            PHDOT                          RDIFF
 .00000000E+00 .00000000E+00 .00000000E+00 .00000000E+00
 .20000000E+00 .37349732E+01-.12129928E-03 .10935693E-04
 .40000000E+00 .74679195E+01-.13286782E-03 .41326405E-04
 .60000000E+00 .11196817E+02-.18179352E-04 .92184038E-04
 .80000000E+00 .14919851E+02 .87390236E-04 .16393459E-03
      :             :             :             :
 .11240000E+03 .40385227E+02 .36613371E-04 .36995390E-01              -.81835509E+02
 .11250000E+03 .40229430E+02-.50482039E-04 .37005210E-01              -.30455650E+02
 SHADOW ENTRY/EXIT AT 2.051830578427 (RAD) TIME= 112.5999999999
 .11260000E+03 .40073681E+02-.94081161E-04 .37016396E-01               .21219670E+02
 .11270000E+03 .39917980E+02-.31215428E-04 .37028444E-01               .73192539E+02
 .11280000E+03 .39762327E+02-.18842581E-03 .37037442E-01               .12546507E+03
      :             :             :             :
```

Computer Program III

Listing of Sample Program to Compute Equilibrium Temperature

```
      PROGRAM EQTMP (INPUT,OUTPUT,TAPE32,TAPE33)
C      ---------------------------------------------------
C     THIS PROGRAM COMPUTES EQUILIBRIUM TEMPERATURE (TMPEQ).
C     ---------------------------------------------------
      REAL IPRM
      PRINT *,'ENTER CODE FOR DIRECT SOLAR, DIRECT EARTH,'
      PRINT *,'AND ALBEDO: 1=YES, 2=NO'
      READ *,NDSOL,NDERT,NALBD
      PI=3.141592
      IPRM=PI/2.0
      READ (32,*)R0,TH0,PH0
      READ (32,*)RE,GS,ALBD
      READ (32,*)ABSOL,ABERT1,ABALB1,DERAD
      READ (32,*)ABERT2,ABALB2
      READ (32,*)EPSL1,EPSL2,SIGMA
      READ (32,*)DELTA
      READ (32,*)XASDE1,XASDE2,XASRF
C     ***
C     DIRECT SOLAR RADIATION HEAT INPUT (QDSOL):
C     ***
      IF (NDSOL .EQ. 1) THEN
      CBTS=SIN(IPRM)*SIN(TH0+PH0)
      QDSOL=DELTA*ABSOL*GS*XASDE1*ABS(CBTS)
      ELSE
      QDSOL=0.0
      END IF
      PRINT *,'DIR. SOL.= ',QDSOL
C     *****
C     VIEW FACTORS:
C     *****
      IF (PH0 .LT. 0.0) PH0=-PH0
      IF (PH0 .GT. 2.0*PI) PH0=PH0-2.0*PI
      IF (PH0 .GT. PI) PH0=PH0-PI
      GMMA=ASIN(RE/R0)
      BTR=ABS(PH0-PI/2.0)
      XX=(PI/2.0) - GMMA
      IF (BTR .GE. 0.0 .AND. BTR .LE. XX) THEN
      FE1=(SIN(GMMA)**2)*(COS(BTR))
      FE2=0.0
      PRINT *,'FE1= ',FE1,'FE2= ',FE2
      ELSE
      F1=1.0/(TAN(GMMA)*TAN(BTR))
      F2=COS(GMMA)/SIN(BTR)
```

```
      F3=SQRT((SIN(GMMA))**2-(COS(BTR))**2)
      PT1=(SIN(GMMA)**2)*COS(BTR)*ACOS(-F1)
      PT2=ACOS(F2)-COS(GMMA)*F3
      FE1=(PT1+PT2)/PI
      BTR=PI-BTR
      F1=1.0/(TAN(GMMA)*TAN(BTR))
      F2=COS(GMMA)/SIN(BTR)
      F3=SQRT((SIN(GMMA))**2-(COS(BTR))**2)
      PT1=(SIN(GMMA)**2)*COS(BTR)*ACOS(-F1)
      PT2=ACOS(F2)-COS(GMMA)*F3
      FE2=(PT1+PT2)/PI
      END IF
      PRINT *,'FE1= ',FE1,'FE2= ',FE2
C     *
      ASDE1=XASDE1
      ASDE2=XASDE2
C     ***
C     DIRECT EARTH RADIATION HEAT INPUT (QDERT):
C     ***
      IF (NDERT .EQ. 1) THEN
      QDERT=(ABERT1*FE1*ASDE1+ABERT2*FE2*ASDE2)*DERAD
      ELSE
      QDERT=0.0
      END IF
      PRINT *,'DIR. EARTH = ',QDERT
C     ***
C     EARTH'S ALBEDO RADIATION HEAT INPUT (QALBD):
C     ***
     IF (NALBD .EQ. 1) THEN
      ALBRAD=ALBD*GS
      CBETA=SIN(IPRM)*COS(TH0)
      IF (CBETA .LT. 0.0) CBETA=0.0
      QALBD=(DELTA)*(ABALB1*ASDE1*FE1+ABALB2*ASDE2*
+     FE2)*ALBRAD*CBETA
      ELSE
      QALBD=0.0
      END IF
      PRINT *,'ALBEDO HEAT= ',QALBD
C     **
C     TOTAL HEAT INPUT (QIN):
C     **
      QIN=QDSOL + QDERT +QALBD
      PRINT *,'HEAT INPUT= ',QIN
C     **
      TMPEQ=(QIN/((EPSL1)*SIGMA*XASRF))**0.25
      PRINT *,'EQUILIBRIUM TEMP (DEGREE KELVIN)= ',TMPEQ
      ALT=R0-RE
      PRINT *,'ALT= ',ALT,' THETA= ',TH0,' PHI= ',PH0
      END
```

Sample Input Data

Tape 32

```
6574.33,0.0,1.5707963
6374.33,1353.0E+06,0.3
1.00,1.00,1.00,237.0E+06
1.00,1.00
1.00,1.00,5.670E-02
1
8.7518784E-04,8.7518784E-04,1.750376E-03
```

Sample Run Session and Output Data

```
FORTRAN
 READY.
OLD,EQTEMP
 READY.
GET,TAPE32
 READY.
RUN

 ENTER CODE FOR DIRECT SOLAR, DIRECT EARTH,
 AND ALBEDO: 1=YES, 2=NO
? 1,1,1


 EQUILIBRIUM TEMP (DEGREE KELVIN)= 362.4644842124
 ALT= 200. THETA= 0. PHI= 1.5707963

SRU      0.816 UNTS.

 RUN COMPLETE.
```

Computer Program IV

Listing of Sample Program to Compute Combined Effects of Radiation Pressures and Differential Gravitational Forces

```
      PROGRAM PRSSEFF (INPUT,OUTPUT,TAPE50,TAPE51,TAPE52)
C- ---------------------------------------------
C  THIS PROGRAM COMPUTES R, THETA, X AND PHI
C    AND THEIR FIRST TIME DERIVATIVES
C  FOR AN AXIALLY FLEXIBLE DUMBBELL STRUCTURE
C  ORBITING IN SPACE WITH PLANAR MOTION
C   UNDER DIFF. GRAVITATIONAL FORCE AND
C   RADIATION PRESSURE EFFECTS.
C  SUN LIES IN THE ORBIT PLANE. STRUCTURAL SURFACE
C  IS ASSUMED TO BE COMPLETELY ABSORBING TO RACIATION.
C   NOTE: THIS PROGRAM COMPUTES DIRECT SOLAR EFFECTS
C         FOR A COMPLETELY ABSORBING SURFACE IN
C         AN ARBITRARY POSITION.
C          BUT, IT CAN COMPUTE DIRECT EARTH
C          AND ALBEDO EFFECTS ONLY FOR A
C         SPECIAL POSITION WHEN THE SPACE STRUCTURE
C         IS AT RIGHT ANGLE TO THE EARTH-STRUCTURE
C         LINE, THAT IS, PHI = 90 DEGREES. THIS
C         CONFIGURATION WILL EXPERIENCE MAXIMUM
C         EFFECTS DUE TO DIRECT EARTH AND ALBEDO
C         RADIATION.
C ---------------------------------------------
C
C    RAMESH B. MALLA          AUG.11, 1985
C   ---------------------------------------------
C
C   SIMULTANEOUS  NONLINEAR COUPLED DIFFERENTIAL
C  EQUATIONS ARE SOLVED BY NUMERICAL ANALYSIS USING
C    5TH AND 6TH. ORDER RUNGE-KUTTA-VERNER METHOD
C    (IMSL SUBROUTINE PACKAGE: DVERK)
C-  ---------------------------------------------
C
      DIMENSION Y(8)
       DIMENSION C(24),W(8,9)
      REAL IPRM
      COMMON XM,XM1,XM2,XMBAR,XMU,UGC,XE,XA,XS,XKA,RM,
     +  RE,NDSOL,NDERT,NALBD,
     +  ABSOL,ABERT,ABALB,
     +   XASDE,
     +   PI,IPRM,NDELTA,NCOUNT,RDIFF1,
     +  DSPRSS,DEPRSS,ALPRSS,
     +  Q1,Q2,Q3,Q4,XLVA
      EXTERNAL FCN1
C       ***
```

```
      PRINT *,'ENTER CODE FOR DIRECT SOLAR, DIRECT EARTH,'
      PRINT *,'AND ALBEDO: 1=YES, 2=NO'
      PRINT *,'ENTER "1" FOR DIRECT EARTH AND ALBEDO'
      PRINT *,'RADIATION, ONLY IF INVESTIGATING A'
      PRINT *,'SPECIAL CASE, PHI = 90 DEGREES.'
      PRINT *,'OTHETWISE, THESE VALUES MUST BE "2".'
      READ *,NDSOL,NDERT,NALBD
      WRITE (51,*) '    ***RADIATION PRESSURE EFFECTS***'
      WRITE (51,*) '    '
      WRITE (52,*) '    ***RADIATION PRESSURE EFFECTS***'
      WRITE (52,*) '    '
      IF (NDSOL .EQ. 1 .AND. NDERT .NE. 1 .AND. NALBD
     +   .NE. 1)THEN
      WRITE (51,*)'**DIRECT SOLAR EFFECT ONLY **'
      WRITE(52,*) '**DIRECT SOLAR EFFECT ONLY **'
      ELSE
      END IF
      IF (NDSOL .NE. 1 .AND. NDERT .EQ. 1 .AND. NALBD
     +   .NE. 1) THEN
      WRITE (51,*) '**DIRECT EARTH RADIATION EFFECT ONLY **'
      WRITE(52,*) '**DIRECT EARTH RADIATION EFFECT ONLY **'
      ELSE
      END IF
      IF (NDSOL .NE. 1 .AND. NDERT .NE. 1 .AND. NALBD
     +   .EQ. 1) THEN
      WRITE (51,*) '**ALBEDO EFFECT ONLY**'
      WRITE(52,*) '**ALBEDO EFFECT ONLY**'
      ELSE
      END IF
      IF (NDSOL .EQ. 1 .AND. NDERT .EQ. 1 .AND. NALBD
     +    .EQ. 1) THEN
         WRITE (51,*) '**TOTAL RADIATION PRESSURE EFFECTS**'
         WRITE(52,*) '**TOTAL RADIATION PRESSURE EFFECTS**'
      ELSE
      END IF
      IF (NDSOL .EQ. 1 .AND. NDERT .NE. 1 .AND. NALBD
     +       .EQ. 1) THEN
       WRITE (51,*) '***DIRECT SOLAR AND ALBEDO EFFECTS***'
       WRITE(52,*) '**DIRECT SOLAR AND ALBEDO EFFECTS**'
      ELSE
      END IF
       PI=3.141592
C      ***
      WRITE (51,*) 'UNITS ARE IN NEWTON, WATT, KILOMETER AND'
      WRITE (51,*)'MINUTES (ANGLE IN RADIAN, TEMP. IN KELVIN)'
      WRITE(52,*) 'UNITS ARE IN NEWTON, WATT, KILOMETER AND'
      WRITE(52,*)'MINUTES (ANGLE IN RADIAN, TEMP. IN KELVIN)'
      READ (50,*) RM,XM2,GE,RE,UGC
      READ (50,*) XE,XHT,XS
      READ (50,*) R0,TH0,X0,PH0
      READ (50,*) RDOT,THDOT,XDOT,PHDOT
```

```
      READ (50,*) ABSOL,ABERT,ABALB
      READ (50,*)XASDE
      READ (50,*) DSPRSS,DEPRSS,ALPRSS
      READ (50,*) IPRM,NDELTA
      READ (50,*)TOL
      XM1=RM*XM2
      XA=0.05*XS*XHT
      XKA=(XE*XA)/XS
      XMU=GE*(RE**2.)
      XM=XM1+XM2
      XMBAR=(XM1*XM2)/XM
C       ***
      WRITE (51,*)' M1= ',XM1,' M2= ',XM2,' M1/M2= ',RM
      WRITE (51,*)' ACC.GRAV.= ',GE,' RADIUS OF EARTH= ',RE
      WRITE (51,*)' ELAST MOD= ',XE,' X-AREA OF LINK= ',XA
      WRITE (51,*)' STIFFNESS= ',XKA,' REF LENGTH= ',XS
      WRITE (51,*)' UNIVERSAL GRAV. CONST.= ',UGC
      WRITE (51,*)'GRAV. CONST.= ',XMU
      WRITE (51,*)' TOTAL MASS= ',XM,' REDUCED MASS= ',XMBAR
      WRITE (51,*)'***'
      WRITE (51,*)'DIRECT SOLAR RADIATICN PRESSURE = ',DSPRSS
      WRITE (51,*)'DIRECT EARTH RADIATION PRESSURE AT'
      WRITE (51,*)'   THE SURFACE OF THE EARTH = ',DEPRSS
      WRITE (51,*)'ALBEDO RADIATION PRESSURE AT THE'
      WRITE (51,*)'   EARTH SURFACE = ',ALPRSS
      WRITE (51,*) 'ABSORPTANCE TO DIRECT SOLAR'
      WRITE (51,*) '   RADIATION= ',ABSOL
      WRITE (51,*) 'ABSORPTANCE TO DIRECT EARTH'
      WRITE (51,*) '  RADIATION= ',ABERT
      WRITE (51,*) 'ABSORPTANCE TO ALBEDO RADIATION= ',ABALB
      WRITE (51,*) 'TOTAL AREA OF ONE SIDE OF THE  STRUCRURE'
      WRITE (51,*) '   EFFECTIVE TO RADIATION PRESSURE = ',XASDE
      WRITE (51,*) '***'
      WRITE (51,*) 'INCLINATION OF SUN FROM NORMAL TO'
      WRITE (51,*) '   ORBIT PLANE= ',IPRM,' (RAD)'
      WRITE (51,*)TOL
      WRITE (51,*)'****'
      WRITE(52,*)' M1= ',XM1,' M2= ',XM2,' M1/M2= ',RM
      WRITE(52,*)' ACC.GRAV.= ',GE,' RADIUS OF EARTH= ',RE
      WRITE(52,*)' ELAST MOD= ',XE,' X-AREA OF LINK= ',XA
      WRITE(52,*)' STIFFNESS= ',XKA,' REF LENGTH= ',XS
      WRITE(52,*)' UNIVERSAL GRAV. CONST.= ',UGC
      WRITE(52,*)'GRAV. CONST.= ',XMU
      WRITE(52,*)' TOTAL MASS= ',XM,' REDUCED MASS= ',XMBAR
      WRITE(52,*)'***'
      WRITE(52,*) 'DIRECT SOLAR RADIATION PRESSURE= ',DSPRSS
      WRITE (52,*) 'DIRECT EARTH RADIATION PRESSURE AT THE '
      WRITE (52,*) '  EARTH SURFACE= ',DEPRSS
      WRITE (52,*) 'ALBEDO RADIATION PRESSURE AT THE'
      WRITE (52,*) '  EARTH SURFACE= ',ALPRSS
      WRITE(52,*) 'ABSORPTANCE TO DIRECT SOLAR RADIATION= ',ABSOL
```

```
      WRITE(52,*) 'ABSORPTANCE TO ALBEDO RADIATION = ',ABALB
      WRITE(52,*) 'ABSORPTANCE TO DIRECT EARTH RADIATION=  ',ABERT
      WRITE(52,*) '***'
      WRITE(52,*) 'TOTAL AREA OF ONE SIDE OF THE  STRUCTURE'
      WRITE(52,*) 'EFFECTIVE TO RADIATION PRESSURE= ',XASDE
      WRITE(52,*) '***'
      WRITE(52,*) 'INCLINATION OF SUN FROM NORMAL TO'
      WRITE(52,*) '   ORBIT PLANE= ',IPRM,' (RAD)'
      WRITE(52,*)TOL
      WRITE(52,*)'***'
      NW=8
      N=8
      T=0.0
      Y(1)=R0
      Y(2)=TH0
      Y(3)=X0
      Y(5)=RDOT
      Y(6)=THDOT
      Y(7)=XDOT
      IF (NDERT .EQ. 1 .OR. NALBD .EQ. 1) THEN
         Y(4)=1.5707963
       Y(8)=0.0
      ELSE
       Y(4)=PH0
      Y(8)=PHDOT
      END IF
      IND=1
C       ***
      RCRAT=Y(1)/R0
      XRAT=Y(3)/XS
      CALL RADFRC (N,T,Y,QR,QTH,QX,QPH)
      Q1=QR
      Q2=QTH
      Q3=QX
      Q4=QPH
      WRITE (51,10)
   10  FORMAT ('TIME',15X,'RC',10X,'THETA',10X,'X',13X,'PHI',
     +   11X,'THDOT',9X,'RC/R0',10X,'X/XS',12X,'L')
      WRITE(52,15)
   15  FORMAT ('TIME',12X,'RDOT',10X,'XDOT',10X,'PHDOT',13X,
     +    'QR',12X,'QTH',12X,'QX',12X,'QPH',12X,'RDIFF')
      WRITE (51,20)T,(Y(K),K=1,4),Y(6),RCRAT,XRAT,XLVA
      20  FORMAT (9E14.8)
      WRITE(52,25)T,Y(5),Y(7),Y(8),QR,QTH,QX,QPH
      25  FORMAT (8E14.8)
       NCOUNT=0
      TEND=0.0
       DTEND=0.2
         DO 50 K=1,4000
      TEND=TEND+DTEND
      CALL DVERK(N,FCN1,T,Y,TEND,TOL,IND,C,NW,W,IER)
```

```
      IF (IND.LT.0.OR.IER.GT.0) GO TO 30
      CALL RADFRC (N,T,Y,QR,QTH,QX,QPH)
      Q1=QR
      Q2=QTH
      Q3=QX
      Q4=QPH
      IF (Y(2) .LE. (2.0*PI)) NORB=0
      IF (Y(2) .GE. (2.0*PI)) NORB=1
      IF (Y(2) .GE. (4.0*PI)) NORB=2
      IF (Y(2) .GE. (6.0*PI)) NORB=3
      IF (Y(2) .GE. (8.0*PI)) NORB=4
      THETA1=(1.0+4.0*NORB)*PI/2.0
      THETA2=THETA1+PI
      IF (Y(2) .GT. THETA1 .AND. Y(2) .LT.THETA2) THEN
      CALL SHADOW (N,T,Y,TEND,RDIFF)
       DTEND=0.1
      ELSE
       NCOUNT=0
       DTEND=0.2
      END IF
      RCRAT=Y(1)/R0
      XRAT=Y(3)/XS
      WRITE (51,40)TEND,(Y(L),L=1,4),Y(6),RCRAT,XRAT,XLVA
      40  FORMAT (9E14.8)
      IF (Y(2) .GT. THETA1 .AND. Y(2) .LT.THETA2) THEN
      WRITE(52,45)TEND,Y(5),Y(7),Y(8),QR,QTH,QX,QPH,RDIFF
     45  FORMAT (9E14.8)
      ELSE
        WRITE(52,48)TEND,Y(5),Y(7),Y(8),QR,QTH,QX,QPH
      48  FORMAT (8E14.8)
      END IF
      50  CONTINUE
      STOP
      30  CONTINUE
      STOP
      END
C     ---------------------------------------------
C     ---         SUBROUTINES          --------
C     ------------------------------------------------
C
C      **********
C      ---------------------------------------------
C      SUBROUTINE  *FC1*
C      ---------------------------------------------
C      **********
      SUBROUTINE FCN1 (N,T,Y,YD)
       DIMENSION Y(N),YD(N)
       REAL IPRM
      COMMON XM,XM1,XM2,XMBAR,XMU,UGC,XE,XA,XS,XKA,RM,
     +  RE,NDSOL,NDERT,NALBD,
     +   ABSOL,ABERT,ABALB,
```

```
+    XASDE,
+    PI,IPRM,NDELTA,NCOUNT,RDIFF1,
+   DSPRSS,DEPRSS,ALPRSS,
+   Q1,Q2,Q3,Q4,XLVA
    YD(1)=Y(5)
    YD(2)=Y(6)
    YD(3)=Y(7)
    YD(4)=Y(8)
    QR=Q1
    QTH=Q2
    QX=Q3
    QPH=Q4
    A=Y(1)**2.
    B=(Y(3)**2./XM**2.)
    CC=COS(Y(4))
    D=2.*(1./XM)*Y(1)*Y(3)*CC
    R1=(A+(XM2**2.)*B+D*XM2)**0.5
    R2=SQRT(A+(XM1**2.)*B-D*XM1)
    X1=(XM2/XM)*Y(3)
    X2=(XM1/XM)*Y(3)
    DUDX=XKA*(Y(3)-XS)
    E=(XM1*(Y(1)+X1*CC))/R1**3.
    F=(XM2*(Y(1)-X2*CC))/R2**3.
    YD(5)=(Y(1)*(Y(6))**2.)-(XMU/XM)*(E+F)+(QR/XM)
    G=SIN(Y(4))
    BH=XMU*((1./R2**3.)-(1./R1**3.))*G
    YD(6)=(-2.)*(Y(5)/Y(1))*Y(6)+(XMBAR/XM)*BH*(Y(3)/Y(1))
+         +((QTH-QPH)/(XM*Y(1)**2))
    BI=Y(6)+Y(8)
    BJ=(X1+Y(1)*CC)/(R1**3.)
    BK=(Y(1)*CC-X2)/(R2**3.)
    GRV=(UGC*XM1*XM2)/(Y(3)**2.)
    YD(7)=Y(3)*(BI**2.)-XMU*(BJ-BK)-(DUDX/XMBAR)-(GRV/XMBAR)
+             +(QX/XMBAR)
    BL=((XMBAR/XM)*(Y(3)/Y(1)))+(Y(1)/Y(3))
    IF (NDERT .EQ. 1 .OR. NALBD .EQ.1 ) THEN
       YD(8)=0.0
    ELSE
    YD(8)=2.*(Y(5)/Y(1))*Y(6)-2.*(Y(7)/Y(3))*BI-(BL*BH)
+         +QPH/(XMBAR*(Y(3)**2))-(QTH-QPH)/(XM*(Y(1)**2))
    END IF
    RETURN
    END
C     ************
C    ------------------------------------------ --------
C     SUBROUTINE TO DETERMINE EARTH SHADOW ENTRY AND EXIT
C    ------------------------------------------------------
C    ************
      SUBROUTINE SHADOW (N,T,Y,TEND,RDIFF)
      DIMENSION Y(N)
      REAL IPRM
```

```
      COMMON XM,XM1,XM2,XMBAR,XMU,UGC,XE,XA,XS,XKA,RM,
+     RE,NDSOL,NDERT,NALBD,
+     ABSOL,ABERT,ABALB,
+     XASDE,
+     PI,IPRM,NDELTA,NCOUNT,RDIFF1,
+    DSPRSS,DEPRSS,ALPRSS,
+   Q1,Q2,Q3,Q4,XLVA
      CSQ=(COS(Y(2)))**2
     SSQ=(SIN(IPRM))**2
     RSH=RE/SQRT(1-CSQ*SSQ)
     RDIFF=RSH-Y(1)
     IF (NCOUNT .EQ. 0) GO TO 300
      IF (RDIFF1 .GT. 0 .AND. RDIFF .LT. 0 .OR.
+         RDIFF1 .LT. 0 .AND. RDIFF .GT. 0) THEN
        NDELTA=ABS(NDELTA-1)
    PRINT *,'SHADOW ENTRY/EXIT AT ',Y(2),' (RAD)',' TIME= ',TEND
     WRITE(52,*) 'SHADOW ENTRY/EXIT AT ',Y(2),' (RAD)',' TIME= ',TEND
       ELSE
      NDELTA=NDELTA
     END IF
    300  RDIFF1=RDIFF
      NCOUNT=NCOUNT+1
      RETURN
     END
C      ****
C      ---------------------------------------------
C     SUBROUTINE TO DETERMINE GENERALIZED FORCING
C     FUNCTIONS DUE TO RADIATION PRESSURE.
C     ------------------------------------------------
C     *****
      SUBROUTINE RADFRC (N,T,Y,QR,QTH,QX,QPH)
      DIMENSION Y(N)
      REAL IPRM
      COMMON XM,XM1,XM2,XMBAR,XMU,UGC,XE,XA,XS,XKA,RM,
+     RE,NDSOL,NDERT,NALBD,
+     ABSOL,ABERT,ABALB,
+     XASDE,
+     PI,IPRM,NDELTA,NCOUNT,RDIFF1,
+   DSPRSS,DEPRSS,ALPRSS,
+   Q1,Q2,Q3,Q4,XLVA
C    *************
    X1=(XM2/XM)*Y(3)
    X2=(XM1/XM)*Y(3)
    IF (XM1 .GE. XM2) XLVA=(Y(3)/2)-X2
    IF (XM1 .LE. XM2) XLVA=X1-(Y(3)/2)
    SQLVA=XLVA**2
    A=Y(1)**2
    CC=COS(Y(4))
    G=SIN(Y(4))
    RP=SQRT(A+SQLVA+2*Y(1)*XLVA*CC)
C    **********
```

```
C   GENERALIZED FORCES DUE TO DIRECT SOLAR RADIATION
C   **************
    IF (NDSOL .EQ. 1) THEN
    ETA=Y(2)+Y(4)
    CETA=COS(ETA)
    SETA=SIN(ETA)
    S1=CETA*SIN(IPRM)
    S2=-SETA*SIN(IPRM)
    S3=-COS(IPRM)
    S01=COS(Y(2))*SIN(IPRM)
    S02=-SIN(Y(2))*SIN(IPRM)
    S03=-COS(IPRM)
    CBTS=SETA*SIN(IPRM)
    DSFACT=NDELTA*DSPRSS*ABS(CBTS)*XASDE
    XLDS=Y(1)*SIN(Y(2))+XLVA*SETA
    FDS=DSFACT*SQRT(S1**2+S2**2)
C     ***
    DSQR=-DSFACT*S01
    DSQTH=XLDS*FDS
    DSQX=-DSFACT*S1
    DSQPH=-DSFACT*XLVA*S2
    ELSE
    DSQR=0.0
    DSQTH=0.0
    DSQX=0.0
    DSQPH=0.0
    END IF
C   ***************
C   GENERALIZED FORCES DUE TO DIRECT EARTH RADIATION
C   **************
    IF (NDERT .EQ. 1) THEN
    DEFACT=(DEPRSS)*XASDE
    DEQR=DEFACT*((RE/Y(1))**2)
    DEQTH=-DEQR*XLVA
    DEQX=0.0
    DEQPH=-DEQR*XLVA
    ELSE
    DEQR=0.0
    DEQTH=0.0
    DEQX=0.0
    DEQPH=0.0
    END IF
C   ***************
C   GENERALIZED FORCES DUE TO ALBEDO RADIATION
C   ***************
    IF (NALBD .EQ. 1) THEN
    CBETA=SIN(IPRM)*COS(Y(2))
    IF (CBETA .LT. 0.0) CBETA=0.0
    ALFACT=NDELTA*(ALPRSS)*XASDE
    ALQR=ALFACT*CBETA*((RE/Y(1))**2)
    ALQTH=-DEQR*XLVA
```

```
      ALQX=0.0
      ALQPH=-ALQR*XLVA
      ELSE
      ALQR=0.0
      ALQTH=0.0
      ALQX=0.0
      ALQPH=0.0
      END IF
C     ******************************
C      TOTAL GENERALIZED FORCES AND MOMENTS
C      ****************************************
      QR=DSQR+DEQR+ALQR
      QTH=DSQTH+DEQTH+ALQTH
      QX=DSQX+DEQX+ALQX
      QPH=DSQPH+DEQPH+ALQPH
C     ************************************
      RETURN
      END
```

Sample Input Data

Tape 50

```
1.000000,5.000E+05,3.5316E+1,6.37433E+3,8.64432E-16
6.689496E+11,4.899E-3,1.0
6.5743300000E+3,0.000,1.0000230,0.00000000
0.0,8.8830000000E-02,0.0,0.00
1.00,1.00,1.00
8.7518784E-04
4.66000,0.497950,1.206580
1.570796,1
1.0E-06
```

Sample Run Session

```
FORTRAN
 READY.
PRIMARY,PREFF
 READY.
FINDLIB,IMSL
 READY.
X,LIBRARY,IMSL
 READY.
GET,TAPE50
 READY.
RUN

 ENTER CODE FOR DIRECT SOLAR, DIRECT EARTH,
 AND ALBEDO: 1=YES, 2=NO
 ENTER '1' FOR DIRECT EARTH AND ALBEDO
 RADIATION, ONLY IF INVESTIGATING A
 SPECIAL CASE, PHI = 90 DEGREES.
 OTHETWISE, THESE VALUES MUST BE '2'.
? 1,2,2

    STOP

SRU       6.217 UNTS.

 RUN COMPLETE.
```

Sample Outpute Data

Tape 51

```
      ***RADIATION PRESSURE EFFECTS***
 **DIRECT SOLAR EFFECT ONLY **
 UNITS ARE IN NEWTON, WATT, KILOMETER AND
 MINUTES (ANGLE IN RADIAN, TEMP. IN KELVIN)
  M1= 500000. M2= 500000. M1/M2= 1.
  ACC.GRAV.= 35.316 RADIUS OF EARTH= 6374.33
  ELAST MOD= 6.489496E+11 X-AREA OF LINK= .00024495
  STIFFNESS= 163859204.52 REF LENGTH= 1.
  UNIVERSAL GRAV. CONST.= 8.64432E-16
 GRAV. CONST.= 1.434962441423E+9
  TOTAL MASS= 1000000. REDUCED MASS= 250000.
 ***
 ABSORPTANCE TO DIRECT SOLAR
    RADIATION= 1.
 ABSORPTANCE TO DIRECT EARTH
   RADIATION= 1.
 ABSORPTANCE TO ALBEDO RADIATION= 1.
 TOTAL AREA OF ONE SIDE OF THE  STRUCRURE
    EFFECTIVE TO RADIATION PRESSURE = .00007518784
 ***
 INCLINATION OF SUN FROM NORMAL TO
    ORBIT PLANE= 1.570796 (RAD)
 1.E-6
 ****
TIME          RC            THETA         X             PHI           THDOT         RC/RO         X/XS          L
.00000000E+00 .65743300E+04 .00000000E+00 .10000230E+01 .00000000E+00 .88830000E-01 .10000000E+01 .10000230E+01 .00000000E+00
.20000000E+00 .65747035E+04 .17745327E-01 .10000257E+01 .48450057E-06 .88819907E-01 .10000568E+01 .10000257E+01 .00000000E+00
.40000000E+00 .65758239E+04 .35526618E-01 .10000305E+01 .50428107E-05 .88789645E-01 .10002272E+01 .10000305E+01 .00000000E+00
.60000000E+00 .65774904E+04 .53279844E-01 .10000314E+01 .17488938E-04 .88739260E-01 .10005111E+01 .10000316E+01 .00000000E+00
      :             :             :             :             :             :             :             :             :
.11230000E+03 .22270067E+05 .28495100E+01 .10000059E+01 .29872129E+01 .77414020E-02 .33874276E+01 .10000059E+01 .00000000E+00
.11240000E+03 .22276113E+05 .28502040E+01 .99999932E+00 .29909240E+01 .77372001E-02 .33883473E+01 .99999932E+00 .00000000E+00
.11250000E+03 .22282144E+05 .28510575E+01 .10000079E+01 .29946361E+01 .77330125E-02 .33892646E+01 .10000079E+01 .00000000E+00
.11260000E+03 .22288159E+05 .28518306E+01 .10000002E+01 .29983491E+01 .77288391E-02 .33901795E+01 .10000002E+01 .00000000E+00
.11270000E+03 .22294159E+05 .28526033E+01 .10000045E+01 .30020632E+01 .77246798E-02 .33910921E+01 .10000045E+01 .00000000E+00
.11280000E+03 .22300143E+05 .28533755E+01 .10000050E+01 .30057781E+01 .77205347E-02 .33920023E+01 .10000050E+01 .00000000E+00
.11290000E+03 .22306111E+05 .28541474E+01 .99999986E+00 .30094940E+01 .77164037E-02 .33929102E+01 .99999986E+00 .00000000E+00
      :             :             :             :             :             :             :             :             :
.29970000E+03 .68064164E+04 .57760108E+01 .99999930E+00 .77295318E+01 .80761045E-01 .10474705E+01 .99999930E+00 .00000000E+00
.29990000E+03 .68662913E+04 .57922500E+01 .99999430E+00 .77218729E+01 .81436333E-01 .10444093E+01 .99999430E+00 .00000000E+00
.30010000E+03 .68467703E+04 .58085847E+01 .99999180E+00 .77140506E+01 .81901367E-01 .10414400E+01 .99999180E+00 .00000000E+00
.30030000E+03 .68278618E+04 .58250106E+01 .99999473E+00 .77060621E+01 .82355615E-01 .10385639E+01 .99999473E+00 .00000000E+00
.30050000E+03 .68095745E+04 .58415262E+01 .99999951E+00 .76979051E+01 .82798545E-01 .10357823E+01 .99999951E+00 .00000000E+00
.30070000E+03 .67919168E+04 .58581292E+01 .10000003E+01 .76895770E+01 .83229628E-01 .10330964E+01 .10000003E+01 .00000000E+00
      :             :             :             :             :             :             :             :             :
```

Sample Output Data (continued ...)

Tape 52

```
    ***RADIATION PRESSURE EFFECTS***
**DIRECT SOLAR EFFECT ONLY **
UNITS ARE IN NEWTON, WATT, KILOMETER AND
MINUTES (ANGLE IN RADIAN, TEMP. IN KELVIN)
 M1= 500000. M2= 500000. M1/M2= 1.
 ACC.GRAV.= 35.314 RADIUS OF EARTH= 6374.33
 ELAST MOD= 6.489496E+11 X-AREA OF LINK= .00024495
 STIFFNESS= 163859204.52 REF LENGTH= 1.
 UNIVERSAL GRAV. CONST.= 0.644332E-16
GRAV. CONST.= 1.43496244423E+9
 TOTAL MASS= 1000000. REDUCED MASS= 250000.
***
DIRECT SOLAR RADIATION PRESSURE= 4.66
DIRECT EARTH RADIATION PRESSURE AT THE
  EARTH SURFACE= .49795
ALBEDO RADIATION PRESSURE AT THE
  EARTH SURFACE= 1.20650
ABSORPTANCE TO DIRECT SOLAR RADIATION= 1.
ABSORPTANCE TO ALBEDO RADIATION = 1.
ABSORPTANCE TO DIRECT EARTH RADIATION=  1.
***
TOTAL AREA OF ONE SIDE OF THE  STRUCTURE
EFFECTIVE TO RADIATION PRESSURE= .00067518784
***
INCLINATION OF SUN FROM NORMAL TO
   ORBIT PLANE= 1.570796 (RAD)
1.E-6
***
TIME          RDOT          XDOT          PHDOT         QR            QTH           QX            QPH           RDIFF
.00000000E+00 .00000000E+00 .00000000E+00 .00000000E+00 .00000000E+00 .00000000E+00 .00000000E+00 .00000000E+00
.20000000E+00 .37349732E+01-.10453427E-03 .96173460E-05-.72440412E-04 .84620377E-02-.72440411E-04 .00000000E+00
.40000000E+00 .74679195E+01-.83249480E-04 .39019136E-04-.14478954E-03 .33839504E-01-.14478951E-03 .00000000E+00
      :             :             :             :             :             :             :             :
.11230000E+03 .60541073E+02-.96500834E-04 .37105442E-01 .14863473E-02 .11292277E+02-.15083422E-02 .00000000E+00-.13292199E+03
.11240000E+03 .60385228E+02 .45938339E-04 .37116107E-01 .14709380E-02 .11160597E+02-.15768071E-02 .00000000E+00-.81835526E+02
.11250000E+03 .60229431E+02 .19757507E-04 .37125233E-01 .14554661E-02 .11029154E+02-.15451437E-02 .00000000E+00-.30455467E+02
SHADOW ENTRY/EXIT AT 2.051830578436 (RAD) TIME= 112.5999999999
.11260000E+03 .60073681E+02-.78918953E-04 .37135465E-01 .14399496E-02 .10897952E+02-.15533529E-02 .00000000E+00 .21219453E+02
.11270000E+03 .59917981E+02 .11221422E-03 .37144856E-01 .00000000E+00 .00000000E+00 .00000000E+00 .00000000E+00 .73192522E+02
      :             :             :             :             :             :             :             :
.29970000E+03-.10212065E+03 .89347380E-04-.37889980E-01-.28771955E-02-.11009504E+02-.19435065E-02 .00000000E+00
.29990000E+03-.99122681E+02 .10270391E-03-.38700793E-01-.29208945E-02-.10721547E+02-.19326265E-02 .00000000E+00
.30010000E+03-.96080979E+02-.78221747E-05-.39524451E-01-.29639188E-02-.10426017E+02-.19212723E-02 .00000000E+00
.30030000E+03-.92976307E+02-.10942995E-03-.40361200E-01-.30062102E-02-.10122982E+02-.19094675E-02 .00000000E+00
      :             :             :             :             :             :             :             :
```

APPENDIX F

GLOSSARY OF TERMS USED IN COMPUTER PROGRAMS

The following is a glossary showing the correpondence between the variables in the computer programs and those used in the theoretical analysis.

Notations Used in Computer Programs	Corresponding Natations in Analysis
ABALB	a_r
ABALB1	a_{r1}
ABALB2	a_{r2}
ABERT	a_e
ABERT1	a_{e1}
ABERT2	a_{e2}
ABSOL	a_s
ALBD	A_r
ALPRSS	P_{alb}
ALQR	$(Q_r)_{alb}$
ALQTH	$(Q_\theta)_{alb}$
ALQX	$(Q_x)_{alb}$
ALQPH	$(Q_\phi)_{alb}$
BTR	β_r

CBETA	$\cos\beta$
CBTS	$\cos\beta_s$
DEPRSS	p_{de}
DEQR	$(Q_r)_{de}$
DEQTH	$(Q_\theta)_{de}$
DEQX	$(Q_x)_{de}$
DEQPH	$(Q_\phi)_{de}$
DERAD	E_e
DGF	ΔF_g
DSPRSS	p_{ds}
DSQR	$(Q_r)_{ds}$
DSQTH	$(Q_\theta)_{ds}$
DSQX	$(Q_x)_{ds}$
DSQPH	$(Q_\phi)_{ds}$
DUDX	dU_e/dx
EPSL	ϵ
ETA	η
FE1	F_{e1}
FE2	F_{e2}
GE	g
GMMA	γ
GRV	V_m
GS	G_s
IGF	F_{g0}
IPRM	i'
NDELTA	δ

PHDOT	$\dot{\phi}_0$; $\dot{\phi}$
PHO	ϕ_0
QALBD	$\dot{q}_r$
QDERT	$\dot{q}_e$
QDSOL	$\dot{q}_s$
QIN	$\dot{q}_{in}$
QOUT	$\dot{q}_{out}$
QR	Q_r
QTH	Q_θ
QX	Q_x
QPH	Q_ϕ
UGC	G
RDOT	$\dot{r}_0$; $\dot{r}_c$
RC	r_c
RDIFF	$(r_{sb} - r_c)$
RE	R
RM	m_1/m_2
RP	r_p
RO	r_0
RSH	r_{sb}
R1	r_1
R10	r_{10}
R2	r_2
R20	r_{20}
SIGMA	σ
SPHT	c

S1	S_1
S2	S_2
S3	S_3
SO1	S_{O1}
SO2	S_{O2}
SO3	S_{O3}
T; TIME	t
TGF	F_g
THDOT	$\dot{\theta}_O$; $\dot{\theta}$
THO	θ_O
TMPO	T_O
TMPS	T_s
TPROP	E_α
X	x
XA	A_{cs}
XASDE	A_{sd}
XASD1	A_{sd1}
XASD2	A_{sd2}
XASRF	A_{sf}
XDOT	$\dot{x}_O$; $\dot{x}$
XE	E
XHT	h
XKA	K_a
XLVA; L	l_p
XM	m
XMASS	M

XM1	m_1
XM2	m_2
XMBAR	$\bar{m}$
XMU	μ
XS	x_s
XO	x_o
X1	x_1
X2	x_2
Y(1)	r_c
Y(2); THETA	θ
Y(3)	x
Y(4)	ϕ
Y(5)	$\dot{r}_c$
Y(6)	$\dot{\theta}$
Y(7)	$\dot{x}$
Y(8)	$\dot{\phi}$
Y(9)	T
YD(5)	$\ddot{r}_c$
YD(6)	$\ddot{\theta}$
YD(7)	$\ddot{x}$
YD(8)	$\ddot{\phi}$
YD(9)	$\dot{T}$

APPENDIX II

Finite Deformations, Thermal Stresses and Inflation Instability of Axisymmetric Membrane Structures

LIST OF SYMBOLS

(r,z)	Coordinates of a point on undeformed axisymmetric membrane
(ρ,η)	Coordinates of the point (r,z) on the deformed membrane
ds	Length of an undeformed element in meridional direction
dS	Length of the element on the deformed membrane in meridional direction
λ_1	Principal stretch ratio in the meridional direction
λ_2	Principal stretch ratio in the circumferential direction
λ_3	Principal stretch ratio in the normal to the deformed middle surface
S_0	Generating curve of an undeformed membrane
S_1	Curve corresponding to S_0 on the deformed membrane
N_1	Principal stress resultant in the meridional direction
N_2	Principal stress resultant in the circumferential direction
K_1	Principal curvature in the meridional direction
K_2	Principal curvature in the circumferential direction
R_1	Radius of curvature in the meridional direction
R_2	Radius of curvature in the circumferential direction
p	Internal pressure in the outward normal direction
p_α	$=pr/(2h_0C_1)$
F	Axial force

LIST OF SYMBOLS (continued)

F_α	$=F/(4\pi h_0 r C_1)$
ϕ	Angle between the ρ axis and the tangent to the meridian on the deformed membrane
W	$=W(I_1,I_2,T)$. Strain energy function per unit undeformed volume
w	$=w(\lambda_1,\lambda_2,T)$. Strain energy function per unit volume
I_1	First invariant of total extension
I_2	Second invariant of total extension
h_0	Thickness of the undeformed membrane
C_1,C_2	Mooney material constants
R_c	Gas constant
ρ_c	Density of the membrane
M_c	Number average molar mass of the chain length
T_0	Initial temperature of the membrane
T	Final temperature of the membrane
u,v,ω	Basic dependent variables for generally axisymmetric membranes
U	Internal energy of the membrane
W	Work done on the membrane by external forces
Q	Value of the heat supplied to the membrane
S	Entropy
A	Helmholtz free energy
α	Thermal expansion coefficient of the membrane

LIST OF SYMBOLS (continued)

α_c	Thermal expansion coefficient of the cord
*	represents the state of free stress
-	represents the isothermal processes
Λ_1, Λ_2	Stretch ratios of the deformed membrane in the centre plane
z_α	$=z/r$
$\bar{\rho}$	Radius of the deformed membrane in the center plane
$\bar{\rho}_\alpha$	$=\bar{\rho}/r=\Lambda_2$
ρ_α	$=\rho/r=\lambda_2$
η_α	$=\eta/r=\lambda_2$
$N_{1\alpha}$	$N_1/(2h_0C_1)$. Dimensionless stress resultant in the meridional direction
$N_{2\alpha}$	$N_2/(2h_0C_1)$. Dimensionless stress resultant in the circumferential direction
Γ	C_2/C_1. Ratio of the Mooney material constants
L_0	A half of length of the undeformed membrane
L	A half of length of the deformed membrane
$L_{0\alpha}$	L_0/r. Dimensionless length of the undeformed membrane
L_α	L/r. Dimensionless length of the deformed membrane
τ_1, τ_2	Lagrange multipliers
p_{cr}	Critical pressure

LIST OF SYMBOLS (continued)

Γ_{cr} Critical material constant

CHAPTER I

INTRODUCTION

The problem of investigating large deformations of very thin, flexible structures began to assume importance nearly two decades ago when small pneumatic structures were constructed for civil [54] as well as military use [2], and when space inflatable structures [2] [34] were deployed. Usually these structures were designed to act as coverings over some area on the ground, or as space vehicles and their components, such as communication satellites. They were constructed of light weight, flexible membranes, and combine the inherent strength and reliability of material used in tension with the structural efficiency of the shell. In space science, flexible structures have special importance. No other type of structure can provide the light weight and compactness required for launching into space and the speed and ease of erection as a pneumatic structure. Recently, serious attention has been given to the development of design criteria for large space structures. The possible deployment of very large space structures having characteristic lengths of several kilometers [26] gives rise to a number of new and significant problems.

Large space structures will be deployed in a complex space environment. The deformations and the stresses of the structures will be influenced by various physical factors. They will be exposed to a wide variety of temperature varying from $-105^{\circ}C$ to $121^{\circ}C$ [2] during

orbit. Thermal deformations, thermal stresses, thermal vibrations as well as thermally induced instability may occur. Since the external pressure is approximately zero, the instability caused by internal pressure may be a significant problem. In addition, there are various environmental factors, such as radiation pressure, loading due to high energy electrons and protons, and the albedo effects, etc. Among these factors, the effects of the change of temperature and the difference between internal and external pressure on the structures are the most essential. Under some conditions, there is no doubt that an inflated membrane structure can be used as a substructure or element of a large truss-like space structure. Therefore, the investigation of mechanical and thermal properties of flexible membrane structures is one of the significant problems for large space structures. In most of the early works on flexible structures, the analysis and design criteria were based on simplified linear small deflection theories. Obviously, these are not suitable for large space structures in complex space environments. We must develop a theory of nonlinear membrane behavior with the effects of both mechanical and thermal loadings.

Thin membrane shell theory has a long history [29]. The theory of large deformations of nonlinear elastic membranes was presented systematically by Adkins and Rivlin [1], Green and Zerna [14], and Green and Adkins [15] after the Second World War. During the past thirty years, considerable progress in development of the theory has been made [See 5, 28, 38, 40]. So far the nonlinear membrane theory has been

successfully applied to a number of problems (For example, [8, 9, 16, 18, 21-23, 25, 30, 35, 41, 45, 46, 49, 53, 56]). Because of the nonlinearity of the equations involved, the application of the theory to particular problems is in general very difficult. Fortunately, the solvable problems in which there is a high degree of symmetry are often very important in practice.

Particular attention has been paid to axisymmetric membranes due to their importance in various membrane structures, and they have been studied by many authors (see [9, 14, 15, 21, 35, 49, 53], for example). In the early works, the problem was formulated in terms of eight coupled equations for the determination of eight unknowns and the solutions were obtained numerically. For such a large system of equations, the choice of boundary conditions and constants of integration is often very complicated and computation is often quite tedious. In order to simplify the equations and the computation, two different approaches were developed. Yang and Feng [53] reduced the number of equations by means of a proper choice of variables. The governing equations were simplified to a set of three first order ordinary differential equations. In the other side, Wu [49], Kydoniefs and Spencer [21], and Kydoniefs [22] reduced the governing equations to a set of quadratures in terms of the existence of a first integral for the special case in which either the undeformed or deformed profile is a circular cylinder. Both ways are efficient for the simplification of the problem. Essentially, each of them is a method for the reduction of order of the

system of differential equations. All of the investigations on deformations, stresses and stability of nonlinear membranes mentioned above have been concerned only with mechanical loadings with no consideration of thermal effect.

The purpose of our work is to develop the theory of nonlinear axisymmetric membranes with changes of temperature. The emphasis is on the effect of the thermal factor on constitutive relations, deformations, stresses and stability of axisymmetric membranes. The basic goal of the theory of axisymmetric membranes is to determine finite deformations and thermal stresses. The best method of achieving the goal is the one involving a minimum number of differential equations with a minimum number of variables and choosing the boundary conditions and parameters with ease.

In this dissertation, first we present a suitable mathematical model of nonlinear axisymmetric membranes based on the theory of axisymmetric membranes and thermodynamics. Then the problem of finite deformations and thermal stresses of axisymmetric membranes with some additional conditions is reformulated by taking advantages of the two methods mentioned above. Under constant pressure the governing equations have been simplified to a set of two first order ordinary differential equations with explicit derivatives. The important class of problems in which the undeformed profile is a circular cylinder may be characterized by a first order ordinary differential equation. Since the number of equations and variables is reduced to the minimum

possible, the problem is greatly simplified and the method is convenient for application to engineering problems. In order to investigate inflated instability analytically, we have presented an efficient approximate procedure. Although the procedure is demonstrated by the case of an initially circular cylinder as an example, it can be applied to a wide range of problems.

Mathematical models of axisymmetric membranes under mechanical and thermal loadings are given in Chapter 2. In section 2.1 the theory of nonlinear membranes in isothermal processes is reviewed briefly. The detailed analysis of the thermodynamic processes of deformations of nonlinear membranes is discussed in section 2.2. Based on sections 2.1, 2.2, the mathematical model of general axisymmetric membranes is derived in section 2.3. For the special cases of constant pressure and an initially circular cylinder with constant pressure, simplified mathematical models are developed in section 2.4. The application of the mathematical models to a particular structure is given in Chapter III. We discuss the boundary value problem of an initially circular cylindrical membrane reinforced by flexible cords at both ends first. The numerical results on the deformations, the thermal stress resultants, and inflated instability are represented in section 3.2, 3.3, and 3.4 respectively. Finally, in section 3.5 and 3.6, we have developed an efficient approximate procedure with application to instability.

CHAPTER II

FORMULATIONS

Classical membrane theory has been widely used as a first approximation in the analysis of membranes and shells, and in various analogue to solve other problems, for example the torsion problem in classical elasticity. Currently there are many important problems involving membranes. They include inflatable structures, fluid containers, weather balloons, communication satellites, oil slick containment apparatus, and many problems in biological engineering. In many of these there is symmetry with regard to one or two coordinates and the problems may be solved exactly for a general material. Axisymmetric behavior of membranes is one of the important and practical problems.

In this dissertation, we investigate finite deformations, thermal stresses, and instability of the inflated axisymmetric membrane. In particular, the influence of change of temperature is considered.

For simplification the following assumptions are made in this dissertation:

(1) The undeformed and deformed profiles of the membranes are axisymmetric. The axis of symmetry before deformation coincides with that after deformations. Also the loadings are axisymmetric about the axis.

(2) The membranes are composed of an incompressible, homogeneous, isotropic, elastic material with very thin uniform thickness h_0 before deformation. This assumption enables us to use membrane theory and ensures that the strain energy function of the system exists.

(3) The temperature of the entire system is uniform at any moment and varies slowly with time. The thermodynamic processes can be assumed to be reversible.

2.1 GENERAL MEMBRANE THEORY

In this section we derive equations for nonlinear axisymmetric membranes under a uniform internal pressure and an axial force.

We assume the undeformed and the deformed profiles are generated by revolution of plane curves S_0 and S_1 through an angle 2π about an axis Z respectively. The geometry of an axisymmetric membrane can be described by polar coordinates. We suppose that (r,z) is any point of the middle surface of the undeformed membrane , ds is arc length measured along the meridian through the point, and the undeformed configuration of the membrane is given as

$$z = z(r) \tag{2.1}$$

After deformation the point (r,z) is displaced to a new position (ρ,η). The corresponding arc length measured along the corresponding meridian in the deformed membrane is denoted by dS. The situation in the undeformed and deformed membrane is illustrated in Figure 1.

From the symmetry of the system it follows that the principal directions of strain coincide with the meridian, the line of latitude and the normal to the deformed middle surface. The principal stretch ratios in the those principal directions are denoted by λ_1, λ_2 and λ_3 respectively. If we choose r as a single independent variable, ρ, η, λ_1, λ_2 and λ_3 may be regarded as functions of r. We then have

$$\lambda_1 = \frac{dS}{ds} = \left(\frac{\rho'^2+\eta'^2}{1+z'^2} \right)^{1/2} \tag{2.2.1}$$

$$\lambda_2 = \rho \ / \ r \tag{2.2.2}$$

$$\lambda_3 = 1 \ / \ \lambda_1\lambda_2 \tag{2.2.3}$$

where the primes denote differentiation with respect to the independent variable r. Equation (2.2.3) comes from the incompressible assumption. Henceforth we shall use the subscript $_1$ and $_2$ to denote the meridional and circumferential directions of the deformed membrane, respectively.

The equilibrium equations in the meridian-tangential and the normal directions of the deformed membrane are

$$\frac{dN_1}{d\rho} + \frac{1}{\rho}(N_1-N_2) = 0 \tag{2.3.1}$$

$$K_1N_1 + K_2N_2 = p \tag{2.3.2}$$

where N_1,N_2 are the stress resultants with dimensions of force per unit edge length of the membrane; K_1, K_2 are the principal curvatures; and P is the internal pressure in the outward normal direction of the membrane.

The principal curvatures and the geometric relation of the deformed surface can be written in the form

$$K_1 = d(\sin\phi)/d\rho \tag{2.4.1}$$

$$K_2 = \sin\phi/\rho \tag{2.4.2}$$

$$tg\phi = \frac{\eta'}{\rho'} \tag{2.4.3}$$

where ϕ is the angle from the ρ axis to the tangent to the meridian.

The principal stress resultants per unit length of the deformed surface are

$$N_1 = N_1(\lambda_1,\lambda_2) \tag{2.5.1}$$

$$N_2 = N_2(\lambda_1,\lambda_2) \tag{2.5.2}$$

where functions N_1 and N_2 depend on the strain energy function of the material under consideration.

For an incompressible material, the third strain invariant $I_3=1$. The strain energy density function W is a function of the strain invariants I_1, I_2 and temperature T

$$W = W(I_1,I_2,T) \tag{2.6}$$

where I_1, I_2 are given by

$$I_1 = \lambda_1^2 + \lambda_2^2 + \frac{1}{\lambda_1^2\lambda_2^2} \tag{2.7.1}$$

$$I_2 = \lambda_1^2\lambda_2^2 + \frac{1}{\lambda_1^2} + \frac{1}{\lambda_2^2} \tag{2.7.2}$$

In isothermal processes the stress-strain relations [47] are given by

$$N_1 = 2h_0\left(\frac{\lambda_1}{\lambda_2} - \frac{1}{\lambda_1^3\lambda_2^3} \right) \left(\frac{\partial W}{\partial I_1} + \lambda_2^2 \frac{\partial W}{\partial I_2} \right) \tag{2.8.1}$$

$$N_2 = 2h_0\left(\frac{\lambda_2}{\lambda_1} - \frac{1}{\lambda_1^3\lambda_2^3} \right) \left(\frac{\partial W}{\partial I_1} + \lambda_1^2 \frac{\partial W}{\partial I_2} \right) \tag{2.8.2}$$

For many rubber-like materials a strain energy density function of wide application is the Mooney form [27] which is given by

$$W = C_1(I_1-3)+C_2(I_2-3) \tag{2.9}$$

where C_1, C_2 are material constants with the dimension of stress.

From the Gaussian statistical theory of the cross-linked network [43], we have

$$C_1 = R_c\rho_c T/2M_c \tag{2.10}$$

where R_c, ρ_c, M_c represent the gas constant, density of the membrane and the number average molar mass of the chain lengths respectively.

According to experiment [20], it was found that C_1 increased approximately in proportion to the absolute temperature, in accordance with the statistical theory, while C_2 was substantially independent of temperature.

Thus we have nine equations (2.2-2.4) and (2.8) for the nine unknowns λ_1, λ_2, N_1, N_2, ρ, η, K_1, K_2 and ϕ. The system of equations can be solved by various numerical procedures. Obviously for such a

large system of equations the process of computation is often quite tedious and is not economical.

One method for simplification is to make the system of equations be partially uncoupled, i.e. the system of equations is divided into several small systems of equations independent of each other. The general solutions are obtained by means of solving each small subsystem of equations respectively.

Let us analyse the system of equations which includes ordinary differential equations and algebraic equations. From equation (2.4) it follows that

$$\sin\phi = \Phi(\rho', \eta')$$

$$K_1 = K_1(\rho'', \eta'', \rho', \eta')$$

$$K_2 = K_2(\rho', \eta')$$

By substitution of above functions, equations (2.1) and equations (2.5) into equations (2.3), we can make out that each of equation (2.3.1) and equation (2.3.2) is a second order ordinary differential equation with regard to variables ρ, η. Therefore, if we choose ρ, η as basic functions, the system of equations is equivalent to a fourth order ordinary differential equation involving ρ, η. Alternatively, if λ_1, λ_2 can be chosen as the basic functions. Since λ_1 is a function of ρ', η', the system of equations is equivalent to a third order ordinary differential equation after uncoupling.

For the reason, Yang and Feng [53] have simplified the governing equations to a set of three first order ordinary differential equations with explicit derivatives either in terms of λ_1, λ_2 or in terms of the three new variables u, v, ω defined as follows:

$$u(r) = (\rho'^2+\eta'^2)^{1/2} \tag{2.11.1}$$

$$v(r) = \rho/r = \lambda_2 \tag{2.11.2}$$

$$\omega(r) = \rho' \tag{2.11.3}$$

Equations (2.6) can be derived by simple manupulations to the following first order system

$$\frac{du}{dr} = \frac{uz'z''}{1+z'^2} - (1+z'^2)^{1/2}\left[\frac{\omega f_3}{vrf_1} + \frac{\omega-v}{r}\frac{f_2}{f_1} \right] \tag{2.12.1}$$

$$\frac{dv}{dr} = \frac{\omega-v}{r} \tag{2.12.2}$$

$$\frac{d\omega}{dr} = \frac{\omega u'}{u} - u(u^2-\omega^2)^{1/2}\left[\frac{p}{N_1} - \frac{(u^2-\omega^2)^{1/2}}{uvr}\frac{N_2}{N_2} \right] \tag{2.12.3}$$

where

$$f_1 = \frac{\partial N_1}{\partial \lambda_1}, \qquad f_2 = \frac{\partial N_1}{\partial \lambda_2}, \qquad f_3 = N_1 - N_2 \tag{2.13}$$

Equations (2.7) are the basic equations of axisymmetric membrane behavior in isothermal processes.

2.2 THERMAL ANALYSES

In this section, we extend the theory of axisymmetric membranes in isothermal processes to that in non-isothermal processes. Suppose the temperature of the system varies from the uniform temperature T_0 to a new uniform temperature T. The difference of temperature definitely affects the form of the strain energy function and the stress resultants, but does not influence the equilibrium equations and geometric relations. In order to derive the dependence of the strain energy density function on temperature, we assume the material to be an ideal elastomer. This postulate means that deformations of the membrane are associated with changes in the configurational entropy of the system, the internal energy being considered to remain unchanged [4,43]

From the first law of thermodynamics, the change in internal energy dU in any process is given by

$$d\bar{W} = dU - dQ \tag{2.14}$$

where $d\bar{W}$ is the work done on the membrane by external forces; and dQ is the mechanical value of the heat supplied.

The second law of thermodynamics defines the entropy change dS in a reversible process

$$dQ = TdS \tag{2.15}$$

From (2.14) (2.15), it follows for a reversible process

$$d\bar{W} = dU - TdS$$

$$= d(U-TS) + SdT \tag{2.16}$$

$$= dA + SdT$$

where A is the Helmholtz free energy.. Obviously, in a reversible isothermal process the change in the Helmholtz free energy is identical with the work done by the external forces

$$dA = d\bar{W}, \quad (\text{ constant } T) \tag{2.17}$$

Therefore, for a reversible isothermal process the Helmholtz free energy can be defined as the strain energy function.

In reversible non-isothermal processes, Blatz [4] considered the membrane to be subjected to the following two steps of thermodynamic deformations. First, the temperature of the membrane is changed from T_0 to T. In this step, the membrane is stress free and no work is done on it. The change of dimensions of the membrane is

$$l_i^* = l_{i0}^* \exp(\int_{T_0}^{T} \alpha \, dT) \tag{2.18}$$

and

$$V^* = V_0^* \exp(3\int_{T_0}^{T} \alpha \, dT) \tag{2.19}$$

where the superscript * represents the state of free stress; the subscript $_0$ represents the state corresponding to the temperature T_0; l^* is the length in any direction at temperature T; V^* is volume at

temperature T; and α is the thermal expansion coefficient of the membrane.

In the second step the membrane is deformed slowly and isothermally into the final state under the mechanical loads. This step is an isothermal process. The stretch ratios in the step are denoted as $\bar{\lambda}_i$, where ~ represents isothermal condition.

From equation (2.14) the increment in the internal energy is equal to the heat energy TdS added in both steps plus the work done on the membrane in step two:

$$dU = TdS + V^* W_i dI_i \tag{2.20}$$

where the subscript i in W_i *represents the* partial differentiation of the strain energy function with respect to I_i. Letting T, I_i be independent variables, we have

$$dA = -SdT + V^* W_i dI_i \tag{2.21}$$

Noting that

$$-S = \frac{\partial A}{\partial T}, \qquad V^* W_i = \frac{\partial A}{\partial I_i} \tag{2.22}$$

and a well-known property of partial differentials

$$\frac{\partial}{\partial T}\left(\frac{\partial A}{\partial I_i} \right)_T = \frac{\partial}{\partial I_i}\left(\frac{\partial A}{\partial T} \right)_{I_i} \tag{2.23}$$

we have

$$-\frac{\partial S}{\partial I_i} = \frac{\partial V^* W_i}{\partial T} = 3\alpha V^* W_i + V^* W_{iT} \tag{2.24}$$

From equations (2.20), (2.24) it follows that

$$dU = \frac{\partial U}{\partial T}\, dT + V^*\left[(1-3\alpha T)W_i - TW_{iT}\right] dI_i \tag{2.25}$$

For an ideal elastomer

$$\frac{\partial U}{\partial I_i} = 0 \tag{2.26}$$

Therefore, we obtain

$$TW_{iT} = (1-3\alpha T)W_i \tag{2.27}$$

Equations (2.27) are a system of two linear second order partial differential equations in the variables T, I_1, I_2. The solution is obtained by integration (See Appendix A)

$$W(I_1, I_2, T) = \frac{T}{T_0} \exp\left(-3\int_{T_0}^{T} \alpha\, dT\right) W(I_1, I_2, T_0) \tag{2.28}$$

and

$$W(I_1^*, I_2^*, T_0) = 0 \tag{2.29}$$

with

$$I_1^* = I_2^* = 3 \tag{2.30}$$

Equation (2.26) gives the relation between the strain energy density functions at different temperatures T, T_0 with the same strain invariants.

Since no work is done in step one, Equations (2.11) can be used in step two. Substituting equation (2.30) into (2.11), we obtain the strain-stress relations

$$N_1 = 2h_0\left(\frac{\tilde{\lambda}_1}{\tilde{\lambda}_2} - \frac{1}{\tilde{\lambda}_1^3\tilde{\lambda}_2^3}\right)\left(W_1 + \tilde{\lambda}_2^2 W_2\right) \tag{2.31.1}$$

$$N_2 = 2h_0\left(\frac{\tilde{\lambda}_2}{\tilde{\lambda}_1} - \frac{1}{\tilde{\lambda}_1^3\tilde{\lambda}_2^3}\right)\left(W_1 + \tilde{\lambda}_1^2 W_2\right) \tag{2.31.2}$$

where ~ represents the isothermal process, i.e. step two.

We define the total stretch ratios including the two steps as

$$\lambda_i = \frac{l_i}{l_{io}^*} = \tilde{\lambda}_i \exp\left(-\int_{T_0}^{T} \alpha \, dT\right) \tag{2.32}$$

Thus, equations (2.31) become

$$N_1 = 2h_0\left(\frac{\lambda_1}{\lambda_2} - \frac{a^6}{\lambda_1^3\lambda_2^3}\right)\left(W_1 + a^{-2}\lambda_2^2 W_2\right) \tag{2.33.1}$$

$$N_2 = 2h_0\left(\frac{\lambda_2}{\lambda_1} - \frac{a^6}{\lambda_1^3\lambda_2^3}\right)\left(W_1 + a^{-2}\lambda_1^2 W_2\right) \tag{2.33.2}$$

where

$$a = \exp\left(\int_{T_0}^{T} \alpha dT\right) \tag{2.34}$$

For the Mooney material

$$W(I_1, I_2, T) = C_1(I_1 - 3) + C_2(I_2 - 3) \tag{2.35}$$

and equation (2.28) becomes

$$W = \frac{T}{T_0} \exp(-3\int_{T_0}^{T} \alpha \, dT) \left[C_{10}(I_1-3) + C_{20}(I_2-3)\right] \qquad (2.36)$$

where C_{10}, C_{20} are the material constants at T_0; and

$$I_1 = \bar{\lambda}_1^2 + \bar{\lambda}_2^2 + \frac{1}{\bar{\lambda}_1^2\bar{\lambda}_2^2} \qquad (2.37.1)$$

$$I_2 = \frac{1}{\bar{\lambda}_1^2} + \frac{1}{\bar{\lambda}_2^2} + \bar{\lambda}_1^2\bar{\lambda}_2^2 \qquad (2.37.2)$$

Equations (2.33) may be written in terms of dimensionless stress resultants as

$$N_{1\alpha} = C(T) \left(\frac{\lambda_1}{\lambda_2} - \frac{a^6}{\lambda_1^3\lambda_2^3} \right) \left(1+\Gamma a^{-2}\lambda_2^2 \right) \qquad (2.38.1)$$

$$N_{2\alpha} = C(T) \left(\frac{\lambda_2}{\lambda_1} - \frac{a^6}{\lambda_1^3\lambda_2^3} \right) \left(1+\Gamma a^{-2}\lambda_1^2 \right) \qquad (2.38.2)$$

where

$$N_{1\alpha} = N_1/2h_0C_1 \qquad (2.39.1)$$

$$N_{2\alpha} = N_2/2h_0C_1 \qquad (2.39.2)$$

$$\Gamma = C_2/C_1 \qquad (2.39.3)$$

$$C(T) = \frac{T}{T_0} \exp\left(-3\int_{T_0}^{T} \alpha \, dT\right) \qquad (2.39.4)$$

The neo-Hookean material is a special case in which Γ is equal to zero:

$$W(I_1,T) = C_1C(T)(I_1-3) \tag{2.40}$$

For this material the constitutive equations (2.33) are simplified further to

$$N_{1\alpha} = C(T)\left(\frac{\lambda_1}{\lambda_2} - \frac{a^6}{\lambda_1^3\lambda_2^3}\right) \tag{2.41.1}$$

$$N_{2\alpha} = C(T)\left(\frac{\lambda_2}{\lambda_1} - \frac{a^6}{\lambda_1^3\lambda_2^3}\right) \tag{2.41.2}$$

If deformations are small, equations (2.38) naturally become the formulas for small strain (See Appendix B for further details)

2.3 GOVERNING EQUATIONS AND BOUNDARY CONDITIONS

The objective of our research is to determine the deformed profile, the displacements, and stresses of the membrane under mechanical and thermal loadings. From sections 2.1, 2.2 we already have the basic equations for this objective.

We can start by solving for the variables u, v, ω which are concerned with the stretch ratios λ_1, λ_2. If the form of the strain energy function is given, u, v, ω are determined from equations (2.12) by a standard numerical integral:

$$\frac{du}{dr} = \frac{uz'z''}{1+z'^2} - (1+z'^2)^{1/2}\left[\frac{\omega f_3}{vrf_1} + \frac{\omega-v}{r}\frac{f_2}{f_1}\right] \tag{2.12.1}$$

$$\frac{dv}{dr} = \frac{\omega-v}{r} \tag{2.12.2}$$

$$\frac{d\omega}{dr} = \frac{\omega u'}{u} - u(u^2-\omega^2)^{1/2}\left[\frac{p}{N_1} - \frac{(u^2-\omega^2)^{1/2}}{uvr} \frac{N_2}{N_1} \right] \qquad (2.12.3)$$

where

$$f_1 = \frac{\partial N_1}{\partial \lambda_1}, \qquad f_2 = \frac{\partial N_1}{\partial \lambda_2}, \qquad f_3 = N_1 - N_2 \qquad (2.13)$$

The stretch ratios are obtained from equations (2.11) at once as

$$\lambda_1 = \frac{u}{(1+z'^2)^{1/2}} \qquad (2.42.1)$$

$$\lambda_2 = v \qquad (2.42.2)$$

Then we have the stress resultants from equations (2.33)

$$N_1 = 2h_0\left(\frac{\lambda_1}{\lambda_2} - \frac{a^6}{\lambda_1^3\lambda_2^3} \right) \left(W_1 + a^{-2}\lambda_2^2 W_2 \right) \qquad (2.33.1)$$

$$N_2 = 2h_0\left(\frac{\lambda_2}{\lambda_1} - \frac{a^6}{\lambda_1^3\lambda_2^3} \right) \left(W_1 + a^{-2}\lambda_1^2 W_2 \right) \qquad (2.33.2)$$

Finally the deformed profile can be obtained from equations (2.11)

$$\rho = \lambda_2 r \qquad (2.43.1)$$

$$\eta = \int_{r_0}^{r} (u^2-\omega^2)^{1/2} dr + \eta_0 \qquad (2.43.2)$$

Although there are nine equations (2.11), (2.12), (2.33), (2.41) and (2.42) with nine unknown variables u, v, w, λ_1, λ_2, N_1, N_2, ρ, η, the governing equations (2.12) only involve three first order equations

which are uncoupled with the rest of equations. The rest of the variables are easily obtained by algebraic or integral calculations.

In the formulation of the governing equations, the constitutive relations are not specified but are in a general form of stress-stretch ratio relations. The governing equations can be readily applied to problems of different axisymmetric membrane structures if a suitable constitutive equation for corresponding material is used.

Corresponding to the governing equations, there are three boundary conditions in axisymmetric problems of membrane structures. Due to the complexity of the boundary, it is often necessary to simplify these boundary conditions.

If an end of the system is clamped by an inextensible cord, we have a displacement boundary condition

$$v|_{z=0} = \exp\left(\int_{T_0}^{T} \alpha_c dT\right) \tag{2.44}$$

where α_c is the thermal expansion coefficient of the cord.

If the system has symmetry about a plane in the z direction, it is necessary to consider one half of the system only. In this case, we have the displacement boundary condition

$$\omega|_{z=l_0/2} = 0 \tag{2.45}$$

where l_0 is the initial length of the system.

Sometimes we need to use a force boundary condition, for example, the equilibrium condition of force resultant in the z direction.

2.4 SIMPLIFICATION OF THE FORMULAE

As mentioned in the introduction, there are two ways to simplify the formulas of axisymmetric membranes: an partially uncoupling method and a method of reduction of the order of the system of ordinary differential equations. Yang and Feng's method [53] is an uncoupling one. In the present work, we reformulate by means of reduction of the order of these equations.

Let us consider the equilibrium equations. They can be written in the alternate form

$$\frac{d(\rho N_1)}{d\rho} = N_2 \tag{2.46}$$

$$\frac{d(\rho N_1 \sin\phi)}{d\rho} = p\rho \tag{2.47}$$

Equation (2.46) or equation (2.47), together with either one of equations (2.3) can be regarded as the equilibrium equations.

The form of equation (2.46) and equation (2.47) hints that first integrals may be obtained. If we can obtain one or two of the first integrals, the order of the system of ordinary differential equations will be reduced by one or two. The governing equations consisting of three first order ordinary differential equations will be simplified to two or even one first order differential equations. Obviously, this is greatly helpful for the problem of axisymmetric membranes.

Unfortunately, we could not obtain the first integrals in a general case. But if some restrictions which often are not critical are made on the axisymmetric system, our objective can be reached.

We consider in great detail the following three cases.

CASE I. The pressure p is a given function $p(\rho)$ of radius ρ.

For this condition, we choose equation (2.3.1) and equation (2.47) as the equilibrium equations. Integrating equation (2.47), we have

$$\rho N_1 \sin\phi = G(\rho)+B \tag{2.48}$$

where

$$G(\rho) = \int p(\rho)\rho d\rho \tag{2.49}$$

By using geometric relations, we have

$$\sin\phi = \frac{\eta'}{S'} = \frac{(S'^2-\rho'^2)^{1/2}}{S'} \tag{2.50}$$

and

$$S' = (1+z'^2)^{1/2}\lambda_1 \tag{2.51}$$

Substituting equations (2.50), (2.51) into equation (2.49), we obtain

$$\rho' = \pm(1+z'^2)^{1/2}[1 - \frac{(G(\rho)+B)^2}{N_1^2\rho^2}]^{1/2}\lambda_1 \tag{2.52}$$

It is convenient to choose λ_1, λ_2 as dependent variables. From equation (2.2.2), we have

$$\rho' = \lambda_2' r+\lambda_2 \tag{2.53}$$

Combining equations (2.52), (2.53), and (2.33.1), we obtain

$$\lambda_2' = \frac{1}{r}\{-\lambda_2\pm(1+z'^2)^{1/2}\lambda_1[1 -$$

$$\frac{(G(\lambda_2 r)+B)^2}{4\lambda_2^2 r^2 h_0^2 (\frac{\lambda_1}{\lambda_2} - \frac{a^6}{\lambda_1^3\lambda_2^3})^2 (W_1 + a^{-2}\lambda_2^2 W_2)^2}]^{1/2}\} \qquad (2.54)$$

where the + sign is chosen according as ρ is an increasing or a decreasing function of r.

The other equilibrium equation (2.3.1) can be represented by means of λ_1, λ_2 also. Note that

$$\frac{dN_1}{d\rho} = (\frac{\partial N_1}{\partial \lambda_1}\frac{d\lambda_1}{dr} + \frac{\partial N_1}{\partial \lambda_1}\frac{d\lambda_2}{dr})\frac{dr}{d\rho} \qquad (2.55)$$

Introducing equation (2.55) into equation (2.3.1), we have

$$\lambda_1' = -\frac{1}{f_1}[(\frac{f_3}{\lambda_2} + f_2)\lambda_2' + \frac{f_3}{r}] \qquad (2.56)$$

where

$$f_1 = \frac{\partial N_1}{\partial \lambda_1}, \quad f_2 = \frac{\partial N_1}{\partial \lambda_2}, \quad f_3 = N_1 - N_2 \qquad (2.13)$$

In the case with the given function $p(\rho)$, the governing equations are simplified to a set of two first order ordinary differential equations with explicit derivatives:

$$\lambda_1' = -\frac{1}{f_1}[(\frac{f_3}{\lambda_2} + f_2)\lambda_2' + \frac{f_3}{r}] \qquad (2.56)$$

$$\lambda_2' = \frac{1}{r}\{-\lambda_2 \pm (1+z'^2)^{1/2}\lambda_1[1-$$

$$\frac{(G(\lambda_2 r)+B)^2}{4\lambda_2^2 r^2 h_0^2\left(\frac{\lambda_1}{\lambda_2} - \frac{a^6}{\lambda_1^3\lambda_2^3}\right)^2 (W_1 + a^{-2}\lambda_2^2 W_2)^2}\Bigg]^{1/2}\Bigg\} \qquad (2.54)$$

If the pressure p is constant, the governing equations become

$$\lambda_1' = -\frac{1}{f_1}\left[\left(\frac{f_3}{\lambda_2} + f_2\right)\lambda_2' + \frac{f_3}{r}\right] \qquad (2.56)$$

$$\lambda_2' = \frac{1}{r}\Bigg\{-\lambda_2 \pm (1+z'^2)^{1/2}\lambda_1\Bigg[1-$$

$$\frac{(\frac{1}{2}\, p\lambda_2^2 r^2 + B)^2}{4\lambda_2^2 r^2 h_0^2\left(\frac{\lambda_1}{\lambda_2} - \frac{a^6}{\lambda_1^3\lambda_2^3}\right)^2 (W_1 + a^{-2}\lambda_2^2 W_2)^2}\Bigg]^{1/2}\Bigg\} \qquad (2.57)$$

The constant of integration B depends on boundary condition. The set of two equations (2.54) and (2.56) (or (2.56) and (2.57) as p=const), with appropriate boundary conditions, can be solved by standard numerical procedures.

<u>CASE II</u>. The undeformed shape of the membrane is a straight circular cylinder.

Pipkin [32] discovered first that for initially circular membranes, the equilibrium equation (2.46) can be integrated. For the Mooney material, Kydoniefs and Spencer [21], and Wu [49] gave the integrated results.

For convenience, we choose the principal stretch ratios λ_1, λ_2 as basic variables. If $w(\lambda_1, \lambda_2, T)$ ($=W(I_1, I_2, T)$) is the strain energy

density function, then stress resultant equations (2.31) are derived to (Appendix C)

$$N_1 = 2h_0\left(\frac{\bar{\lambda}_1}{\bar{\lambda}_2} - \frac{1}{\bar{\lambda}_1^3\bar{\lambda}_2^3}\right)(W_1 + \bar{\lambda}_2^2 W_2) = \frac{a^2 h_0}{\bar{\lambda}_2}\frac{\partial w}{\partial \lambda_1} \tag{2.58.1}$$

$$N_2 = 2h_0\left(\frac{\bar{\lambda}_2}{\bar{\lambda}_1} - \frac{1}{\bar{\lambda}_1^3\bar{\lambda}_2^3}\right)(W_1 + \bar{\lambda}_1^2 W_2) = \frac{a^2 h_0}{\bar{\lambda}_1}\frac{\partial w}{\partial \lambda_2} \tag{2.58.2}$$

Substituting equations (2.58) into equation (2.46), we have

$$\frac{d(w_{\lambda_1})}{d\lambda_2} = \frac{1}{\lambda_1} w_{\lambda_2} \tag{2.59}$$

Note that

$$d(\lambda_1 w_{\lambda_1}) = w_{\lambda_1} d\lambda_1 + \lambda_1 d(w_{\lambda_1}) \tag{2.60}$$

From equations (2.59), (2.60), we obtain

$$d(\lambda_1 w_{\lambda_1}) = w_{\lambda_1} d\lambda_1 + w_{\lambda_2} d\lambda_2 = dw \tag{2.61}$$

Integrating equation (2.61), we have

$$w - \lambda_1 w_{\lambda_1} = A_1 \tag{2.62}$$

where A_1 is an constant of integration.

This result takes a more complicated appearance when the strain energy function is expressed as a function of strain invariants:

$$W - 2a^{-2}\left(\lambda_1^2 - \frac{a^6}{\lambda_1^2\lambda_2^2}\right)(W_1 + a^{-2}\lambda_2^2 W_2) = A_1 \tag{2.63}$$

Equation (2.63) is an algebraic equation involving the stretch ratios λ_1, λ_2 which determines the functional relation between λ_1, λ_2.

$$\lambda_1 = \lambda_1(\lambda_2, A) \tag{2.64}$$

If p is an unknown function of ρ, the equilibrium equation (2.47) cannot be integrated. But we can express it in terms of a differential equation with respect to λ_1, λ_2.

Substituting the geometric relations

$$K_1 = \frac{r_0(\lambda_1'\lambda_2' - \lambda_1\lambda_2'')}{\lambda_1(\lambda_1^2 - r_0^2\lambda_2'^2)^{1/2}} \tag{2.65.1}$$

$$K_2 = \frac{(\lambda_1^2 - r_0^2\lambda_2'^2)^{1/2}}{r_0\lambda_1\lambda_2} \tag{2.65.2}$$

into the equilibrium equation (2.3.2) and letting $\lambda' = \mu$, we have

$$\lambda_2' = \mu \tag{2,66.1}$$

$$\mu' = \frac{\lambda_1'\mu}{\lambda_1} + \frac{\lambda_1(\lambda_2,A)[\lambda_1^2(\lambda_2,A) - r^2\mu^2)^{1/2}}{rC[\frac{\lambda_1(\lambda_2,A)}{\lambda_2} + \frac{a^6}{\lambda_1^3(\lambda_2,A)\lambda_2^3}](W_1 + a^{-2}\lambda_2^2 W_2)} \{ p -$$

$$\frac{C[\lambda_1^2(\lambda_2,A) - r^2\mu^2]^{1/2}}{r\lambda_1\lambda_2}[\frac{\lambda_2}{\lambda_1(\lambda_2,A)} - \frac{a^6}{\lambda_1^3(\lambda_2,A)\lambda_2^3}][W_1 + a^{-2}\lambda_1^2(\lambda_2,A)W_2]\} \tag{2.66.2}$$

Thus, for initially circular cylindrical membranes, the governing equations are simplified to a set of two first order ordinary

differential equations with the constant of integration A. The system of equations is valid and exact for an arbitrary axisymmetric distribution of the pressure p.

CASE III. Initially circular cylindrical membrane and given pressure function $p(\rho)$.

In this case, there exist two first integrals. Integrating equation (2.46), we obtain equation (2.63)

$$W-2a^{-2}\left(\lambda_1^2-\frac{a^6}{\lambda_1^2\lambda_2^2}\right)\left(W_1+a^{-2}\lambda_2^2W_1\right) = A_1 \tag{2.63}$$

or equation (2.64)

$$\lambda_1 = \lambda_1(\lambda_2, A) \tag{2.64}$$

Integrating equation (2.47), we have

$$\sin\phi = \frac{G(\lambda_2 r)+B}{r\lambda_2 C(T)\left(\frac{\lambda_1}{\lambda_2}-\frac{a^6}{\lambda_1^2\lambda_2^2}\right)\left(W_1+\lambda_2^2W_2\right)} \tag{2.67}$$

Noting the geometric relation

$$\sin\phi = \frac{(\lambda_1^2-r^2\lambda_2'^2)^{1/2}}{\lambda_1} \tag{2.68}$$

Equation (2.65) can be written

$$\lambda_2' = \frac{\lambda_1(\lambda_2,A)}{r}\left\{1-\frac{[G(\lambda_2 r)+B]^2}{\lambda_2^2C^2\left[\frac{\lambda_1(\lambda_2,A)}{\lambda_2}-\frac{a^6}{\lambda_1^2(\lambda_2,A)\lambda_2^2}\right]^2\left[W_1+a^{-2}\lambda_2^2W_2\right]^2}\right\}^{1/2} \tag{2.69}$$

The governing equations are simplified to a first order ordinary differential equation with two constants of integration.

If the pressure p is a constant and the membrane is made of the Mooney material, equation (2.63) becomes (Appendix D)

$$\frac{\lambda_1^2(\lambda_2^4+\Gamma a^4)+(3a^6-\lambda_1^4\lambda_2^2)(1+\Gamma a^{-2}\lambda_2^2)}{\lambda_1^2\lambda_2^2} = A \qquad (2.70)$$

or

$$(\lambda_2^2+\Gamma a^{-2}\lambda_2^4)\lambda_1^4-(\lambda_2^4-A\lambda_2^2+\Gamma a^4)\lambda_1^2-(3a^6+3\Gamma a^4\lambda_2^2) = 0 \qquad (2.71)$$

where A is a constant of integration.

Regarded as a quadratic equation for λ_1^2, this equation has only one positive root, so that

$$\lambda_1^2 = \frac{\lambda_2^4-A\lambda_2^2+\Gamma a^4+[(\lambda_2^4-A\lambda_2^2+\Gamma a^4)+12a^6\lambda_2^2(1+\Gamma a^{-2}\lambda_2^2)^2]^{1/2}}{2\lambda_2^2(1+\Gamma a^{-2}\lambda_2^2)} \qquad (2.72)$$

The governing equation becomes

$$\lambda_2' = \frac{\lambda_1(\lambda_2,A)}{r}\left\{1-\frac{(-\frac{1}{2}pr^2\lambda_2^2+B)^2}{C^2\lambda_2^2\left[\frac{\lambda_1(\lambda_2,A)}{\lambda_2}-\frac{a^6}{\lambda_1^3(\lambda_2,A)\lambda_2^3}\right]^2(C_1+C_2a^{-2}\lambda_2^2)^2}\right\}^{1/2}$$

(2.73)

The constants of integration A, B can be determined by appropriate boundary conditions. The stretch ratio λ_2 is obtained by integrating

equation(2.73) together with a boundary condition. Then the stretch ratio λ_1 is calculated from equation (2.72).

For the neo-Hookean material, the basic equations have a simpler form

$$\lambda_1^2 = \frac{1}{2}\{\lambda_2^2 - A + [(\lambda_2^2 - A)^2 + \frac{12a^6}{\lambda_2^2}]^{1/2}\} \tag{2.74}$$

$$\lambda_2' = \frac{\lambda_1}{r}\{1 - \frac{(\frac{1}{2}\, pr^2\lambda_2^2 + B)^2}{C_1^2 C^2 \lambda_2^2 [\frac{\lambda_1(\lambda_2, A)}{\lambda_2} - \frac{a^6}{\lambda_1(\lambda_2, A)\lambda_2^3}]^2}\}^{1/2} \tag{2.75}$$

CHAPTER III

AN INITIALLY CIRCULAR CYLINDRICAL MEMBRANE REINFORCED AT BOTH ENDS BY FLEXIBLE CORDS

Due to light weight and ease of erection in space, inflatable systems are of interest for potential large space structures. Here we consider a thin-skinned cylindrical shell reinforced by flexible cord-like ribs as substructures of larger, somewhat more rigid systems, as indicated in Figure 2. It is possible that this type of membrane structure may be deployed in space as a substructure of more rigid large space structures in the near future. Since the membrane structure consists of many of the same cylindrical modules reinforced by cords at each ends, we only need to investigate one unit.

Suppose the undeformed configuration is a straight cylinder with length $2L_0$, radius r and thickness h_0. The system is subjected to an internal pressure p and an axial tension F. The stiffness of the cords is assumed to be much larger than that of the membrane so that the deformations of the cords can be neglected. In an earth orbit the system will be exposed to a wide variety of temperature. Due to the symmetry of the system in the axial direction, we only consider a half of the structure, shown in Figure 3.

The governing equations given in sections 2.3 and 2.4 are valid for any strain energy function of an ideal elastomer. In this chapter, in

order to present some numerical results, we assume that the cylindrical membrane is composed of a Mooney material.

3.1 BOUNDARY-VALUE PROBLEM

First we follow the theory of section 2.3 to construct the governing equations. We choose the axial coordinate z of the undeformed membrane as the independent variable instead of the constant radius r. The governing equations can be written in terms of the stretch ratios λ_1, λ_2.

By introducing the dimensionless quantities

$$z_\alpha = z/r \ , \qquad \rho_\alpha = \rho/r \ , \qquad \eta_\alpha = \eta/r \tag{3.1}$$

equations (2.2), (2.4) become

$$\lambda_1 = (\dot{\rho}_\alpha^2+\dot{\eta}_\alpha^2)^{1/2} \tag{3.2.1}$$

$$\lambda_2 = \rho_\alpha \tag{3.2.2}$$

$$K_1 = \frac{\dot{\lambda}_1\dot{\lambda}_2 - \lambda_1\ddot{\lambda}_2}{r\lambda_1^2(\lambda_1^2 - \dot{\lambda}_2^2)^{1/2}} \tag{3.3.1}$$

$$K_2 = \frac{(\lambda_1^2 - \dot{\lambda}_2^2)^{1/2}}{r\lambda_1\lambda_2} \tag{3.3.2}$$

where the dot denotes differentiation with respect to z_α.

Substituting equations (2.38), (3.3) into (2.3) and letting

$$\mu = \dot{\lambda}_2 \ , \qquad p_\alpha = pr/2h_0C_1$$

we obtain the governing equations

$$\dot{\lambda}_1 = \frac{\lambda_1^4 \lambda_2^3 \mu}{(\lambda_1^4\lambda_2^2+3a^6)(1+\Gamma\lambda_2^2 a^{-2})} \left[\frac{1}{\lambda_1} - \frac{3a^6}{\lambda_1^3\lambda_2^4} - \Gamma a^{-2}\lambda_1 - \frac{\Gamma a^4}{\lambda_1\lambda_2^4}\right] \tag{3.4.1}$$

$$\dot{\lambda}_2 = \mu \tag{3.4.2}$$

$$\dot{\mu} = \frac{\dot{\lambda}_1\mu}{\lambda_1} + \frac{(\lambda_1^2-\mu^2)\left(\frac{\lambda_2}{\lambda_1} - \frac{a^6}{\lambda_1^3\lambda_2^3}\right)(1+\Gamma a^{-2}\lambda_1^2)}{\lambda_2\left(\frac{\lambda_1}{\lambda_2} - \frac{a^6}{\lambda_1^3\lambda_2^3}\right)(1+\Gamma a^{-2}\lambda_2^2)}$$

$$- \frac{\lambda_1 (\lambda_1^2-\mu^2)^{1/2} p_\alpha}{C(T)\left(\frac{\lambda_1}{\lambda_2} - \frac{a^6}{\lambda_1^3\lambda_2^3}\right)(1+\Gamma a^{-2}\lambda_2^2)} \tag{3.4.3}$$

The boundary conditions can be written in the form

$$\lambda_2\Big|_{z_\alpha=0} = R/r = \exp\left(\int_{T_0}^{T} \alpha_c dT\right) \tag{3.5.1}$$

$$\mu\Big|_{z_\alpha=1} = 0 \tag{3.5.2}$$

$$2\pi R \frac{(\lambda_1^2-\mu^2)^{1/2}}{\lambda_1} N_1 \Big|_{z_\alpha=0} = F \tag{3.5.3}$$

where R is the radius at $z_\alpha=0$ after deformation. The third boundary condition corresponds to axial equilibrium. In terms of displacements the third boundary condition has the following form

$$C(T)(\lambda_1^2 - \mu^2)^{1/2}\left(1 - \frac{a^6}{\lambda_1^4\lambda_2^2}\right)\left(1+\Gamma a^{-2}\lambda_2^2\right)\Big|_{z_\alpha=0} = F_\alpha \tag{3.6}$$

where

$$F_\alpha = \frac{F}{4\pi h_0 r C_1} \tag{3.7}$$

It is more convenient for numerical computation to choose a displacement boundary condition instead of equations (3.6). For example, we can assume that

$$\lambda_1 \Big|_{z_\alpha = 0} = \lambda_{10} \tag{3.8}$$

Then the corresponding axial force can be obtained from equation (3.7).

Equations (3.4), (3.5) (or either of (3.6) and (3.8) replacing (3.5.3)) form the boundary-value problem for the determination of the deformed profile of the system under mechanical and thermal loadings. The stress resultants are given by equations (2.38).

This boundary value problem can be solved by standard numerical procedures. In this paper, we apply a shooting and matching method which uses initial value techniques and a modified Newton iteration. The parameters in the method may be, but need not be, the boundary values; they may include the pressure p_α, the axial force F_α, and the ratio Γ of the material constants. One of the programs used is shown in Appendix F.

The simplest way is to apply the simplified formulas in section 2.4 to the problem. From axial equilibrium, it follows (Appendix E) that

$$B = \frac{F}{2\pi} - \frac{1}{2} p r^2 \tag{3.9}$$

Thus we obtain the boundary value problem expressed by

$$\dot{\lambda}_2=\lambda_1(\lambda_2,A)\left[1-\frac{(p_\alpha\lambda_2^2-p_\alpha+2F_\alpha)^2}{4C^2(T)\lambda_2^2\left(\frac{\lambda_1(\lambda_2,A)}{\lambda_2}-\frac{a^6}{\lambda_1(\lambda_2,A)\lambda_2^3}\right)^2(1+\Gamma a^{-2}\lambda_2^2)^2}\right]^{1/2}$$

(3.10)

and

$$\lambda_2\Big|_{z_\alpha=0}=\Lambda_{20}=\exp\left(\int_{T_0}^{T}\alpha_c dT\right) \tag{3.11.1}$$

$$p_\alpha(\Lambda_2^2-1)+2F_\alpha=2C(T)\Lambda_2\left(\frac{\Lambda_1}{\Lambda_2}-\frac{a^6}{\Lambda_1\Lambda_2^3}\right)(1+\Gamma a^{-2}\Lambda_2^2) \tag{3.11.2}$$

where

$$\lambda_1(\lambda_2,A)=\left\{\frac{\lambda_2^4-A\lambda_2^2+\Gamma a^4+[(\lambda_2^4-A\lambda_2^2+\Gamma a^4)^2+12a^6\lambda_2^2(1+\Gamma a^{-2}\lambda_2^2)^2]^{1/2}}{2\lambda_2^2(1+\Gamma a^{-2}\lambda_2^2)}\right\}^{1/2}$$

(3.12)

This boundary value problem includes a first order ordinary differential equation with an explicit derivative, two boundary conditions, and a constant A. The two boundary conditions are applied to determination of two constants (constant A and the constant of integration which will appear when equation (3.10) is integrated)

It is not difficult to solve the boundary value problem by the shooting and iterative methods. The numerical methods are described briefly as follows.

If the pressure p_α, the axial force F_α, the temperature T, and the material constant Γ are given, we choose an estimated value of the constant A. Note that at $z_\alpha=0$, we have from equation (3.12)

$$A = \frac{(1+\Gamma a^{-2})\,(3a^6-\Lambda_{10}^4) + \Gamma a^4 \Lambda_{10}^2}{\Lambda_{10}^2} \tag{3.13}$$

Therefore, constant A really corresponds to the value Λ_{10} of the stretch ratio λ_1 at $z_\alpha=0$. Integrating equation (3.10) by starting with the boundary condition (3.11.1), we have numerical results on λ_2 as well as λ_1 from (3.12). Next, check the boundary condition (3.11.2) by means of the results at $z_\alpha=L_0/r$. If equation (3.11.2) is not satisfied, we guess a new estimated value A (or corresponding Λ_{10}) and repeat the computation until the condition is satisfied. Finally, λ_1, λ_2 and A are determined.

We may assume any of the parameters p_α, F_α, T, and Γ is unknown for example p_α. The rest of the parameters and constant A are given. In this case we have numerical values of λ_1, λ_2, p_α by means of the above mentioned computational method. Similarly, any of F_α, Γ, T can be chosen as a parameter to be determined. One of the programs we made is given in Appendix G.

3.2 DEFORMED PROFILES AND DISTRIBUTIONS OF STRETCH RATIOS

The problem of an axisymmetric membrane which has an initially circular cylindrical form and is attached to and sealed by a rigid plug at each end has been investigated by Kydoniefs and Spencer [21], Wu [49], Yang and Feng [53] Matsikoudi-Iliopoulou [25], and Lee [23]. Reference [53] investigated the special case in which pressure is zero. The others imposed a special relation ($F=\pi r^2 p$) between the pressure and the axial force of the system. Our work removes these constrained conditions and allows one to choose any arbitrary realistic values for the pressure and the axial force independently. Moreover, none of the previous works have considered changes of temperature. Therefore, those works are special cases of the problem we investigated.

The factors influencing the deformations of the membrane include the pressure p_α, the axial force F_α, the temperature T, and the ratio Γ of material constants of the membrane.

Figures 4-6 are plots of the effect of variations of the pressure p_α on the profile and stretch ratios for constant value of F_α, Γ, T. As can be expected, the radius and stretch ratios of the deformed membrane increase with increasing the pressure p_α at the beginning. As p_α increases, p_α passes through a maximum and then decreases. Similar phenomena have been observed in other inflation problems (references [1, 8, 15, 21]). This shows the phenomenon of inflated instability of

the membrane. The problem of instability will be analysed in section 3.4 in detail.

The variation of the deformed profile and stretch ratios as the axial force changes are given in Figures 7-9. Opposite to the case [53], in which the pressure p is equal to zero, the radius of the deformed profile increases with increasing the axial force. This is a very interesting "barrel shape" phenomenon and can be qualitatively explained as follows. When $p_\alpha=0$, the system is similar to a membrane in the state of simple extension. As the axial force increases, the dimension in the axial direction increases, while the other dimensions (circumferential direction and thickness) are correspondingly reduced. This is the so-called "neck" [53]. If p_α is not equal to zero, the extension in the axial direction makes the thickness and the cross sectional area in the central plane reduce and the total area of the membrane increases. The thinner state of the membrane cannot resist the pressure. Finally, the membrane equilibrates in the state of a larger deformation.

Another phenomenon worthy of note is that in a given condition, λ_1 is almost a constant value throughout the membrane, while the change of λ_2 is much larger than that of λ_1 along axis z_α. The condition is important. The results show that as Λ_2 is less than 3 (Λ_2 is the stretch ratio in the circumferential direction on the central plane), the change of λ_1 along axis z_α does not exceed 15 percent of λ_1.

Obviously Γ is a quantity similar to the modulus of elasticity. The radius ρ_α and stretch ratios λ_1, λ_2 reduce with increasing Γ, as shown in Figure 10-12.

Figures 13-15 show how a change of temperature influences the deformations of the membrane. The most important property is that under conditions of constant loadings the length and radius of the membrane made of the Mooney material decrease on warming, and vice versa. In other words, for the same distribution of the stretch ratios the external loadings (the pressure and the axial force) increase as the temperature is increased. This is a very interesting property of nonlinear membranes made of the Mooney material (rubber-like material) which has a characteristic opposite to other materials such as metals and ceramics. We can qualitatively explain it as follows.

We imagine that the system achieves its final state by undergoing two processes. The first, the system deforms under the external loadings at constant temperature T_0. The curve of configuration changes from curve I to curve II in Figure 16. In the second process, the temperature of the system under the same loadings decreases from T_0 to T. The influence of the change of temperature involves two sides. On the one side, the change compels the system to contract. On the other side, the Mooney coefficient C_1 decreases as temperature drops (see equation (2.10)). As shown in Appendix B, C_1 is a material constant similar to the elastic constant. The system with lower "elastic

constant" does not equilibrate under the same loadings and is imposed a state of larger deformations. Since the coefficient of thermal expansion of the membrane is small and the change of temperature influences the value of the material constant C_1 strongly, the latter dominates the second process. So, the system is deformed from curve II to curve III as temperature drops. This phenomenon is similar to the Gough-Joule effect [10, 13, 33] and is consistent completely with the theory of thermodynamics of the Mooney material. According to the theory, deformations are associated with changes in the configurational entropy of the membrane, the internal energy being considered to remain unchanged [43, 54].

3.3 THERMAL STRESS RESULTANTS

In comparison with large deformations of membranes, the references on the thermal stress state of membrane structures are few [6, 17, 33, 43, 54]. Most of them give only general principles or thermal analyses of simple extension and compression.

Following the mathematical model given in Chapter II, we obtain some results on the cylindrical membrane made of the Mooney material by numerical methods.

Figures 17 and 18 show the relations between the pressure p_α and the stress resultants. Here we see instability once again. For moderate deformations, the stress resultants increase with raising

pressure. When deformations exceed some limit, larger stress resultants correspond to less pressure.

For values of parameters of interest in large space structures, the influence of increasing the axial force on deformations and stresses is shown in Figures 7-9, 19, and 20. We note that the stress resultant N_{1_α} in the meridional direction is approximately a constant throughout the membrane as the stretch ratio λ_1 in the meridional direction is small. In Figure 19, for example, the change of N_{1_α} for curve 1 is within 6.5 percent of the value at the end. Examining the corresponding stretch ratio λ_1 in the meridional direction in Figure 8 and λ_2 in the circumferential direction in Figure 9, we discover that λ_1 is small (around 1.25) and approximately a constant, while the change of λ_2 along the axis is very obvious (30 percent of the value at the end). This shows that as the stretch ratio λ_1 is very small, the distribution of stress resultant N_{1_α} along the axis has the similar form of distribution with that of the stretch ratio λ_1 and N_{1_α} does not obviously change with increasing λ_2 along the axis. On the other side, in comparison of curve 1 in Figure 20 with curve 1 in Figure 9, N_{2_α} and λ_2 have the similar form of distribution along the axis. These parameters are essentially uncoupled between the meridional and the circumferential directions under the condition of small deformations.

The variation of stress resultants in meridional and circumferential directions with temperature is given in Figure 23, 24. In general, there exist even larger stress resultants in the meridional direction in the condition of a low temperature than in that of a high temperature. Therefore, the membrane structure is easily destroyed when overcooled.

The dependence of stress resultants on the ratio Γ of material constants is illustrated in Figure 21, 22.

The maximum meridional stress resultant occurs at the end adjacent to the cord. The maximum circumferential stress resultant is encountered in the centre symmetric plane. When the loadings (pressure p_α and axial force F_α) or temperarure T vary, the positions where material is destroyed first are the centre symmetric plane or the end adjacent to the cord.

3.4 INFLATED INSTABILITY

The problem of instability of a cylindrical membrane subjected to uniform pressure and axial force has been considered many times in the past. The excellent paper by Corneliussen and Shield [6] gave a quite complete analysis of the stability of an inflated tube. Further results were obtained by Alexander [3], Shield [39], Fourney and Stern [12], and Ratner [37]. The above works only investigated a special case in which they assumed no change in shape, i.e., the membrane is not only

initially, but is always a circular cylindrical tube. For the boundary condition of being sealed at each end by rigid plugs, Kydoniefs and Spencer [21] pointed out the existance of inflated instability of a cylindrical membrane. Moreover, none of these studies considered the effect of temperature on the instability in the circumferential direction. In this section, we will analyze the characteristics, the types, and regulation of the instability.

We consider the stretch ratio in the centre symmetrical plane in the circumferential direction denoted by Λ_2. From the numerical results, we can plot many p_α-Λ_2 functional relations for different parameters. The function curves can be classified into three kinds, as shown in Figure 25. Curve I includes two segments corresponding to stable and unstable regions, respectively. Before achieving its maximum value, the pressure p_α increases with Λ_2 rapidly. If p_α exceeds $p_{\alpha max}$, no equilibrium state exists at all and the deformations grow infinitely. Curve III corresponds to a stable relation, and there exists no maximum value of the pressure. Thus Λ_2 increases with the pressure p_α monotonically. What is worthwhile to be noted is curve II. Here there exist a maximum and a minimum value of the pressure p. Curve II is divided into three segments. Segments 1,3 correspond to a stable part, and segment 2 is an unstable region. Let us imagine the process of change of the equilibrium point. At the beginning, the equilibrium point moves along segment 1 with increasing value of p_α. When the

equilibrium point passes the point corresponding to $p_{\alpha max}$, it jumps from point A to B without moving along segment 2. In the inverse process, the equilibrium point jumps back from C to D. Segment 2 corresponds to an impossible state. This is the important jump phenomenon associated with nonlinear mechanics.

The foundations of the theory of stability of the forms of equilibrium is provided by the fact that a new adjacent, different form of equilibrium is stable one, while the original form is unstable. The loss of stability consists in the system passing to the adjacent form of equilibrium, with any infinitesimal perturbation of the original form of equilibrium being sufficient to bring about the transition. However, the loss of stability we found is not expressed as a transition to an adjacent form of equilibrium, but to some completely different form. We define the maximum value of the pressure p_α as the critical value p_{cr}. At $p_\alpha = p_{cr}$, curve I is of the type of infinite growth and curve II is the "jump" type [31].

Stability is influenced by three factors: the axial force F_α, the ratio Γ of material constants, and temperature T. The influence of the axial force F_α on the curve shape is shown in Figure 26. An increment of the axial force F_α contributes to better stability in the circumferential direction. If the axial force decreases, it is possible

that the p_α-Λ_2 curve is transferred from the stable curve III to the unstable curve II.

Figure 27 represents the dependence of stability on the ratio Γ of material constants. As the ratio Γ increases, the membrane becomes more and more stable. For constant F and T, there exists a critical ratio Γ_{cr}. The instability phenomenon appears only below Γ_{cr}.

Figure 28 is a plot of the effect of variation of temperature on stability. We discover that p_{cr} increases if the temperature T is raised. However, the membrane which is stable at a low temperature may become unstable at a high temperature.

The following qualitative conclusions can be obtained. If we assume that only one of the three factors which influence stability of the membrane changes (the other two being held constant) then increasing the ratio Γ of material constants, or temperature T , or decreasing the axial force F_α will make the critical pressure p_{cr} increase. Raising the temperature or decreasing the axial force F_α or the ratio Γ of material constants probably takes the system from the stable curve I to the unstable curves II or III.

3.5 AN APPROXIMATE PROCEDURE

In the last section, we obtained the p_α-Λ_2 relations from numerical results and discovered some characteristics of inflated instability. It

is the most important to determine the critical pressure p_{cr} as well as the functional relationship of p_{cr} with the factors: F_α, T, Λ.

If inflated instability exists, the governing condition for the onset of the inflated instability is

$$\frac{dp_\alpha}{d\Lambda_2} = 0 \tag{3.14}$$

Since we only obtained numerical results concerning the function $p_\alpha = p_\alpha(\Lambda_2)$, we cannot investigate condition (3.14) analytically.

A classical method of investigating instability is the perturbation method based on a known finite deformation (see [6, 39, 45]). The necessary condition using this method is that the finite deformation is known at the beginning. For this reason the method is often applied to the problem of small deformations superposed on a known finite deformation. All of the papers mentioned above only investigated the inflated instability in the special case in which the membrane before and after a finite deformation has the shape of a given circular cylinder. But the analytical solutions of the problem we are discussing is not explicitly obtainable. Therefore, the method cannot apply directly to the problem we are considering.

Here we derive a new approximate procedure which produces approximate analytical solutions.

The equilibrium equations are rewritten in the form

$$N_1 = \frac{F \pm \pi p(\rho^2 - r^2)}{2\pi\rho \sin\phi} = \frac{F \pm \pi p(\rho^2 - r^2)}{2\pi\rho}\left[1 + \left(\frac{d\rho}{d\eta}\right)^2\right]^{1/2} \tag{3.15.1}$$

$$\frac{N_1}{R_1} + \frac{N_2}{R_2} = p \tag{3.15.2}$$

where R_1, R_2 are the curvature radii in the meridional and circumferential directions respectively. Note that

$$R_2 = [1+(\frac{d\rho}{d\eta})^2]^{1/2}\rho \tag{3.16}$$

We have

$$N_1 = \frac{F+\pi p(\rho^2-r^2)}{2\pi\rho^2} R_2 = \frac{p'R_2}{2} \tag{2.17.1}$$

$$N_2 = (\frac{2\rho^2}{\rho^2-r^2} - \frac{R_2}{R_1})N_1 = \frac{R_2F}{\pi(\rho^2-r^2)} \tag{2.17.2}$$

From the numerical results in section (3.2) we found that the deformed profile is like a barrel-shaped cylinder. For the first approximation, we now postulate that the meridian curve of the deformed profile is a circular arc (see Figure 29). The equation of the circular arc can be represented by

$$R_1 = \frac{(\bar{\rho}-\rho)^2+(L-\eta)^2}{2(\bar{\rho}-\rho)} \tag{3.18}$$

where $\bar{\rho}$ represents the radius at $z=L_0$. For simplification, we assume that the deformation of radius ρ at $z=0$ can be neglected, i.e. $\rho|_{z=0}=r$. At $z=0$ we have

$$R_1 = \frac{(\bar{\rho}-r)^2+L^2}{2(\bar{\rho}-r)} \tag{3.19}$$

Differentiation of equation (3.18) yields

$$\frac{d\rho}{d\eta} = \frac{L-\eta}{[R_1^2-(L-\eta)^2]^{1/2}} \tag{3.20}$$

From equation (3.16), we obtain

$$R_2=\{1+\frac{\bar{\rho}^2-r^2-L^2}{[(\bar{\rho}-r)^4+2(\bar{\rho}-r)^2(4L\eta-2\eta^2-L^2)+L^4]^{1/2}}\}\ R_1 \tag{3.21}$$

The equilibrium equations become

$$N_1=\{1+\frac{\bar{\rho}_\alpha^2-L_\alpha^2-1}{[(\bar{\rho}_\alpha-1)^4+2L_\alpha^2(\bar{\rho}_\alpha-1)^2(4\eta_\alpha-2\eta_\alpha^2-1)+L_\alpha^4]^{1/2}}\}$$

$$\cdot\frac{[(\bar{\rho}_\alpha-1)^2+L_\alpha^2]p'r}{4(\bar{\rho}_\alpha-1)} \tag{3.22.1}$$

$$N_2=\frac{2\rho_\alpha^2 N_1}{\rho_\alpha^2-1}-\{1+\frac{\bar{\rho}_\alpha^2-L_\alpha^2-1}{[(\bar{\rho}_\alpha-1)^4+2L_\alpha^2(\bar{\rho}_\alpha-1)^2(4\eta_\alpha-2\eta_\alpha^2-1)+L_\alpha^4]^{1/2}}\}$$

$$[N_1+\frac{F}{\pi\ (\rho_\alpha^2-1)}\cdot\frac{(\bar{\rho}_\alpha-1)^2+L_\alpha^2}{2(\bar{\rho}_\alpha-1)}] \tag{3.22.2}$$

where the dimensionless quantities are defined as

$$\bar{\rho}_\alpha=\frac{\bar{\rho}}{r}=\Lambda_2,\quad \rho_\alpha=\frac{\rho}{r}=\lambda_2,\quad \eta_\alpha=\frac{\eta}{r},\quad L_\alpha=\frac{L}{r} \tag{3.23}$$

Substituting equations (2.33) for the stress resultants, we have

$$2h_0(\frac{\lambda_1}{\lambda_2}-\frac{a^6}{\lambda_1\lambda_2^3})(W_1+a^{-2}\lambda_2^2W_2)$$

$$=\{1+\frac{\Lambda_2^2-L_\alpha^2-1}{[(\Lambda_2-1)^4+2L_\alpha^2(\Lambda_2-1)^2(4\eta_\alpha-2\eta_\alpha^2-1)+L_\alpha^4]^{1/2}}\}\frac{[(\Lambda_2-1)^2+L_\alpha^2]p'r}{4(\Lambda_2-1)}$$

(2.24.1)

$$2h_0\left(\frac{\lambda_2}{\lambda_1} - \frac{a^6}{\lambda_1\lambda_2^3}\right)(W_1+a^{-2}\lambda_1^2W_2) = \frac{2\lambda_2^2N_1}{\lambda_2^2-1}$$

$$-\left\{1+\frac{\Lambda_2^2-L_\alpha^2-1}{[(\Lambda_2-1)^4+2L_\alpha^2(\Lambda_2-1)^2(4\eta_\alpha-2\eta_\alpha^2-1)+L_\alpha^4]^{1/2}}\right\}$$

$$.\left[N_1+\frac{F}{\pi(\Lambda_2-1)}.\frac{(\Lambda_2-1)^2+L_\alpha^2}{2(\Lambda_2-1)^2}\right] \qquad (3.24.2)$$

At $\eta=L$ ($\eta_\alpha=L_\alpha$), equations (3.24) become

$$\left(\frac{\Lambda_1}{\Lambda_2} - \frac{a^6}{\lambda_1\lambda_2^3}\right)(W_1+a^{-2}\Lambda_2^2W_2)=\frac{2F_\beta+p_\beta(\Lambda_2^2-1)}{2\Lambda_2} \qquad (3.25.1)$$

$$\left(\frac{\Lambda_2}{\Lambda_1} - \frac{a^6}{\Lambda_1\Lambda_2^3}\right)(W_1+a^{-2}\Lambda_1^2W_2)=\left[\frac{2\Lambda_2^2}{\Lambda_2^2-1} - \frac{2\Lambda_2(\Lambda_2-1)}{(\Lambda_2-1)^2+L_\alpha^2}\right]\left(\frac{\Lambda_1}{\Lambda_2} - \frac{a^6}{\Lambda_1\Lambda_2^3}\right)$$

$$.(W_1+a^{-2}\Lambda_2^2W_2) - \frac{2\Lambda_2F_\beta}{\Lambda_2^2-1} \qquad (3.25.2)$$

where

$$p_\beta = pr/2h_0, \qquad F_\beta = \frac{F}{4\pi h_0 r}$$

The length of the deformed cylinder is determined by

$$L_\alpha = \int_1^{\Lambda_2} tg\phi \, d\lambda_2 \qquad (3.26)$$

Because the function tgϕ is very complicated, an analytical result cannot be obtained. Note that λ_1 is almost a constant if deformations are not very large, for example λ_1 3. We assume that λ_1 is constant along the axial direction and have

$$\lambda_1 = \Lambda_1, \qquad S = \Lambda_1 L_0 \tag{3.27}$$

From the geometry of the circular arc, we have

$$L = R_1 \sin\frac{\Lambda_1 L_0}{R_1} \tag{3.28}$$

Expanding the right hand of equation (3.28) to the third degree in $\frac{\Lambda_1 L_0}{R_1}$ and combining equation (3.19), we obtain

$$3L_\alpha^5 - 3L_{0\alpha}\Lambda_1 L_\alpha^4 + 6(\Lambda_2-1)^2 L_\alpha^3 - 6L_{0\alpha}\Lambda_1(\Lambda_2-1)^2 L_\alpha^2 + 3(\Lambda_2-1)^4 L_\alpha +$$
$$2L_{0\alpha}^3\Lambda_1^3(\Lambda_2-1)^2 - 3L_{0\alpha}\Lambda_1(\Lambda_2-1)^4 = 0 \tag{3.29}$$

where

$$L_{0\alpha} = \frac{L_0}{r} \tag{3.30}$$

Equation (3.25) and (3.29) with three unknown variables form the governing equations in the approximate procedure. The assumed deformed profile (circular arc) satisfied the geometric boundary conditions (on Λ_2). So, the function of the deformed profile is an admissible function. The first of the equilibrium equation (3.25.1) is an exact equation. Only the second equilibrium equation is satisfied

approximately. Therefore, we can predict that the error will not be large.

We used a hybrid algorithm, which is a variation of Newton's method, to solve the set of equations. One of the program used is shown in Appendix H. The numerical results are close to those we expect. If the membrane is made of the Mooney material, for $F_\alpha = 1.391$, $\Gamma = 0.05$, $L_0 = 1.0$, the approximate solution is compared with the exact solution, as shown in Figure 30 and 31.

Figure 30 shows the deformed profiles for $p_\alpha = 0.94$, 1.03 by the exact method and approximate method. When deformations are moderate, the errors are very small. For example, for $p_\alpha = 0.94$, corresponding deformations are $\Lambda_1 = 1.77$, $\Lambda_2 = 1.4$, $L_\alpha = 1.67$, while the approximate results of the deformations are $\Lambda_1 = 1.768$, $\Lambda_2 = 1.398$, $L_\alpha = 1.706$. The errors are all less than 2 percent. When deformations are larger, for example $\Lambda_1 = 2.139$, $\Lambda_2 = 1.732$, $L_\alpha = 1.955$, the errors of the approximate solutions are in the usual range of allowable error and all of them are less than 9 percent. The functional relationship $p_\alpha(\Lambda_2)$ from the two methods is shown in Figure 31. We find that the approximate solution is very close to the exact solution. The above results state clearly that the approximate procedure is efficient for moderate deformations. Foster [11], Wu [52] gave an approximate procedure for very large deformations

(λ_1 2). Here, the approximate procedure we developed is just complementary to their method.

The approximate procedure is based on two additional assumptions (circular arc and constant λ_1) and the approximate expansion of equation (3.28). The second additional assumption (λ_1=const.) comes from the calculated results (section (3.2)). For the first additional assumption (circular arc), we give the following analysis.

From geometric relations, it is easy to derive

$$\frac{dK_2}{d\lambda_2} = \frac{1}{\lambda_2} (K_1 - K_2) \tag{3.31}$$

If the shape of the deformed profile is like a football being cut down the two ends, it is obvious that K_2 K_1, or R_2 R_1. It follows that $dK_2/d\lambda_2$ 0. Therefore, $K_2$is a monotone decreasing function of λ_2. In the central symmetric plane ($z=L_0$), R_2 reaches its maximum value. Let us observe the equilibrium equations (3.17). Note that the part G in the parentheses in the right of equation (3.17.2) is

$$G = \frac{2\rho^2}{\rho - r^2} - \frac{R_2}{R_1} \tag{3.32}$$

At $z=L_0$, if $\Lambda_2=2$ we have

$$\frac{2\bar{\rho}^2}{\bar{\rho} - r^2} = \frac{8}{3}$$

Since the function $2\rho^2/(\rho^2-r^2)$ reaches its minimum value at $z=L_0$, we find

$$\frac{2\rho^2}{\rho^2-r^2} \geq \frac{8}{3}, \qquad \text{if} \quad \Lambda_2 \leq 2 \tag{3.33}$$

and

$$\frac{R_2}{R_1} < 1 \tag{3.34}$$

Obviously, $2\rho^2/(\rho^2-r^2)$ is the dominate part of the function G. If the radius of curvature in the meridian direction is replaced by a constant radius, only the minor term R_2/R_1 is influenced. Thus, the replacement of the deformed profile by the circular arc only produces a slight effect in the second equilibrium equation and does not change the first one.

According to the above analysis and the approximate expansion, we discover that the larger R_1 is, the smaller the errors will be.

For a more accurate solution, we can use the perturbation method based on the approximate solution.

The main advantage of the approximate procedure is that we can investigate the problem of inflated instability by means of analytical expressions (3.25) and (3.29). We will discuss this in detail in the next section.

3.6 APPROXIMATE PROCEDURE: INFLATED INSTABILITY

The governing condition for inflated instability derived in the last section is

$$p'_\alpha = 0 \tag{3.14}$$

The difficulty of the problem investigated analytically is that we cannot obtain the analytical expression $p_\alpha = p_\alpha(\Lambda_2)$. Many approximate methods, for example the Ritz method [30, 41], only yield numerical results by numerical integral. The approximate method we developed has given a set of algebraic equations. From this set of equations we can obtain the critical pressure p_{cr} and the curves of p_{cr} with variation of any of the parameters F_α, Γ, T by means of the maximum principle.

We have the basic algebraic equations

$$p_\alpha(\Lambda_1,\Lambda_2,L_\alpha) = \frac{2}{\Lambda_2-1}\left[\left(\Lambda_1 - \frac{a^6}{\Lambda_1\Lambda_2^2}\right)(1+\Gamma a^{-2}\Lambda_2^2) - F_\alpha\right] \tag{3.35.1}$$

$$f_1(\Lambda_1,\Lambda_2,L_\alpha) = \left(\frac{\Lambda_2}{\Lambda_1} - \frac{a^6}{\Lambda_1\Lambda_2^3}\right)(1+\Gamma a^{-2}\Lambda_1^2) + \frac{2\Lambda_2 F_\alpha}{\Lambda_2-1}$$

$$-\left[\frac{2\Lambda_2^2}{\Lambda_2-1} + \frac{2\Lambda_2(\Lambda_2-1)}{(\Lambda_2-1)^2+L_\alpha^2}\right]\left(\frac{\Lambda_1}{\Lambda_2} - \frac{a^6}{\Lambda_1\Lambda_2^3}\right)(1+\Gamma a^{-2}\Lambda_2^2) = 0 \tag{3.35.2}$$

$$f_2(\Lambda_1,\Lambda_2,L_\alpha) = 3L_\alpha^5 - 3L_{0\alpha}\Lambda_1 L_\alpha^4 + 6(\Lambda_2-1)^2 L_\alpha^3 - 6L_{0\alpha}\Lambda_1(\Lambda_2-1)^2 L_\alpha^2 +$$

$$3(\Lambda_2-1)^4 L_\alpha + 2L_{0\alpha}^3\Lambda_1^3(\Lambda_2-1)^2 - 3L_{0\alpha}\Lambda_1(\Lambda_2-1)^4 = 0 \tag{3.35.3}$$

The variables $\Lambda_1, \Lambda_2, L_\alpha$ in the equation (3.35.1) are not independent, but are interrelated by two constraint conditions (3.35.2), (3.35.3).

According to the Lagrange multiplier method, we set τ_1, τ_2 be multipliers and assume a new function

$$F_p = p_\alpha(\Lambda_1, \Lambda_2, L_\alpha) + \tau_1 f_1(\Lambda_1, \Lambda_2, L_\alpha) + \tau_2 f_2(\Lambda_1, \Lambda_2, L_\alpha) \qquad (3.36)$$

The necessary conditions for rendering F_p a maximum with no constraints are

$$\frac{\partial F_p}{\partial \Lambda_1} = 0, \qquad \frac{\partial F_p}{\partial \Lambda_2} = 0, \qquad \frac{\partial F_p}{\partial L_\alpha} = 0 \qquad (3.37)$$

From equations (3.35)-(3.37) we obtain

$$\frac{2}{\Lambda_2^2-1}\left[\left(1+\frac{3a^6}{\Lambda_1\Lambda_2^4}\right)\left(1+\Gamma a^{-2}\Lambda_2^2\right)\right]+\tau_1\left\{\left(-\frac{\Lambda_2}{\Lambda_1^2}+\frac{3a^6}{\Lambda_1\Lambda_2^3}\right)\left(1+\Gamma a^{-2}\Lambda_1^2\right)+\right.$$

$$\left.2\Gamma a^{-2}\Lambda_1\left(\frac{\Lambda_2}{\Lambda_1^3}-\frac{a^6}{\Lambda_1\Lambda_2^3}\right)-2\Lambda_2\left[\frac{\Lambda_2}{\Lambda_2^2-1}-\frac{\Lambda_2^2-1}{(\Lambda_2^2-1)^2+L_\alpha^2}\right]\left(1+\frac{a^6}{\Lambda_1\Lambda_2^4}\right)\left(1+\Gamma a^{-2}\Lambda_2^2\right)\right\}+$$

$$\tau_2\left[-3L_{0\alpha}L_\alpha^4-6L_{0\alpha}(\Lambda_2^2-1)^2L_\alpha^2+6L_{0\alpha}^3\Lambda_1^2(\Lambda_2^2-1)^2-3L_{0\alpha}(\Lambda_2^2-1)^4\right]=0$$

$$(3.38.1)$$

$$\frac{4\Lambda_2}{(\Lambda_2^2-1)^2}\left[F_\alpha-\left(\Lambda_1-\frac{a^6}{\Lambda_1\Lambda_2^4}\right)\left(1+\Gamma a^{-2}\Lambda_2^2\right)\right]+\frac{4}{\Lambda_2^2-1}\left[-\frac{a^6}{\Lambda_1\Lambda_2^3}\left(1+\Gamma a^{-2}\Lambda_2^2\right)\right.$$

$$\left.+\Gamma a^{-2}\Lambda_2\left(\Lambda_1-\frac{a^6}{\Lambda_1\Lambda_2^4}\right)\right]+\tau_1\left\{\left(\frac{1}{\Lambda_1}+\frac{3a^6}{\Lambda_1\Lambda_2^5}\right)\left(1+\Gamma a^{-2}\Lambda_1^2\right)-\frac{2F_\alpha(\Lambda_2^2+1)}{(\Lambda_2^2-1)^2}\right.$$

$$+2\left[\frac{\Lambda_2^2+1}{(\Lambda_2-1)^2}-\frac{L_\alpha^2-(\Lambda_2-1)^2}{((\Lambda_2-1)^2+L_\alpha^2)^2}\right](\Lambda_1-\frac{a^6}{\Lambda_1\Lambda_2^3})(1+\Gamma a^{-2}\Lambda_2^2)$$

$$-\frac{4a^6}{\Lambda_1\Lambda_2^3}\left[\frac{\Lambda_2}{\Lambda_2-1}-\frac{\Lambda_2-1}{(\Lambda_2-1)^2+L_\alpha^2}\right](1+\Gamma a^{-2}\Lambda_2^2)$$

$$-4\Gamma a^{-2}\Lambda_2\left[\frac{\Lambda_2}{\Lambda_2-1}-\frac{\Lambda_2-1}{(\Lambda_2-1)^2+L_\alpha^2}\right](\Lambda_1-\frac{a^6}{\Lambda_1\Lambda_2^3})$$

$$+\tau_2[24(\Lambda_2-1)L_\alpha^3-12L_{0\alpha}\Lambda_1(\Lambda_2-1)L_\alpha^2+12(\Lambda_2-1)^3L_\alpha^3-12L_{0\alpha}\Lambda_1(\Lambda_2-1)^3$$

$$+4L_{0\alpha}^3\Lambda_1^3(\Lambda_2-1)] = 0 \qquad (3.38.2)$$

$$\tau_1\{-\frac{4L_\alpha\Lambda_2(\Lambda_2-1)}{[(\Lambda_2-1)^2+L_\alpha^2]^2}(\frac{\Lambda_1}{\Lambda_2}-\frac{a^6}{\Lambda_1\Lambda_2^3})(1+\Gamma a^{-2}\Lambda_2^2)\}+\tau_2\{15L_a^4-12L_{0\alpha}\Lambda_1L_\alpha^3$$

$$+18(\Lambda_2-1)^2L_\alpha^2-12L_{0\alpha}\Lambda_1(\Lambda_2-1)^2L_\alpha+3(\Lambda_2-1)^4\} = 0 \qquad (3.38.3)$$

From the five equations (3.38), (3.35.2),and (3.35.3), we can determine the five unknown quantities: $\Lambda_1, \Lambda_2, L_\alpha, \tau_1, \tau_2$. Then the corresponding maximum p_{cr} can be obtained from equation (3.35.1). If any of the parameters: F_α, Γ, T varies, p_{cr} changes also. Thus we can obtain the functional relations of p_{cr} with the parameters. From the functional relations, we can analyze unstable areas for the parameters.

We obtain the numerical results by means of the modified Newton's method (one of the programs used is given in Appendix I). Figure 32

represents the functional relations of p_{cr} with axial force F_α at $T=293^\circ K$. We call the curves as the critical curves p_{cr}-F_α for the values of given T and Γ. For the points below a critical curve, the system is stable, while for the points above the critical curve, the system shows instability. If the axial force F_α increases, the critical pressure p_{cr} decreases. When the axial force F_α reaches a certain value, the critical curve is terminated with a point. The value of the axial force corresponding to the terminal point is called the critical force $F_{\alpha cr}$ for the given T and Γ. If the axial force exceeds $F_{\alpha cr}$, there exists no instability.

The plane p_{cr}-F_α can be divided into three areas, as shown in Figure 33. Part III is an definitely stable area, which corresponds to the type of curve III in Figure 25. Part II is an unstable area, which corresponds to the region on the right segments of the critical pressure p_{cr} on curve I and curve II. Part I is a stable area, which corresponds to the region on the left segments of the critical pressure p_{cr} on curve I and curve II. There are different critical curves for different Γ and T. For example, curve I and curve II in Figure 32 correspond to $\Gamma=0.02$, 0.05 respectively. We discover that the critical axial force $F_{\alpha cr}$ decreases and the definitely stable area, part II, is enlarged as the material constant Γ increases. That means that the system is getting more and more stable with increasing value of material constant .

The dependence of the critical pressure p_{cr} on the ratio Γ of material constants is illustrated in Figure 34 at $T=293^{\circ}K$. For a given value of the axial force, the critical pressure increases with increment of the ratio Γ. Similar to Figure 32, there exists the critical ratio Γ_{cr} and the plane $p_{cr}\neg\Gamma$ can be divided into three areas. If the axial force increases, the definitely stable area is enlarged, but the critical pressure p_{cr} decreases for the same material constant Γ.

CHAPTER IV

CONCLUSIONS AND RECOMMENDATIONS

The objective of this study has been to develop a theory of axisymmetric membranes under combined mechanical and thermal loadings and to investigate the behavior of their deformations, thermal stresses, and instability. A mathematical model is established on the basis of the theory of nonlinear membranes and thermodynamics. The nonlinear relations of deformations and thermal stresses with loadings (p_α, F_α, T) and the material constant Γ are represented by the mathematical model.

We discover that the mathematical model can be simplified in some cases. The keys for simplification are to make the set of governing equations be uncoupled by means of an appropriate choice of variables and to make use of the first integrals if they exist. For a given $p(\rho)$, the governing equations are simplified to a set of two first order ordinary differential equations. For an initially circular cylindrical membrane, the number of the governing equations is reduced to one.

Due to the nonlinearity of the governing equations, not only is the numerical computation complex, but also it is difficult to investigate the problem of instability. Therefore, we developed an approximate procedure for moderate deformations. The results we obtained indicate that the approximate method is useful for investigation of deformations, thermal stresses, and especially instability.

For an initially circular cylindrical membrane, we gave numerical

results. The loadings (p_α, F_α, T) and the material constant Γ exist a strong influence on the nonlinear deformatioms, the thermal stresses, and the instability

There are some interesting phenomena for finite deformations of nonlinear membranes made of the Mooney material, such as contraction on warming, "barrel-shape" phenomenon as the axial force increases, nearly constant stretch ratio in meridional direction, etc. All of these phenomena should be noted for applications of axisymmetric membranes.

Stress concentration is a considerable problem. The numerical results point out that the maximum value of meridional stress resultant exists near the cords, while that of the circumferential stress resultant exists on the centre symmetrical plane.

Instability of membrane structures is a very serious problem. There exist two types of unstable phenomena. In the case of small Γ, small F_α, and high temperature T, there exists a critical pressure p_{cr}. If the pressure p_{cr} is exceeded, the membrane structure will inflate boundlessly until it is destroyed. The other unstable phenomenon is the jump phenomenon which is in important property of nonlinear system.

We investigated instability. According to the behavior of the inflation curves p_α-Λ_2, the state of the system in stability can be classified into three types. Some important concepts, critical curve and critical parameters, are presented. The effect of variation of

parameters on the unstable areas are discussed by means of the approximate procedure.

We paid attention to the influence of temperature on membrane structures. In general, decreasing the temperature makes deformations and stress resultants increase such that the system is destroyed ever more easily, while increasing temperature possibly transforms a stable system into an unstable one.

Further studies are recommended in the following areas:

1. Effect of thermal gradients on the nonlinear membrane.

In this dissertation we assume that the temperature of the membrane is uniform at any moment and varies slowly with time. This is just the first approximation to a practical case. In fact, even when a membrane structure is in sunlight, the side toward the sun is at a significantly higher temperature than the side away from the sun. The nonuniform distribution of temperature may give rise to thermally induced deformation, possible skin buckling, and overall distortion. It is very difficult to develop an expression for the membrane with a nonuniform distribution temperature. The difficulty comes from loss of axisymmetry. As the first step, one could consider a small deformation induced by the thermal gradients superposed on the known finite deformation studied in this dissertation.

2. Oscillations of membrane structures.

Membrane structures will oscillate under external excitations, for example thermally induced oscillation. This may cause anomalous motion of the system.

As the first step, we can assume an axisymmetric problem. The natural frequencies and modes could be obtained by numerical methods.

3. Wrinkling

Wrinkling is a important phenomenon in instability which often appears in thin membrane structures. A wide variety of temperature occur in space and also membrane structures could have complex boundary conditions which correspond to various types of attachment. In this case may lead to wrinkling.

Wrinkling of thin membranes in a constant temperature was studied by other authors before [24, 35, 49, 50]. The theory has to be extended to non-isothermal processes. The first step is to develop a new formulation.

4. More accurate constitutive relation.

The Mooney equation is only the first approximation to constitutive relations of rubber-like material. We also discovered in our study that the solution is very sensitive to values of the material constant Γ in the Mooney equation. A realistic solution may require some more accurate constitutive relations.

REFERENCES

[1] Adkins, J. E. and Rivlin, R. S., Large Elastic Deformations of Thin Shells, Phil. Trans. A 244, pp 505-531 (1952).

[2] Aerospace Expandable Structures - Conference Transactions, Flight Dynamics Laboratory (1963).

[3] Alexander, H., the Tensile Instability of an Inflated Cylindrical Membrane as Affected by an Axial Load, Int. J. Mech. Sci. 13, pp87-95 (1971).

[4] Blatz, P. J., Applications of Large Deformation Theory to the Thermomechanical Behavior of Rubberlike Polymer-Porous, Unfilled, and Filled, Eirich, F. R., Ed., Rheology-Theory and Applications Vol. 5, pp 1-56 (1969).

[5] Carlson, d. e. and Shield, R. T., Eds., Finite Elasticity, IUTAM Symp. (Lehigh University, 1980), Matinus Nijhoff, Hague, Netherlands (1982).

[6] Conneliussen, A. H. and Shield, R. T., Finite Deformations of Elastic Membranes With Application to the Stability of an Inflated and Extended Tube, Arch. Rat. Mech. Anal. 7, pp 273-304 (1961).

[7] Dreyer, W., On Thermodynamics and Kinetic Theory of Ideal Rubber Membranes, J. Appl. Mech. 48, pp 345-350 (1981).

[8] Feng, W. W. and Yang W. H., On the Contact problem of an Inflated Spherical Nonlinear Membrane, J. Appl. Mech. 40, pp 209-214 (1973).

[9] Feng, W. W., Axisymmetric Finite-Deformation Membrane Problem, CONF-810621-327 (1980).

[10] Flory, P. J., Principle of Polymer Chemistry, Cornell University Press, New York (1963).

[11] Foster, H. O., Very Large Deformations of Axially Symmetrical Membranes Made of Neo-Hookean Materials, Int. J. Engng Sci. 5, pp 95-117 (1967).

[12] Fourney, W. L. and Stern, M., Further Results on the Stability of a Finitely Deformed Thin Cylindrical Shell, Int. J. Engng. Sci., Vol. 10, pp 613-622 (1972).

[13] Gent, A. M. N., Rubber and Rubber Elasticity: A Review, J. Polymer Sci.: Symp. 48, pp 1-17 (1974).

[14] Green, A. E. and Zerna, W., Theoretical Elasticity, Oxford (1960).

[15] Green, A. E. and Adkins, J. E., Large Elastic Deformations, Oxford (1970).

[16] Hart-Smith, L. J., and Crisp, J. D. C., Large elastic Deformations of thin Rubber Membranes, Int. J. Engng Sci. 5, pp 1-24 (1967).

[17] Hearle, J. W. S., etc., Polymers and Their Properties, Vol 1: Foundations of Structures and Mechanics (1982).

[18] Hill, J. M., A Survey of the Solved Problems for Rubber - Part 1 - Universal Deformations, Int. J. Mech. Eng. Ed., Vol. 10, pp 129-140 (1982).

[19] Hill, J. M., A survey of the Solved Problems for Rubber - Part 2 - Partial and Approximate Solutions, Int. J. Mech. Eng. Ed., Vol. 10, pp 153-168 (1982).

[20] Kawabata, S., Fracture and Mechanical Behavior of Rubber-Like Polymers Under Finite Deformation in Biaxial Stress Field, J. Mocromol. Sci.- Phys., B8 (3-4), pp605-630 (1973).

[21] Kydoniefs, A. D. and Spencer, A. L. M., Finite Axisymmetric Deformation of an Initially Cylindrical Elastic Membranes, Quart. Mech. Appl. Math. 22, pp 87-95 (1969).

[22] Kydoniefs, A. D., Finite Axisymmetric Deformations of Elastic Membranes, Int. J. Engng Sci. 10, pp 939-946 (1972).

[23] Lee, J. S., Large Elastic Deformations of Thin Tubes, Graduate Aeronautical Laboratories (1964).

[24] Mansfield, E. H., Load Transfer via a Wrinkled Membrane, Proc. Roy. Soc. Lond. (a), Vol. 316, pp 269-289 (1970).

[25] Matsikoudi-Iliopoulou, M. and Lianis, G., Nonlinear Axisymmetric Deformation of Membranes with Torsion, Acta Mech. 42, pp 153-170 (1982).

[26] Meirovitch, L., ed., Dynamics and control of Large Flexible Spacecraft, AIAA Symposium, 1st (1977), 2nd (1979), and 3rd (1981).

[27] Mooney, M., J Appl. Phys. 11, pp 582-592 (1940).

[28] NaghDi P. M. and Tang, P. Y., Large Deformation Possible in Every Isotropic Elastic Membrane, Phil. Trans. Roy. Soc. Lond., Vol. A287, pp 145-187 (1977).

[29] Nash, W. A., Bibliography on Shells and Shell-like Structures, TMB Report No. 863, U.S. Navy Dept. (1954), and Bibliography on Shells and Shell-like Structures (1954-1956), DA-0100009-ORD-404, U.S. Army (1957).

[30] Nielan, P. E., Large Deformations of Nonlinear Axisymmetric Membranes: a Variational Approach, SAND-82-8053 .

[31] Panovka, Y. G. and Gubanova I. I., Stability and Oscillations of Elastic Systems, Consultant Bureau, New York (1965)

[32] Pipkin, A. C., Integration of an Equation in Membrane Theory, ZAMP, Vol. 19, pp819-820 (1968).

[33] Price, C., Thermodynamics of Rubber Elasticity,Proc. R. Soc. Land. A 351, pp 331-350 (1976).

[34] Proceedings of the First International Colloquium on Pneumatic Structures, Stuttgart, Germany (1967).

[35] Pujara, P. and Lardner, T. J., Deformations of Elastic Membranes - Effect of Different Constitutive Relations, J. Appl. Math. Phys. 29, pp 315-327 (1978).

[36] Pujara, P. and Lardner, T. J., A Model for Cell Division, J. Biomechanics, Vol. 12, pp 293-299 (1979).

[37] Ratner, A.M., Tensile Stability of Cylindrical Membranes, Int. J. Nonlinear Mech. 18, pp 69-84 (1983).

[38] Rivlin, R. S., Ed., Finite Elasticity (1970).

[39] Shield, R. T., On the stability of Finitely Deformed Elastic Membranes, Part 2: Stability of Inflated Cylindrical and Spherical Membranes, ZAMP, Vol. 23, pp 16-34 (1972).

[40] Shield, R. S., Equilibrium Solutions in Finite Elasticity, J. Appl. Mech., Vol. 50, pp 1171-1180 (1983).

[41] Tang, S. C., Large Strain Analysis of an inflating Membrane, Computers and Structures 15, pp 71-78 (1982).

[42] Tielking, J. T. and Feng, W. W., The Application of the Minimum Potential Energy Principle to Nonlinear Axisymmetric Membrane Problem, J. of Appl. Mech., Vol. 41, pp 491-496 (1974).

[43] Treloar, L. R. G., The Physics of Rubber Elasticity, Oxford Uni., 3rd Ed. (1975).

[44] Treloar, L. R. G., The Mechanics of Rubber Elasticity, Proc. Roy. Soc. Lond. A351, pp 301-330. (1976).

[45] Vanghan, H., Axisymmetric and Asymmetric Instability in Elastic Solid Cylinders Under Finite Axial Strain, ZAMP, Vol. 22, pp865-875 (1971).

[46] Vanghan, H., Inflation of Finitely Stretched Circular Membrane, Quart. Mech. Appl. Math. 34, pp 111-127 (1981)

[47] Ward, I. M., Mechanical Properties of Solid Polymer.

[48] Well, N. A., Tensile Instability of Thin-Walled Cylinders of Finite Length, Int. J. Mech. Sci. 5, pp 487-506 (1963).

[49] Wu, C. H., On Certain Integrable Nonlinear Membrane Solutions, Quart. Appl. Math. 28, pp 81-90 (1970).

[50] Wu, C. H., The Wrinkling Axisymmetric Air Bags Made of Inextensible Membrane, J. Appl. Mech., Vol. 41, pp 963-968 (1974).

[51] Wu, C. H., Nonlinear Wrinkling of Revolution Membranes, J. Appl. Mech., Vol. 45, pp 533-538 (1978).

[52] Wu, C. H., Large Finite Strain Membrane Problem, Quart. Appl. Math., Vol.36, pp347-359 (1979).

[53] Yang, W. H. and Feng, W. W., On Axisymmetrical Deformations of Nonlinear Membranes, J. appl. Mech. 37, 1002-1011 (1970).

[54] Young, R. J., Introductions to Polymers (1981).

[55] Younger, D. G., Edmisston, R. M. and Crum, R. G., Nonrigid and Semirigid Structures for Expandable Spacecraft, ASD-TDR-62-586, Flight Dynamics Laboratory (1963).

[56] Yu, L. K., and Valanis, K. C., The Inflation of Axially Symmetric Membranes by Linearly Varying Hydrostatic Pressure, Trans. of the Soc. of Rheology, Vol. 14, pp 159-163 (1970).

AD-A172 080 PARAMETRIC INVESTIGATION OF FACTORS INFLUENCING THE MECHANICAL BEHAVIOR O..(U) MASSACHUSETTS UNIV AMHERST DEPT OF CIVIL ENGINEERING W A WASH ET AL. 30 MAY 86 5/5

UNCLASSIFIED AFOSR-TR-86-0858 AFOSR-83-0025 F/G 22/2 NL

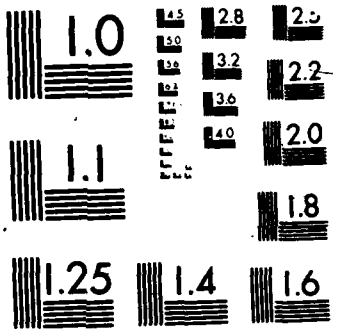
1.0
2.8
3.2
3.6
4.0
2.2
2.0
1.8
1.1
1.25
1.4
1.6

APPENDICES

APPENDIX A

DERIVATION OF EQUATION (2.28)

Equations (2.27) can be written as

$$T\frac{\partial^2 W}{\partial T \partial I_1} = (1 - 3\alpha T)\frac{\partial W}{\partial I_1} \tag{A-1}$$

$$T\frac{\partial^2 W}{\partial T \partial I_2} = (1 - 3\alpha T)\frac{\partial W}{\partial I_2} \tag{A-2}$$

Integrating equations (A-1), (A-2) with respect to T from T_0 to T, we obtain

$$\frac{\partial W(T, I_1, I_2)}{\partial I_1} = \frac{T}{T_0}\exp(-3\int_{T_0}^{T}\alpha\, dT)\frac{\partial W(T_0, I_1, I_2)}{\partial I_1} \tag{A-3}$$

$$\frac{\partial W(T, I_1, I_2)}{\partial I_2} = \frac{T}{T_0}\exp(-3\int_{T_0}^{T}\alpha\, dT)\frac{\partial W(T_0, I_1, I_2)}{\partial I_2} \tag{A-4}$$

Equations (A-3), (A-4) are a system of first order partial differential equations. In order to solve the equations we integrate equation (A-3) first from I_1^* to I_1 at constant I_2^*.

$$W(T, I_1, I_2^*) - W(T, I_1^*, I_2^*) = \frac{T}{T_0}\exp(-3\int_{T_0}^{T}\alpha\, dT)$$

$$[W(T_0, I_1, I_2^*) - W(T_0, I_1^*, I_2^*)] \tag{A-5}$$

Then integrating equation (A-4) from I_2^* to I_2 at constant I_1, we have

$$W(T, I_1, I_2) - W(T, I_1, I_2^*) = \frac{T}{T_0}\exp(-3\int_{T_0}^{T}\alpha\, dT)$$

$$[W(T_0, I_1, I_2) - W(T_0, I_1, I_2^*)] \tag{A-6}$$

Note that

$$W(T_0, I_1^*, I_2^*) = W(T, I_1^*, I_2^*) = 0 \qquad \text{(A-7)}$$

Combining equations (A-5), (A-7), we obtain

$$W(T, I_1, I_2) = \frac{T}{T_0} \exp(-3\int_{T_0}^{T} \alpha \, dT) \, W(T_0, I_1, I_2) \qquad \text{(A-8)}$$

APPENDIX B

FORMULAE FOR SMALL STRAIN

The initial length elements in meridional and circumferential directions are denoted by l^*_{10}, l^*_{20} respectively, the length elements after expansion of free stress l^*_1, l^*_2, the final length elements l_1, l_2. Similarly, ε^*_1, ε^*_2 represent the strain after expansion of free stress, ε_1, ε_2 the final strain. If thermal expansion coefficient α and strain ε_i are small, the terms of the second order and more than two of α, ε_i can be neglected. Therefore, we have

$$\exp(-\int_{T_0}^{T} \alpha \, dT) = 1 - \alpha\Delta T \qquad \text{(B-1)}$$

$$l^*_1 = l^*_{10}(1+\alpha\Delta T) \qquad \text{(B-2)}$$

$$\lambda_1 = l_1/l^*_1 = (1+\varepsilon_1)\ (1-\alpha\Delta T) \qquad \text{(B-3)}$$

$$\lambda_2 = (1+\varepsilon_2)\ (1-\alpha\Delta T) \qquad \text{(B-4)}$$

The factors of equations (2.33) can be written as

$$\frac{\lambda_1}{\lambda_2} - \frac{1}{\lambda_1^3\lambda_2^3} = 4\varepsilon_1+2\varepsilon_2-6\alpha\Delta T \qquad \text{(B-5)}$$

$$\frac{\lambda_2}{\lambda_1} - \frac{1}{\lambda_1^3\lambda_2^3} = 2\varepsilon_1+4\varepsilon_2-6\alpha\Delta T \qquad \text{(B-6)}$$

$$C_1+C_2\lambda_2^2 = b_1+b_2\varepsilon_2-b_2\alpha\Delta T \qquad \text{(B-7)}$$

$$C_1+C_2\lambda_1^2 = b_1+b_2\varepsilon_1-b_2\alpha\Delta T \qquad \text{(B-8)}$$

where

$$b_1 = C_1+C_2 \quad , \quad b_2 = 2C_2 \qquad \text{(B-9)}$$

Substituting equations (B-1), (B-5)-(B-8) into (2.34), we have

$$\sigma_1 = a_1(2\varepsilon_1+\varepsilon_2-3\alpha\Delta T) \qquad \text{(B-10)}$$

$$\sigma_2 = a_1(\varepsilon_1+2\varepsilon_2-3\alpha\Delta T) \qquad \text{(B-11)}$$

where

$$a_1 = 4b_1 \qquad \text{(B-12)}$$

The classical relations between strain-stress for small deformations are

$$\sigma_1 = \frac{E}{1-\mu^2}(\varepsilon_1+\mu\varepsilon_2) - \frac{E\alpha\Delta T}{1-\mu} \qquad \text{(B-13)}$$

$$\sigma_2 = \frac{E}{1-\mu^2}(\varepsilon_2+\mu\varepsilon_1) - \frac{E\alpha\Delta T}{1-\mu} \qquad \text{(B-14)}$$

Considering incompressibility of material

$$\varepsilon_1+\varepsilon_2+\varepsilon_3 = 0 \qquad \text{(B-15)}$$

we obtain $\mu=0.5$. Therefore, equations (B-13), (B-14) become into

$$\sigma_1 = \frac{2E}{3}(2\varepsilon_1+\varepsilon_2-3\alpha\Delta T) \qquad \text{(B-16)}$$

$$\sigma_2 = \frac{2E}{3}(\varepsilon_1+2\varepsilon_2-3\alpha\Delta T) \qquad \text{(B-17)}$$

In comparison of equations (B-10), (B-11) with equations (B-16), (B-17), we discover that

$$E = 6(C_1+C_2) \qquad \text{(B-18)}$$

The result agrees with reference [3].

APPENDIX C

DERIVATION OF STRESS-STRAIN RELATIONS

We consider a square element of a membrane with thickness h_0, length and width 1 before deformations. The element in the deformed state has lengths λ_1, λ_2 and $\lambda_3 h_0$ of the sides. Let f_i be the force acting on per unit deformed faces; N_i the resultant force per unit length in the deformed state; $w(\lambda_1,\lambda_2)$ the strain energy function per unit undeformed volume. From the virtual work principle, the work done in an infinitesimal displacement from λ_i to $\lambda_i+d\lambda_i$ is

$$dw = f_1 d\tilde{\lambda}_1 + f_2 d\tilde{\lambda}_2$$

$$= \frac{N_1}{h_0\lambda_1\lambda_3} d\tilde{\lambda}_1 + \frac{N_2}{h_0\lambda_2\lambda_3} d\tilde{\lambda}_2 \qquad \text{(C.1)}$$

Due to incompressibility, equation (C.1) can be rewritten

$$dw = \frac{\tilde{\lambda}_2 N_1}{h_0} d\tilde{\lambda}_1 + \frac{\tilde{\lambda}_1 N_2}{h_0} d\tilde{\lambda}_2 \qquad \text{(C.2)}$$

From the above equation, we have

$$N_1 = \frac{h_0}{\lambda_2}\frac{\partial w}{\partial \lambda_1}, \qquad N_2 = \frac{h_0}{\lambda_1}\frac{\partial w}{\partial \lambda_2} \qquad \text{(C.3)}$$

If the strain energy function is expressed as a function of strain invariants, we have

$$N_1 = \frac{h_0}{\lambda_2} \left(\frac{\partial W}{\partial I_1} \frac{\partial I_1}{\partial \lambda_1} + \frac{\partial W}{\partial I_2} \frac{\partial I_2}{\partial \lambda_2} \right) \tag{C.4.1}$$

$$N_2 = \frac{h_0}{\lambda_1} \left(\frac{\partial W}{\partial I_1} \frac{\partial I_1}{\partial \lambda_2} + \frac{\partial W}{\partial I_2} \frac{\partial I_2}{\partial \lambda_2} \right) \tag{C.4.2}$$

Calculating $\frac{\partial I_i}{\partial \lambda_j}$ $(i,j=1,2)$ from the representations of strain invariants and noting equation (2.32), we obtain equations (2.58).

APPENDIX D

DERIVATION OF EQUATIONS (2.70) AND (2.71)

Combining equations (2.28), (2.35) and (2.63), we can obtain equations (2.70) and (2.72) easily, where

$$A = \frac{a^5 T_0}{C_1 \bar{T}} A_1 \tag{D.1}$$

Equation (2.70) can be obtained from equilibrium equation (2.46) and constitutive equations (2.38) also. By substituting equations (2.38) into equation (2.46), we obtain by simple manipulation

$$[\lambda_1^4\lambda_2^4+3a^6\lambda_2^2+\Gamma a^{-2}(\lambda_1^4\lambda_2^6+3a^6\lambda_2^4)]d\lambda_1^2+$$

$$[3a^6\lambda_1^2-\lambda_1^4\lambda_2^4+\Gamma a^{-2}(a^6\lambda_1^4+\lambda_1^6\lambda_2^4)]d\lambda_2^2 = 0 \tag{D.2}$$

Equation (D.2) has an integrating factor $\lambda_1^{-4}\lambda_2^{-4}$ and after multiplication by the factor it becomes

$$d(\lambda_1^2-\lambda_2^2)-3a^6 d(\lambda_1^{-2}\lambda_2^{-2})+\Gamma a^{-2}d(\lambda_1^2\lambda_2^2)-3\Gamma a^4 d\lambda_1^{-2}-\Gamma a^4 d\lambda_2^{-2}=0 \tag{D.3}$$

Integrating the above equation and rearranging the result, we obtain

$$\frac{\lambda_1^2(\lambda_2^4+\Gamma a^4)+(3a^6-\lambda_1^4\lambda_2^2)(1+\Gamma a^{-2}\lambda_2^2)}{\lambda_1^2\lambda_2^2} = A \tag{D.4}$$

This is just equation (2.70).

APPENDIX E

DETERMINATION OF THE CONSTANT OF INTEGRATION B

The equilibrium condition in the axial direction can be expressed in the following form

$$2\pi\Lambda_2 r N_1 \Big|_{z_\alpha = L_\alpha} = F + \int 2\pi p\rho \cos\phi dS \tag{E.1}$$

Noting that

$$\cos\phi = -\frac{d\rho}{dS} \tag{E.2}$$

and p=const, we have

$$\Lambda_2 N_1 \Big|_{z_\alpha = L_\alpha} = -\frac{1}{2} pr\Lambda_2^2 + -\frac{F}{2\pi r} - -\frac{1}{2} pr \tag{E.3}$$

At $z_\alpha = L_\alpha$, equation (2.67) can be written in the form

$$\Lambda_2 N_1 \Big|_{z_\alpha = L_\alpha} = -\frac{1}{2} pr\Lambda_2^2 + B/r \tag{E.4}$$

Thus, we obtain

$$B = -\frac{F}{2\pi} - -\frac{1}{2} pr^2 \tag{E.5}$$

APPENDIX F

PROGRAM 1

```
00010C LARGE SPACE STRUC., YU001, P=PARAM(3), C3=0.0
00020 PROGRAM LSS(INPUT, OUTPUT, TAPE1=INPUT )
00030 DIMENSION C(3,11), PARAM(3), ERROR(3), PARERR(3), W(3,34),
00040+  QT(5),DL(11),R1(11),F1(11),D(3),FUN(3)
00050 COMMON QT,C1,C2,FA,RO,PN,SPA,QY8,C3
00060 EXTERNAL AUX, BCAUX, RNAUX, AUF, PROFILE
00070 DATA NOUT/6/
00080 CALL X04AAF(1,NOUT)
00090 CALL X04ABF(1,NOUT)
00100 TO=293.0
00110 RO=1.0
00120 HO=0.03
00130 MC=4
00140 DEN=940.0
00150 RC=8.31
00160CPN=0.0
00170 N=3
00180 N1=3
00190 IW=34
00200 M1=11
00210 PARAM(1)=2.35
```

```
00220 PARAM(2)=2.71

10230 PARAM(3)=0.00210

00240 PARERR(1)=1.0E-8

00250 PARERR(2)=1.0E-8

00260 PARERR(3)=1.0E-8

00270 ERROR(1)=1.0E-8

00280 ERROR(2)=1.0E-8

00290 ERROR(3)=1.0E-8

00300 T1=343.0

00310 WRITE(NOUT,116)  T1

00320 CM=0.5*RC*DEN/FLOAT(MC)*1.0E-6

00330 C1=T0*CM

00340 C3=0.06

00350 C2=C3*C1

00360 WRITE(NOUT,104)C1,C2

00370 FA=150.0

00380 CALL AUF(QT, T0, T1, H0)

00390 WRITE(NOUT,108) (QT(I),I=1,5)

00400 DO 81 I1=1,7
```

```
00410 SPA=2.4
00420 SPA=SPA-FLOAT(I1)*0.2
00430 WRITE(NOUT,111) SPA
00440 IFAIL=001
00450 CALL D02HBF(PARAM, N1,PARERR, ERROR, N, C, M1, AUX,
00460+  BCAUX, RNAUX, W,  IW, IFAIL)
00470 IF (IFAIL.EQ.0) GO TO 11
00480 WRITE (NOUT, 110) IFAIL
00490 IF (IFAIL.GT.5.OR.IFAIL.EQ.1) GO TO 31
00500 WRITE (NOUT, 120) W(1,2), (W(I,1),I=1,N)
00510 GO TO 31
00520 11  PM=582.5*PARAM(3)
00530 WRITE(NOUT,125) PM
00540 WRITE (NOUT,130) (PARAM(I),I=1,N)
00550 WRITE(NOUT,140)
00560 CALL RNAUX(X,X1,PARAM)
00570 H=(X1-X)/FLOAT(M1-1)
00580 DO 21 I=1,M1
00590      DUM=X+FLOAT(I-1)*H
```

```
00600 WRITE(NOUT, 150) DUM, (C(J,I),J=1,N)
00610 21  CONTINUE
00620 DO 61 I=1,M1
00630 F1(I)=RO*SQRT(C(1,I)**2-C(3,I)**2)
00640 R1(I)=C(2,I)
00650 61  CONTINUE
00660 WRITE(NOUT,115)
00670 CALL PROFILE(RO,H,C,M1,DL,F1,PARAM(3))
00680 DO 41 I=1,M1
00690 DUM=X+FLOAT(I-1)*H
00700 WRITE (NOUT,160) DUM,R1(I),DL(I)
00710 41  CONTINUE
00720 WRITE (NOUT,170)
00730 DO  55 I=1,M1
00740 DUM=X+FLOAT(I-1)*H
00750 TN1=QT(5)*(C(1,I)/C(2,I)-QT(4)**6/C(1,I)**3/C(2,I)**3)
00760+  *(C1+C2*C(2,I)**2*QT(4)**(-2))*58.25
00770 TN2=QT(5)*(C(2,I)/C(1,I)-QT(4)**6/C(1,I)**3/C(2,I)**3)
00780+  *(C1+C2*C(1,I)**2*QT(4)**(-2))*58.25
```

```
00790 WRITE (NOUT,160) DUM,TN1,TN2
00800 55  CONTINUE
00810 PARA3=1.0-QT(4)**6/C(1,1)**4/C(2,1)**2
00820 PARA4=SQRT(C(1,1)**2-C(3,1)**2)
00830 PARA5=C1+C2*C(2,1)**2*QT(4)**(-2)
00840 FC=9.27*2.0*3.1415927*QT(5)*RO*PARA4*PARA5*PARA3
00850 WRITE(NOUT,109) FC
00860 FB=0.01854*3141.5927*C(2,M1)*QT(5)*(C(1,M1)/C(2,M1)-QT(4)**6/
00870+  C(1,M1)**3/C(2,M1)**3)*(C1+C2*C(2,M1)**2*QT(4)**(-2))
00880 WRITE(NOUT,185) FB
00890 31  CONTINUE
00900 81 CONTINUE
00910 91  CONTINUE
00920 101  FORMAT(F8.4)
00930 100  FORMAT(4(1X/),20H LSS PROGRAM RESULTS/1X,3F12.4)
00940 104  FORMAT(1X,4H C1=,F8.4,6X,4H C2=,F8.4)
00950 106  FORMAT(2(1X/),4H PN=,F8.5,/1X)
00960 108  FORMAT(1X,7H QT(I)=,/1X,5F12.5,/1X)
00970 109  FORMAT(3X,5H FA= ,F10.3)
```

```
00980 110  FORMAT(4X,9H0IFAIL = , I3)
00990 111  FORMAT(1X,8H  G1(2)=,F6.3)
01000 115  FORMAT(4X,30H X-VALUE     PROFILE OF STRUC.)
01010 116 FORMAT(3(1X/),4H T1=,F8.2)
01020 120  FORMAT(10H W(1,2) = , F9.4, 10H W(I,1) = ,
01030+       3E10.3)
01040 125  FORMAT(2X,5H  PN=,F8.5)
01050 130  FORMAT(4X,17H0FINAL PARAMETERS/1X, 3F10.5)
01060 140  FORMAT(4X,15H0FINAL SOLUTION/4X,
01070+       35H X-VALUE     COMPONENTS OF SOLUTION )
01080 150  FORMAT(1H ,F10.5,3F10.5)
01090 160  FORMAT (1H ,F10.5,2F10.5)
01100 170 FORMAT(4X,24H X-VALUE          STRESS)
01110 185 FORMAT(3X,5H FB= ,F10.3,/1X)
01120 168  FORMAT(1X,4F12.8,/1X)
01130 169 FORMAT(1X,3F10.5)
01140 END
01150 SUBROUTINE AUX(X, Y, F, PARAM)
01160 DIMENSION  Y(3),F(3),PARAM(3),QT(5)
```

```
01170 COMMON QT,C1,C2,FA,RO,PN,SPA,QY8,C3
01180 QX=Y(1)**2-Y(3)**2
01190CIF(QX.GE.0.0) GO TO 15
01200CQY1=0.6
01210CGO TO 25
01220 QY1=SQRT(QX)
01230C25  CONTINUE
01240 QY2=1.0+C3*Y(2)**2*QT(4)**(-2)
01250 QY4=Y(1)**4*Y(2)**2+3.0*QT(4)**6
01260 QY3=1.0+C3*Y(1)**2*QT(4)**(-2)
01270 QY6=Y(1)/Y(2)-QT(4)**6/(Y(1)**3)/(Y(2)**3)
01280 QY7=Y(2)/Y(1)-QT(4)**6/(Y(1)**3)/(Y(2)**3)
01290 QY8=1.0/Y(1)-3.0*QT(4)**6/Y(1)**3/Y(2)**4-C3*Y(1)
01300+     *QT(4)**(-2)-C3*QT(4)**4/Y(1)/Y(2)**4
01310 S1=Y(1)**4*Y(2)**3*Y(3)/QY4/QY2*QY8
01320 F(1)=S1
01330 F(2)=Y(3)
01340 F(3)=S1*Y(3)/Y(1)+QX*QY3*QY7/QY6/QY2/Y(2)
01350+  -10.0*PARAM(3)*RO*Y(1)*QY1/QT(5)/QY6/QY2/C1
```

```
01360 RETURN

01370 END

01380 SUBROUTINE AUF(QT,TO,T,HO)

01390 DIMENSION QT(5)

01400CCOMMON QT(5)

01410 ALPH1B(T)=2.38*1.0E-5+TANA*(T-TO)

01420 ALPH2A(T)=13.7*1.0E-5+(T-253.0)*TANC

01430 ALPH2B(T)=(T-163.0)*TAND

01440 TANA=(2.38-1.0)*1.0E-5/130.0

01450 TANC=(40.3-13.7)*1.0E-7

01460 TAND=(13.7*1.0E-5-20.0*TANC)/70.0

01470 IF (T.GE.293.0) GO TO 10

01480 QT(1)=0.5*(T-TO)*(ALPH1B(T)+ALPH1B(TO))

01490 GO TO 20

01500 10  ALPH1A=2.38*1.0E-5

01510 QT(1)=ALPH1A*(T-TO)

01520 20  IF (T.GE.233.0) GO TO 30

01530 QT(2)=0.5*(T-233.0)*(ALPH2B(T)+ALPH2A(233.0))

01540+  -(TO-233.0)*(ALPH2A(TO)+ALPH2A(233.0))
```

```
01550 GO TO 40
01560 30  QT(2)=0.5*(T-TO)*(ALPH2A(T)+ALPH2A(TO))
01570 40  QT(3)=EXP(QT(1))
01580 QT(4)=EXP(QT(2))
01590 QT(5)=2.0*HO*T*QT(4)**(-3)/TO
01600 RETURN
01610 END
01620 SUBROUTINE RNAUX(X,X1,PARAM)
01630 DIMENSION PARAM(3)
01640 X=0.0
01650 X1=1.0
01660 RETURN
01670 END
01680 SUBROUTINE BCAUX(G,G1,PARAM)
01690 DIMENSION G(3),G1(3),PARAM(3),QT(5)
01700 COMMON QT,C1,C2,FA,RO,PN,SPA
01710 G(1)=PARAM(1)
01720 G(2)=QT(3)
01730 ZL=G(1)**2-(FA/1000.0/2.0/3.1415927/QT(5)/(1.0-QT(4)**6
```

```
01740+  /G(1)**4/G(2)**2)/(C1+C2*G(2)**2*QT(4)**(-2)))**2
01750 G(3)=SQRT(ZL)
01760 G1(1)=PARAM(2)
01770 G1(2)=SPA
01780 G1(3)=0.0
01790 RETURN
01800 END
01810 SUBROUTINE PROFILE (RO,H,A,M1,DL,F1,PAR)
01820 DIMENSION DL(M1),F1(M1),QT(5),A(3,M1)
01830 COMMON QT,C1,C2,FA,SO,PN,SPA
01840 DL(1)=0.0
01850 DO 51 I=2,M1
01860 DL(I)=DL(I-1)+H/2.0*(F1(I-1)+F1(I))
01870 51  CONTINUE
01880 RETURN
01890 END
```

APPENDIX G

PROGRAM 2

```
00010C LARGE SPACE STRUC., YU020, P=PARAM
00020 PROGRAM LSS(INPUT, OUTPUT, TAPE1=INPUT )
00030 DIMENSION C(1,11), PARAM(1), ERROR(1), PARERR(1), W(1,28),
00040+  QT(5),DL(11),R1(11),F1(11),CX(11),CY(11)
00050 COMMON QT,FA,P,C3,A
00060 EXTERNAL AUX, BCAUX, RNAUX, AUF, PROFILE, SRM
00070 DATA NOUT/6/
00080 WRITE(NOUT, 100)
00090 CALL X04AAF(1,NOUT)
00100 CALL X04ABF(1,NOUT)
00110 T0=293.0
00120 FA=1.4
00130 N=1
00140 N1=1
00150 IW=28
00160 M1=11
00170 PARAM(1)=2.0
00180 PARERR(1)=1.0E-8
00190 ERROR(1)=1.0E-8
00200 T1=293.0
00210 C3=0.05
```

```
00220 WRITE(NOUT,110)  T1, FA, C3
00230 CALL AUF(QT, T0, T1)
00240 WRITE(NOUT,130) (QT(I),I=1,5)
00250 DO 81 I1=1,15
00260 SPA=2.0
00270 SPA=SPA+FLOAT(I1)*0.2
00280 A=((1.0+C3)*(3.0-SPA**4)+C3*SPA**2)/(SPA**2)
00290 WRITE(NOUT,140) A
00300 IFAIL=001
00310 CALL D02HBF(PARAM, N1,PARERR, ERROR, N, C, M1, AUX,
00320+  BCAUX, RNAUX, W,  IW, IFAIL)
00330 IF (IFAIL.EQ.0) GO TO 11
00340 WRITE (NOUT, 150) IFAIL
00350 IF (IFAIL.GT.5.OR.IFAIL.EQ.1) GO TO 31
00360 WRITE (NOUT, 160) W(1,2), (W(I,1),I=1,N)
00370 GO TO 31
00380 11  WRITE(NOUT,170) P
00390 WRITE (NOUT,180) PARAM(1)
00400 WRITE(NOUT,190)
00410 CALL RNAUX(X,X1,PARAM)
00420 H=(X1-X)/FLOAT(M1-1)
00430 DO 21 I=1,M1
00440      DUM=X+FLOAT(I-1)*H
00450 CALL SRM(CX(I), C(1,I), QT(4), C3, A)
```

```
00460 CALL AUX(DUM, C(1,I), CY(I), PARAM(1))
00470 WRITE(NOUT, 200) DUM, CX(I), C(1,I)
00480 21  CONTINUE
00490 DO 61 I=1,M1
00500 F1(I)=SQRT(CX(I)**2-CY(I)**2)
00510 R1(I)=C(1,I)
00520 61  CONTINUE
00530 WRITE(NOUT,210)
00540 CALL PROFILE(H,M1,DL,F1)
00550 DO 41 I=1,M1
00560 DUM=X+FLOAT(I-1)*H
00570 WRITE (NOUT,220) DUM,R1(I),DL(I)
00580 41  CONTINUE
00590 WRITE (NOUT,230)
00600 DO  55 I=1,M1
00610 DUM=X+FLOAT(I-1)*H
00620 TN1=QT(5)*(CX(I)/C(1,I)-QT(4)**6/CX(I)**3/C(1,I)**3)
00630+  *(1.0+C3*C(1,I)**2*QT(4)**(-2))
00640 TN2=QT(5)*(C(1,I)/CX(I)-QT(4)**6/CX(I)**3/C(1,I)**3)
00650+  *(1.0+C3*CX(I)**2*QT(4)**(-2))
00660 WRITE (NOUT,220) DUM,TN1,TN2
00670 55  CONTINUE
00680 31  CONTINUE
00690 81 CONTINUE
```

```
100  FORMAT(4(1X/),20H LSS PROGRAM RESULTS/1X,3F12.4)
110  FORMAT(3(1X/),4H T1=,F8.2,4H FA=,F8.4,7H GAMMA=,F8.4)
130  FORMAT(1X,7H QT(I)=,/1X,5F12.5,/1X)
150  FORMAT(4X,9H0IFAIL = , I3)
140  FORMAT(1X,4H  A=,F8.3)
160  FORMAT(10H W(1,2) = , F9.4, 10H W(I,1) = ,
+       3E10.3)
170  FORMAT(2X,4H  P=,F8.5)
180  FORMAT(4X,17H0FINAL PARAMETERS/1X, 1F10.5)
190  FORMAT(4X,15H0FINAL SOLUTION/4X,
+       35H X-VALUE     COMPONENTS OF SOLUTION )
200  FORMAT(1H ,3F10.5)
210  FORMAT(4X, 30H X-VALUE     PROFILE OF STRUC.)
220  FORMAT (1H ,F10.5,2F10.5)
230 FORMAT(4X,24H X-VALUE          STRESS)
END
SUBROUTINE AUX(X, Y, F, PARAM)
DIMENSION  Y(1),F(1),PARAM(1),QT(5)
COMMON QT,FA,P,C3,A
QY1(V)=1.0+C3*V**2*QT(4)**(-2)
QY2(V,W)=W/V-QT(4)**6/(W**3)/(V**3)
CALL SRM(Z,Y(1),QT(4),C3,A)
CALL SRM(Z1,PARAM(1),QT(4),C3,A)
PS=PARAM(1)**2-1.0
```

```
00940 P=2.0*(QT(5)*PARAM(1)*QY2(PARAM(1),Z1)*QY1(PARAM(1))-FA)/PS
00950 QY3=((P*Y(1)**2+2.0*FA-P)/2.0/Y(1)/QT(5))**2
00960 F(1)=Z*SQRT(ABS(1.0-QY3/(QY2(Y(1),Z)**2)/(QY1(Y(1))**2)))
00970 RETURN
00980 END
00990 SUBROUTINE AUF(QT,TO,T)
01000 DIMENSION QT(5)
01010 ALPH1B(T)=2.38*1.0E-5+TANA*(T-TO)
01020 ALPH2A(T)=13.7*1.0E-5+(T-253.0)*TANC
01030 ALPH2B(T)=(T-163.0)*TAND
01040 TANA=(2.38-1.0)*1.0E-5/130.0
01050 TANC=(40.3-13.7)*1.0E-7
01060 TAND=(13.7*1.0E-5-20.0*TANC)/70.0
01070 IF (T.GE.293.0) GO TO 10
01080 QT(1)=0.5*(T-TO)*(ALPH1B(T)+ALPH1B(TO))
01090 GO TO 20
01100 10  ALPH1A=2.38*1.0E-5
01110 QT(1)=ALPH1A*(T-TO)
01120 20  IF (T.GE.233.0) GO TO 30
01130 QT(2)=0.5*(T-233.0)*(ALPH2B(T)+ALPH2A(233.0))
01140+  -(TO-233.0)*(ALPH2A(TO)+ALPH2A(233.0))
01150 GO TO 40
01160 30  QT(2)=0.5*(T-TO)*(ALPH2A(T)+ALPH2A(TO))
01170 40  QT(3)=EXP(QT(1))
```

```
01180 QT(4)=EXP(QT(2))
01190 QT(5)=T*QT(4)**(-3)/TO
01200 RETURN
01210 END
01220 SUBROUTINE RNAUX(X,X1,PARAM)
01230 DIMENSION PARAM(1)
01240 X=0.0
01250 X1=1.0
01260 RETURN
01270 END
01280 SUBROUTINE BCAUX(G,G1,PARAM)
01290 DIMENSION G(1),G1(1),PARAM(1),QT(5)
01300 COMMON QT
01310 G(1)=QT(3)
01320 G1(1)=PARAM(1)
01330 RETURN
01340 END
01350 SUBROUTINE PROFILE (H,M1,DL,F1)
01360 DIMENSION DL(M1),F1(M1)
01370 DL(1)=0.0
01380 DO 51 I=2,M1
01390 DL(I)=DL(I-1)+H/2.0*(F1(I-1)+F1(I))
01400 51  CONTINUE
01410 RETURN
```

```
01420 END
01430 SUBROUTINE SRM(Z,Y,QC,C3,A)
01440 QZ1=Y**4-A*Y**2+C3*QC**4
01450 QZ2=1.0+C3*QC**(-2)*Y**2
01460 QZ3=QZ1**2+12.0*QC**6*Y**2*QZ2**2
01470 QZ4=SQRT(QZ3)
01480 QZ5=(QZ1+QZ4)/(2.0*Y**2*QZ2)
01490 Z=SQRT(QZ5)
01500 RETURN
01510 END
```

APPENDIX H

PROGRAM 3

```
00010C  APPROXIMATE METHOD, YU021
00020 PROGRAM AM(IMPUT, OUTPUT)
00030 DIMENSION X(3), WK(36), PAR(4)
00040 EXTERNAL FCN
00050 DATA NOUT/6/
00060 N=3
00070 NSIG=4
00080 ITMAX=100
00090 F=1.391
00100 C3=0.05
00110 SL0=1.0
00120 WRITE (NOUT, 80) F, C3, SL0
00130 DO 13 I=1,10
00140 DO 12 K=1,15
00150 X(1)=2.61
00160 X(2)=1.0
00170 X(2)=X(2)+FLOAT(K-1)*0.02
00180 X(3)=2.24
00190CDO 12 I=1,10
00200 R=2.20
00210 R=R+FLOAT(I-1)*0.1
```

```
00220 WRITE (NOUT, 90) R
00230 PAR(1)=R
00240 PAR(2)=F
00250 PAR(3)=C3
00260 PAR(4)=SLO
00270 CALL ZSPOW(FCN, NSIG, N, ITMAX, PAR, X, FNORM, WK, IER)
00280 IF (IER.EQ.129) GO TO 10
00290 IF (IER.EQ.130) GO TO 10
00300 IF (IER.EQ.131) GO TO 10
00310 WRITE (NOUT, 100) (X(J), J=1,3)
00320 SN1=(X(1)/PAR(1)-1.0/(X(1)**3*PAR(1)**3))*
00330+  (1.0+PAR(1)**2*PAR(3))
00340 SN2=(PAR(1)/X(1)-1.0/(PAR(1)**3*X(1)**3))
00350+  *(1.0+X(1)**2*PAR(3))
00360 WRITE (NOUT, 105) SN1,SN2
00370 GO TO 11
00380 10  CONTINUE
00390 WRITE (NOUT, 110) IER
00400 11  CONTINUE
00410 12  CONTINUE
00420 13 CONTINUE
00430 80  FORMAT (1X, 3H F=, F7.5,4X, 4H C3=, F7.5, 4X, 4H LO=, F7.5)
00440 90  FORMAT (2(2X/), 3H R=, F7.5)
00450 100 FORMAT (4X, 4H X1=, F7.4, 4X, 4H X2=, F7.4, 4X, 4H X3=, F7.4)
```

```
105 FORMAT (4X, 4H N1=, F8.5, 4X, 4H N2=, F8.5)
110 FORMAT (1X, 5H IER=, I3)
END
SUBROUTINE FCN(X, F, N, PAR)
DIMENSION X(N), F(N), PAR(4)
F(1)=(X(1)/PAR(1)-1.0/(X(1)**3*PAR(1)**3))*(1.0+PAR(3)*PAR(1)**2)
+     -(2.0*PAR(2)+X(2)*(PAR(1)**2-1.0))/2.0/PAR(1)
F(2)=(PAR(1)/X(1)-1.0/(X(1)**3*PAR(1)**3))*(1.0+PAR(3)*X(1)**2)-
+     2.0*PAR(1)*(PAR(1)/(PAR(1)**2-1.0)-(PAR(1)-1.0)/
+     ((PAR(1)-1.0)**2+X(3)**2))*(X(1)/PAR(1)-1.0/(X(1)**3*PAR(1)
+     **3))*(1.0+PAR(3)*PAR(1)**2)+2.0*PAR(2)*PAR(1)/(PAR(1)**2- +
    1.0)
F(3)=3.0*X(3)**5-3.0*PAR(4)*X(1)*X(3)**4+6.0*(PAR(1)-1.0)**2*X(3)
+     **3-6.0*PAR(4)*X(1)*(PAR(1)-1.0)**2*X(3)**2+3.0*(PAR(1)-1.0)
+     **4*X(3)+2.0*PAR(4)**3*X(1)**3*(PAR(1)-1.0)**2-3.0*PAR(4)
+     *X(1)*(PAR(1)-1.0)**4
RETURN
END
```

APPENDIX I

PROGRAM 4

```
00010C  APPROXIMATE METHOD, YU032, INSTABILITY
00020 PROGRAM AM(IMPUT, OUTPUT)
00030 DIMENSION X(5), WK(75), PAR(3), Y(2), Z(3), G(5)
00040 EXTERNAL FCN, ALG
00050 DATA NOUT/6/
00060 N=5
00070 M1=2
00080 M2=3
00090 NSIG=4
00100 ITMAX=100
00110 F=1.391
00120 C3=0.02
00130 SLO=1.0
00140 DO 13 K=1,20
00150 F=2.60
00160 F=F+FLOAT(K-1)*0.05
00170 WRITE (NOUT, 80) SLO, F, C3
00180 DO 12 J=1,6
00190 X(2)=1.75
00200 X(2)=X(2)+FLOAT(J-1)*0.04
00210 X(1)=2.45
```

```
00220 X(3)=2.25
00230 PAR(1)=SLO
00240 PAR(2)=F
00250 PAR(3)=C3
00260 Z(1)=X(1)
00270 Z(2)=X(2)
00280 Z(3)=X(3)
00290 CALL ALG(Y, Z, G, N, M1, M2, PAR)
00300 X(4)=Y(1)
00310 X(5)=Y(2)
00320 CALL ZSPOW(FCN, NSIG, N, ITMAX, PAR, X, FNORM, WK, IER)
00330 IF (IER.EQ.129) GO TO 10
00340 IF (IER.EQ.130) GO TO 10
00350 IF (IER.EQ.131) GO TO 10
00360 WRITE (NOUT, 100) (X(I), I=1,N)
00370 PMAX=2.0/(X(2)**2-1.0)*(X(2)*(X(1)/X(2)-1.0/(X(1)**3*
00380+     X(2)**3))*(1.0+PAR(3)*X(2)**2)-PAR(2))
00390 WRITE (NOUT, 105) PMAX
00400 GO TO 11
00410 10  CONTINUE
00420CWRITE (NOUT, 110) IER
00430 11  CONTINUE
00440 12  CONTINUE
00450 13  CONTINUE
```

```
00460 80  FORMAT (1X, 5H SLO=, F7.5, 4X, 3H F=, F7.5, 4X, 4H C3=, F7.5)
00470 100 FORMAT (2X, 4H X1=, F7.4, 3X, 4H X2=, F7.4, 3X, 4H X3=, F7.4,
00480+            3X, 4H X4=, F7.4, 3X, 4H X5=, F7.4)
00490 105 FORMAT (12X, 4H PM=, F7.4)
00500 110 FORMAT (1X, 5H IER=, I3)
00510 END
00520 SUBROUTINE FCN(X, F, N, PAR)
00530 DIMENSION X(N), F(N), PAR(3), Y(2)
00540 F(1)=-4.0*X(2)/(X(2)**2-1.0)**2*((X(1)-1.0/(X(1)**3*X(2)**2))*
00550+     (1.0+PAR(3)*X(2)**2)-PAR(2))+4.0/(X(2)**2-1.0)*((1.0+PAR(3)
00560+     *X(2)**2)/(X(1)**3*X(2)**3)+(X(1)-1.0/(X(1)**3*X(2)**2))*X(2)
00570+     *PAR(3))+X(4)*((1.0/X(1)+3.0/(X(1)**3*X(2)**4))*(1.0+PAR(3)
00580+     *X(1)**2)-2.0*PAR(2)*(X(2)**2+1.0)/(X(2)**2-1.0)**2-2.0*
00590+     (-(X(2)**2+1.0)/(X(2)**2-1.0)**2+((X(2)-1.0)**2-X(3)**2)/
00600+     ((X(2)-1.0)**2+X(3)**2)**2)*(X(1)-1.0/(X(1)**3*X(2)**2))*
00610+     (1.0+PAR(3)*X(2)**2)-4.0/(X(1)**3*X(2)**3)*(X(2)/(X(2)**2-
00620+     1.0)-(X(2)-1.0)/((X(2)-1.0)**2+X(3)**2))*(1.0+PAR(3)*X(2)
00630+     **2)-4.0*PAR(3)*X(2)*(X(2)/(X(2)**2-1.0)-(X(2)-1.0)/((X(2)
00640+     -1.0)**2+X(3)**2))*(X(1)-1.0/(X(1)**3*X(2)**2)))+X(5)*(12.0
00650+     *(X(2)-1.0)*X(3)**3-12.0*PAR(1)*X(1)*(X(2)-1.0)*X(3)
00660+     **2+12.0*(X(2)-1.0)**3*X(3)-12.0*PAR(1)*X(1)*(X(2)-1.0)**3
00670+     +4.0*PAR(1)**3*X(1)**3*(X(2)-1.0))
00680 F(2)=(X(2)/X(1)-1.0/(X(1)**3*X(2)**3))*(1.0+PAR(3)*X(1)**2)-
00690+     2.0*X(2)*(X(2)/(X(2)**2-1.0)-(X(2)-1.0)/((X(2)-1.0)**2+X(3)
```

```
00700+      **2))*(X(1)/X(2)-1.0/(X(1)**3*X(2)**3))*(1.0+PAR(3)*X(2)**2)
00710+      +2.0*PAR(2)*X(2)/(X(2)**2-1.0)
00720 F(3)=3.0*X(3)**5-3.0*PAR(1)*X(1)*X(3)**4+6.0*(X(2)-1.0)**2*X(3)
00730+      **3-6.0*PAR(1)*X(1)*(X(2)-1.0)**2*X(3)**2+3.0*(X(2)-1.0)**4
00740+      *X(3)+2.0*PAR(1)**3*X(1)**3*(X(2)-1.0)**2-3.0*PAR(1)*X(1)*
00750+      (X(2)-1.0)**4
00760 F(4)=2.0/(X(2)**2-1.0)*(1.0+3.0/(X(1)**4*X(2)**2))*(1.0+PAR(3)*
00770+      X(2)**2)+X(4)/X(1)**2*(-X(2)+3.0/(X(1)**2*X(2)**3))*(1.0
00780+      +PAR(3)*X(1)**2)+2.0*PAR(3)*X(4)*(X(2)-1.0/(X(1)**2*X(2)
00790+      **3))-2.0*X(2)*X(4)*(X(2)/(X(2)**2-1.0)-(X(2)-1.0)/((X(2)
00800+      -1.0)**2+X(3)**2))*(1.0/X(2)+3.0/(X(1)**4*X(2)**3))*(1.0
00810+      +PAR(3)*X(2)**2)+X(5)*(-3.0*PAR(1)*X(3)**4-6.0*PAR(1)*(
00820+      X(2)-1.0)**2*X(3)**2+6.0*PAR(1)**3*X(1)**2*(X(2)-1.0)**2-3.0
00830+      *PAR(1)*(X(2)-1.0)**4)
00840 F(5)=X(4)*(-4.0*X(2)*(X(2)-1.0)*X(3)*(X(1)/X(2)-          +
     1.0/(X(1)**3*X(2)**3))
00850+      *(1.0+PAR(3)*X(2)**2)/((X(2)-1.0)**2+X(3)**2)**2)+X(5)*(
00860+      15.0*X(3)**4-12.0*PAR(1)*X(1)*X(3)**3+18.0*(X(2)-1.0)**2
00870+      *X(3)**2-12.0*PAR(1)*(X(2)-1.0)**2*X(1)*X(3)+3.0*(X(2)-1.0)
00880+      **4)
00890 RETURN
00900 END
00910 SUBROUTINE ALG(Y, Z, G, N, M1, M2, PAR)
00920 DIMENSION Y(M1), G(N), PAR(3), Z(M2)
```

```
G(2)=15.0*Z(3)**4-12.0*PAR(1)*Z(1)*Z(3)**3+18.0*(Z(2)-1.0)**2
+       *Z(3)**2-12.0*PAR(1)*Z(1)*(Z(2)-1.0)**2*Z(3)+3.0*(Z(2)
+       -1.0)**4
G(1)=-4.0*Z(2)*(Z(2)-1.0)*Z(3)/((Z(2)-1.0)**2+Z(3)**2)**2*
+       (Z(1)/Z(2)-1.0/(Z(1)**3*Z(2)**3))*(1.0+PAR(3)*Z(2)**2)
G(3)=2.0/(Z(2)**2-1.0)*((1.0+3.0/(Z(1)**4*Z(2)**2))*(1.0+
+       PAR(3)*Z(2)**2))
G(4)=(-Z(2)/Z(1)**2+3.0/(Z(1)**4*Z(2)**3))*(1.0+PAR(3)*Z(1)**2
+       )+(Z(2)/Z(1)-1.0/(Z(1)**3*Z(2)**3))*2.0*PAR(3)*Z(1)
+       -2.0*(Z(2)**2/(Z(2)**2-1.0)-Z(2)*(Z(2)-1.0)/((Z(2)-
+       1.0)**2+Z(3)**3))*(1.0/Z(2)+3.0/(Z(1)**4*Z(2)**3))*(1.0
+       +PAR(3)*Z(2)**2)
G(5)=-3.0*PAR(1)*Z(3)**4-6.0*PAR(1)*(Z(2)-1.0)**2*Z(3)**2+
+       6.0*PAR(1)**3*Z(1)**2*(Z(2)-1.0)**2-3.0*PAR(1)*(Z(2)-1.0)
+       **4
G6=G(2)*G(4)-G(1)*G(5)
Y(1)=-G(2)*G(3)/G6
Y(2)=G(1)*G(3)/G6
RETURN
END
```

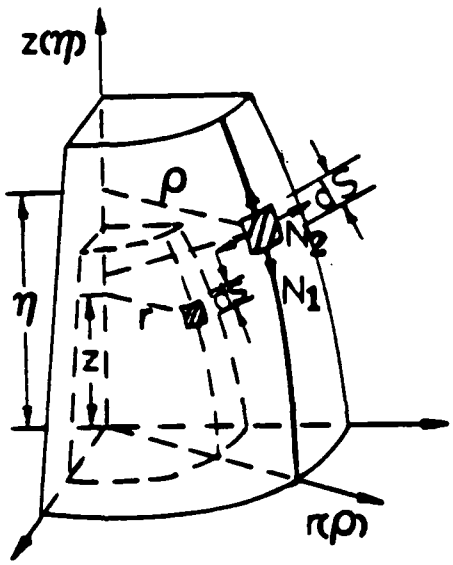

Fig. 1 Undeformed and deformed profile of axisymmetric membrane

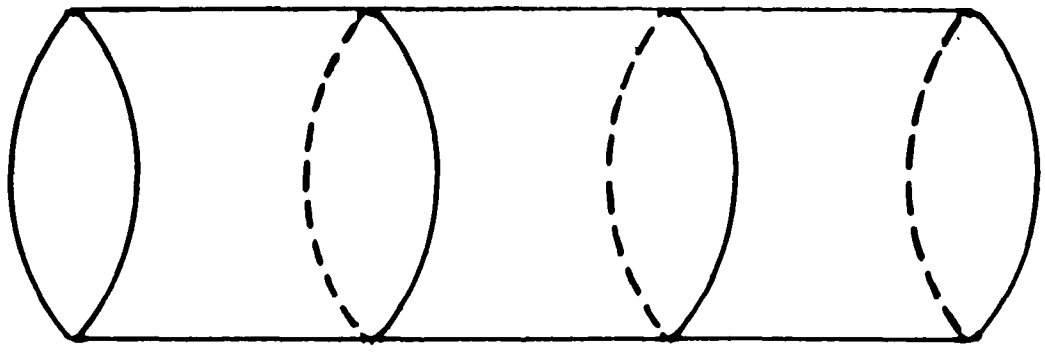

Figure 2. Cylindrical Membrane Shell
Reinforced by Cords.

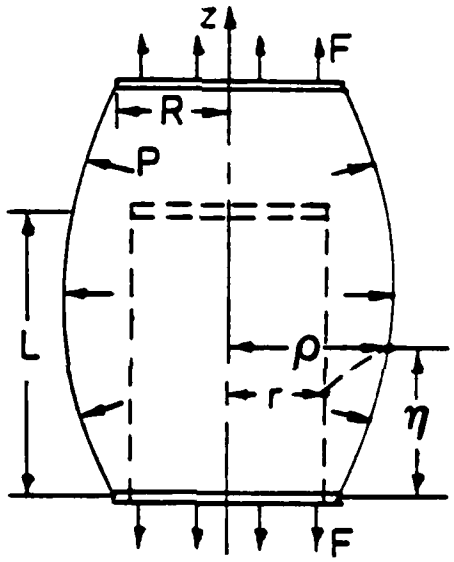

Fig. 3 Circular cylindrical membrane reinforced by flexible cords

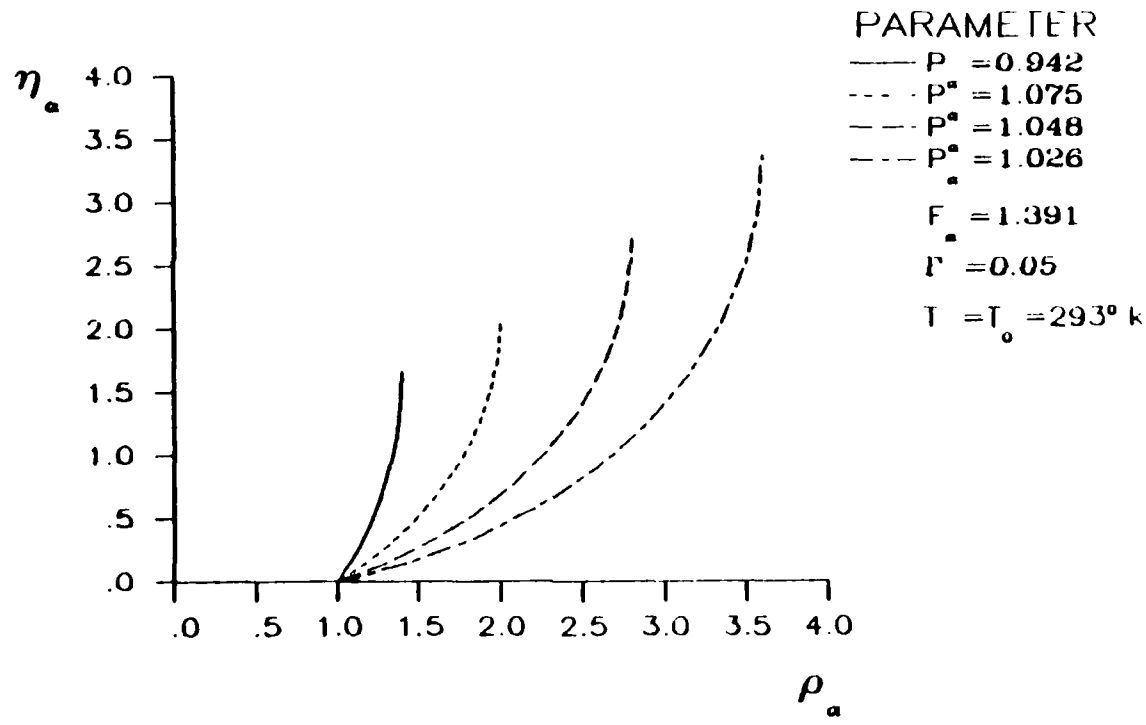

FIGURE 4. CHANGE OF DEFORMED PROFILE WITH PRESSURE.

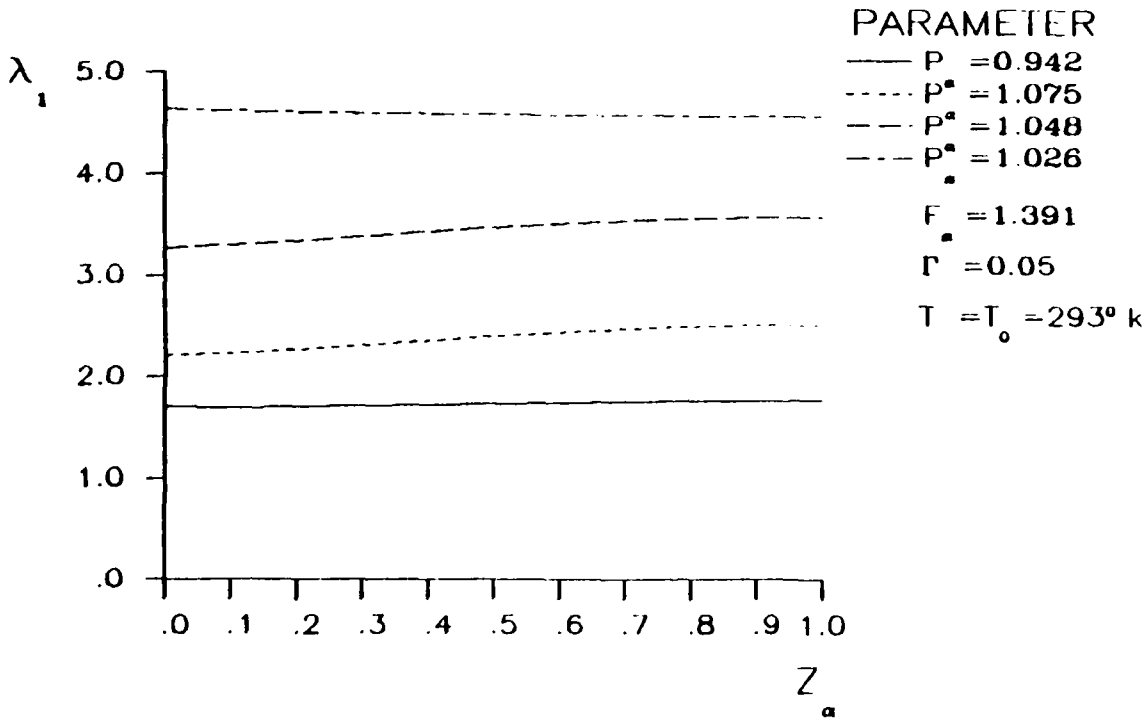

FIGURE 5. PRINCIPAL STRETCH RATIO IN THE MERIDIONAL DIRECTION.

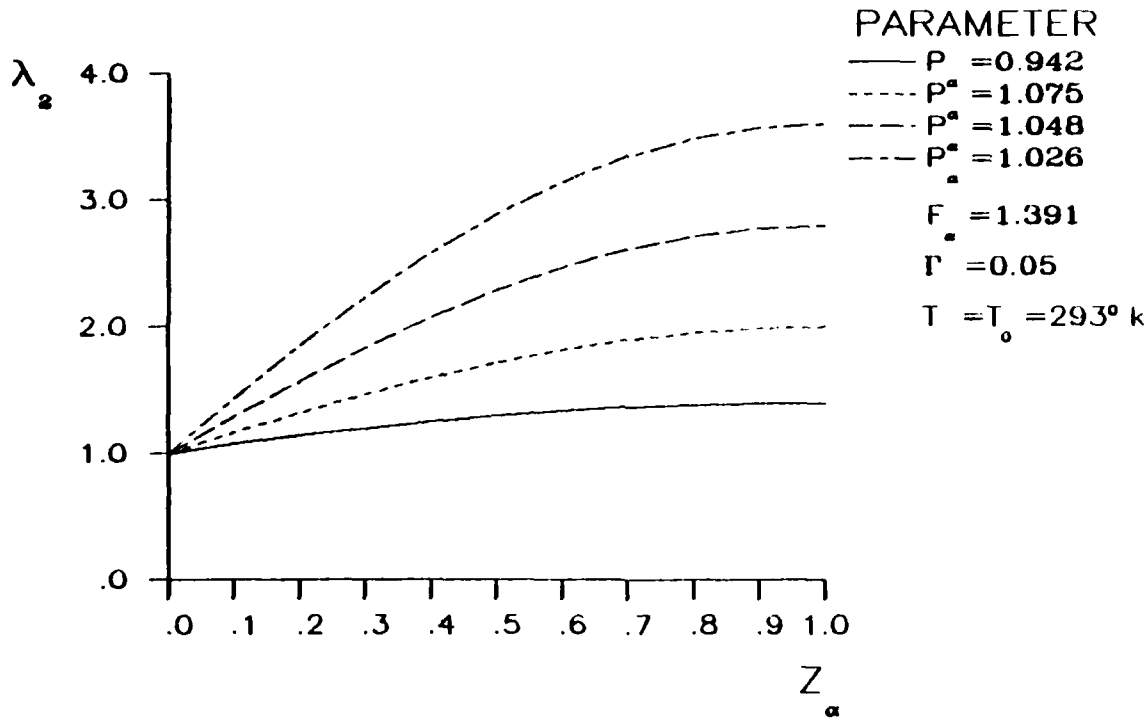

FIGURE 6. PRINCIPAL STRETCH RATIO IN THE CIRCUMFERENTIAL DIRECTION

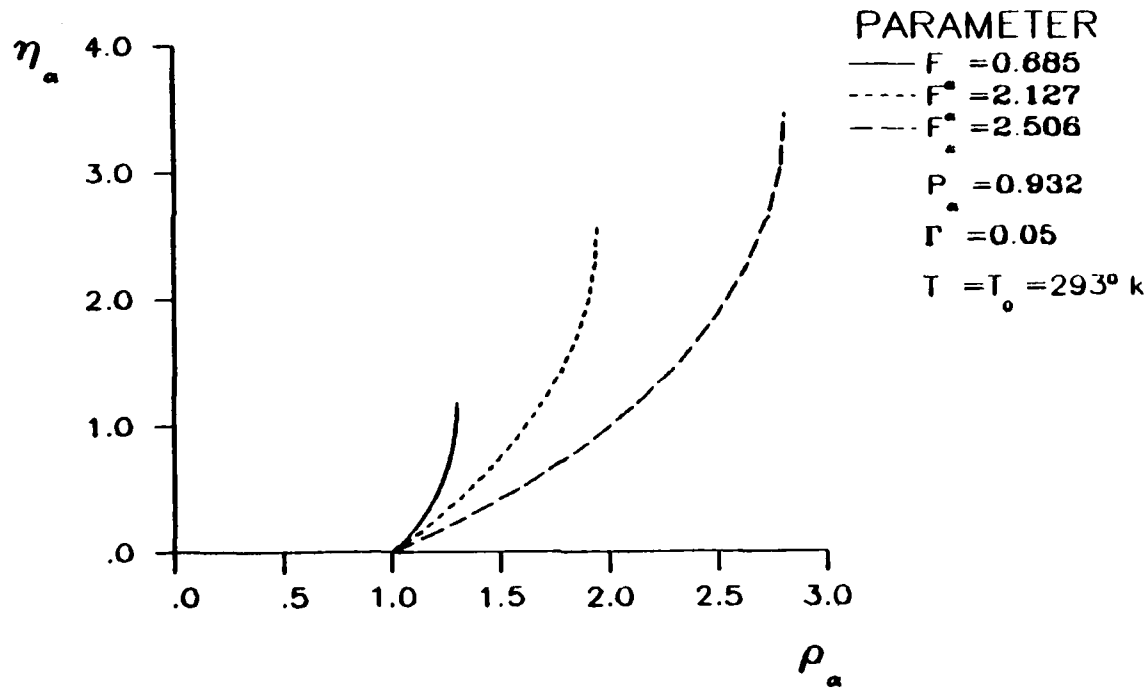

FIGURE 7. CHANGE OF DEFORMED PROFILE WITH AXIAL FORCE.

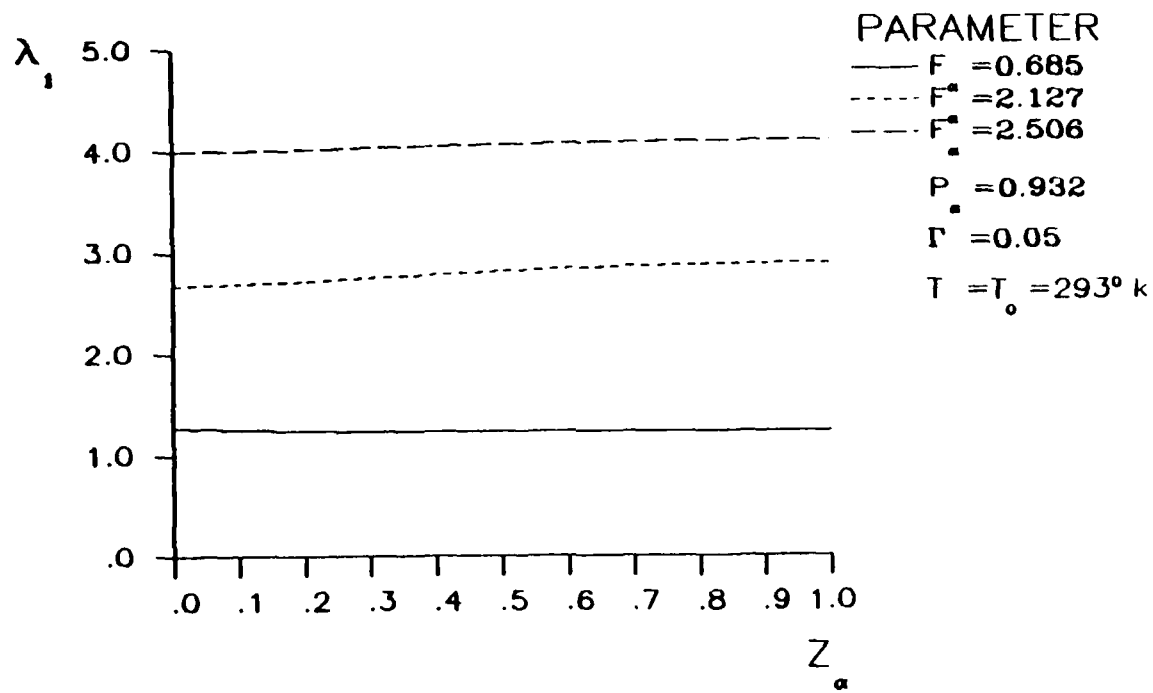

FIGURE 8. PRINCIPAL STRETCH RATIO IN THE MERIDIONAL DIRECTION.

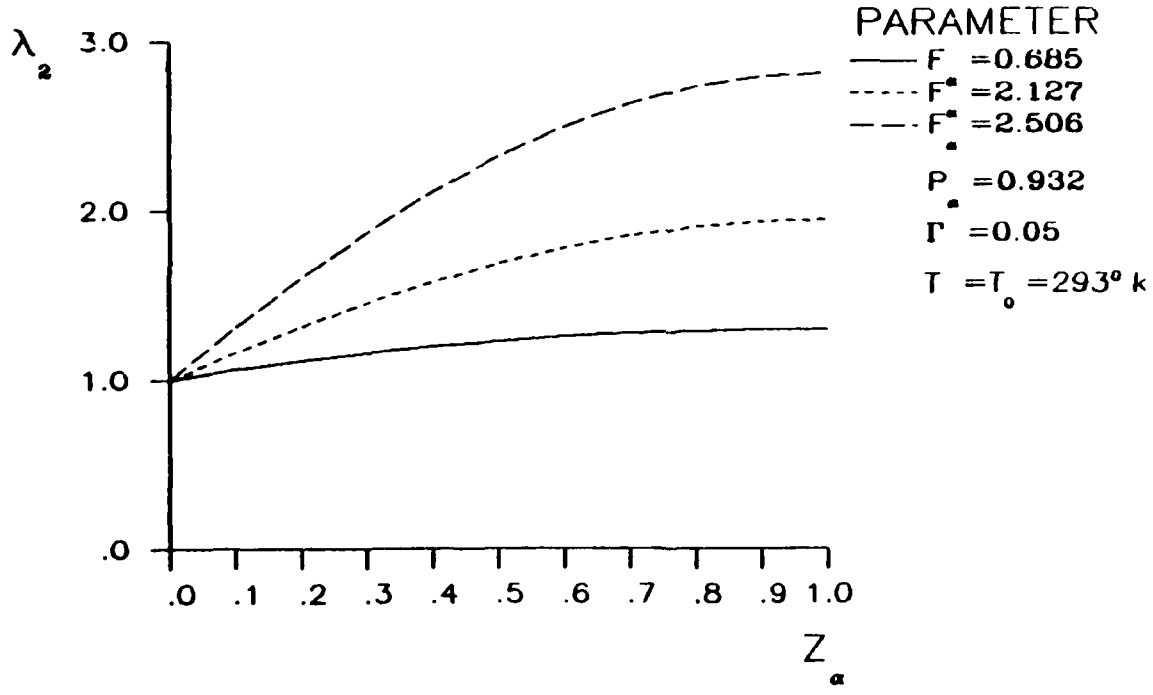

FIGURE 9. PRINCIPAL STRETCH RATIO IN THE CIRCUMFERENTIAL DIRECTION.

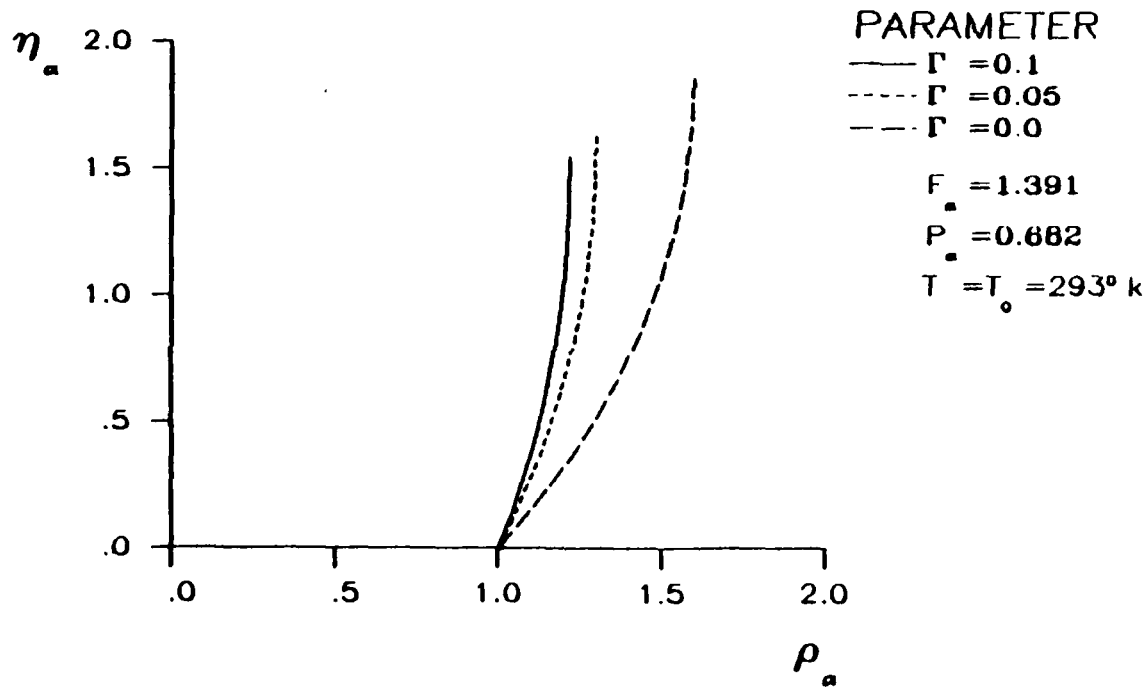

FIGURE 10. CHANGE OF DEFORMED PROFILE WITH THE MATERIAL CONSTANT

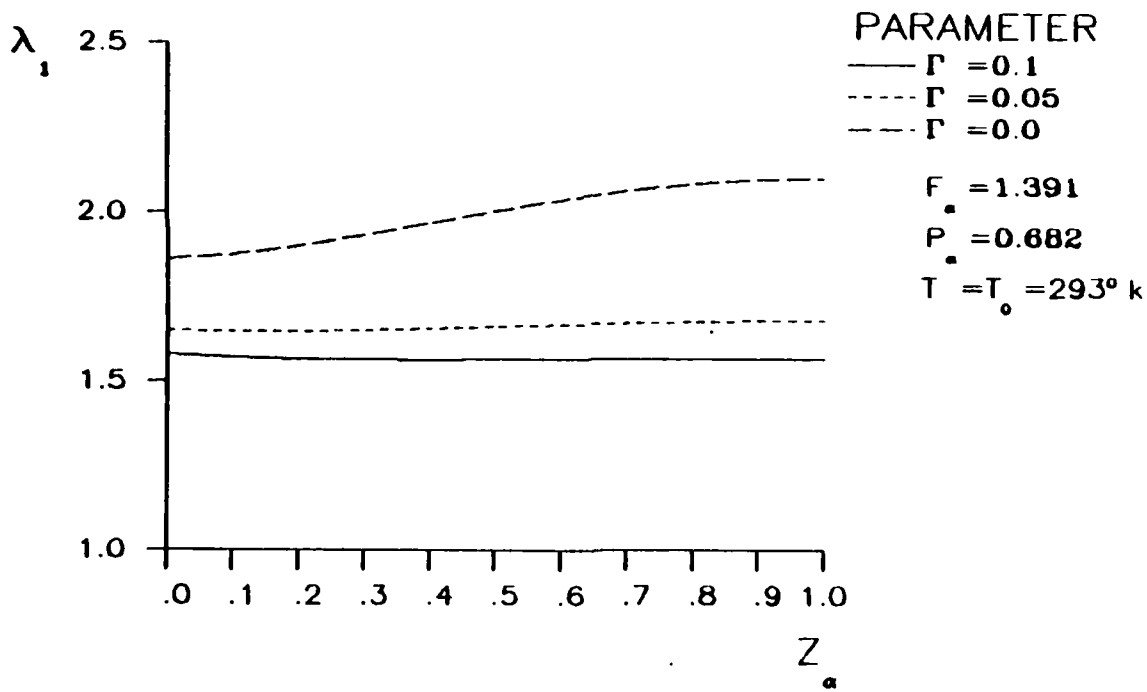

FIGURE 11. PRINCIPAL STRETCH RATIO IN THE MERIDIONAL DIRECTION.

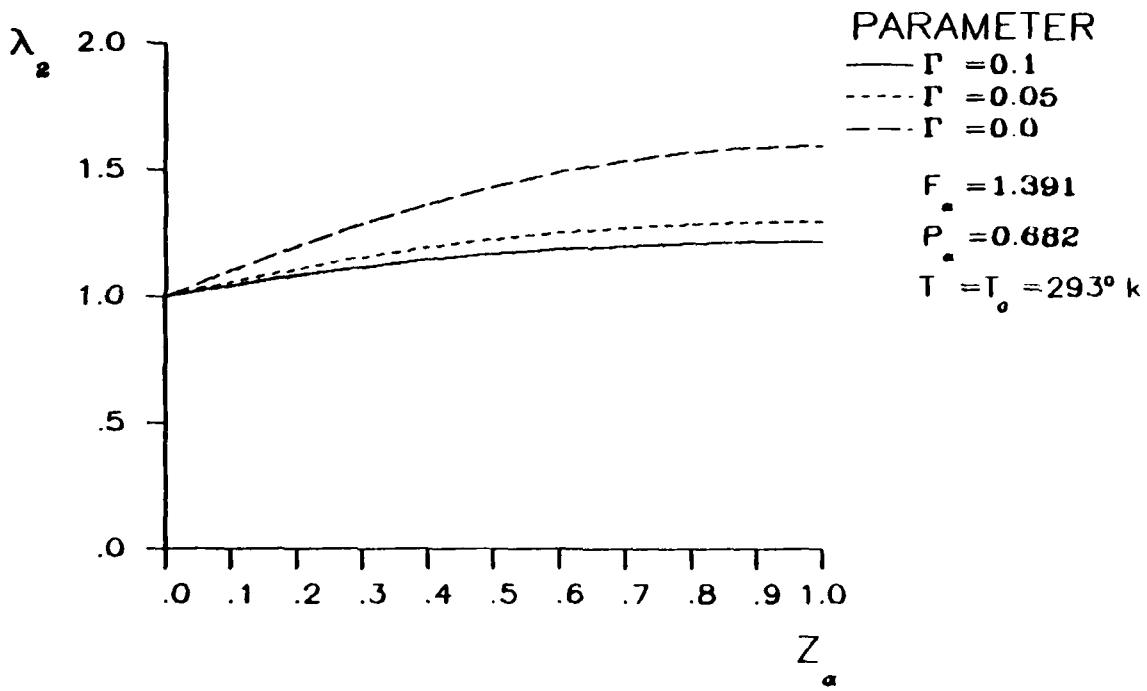

FIGURE 12. PRINCIPAL STRETCH RATIO IN THE CIRCUMFERENTIAL DIRECTION.

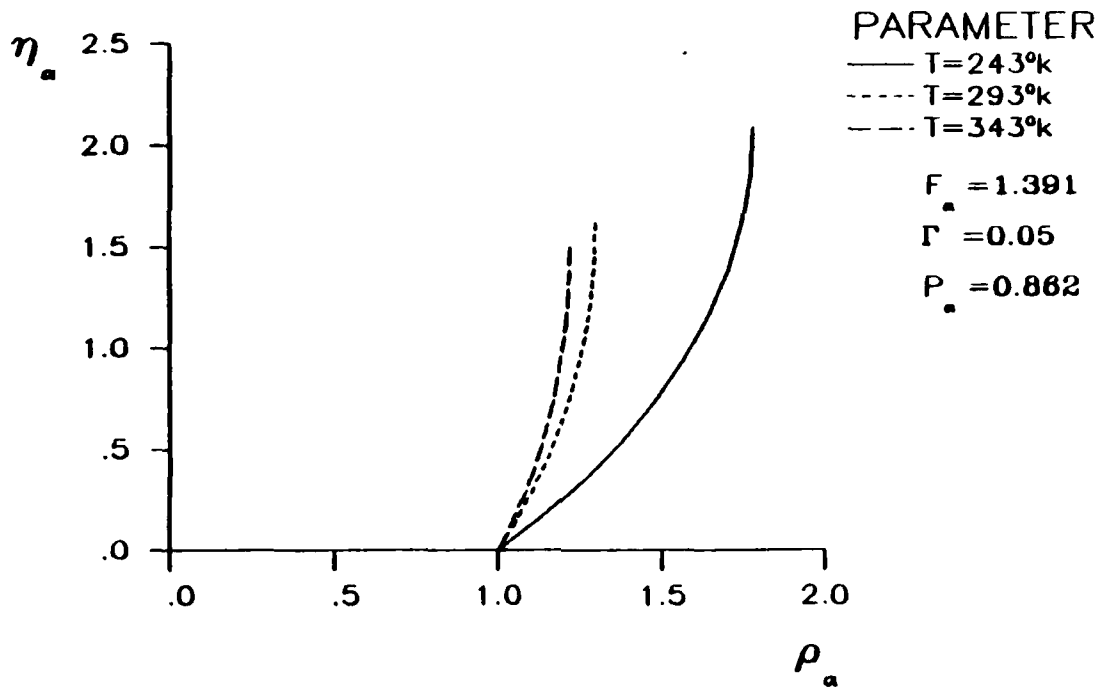

FIGURE 13. CHANGE OF DEFORMED PROFILE WITH TEMPERATURE

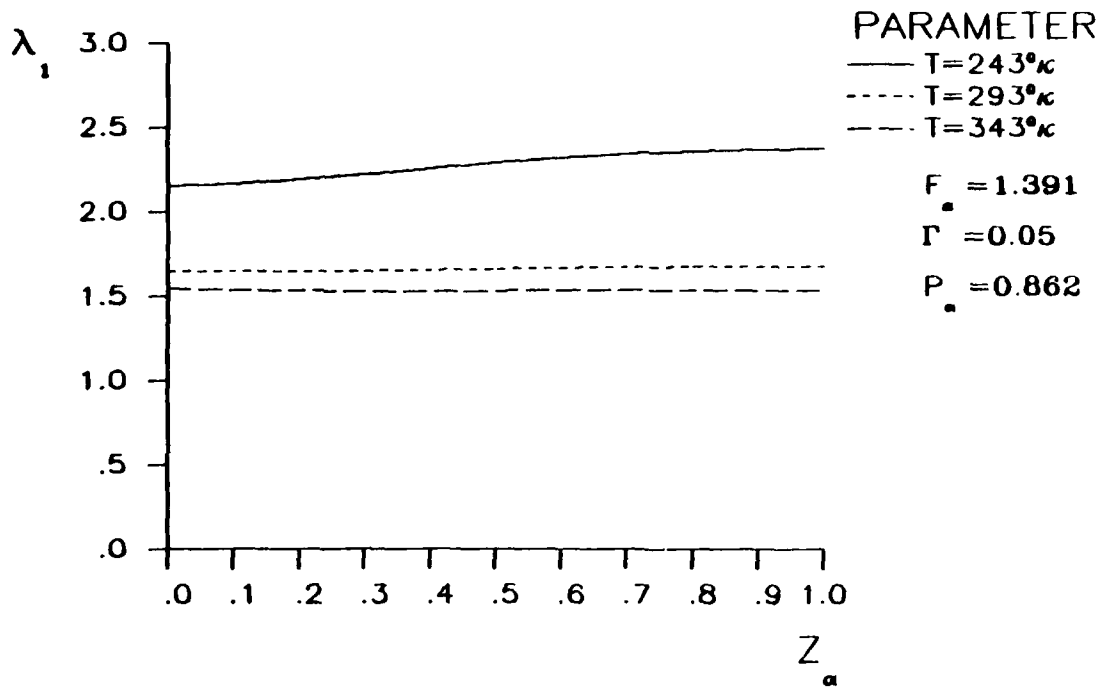

FIGURE 14. PRINCIPAL STRETCH RATIO IN THE MERIDIONAL DIRECTION.

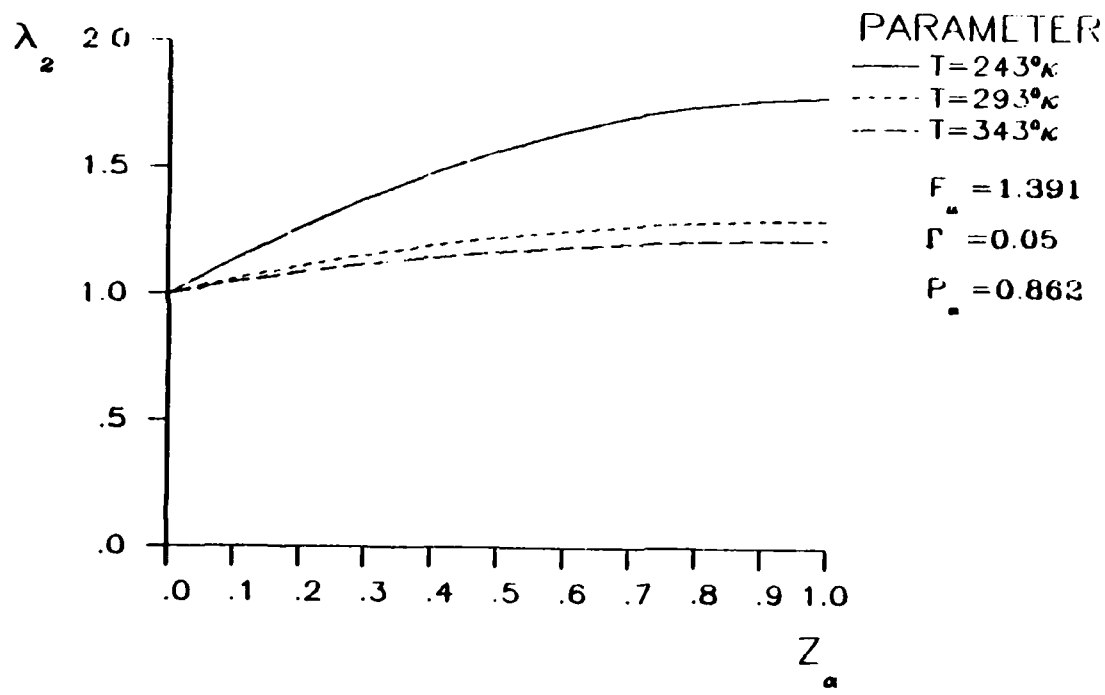

FIGURE 15. PRINCIPAL STRETCH RATIO IN THE CIRCUMFERENTIAL DIRECTION.

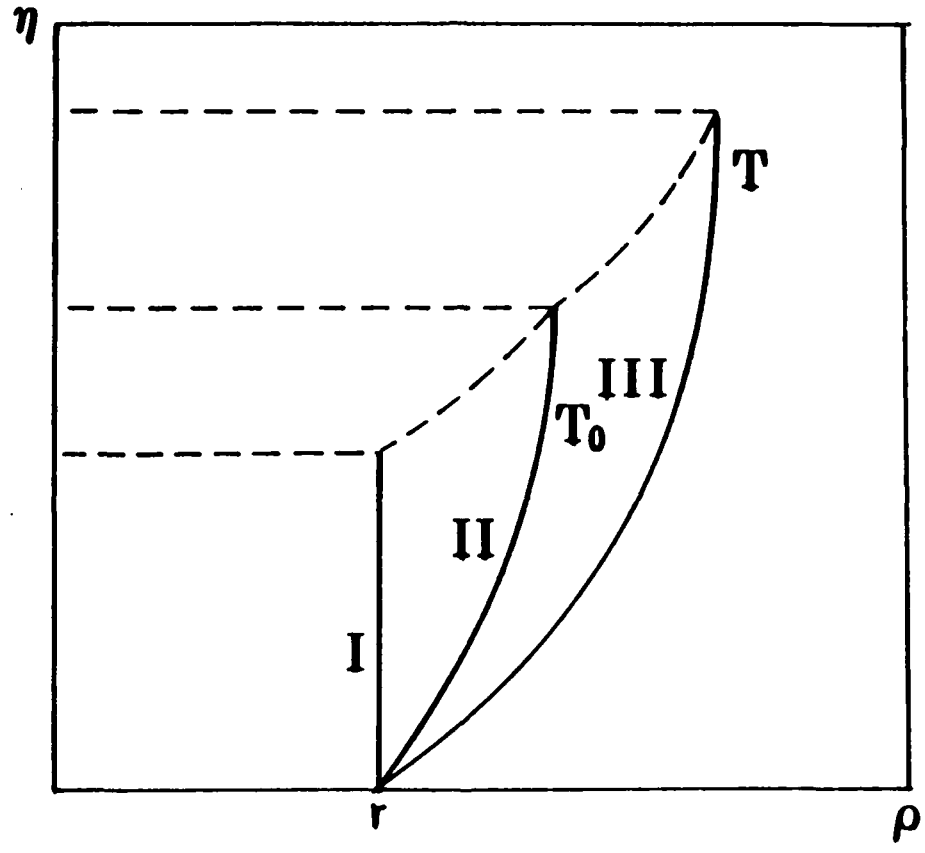

Figure 16. Explanation About Expansion on Cooling.

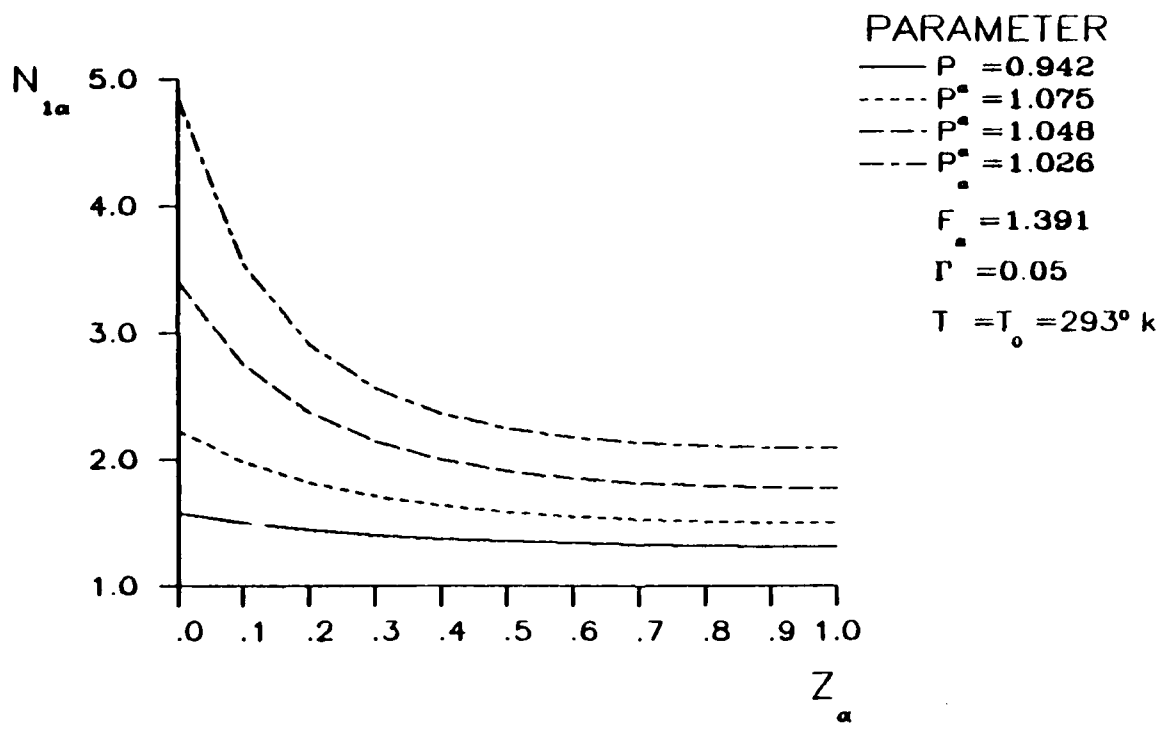

FIGURE 17. STRESS RESULTANT IN THE MERIDIONAL DIRECTION.

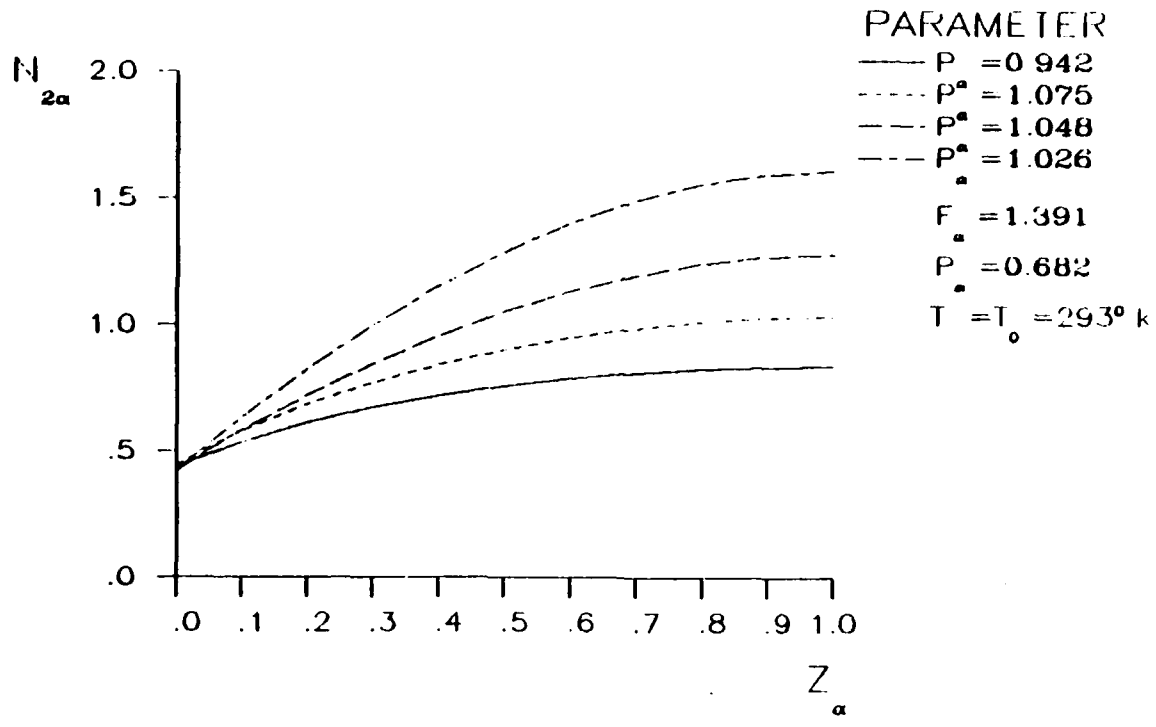

FIGURE 18. STRESS RESULTANT IN THE CIRCUMFERENTIAL DIRECTION.

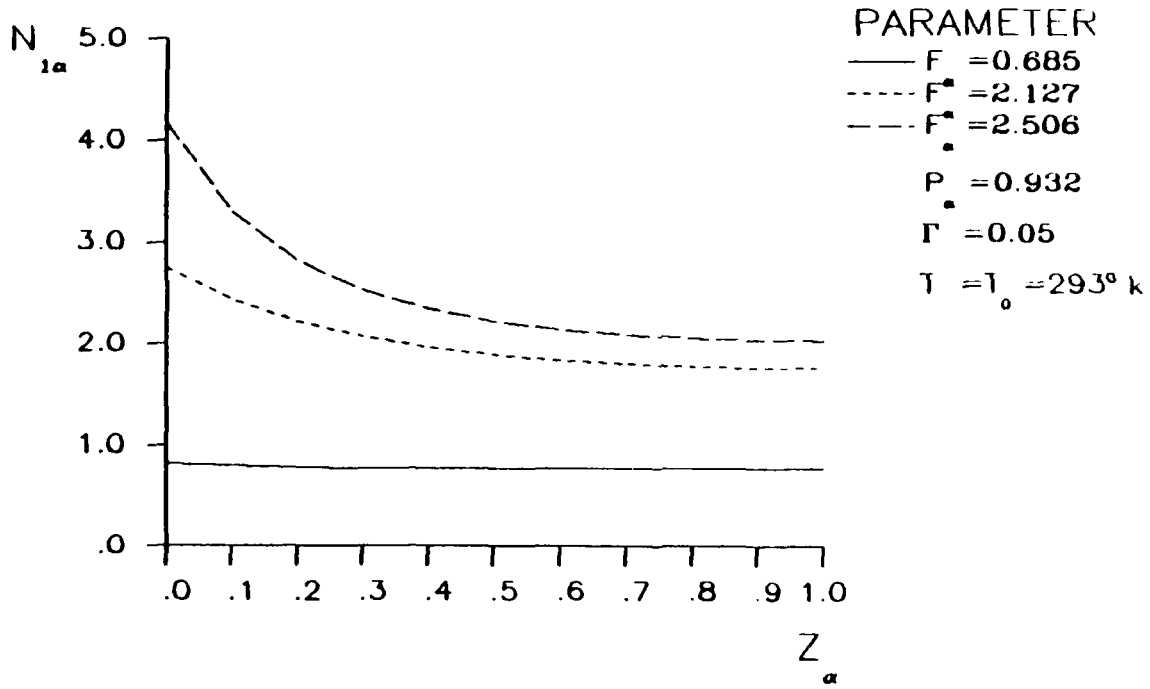

FIGURE 19. STRESS RESULTANT IN THE MERIDIONAL DIRECTION.

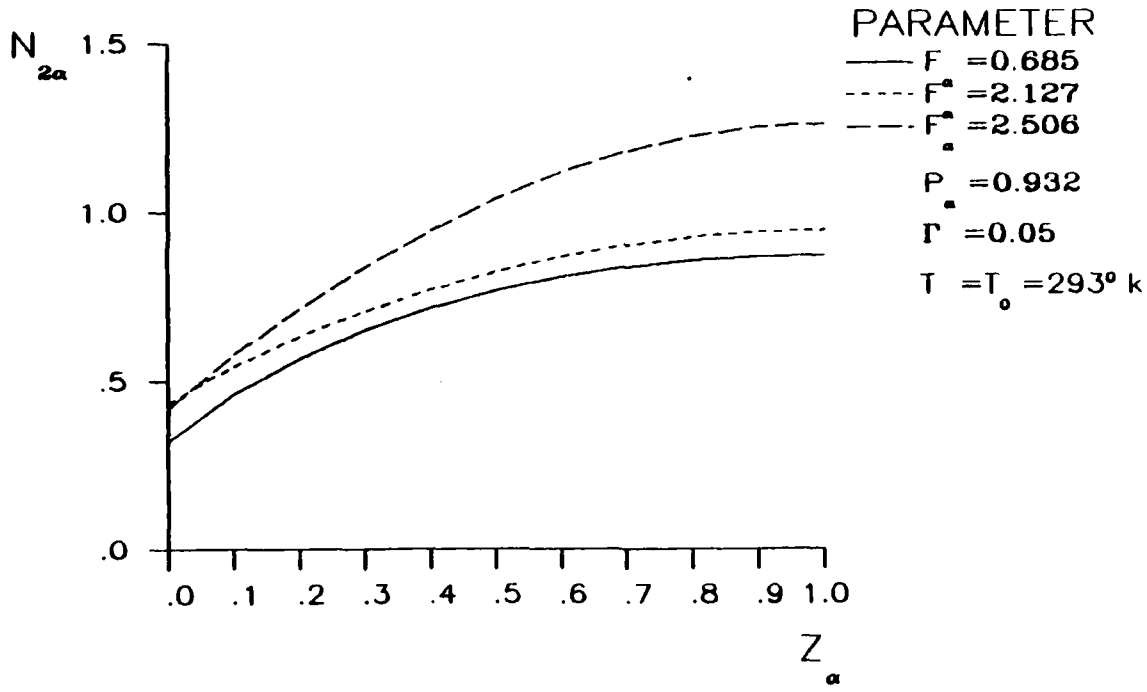

FIGURE 20. STRESS RESULTANT IN THE CIRCUMFERENTIAL DIRECTION.

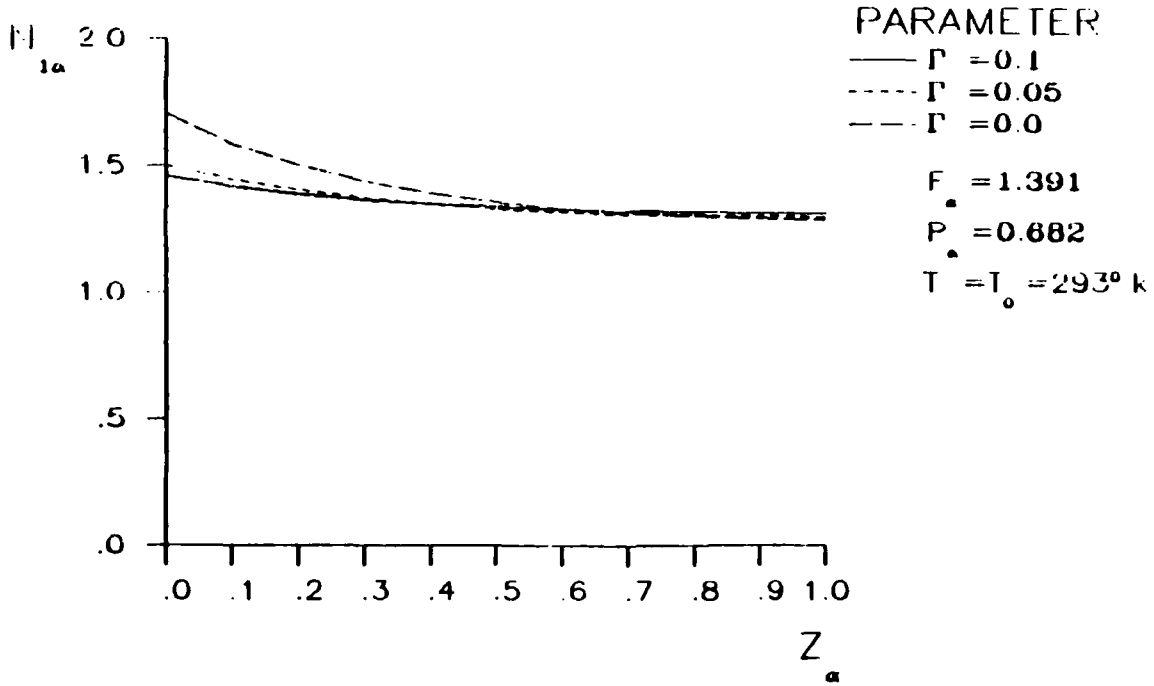

FIGURE 21. STRESS RESULTANT IN THE MERIDIONAL DIRECTION.

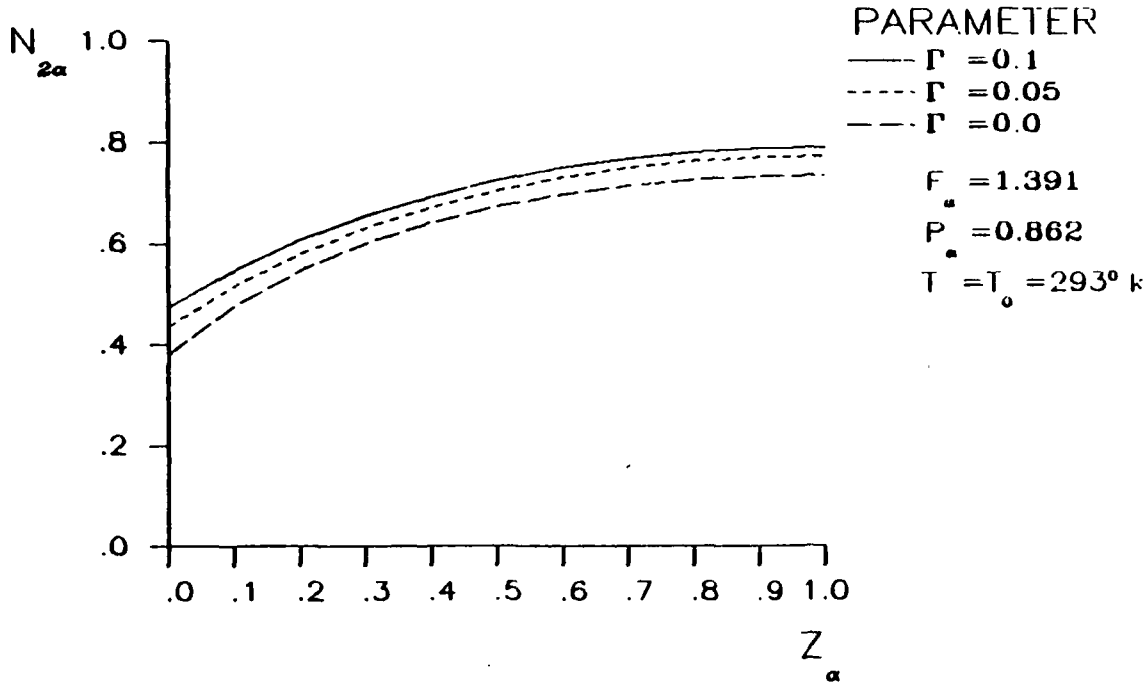

FIGURE 22. STRESS RESULTANT IN THE CIRCUMFERENTIAL DIRECTION.

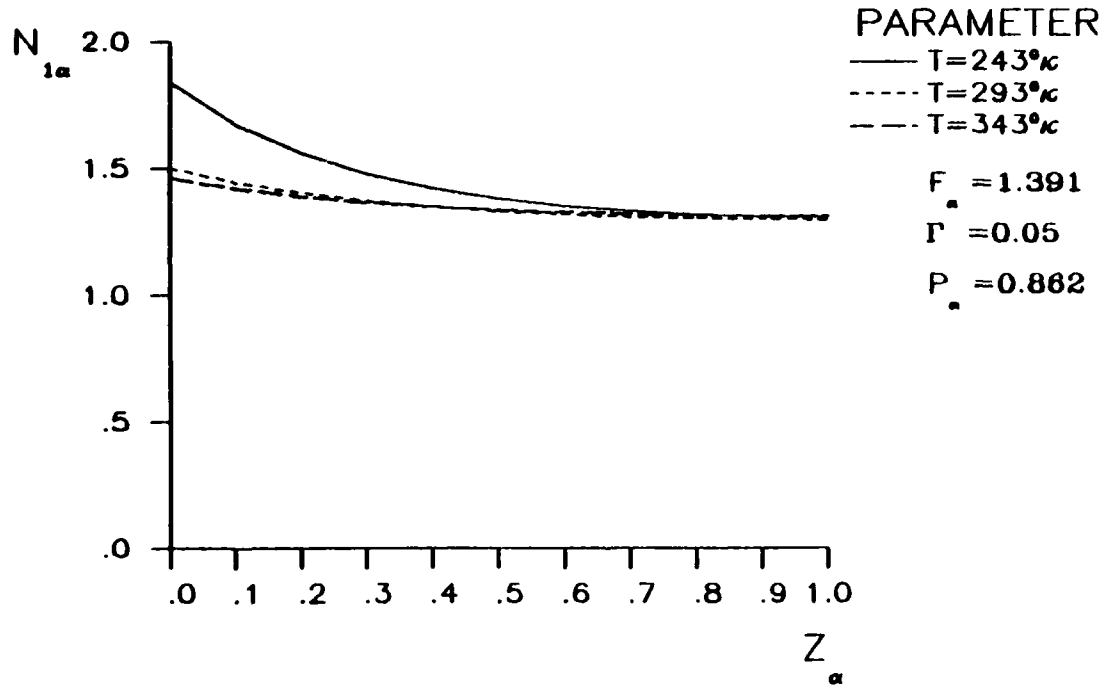

FIGURE 23. STRESS RESULTANT IN THE MERIDIONAL DIRECTION.

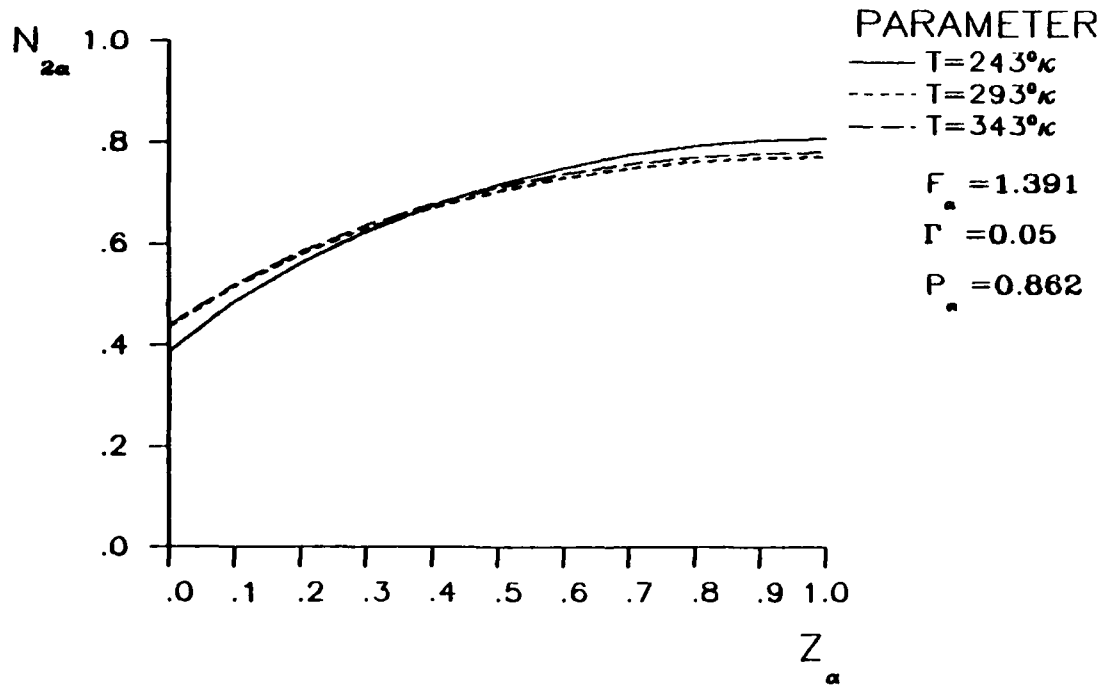

FIGURE 24. STRESS RESULTANT IN THE CIRCUMFERENTIAL DIRECTION.

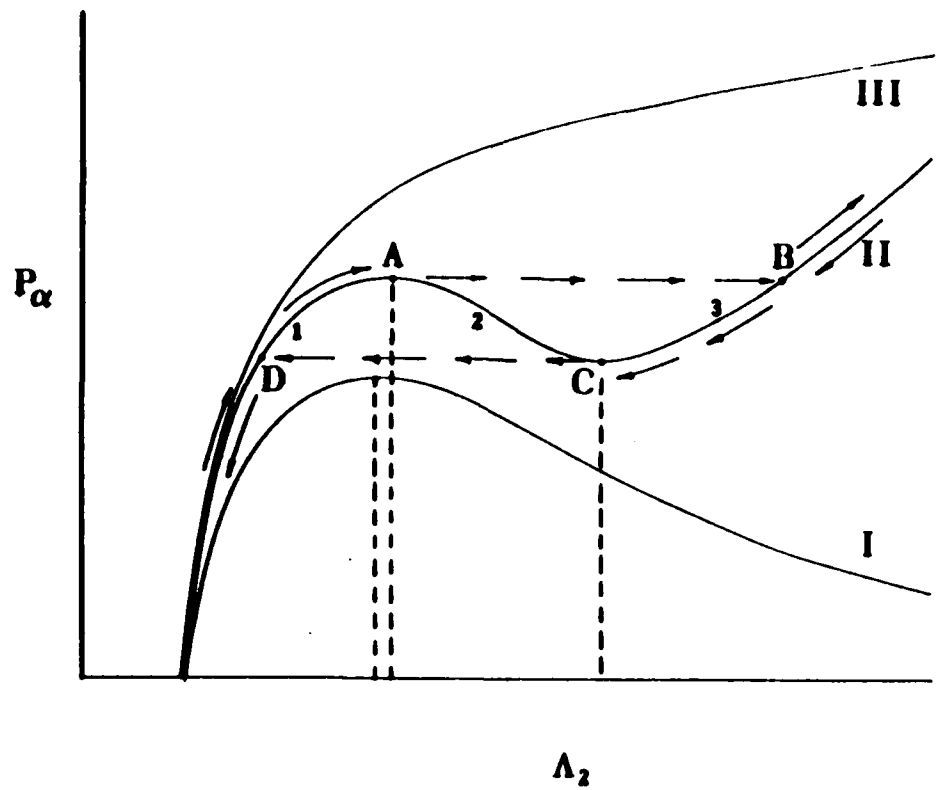

Figure 25. Instability. Jump Phenomenon.

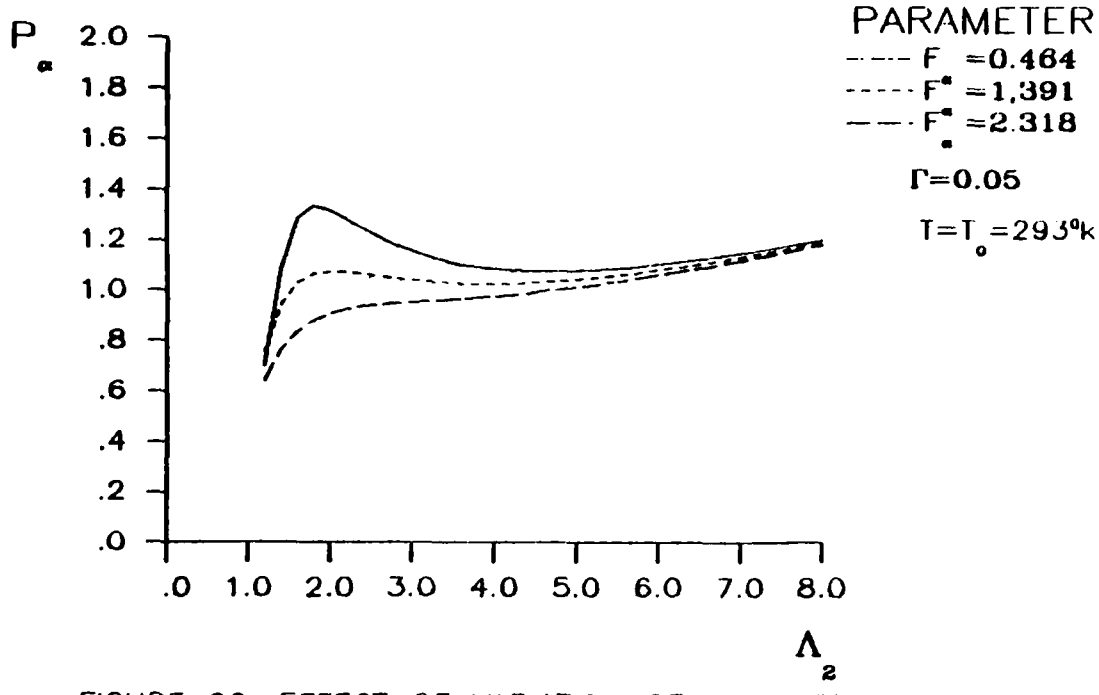

FIGURE 26. EFFECT OF VARIATION OF AXIAL FORCE ON INSTABILITY.

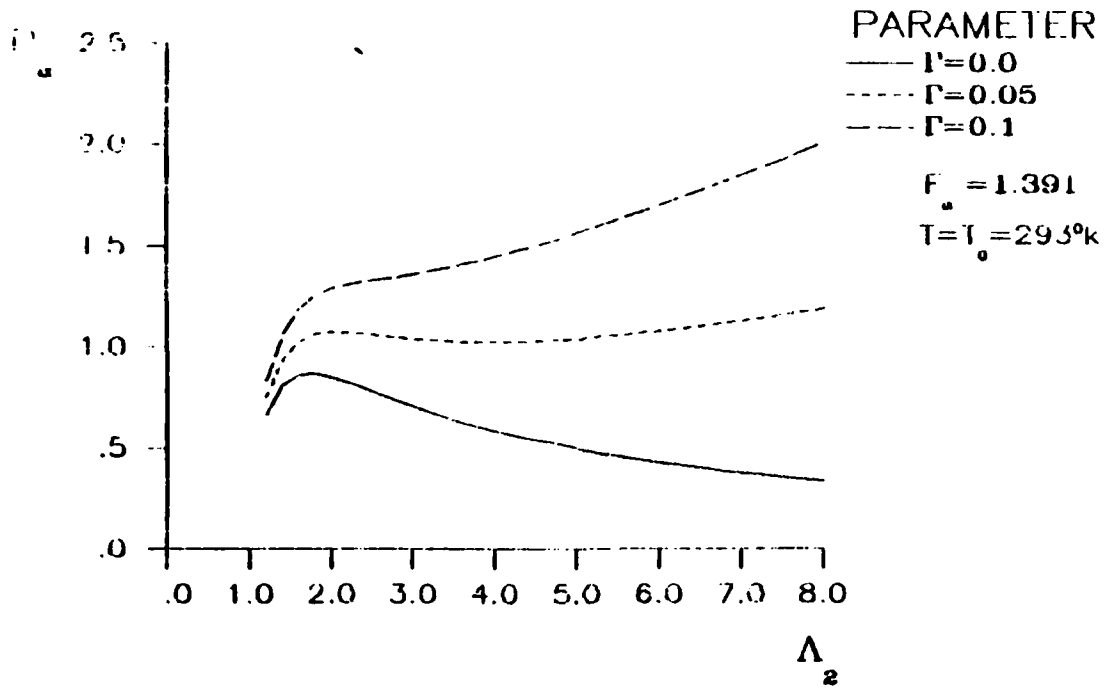

FIGURE 27. EFFECT OF VARIATION OF MATERIAL CONSTANT ON INSTABILITY.

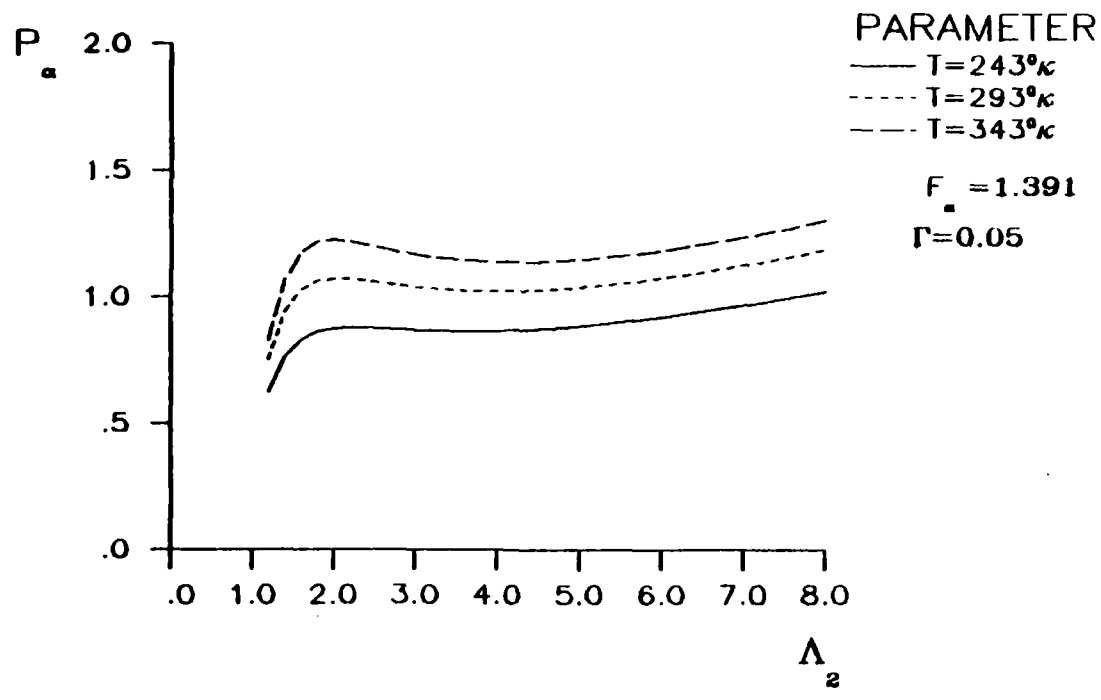

FIGURE 28. EFFECT OF VARIATION OF TEMPERATURE ON INSTABILITY.
ON INSTABILITY.

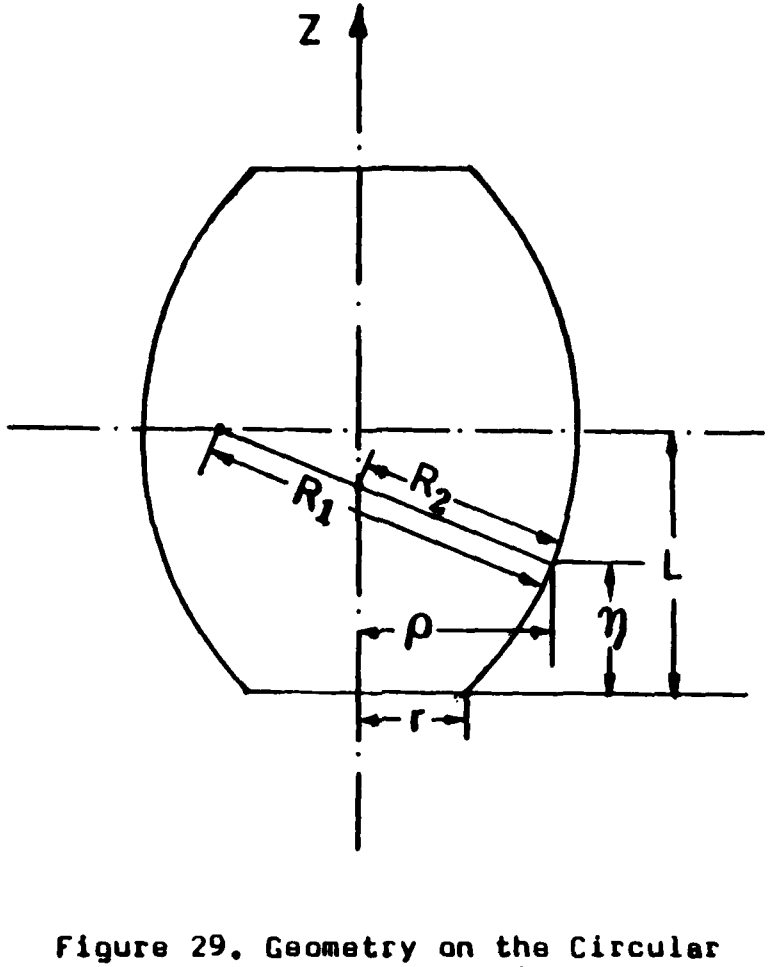

Figure 29. Geometry on the Circular Arc Assumption.

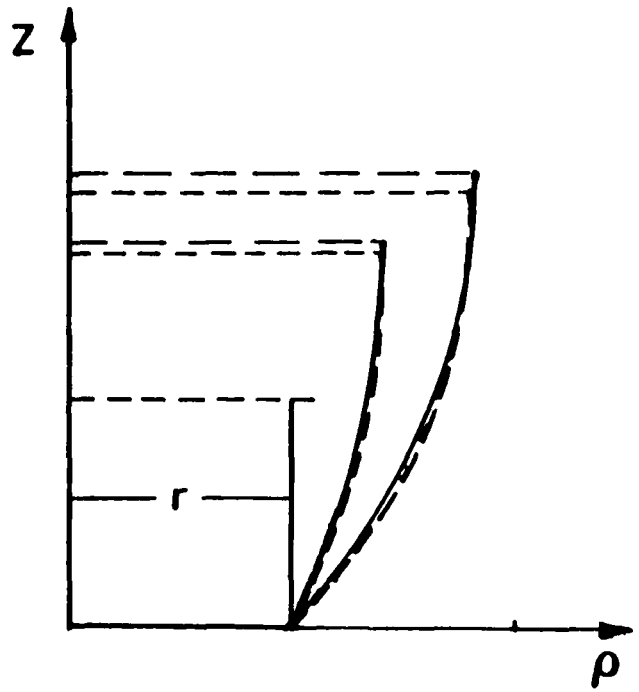

Figure 30. Compare Approximation Solutions With Exact Solutions.

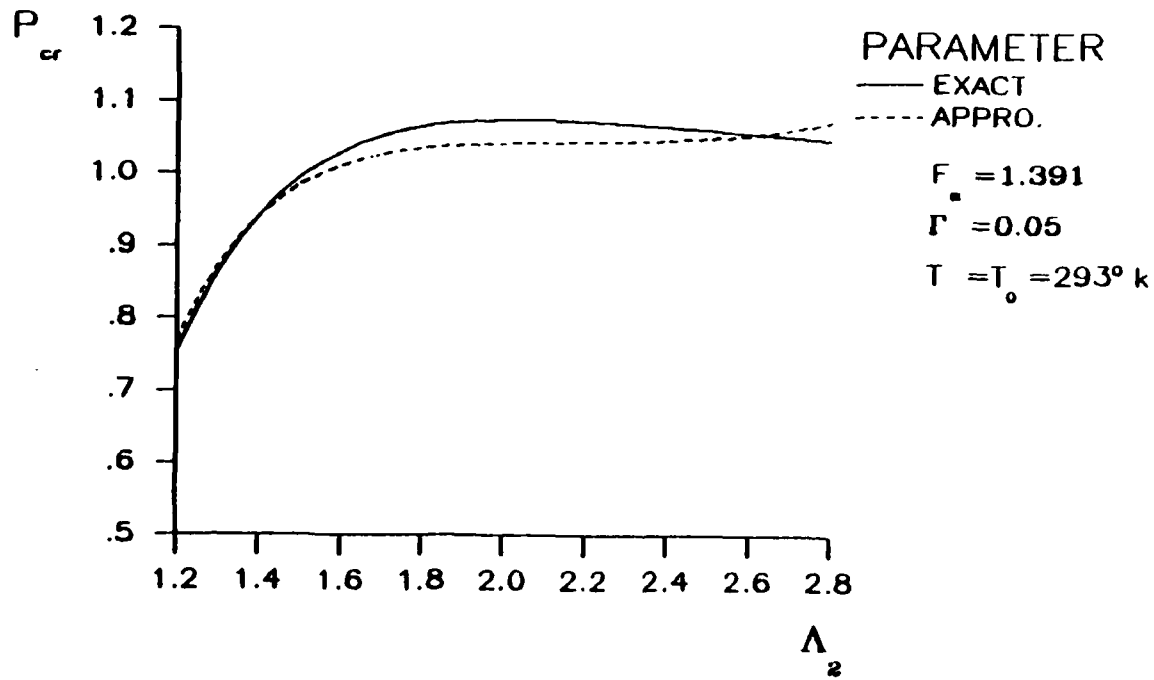

FIGURE 31. COMPARE APPROXIMATE SOLUTION WITH EXACT SOLUTION.

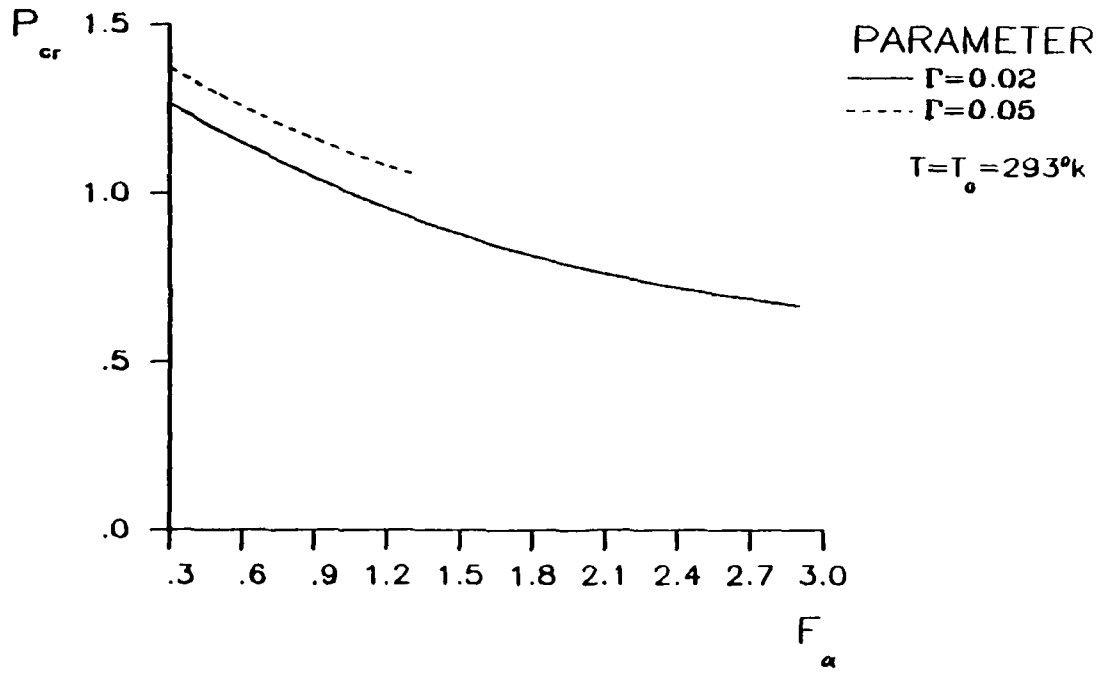

FIGURE 32. CRITICAL CURVE $P_{cr}-F_\alpha$

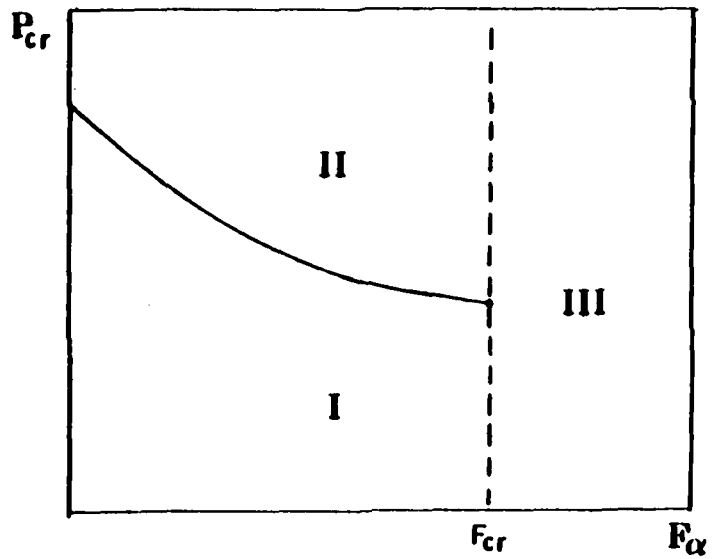

Figure 33. Distribution of stable Regions.

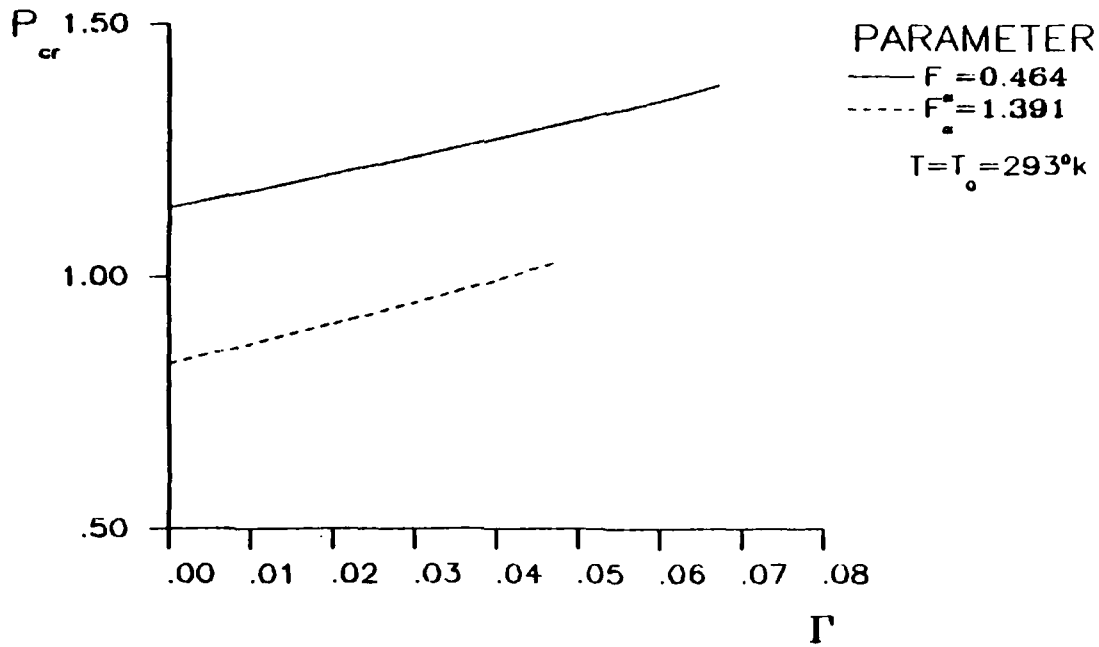

FIGURE 34. CRITICAL CURVE $P_{cr}-\Gamma$.

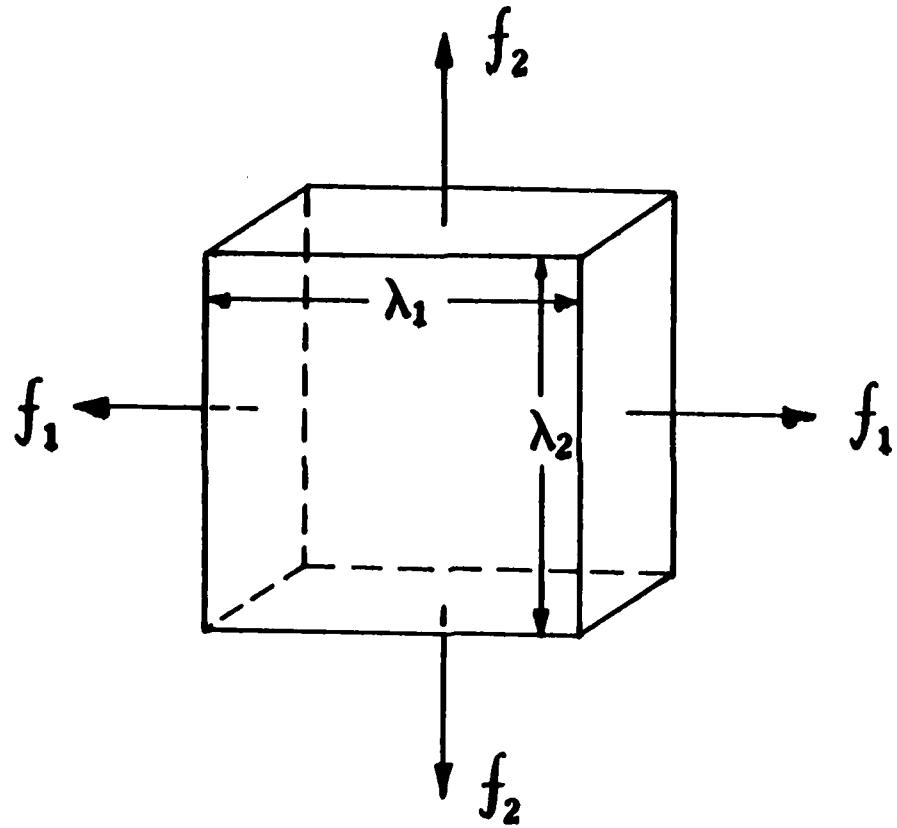

Figure 35. Derivation of Stress Resultant-Stretch Ratio Relations.

END

11-86

DTIC